DISS. ETH NO. 27402

Advanced microfluidic platforms for pathogen detection

A thesis submitted to attain the degree of DOCTOR

OF SCIENCES of ETH ZURICH

(Dr. sc. ETH Zurich)

presented by

Zahra Alsadat Halvorsen

Laurea Magistrale, Polytechnic University of Turin, Italy

born on 25.06.1987

citizen of Iran

accepted on the recommendation of

Prof. Andrew deMello
Prof. Klaus Eyer
Dr. Vincent Revol
Dr. Stavros Stavrakis

2021

To my family and Thomas.

Imagination is the highest form of research.

Albert Einstein

Acknowledgments

I had the honor to spend around four years at the Swiss Federal Institute of Technology, ETH Zürich, and CSEM. With sincerest gratitude, I wish to begin my thesis by acknowledging those who kindly supported me during this dissertation.

I wish to thank Prof. *Andrew J. deMello* for providing me the opportunity to be part of his research group, moreover, to let me follow my ideas. It was an enormous privilege to pursue a Ph.D. in his group, I will always remember him as a great scientist with a spectacular level of intelligence and a very humble attitude. I am particularly grateful to Dr. *Stavros Stavrakis*, Dr. *Philip Howes,* and *Akkapol Suea-Ngam*.

I wish to thank Prof. *Klaus Eyer*, Dr. *Stavros Stavrakis,* and Dr. *Vincent Revol* for accepting to be co-examiners of this thesis. It is an honor to have you on my committee.

I want to thank Prof. *Peter Ryser* for his always guidance and kind support, He is a mentor in my life, I do not know how to thank him enough, without him along with my Ph.D. studies, I could not make it. I want to thank all members of DeMello group and CSEM Alpnach, for their friendship and help. Especially Dr. *Helmut Knapp* and Dr. *Philippe Steiert* for financing my Ph.D. and their always kind support and guidance, I want to particularly thank Dr. *Vincent Revol* for his scientific support, I learned a lot from Noa Schmid and I want to thank him.

I am extremely thankful for all the support of my friends and my family. Special thanks go to my Mom and my sisters, who are always standing behind me. Finally, I would like to thank my amazing husband, I am so lucky to have you, I thank you for accepting me the way I am, thank you for all your love and support.

Abstract

The overarching goal of this thesaural work was to develop novel and powerful microfluidic platforms for the accurate detection and analysis of pathogens. More specifically, studies focused on developing a microfluidic sample preparation module for high-throughput flow cytometric detection of bacteria and the implementation of a field-deployable nucleic acid amplification system.

The first part of the thesis describes the creation of a miniaturized and automated sample preparation platform that interfaces with the optical module of a portable commercial flow cytometer. The integrated system is able, for the first time, to perform fully automated and high-throughput analysis of microbial species in drinking and lake water samples. The utility of the platform as a valuable tool in the water treatment industry is confirmed through the quantitative analysis of contaminated lake water samples on timescales of less than 30 minutes.

The second part of the thesis describes the development of a microfabricated step emulsification device for the high-throughput generation of monodisperse droplet populations that can be used as templates for the production of functional microparticles. As a proof-of-concept, we used this system to produce large quantities of monodisperse PAA hydrogel and PLGA microparticles on short timescales.

Accordingly, the final part of this thesis describes the development of a novel micro-compartmentalized nucleic acid quantification assay based on hydrogel microparticles that can be batch synthesized in large numbers and stored for subsequent application in loop-

mediated isothermal amplification (LAMP)-based procedures. Specifically, we targeted the detection of Methicillin-resistant Staphylococcus aureus (MRSA), the most prevalent AMR pathogen. In our hydrogel LAMP assay (which we term H-LAMP), monodisperse polyacrylamide microbeads were used for particle-templated emulsification of LAMP reaction components, thus achieving micro-compartmentalization of the reaction. The assay was successful in detecting MRSA within 30 minutes, with a limit-of-detection of 1 fg/μL (103 copies/μL). Overall, this new approach enables the direct translation of technical advances in droplet-based microfluidics to the in vitro diagnostics field, whilst circumventing the need for costly, complex, and cumbersome instrumentation. Such a platform has significant potential utility for use in resource-limited environments and represents a significant advance in field-deployable diagnostic tools for pathogen detection and quantification.

This thesis shows the benefit of combining interdisciplinary knowledge in biology, chemistry, and engineering, to develop industry-oriented tools for point of care diagnostics applications, especially for resource-limited areas.

Keywords: flow cytometry, water monitoring, Nucleic Acid Amplification, automation, step emulsification, microfluidics.

Zusammenfassung

Das übergreifende Ziel dieser Thesis liegt darin, neue und effizientere Microfluidics-Platformen zu entwickeln für die präzise und effiziente Erkennung von Pathogenen. Genauer gesagt, konzentrierten sich die Studien auf die Entwicklung eines mikrofluidischen Probenvorbereitungsmoduls für den rapiden Flow-Zytometrischen Nachweis von Bakterien und die Implementierung eines feldtauglichen Nukleinsäure-Amplifikationssystems.

Der erste Teil der Arbeit beschreibt die Erstellung einer miniaturisierten und automatisierten Probe-Analyse-Platform, die mit dem optischen Modul eines tragbaren kommerziellen Flow-Zytometers verbunden ist. Das integrierte System ist zum ersten Mal in der Lage, eine vollständig atumatisierte Hoch-Durchsatz-Analyse von mikrobiellen Spezien in Trink- und Seewasserproben durchzuführen. Die Nützlichkeit der Plattform als wertvolles Werkzeug in der Wasseraufbereitungsindustrie wird durch die quantitative Analyse von kontaminierten Seewasserproben in weniger als 30 Minuten bestätigt.

Der zweite Teil der Arbeit beschreibt die Entwicklung eines mikrofabrizierten Stufen-Emulsifizierungs-Geräts für die Hoch-Durchsatz-Generierung von monodispersen Droplets, die als Vorlagen für die Herstellung von funktionalen Mikropartikeln verwendet werden können. Als Proof-of-Concept haben wir dieses System verwendet, um grosse Mengen an monodispersen PAA-Hydrogel- und PLGA-Mikropartikeln in kurzer Zeit zu produzieren.

Dementsprechend beschreibt der letzte Teil dieser Arbeit die Entwicklung eines neuartigen Micro-Compartmentalized Nukleinsäure-Quantifizierungstests auf der Basis von Hydrogel-Mikropartikeln, die in grosen Mengen im Batch-Verfahren hergestellt und für die spätere Anwendung im Loop-Mediated Isothermal Amplification-Verfahren (LAMP) gelagert

werden können. Speziell haben wir uns auf den Nachweis von Methicillin-resistentem Staphylococcus Aureus (MRSA), dem häufigsten AMR-Erreger, konzentriert. In unserer Hydrogel-LAMP-Probe (die wir als H-LAMP bezeichnen) wurden monodisperse Polyacrylamid-Mikroperlen für die partikelgesteuerte Emulgierung der LAMP-Reaktionskomponenten verwendet, wodurch eine Mikrokompartimentierung der Reaktion erreicht wurde. Die Probe war erfolgreich beim Nachweis von MRSA innerhalb von 30 Minuten mit einer Genauigkeit von 1 fg/μL (103 Kopien/μL). Insgesamt ermöglicht dieser neue Ansatz die direkte Übertragung der technischen Fortschritte im Bereich der Droplet-Microfluidics auf den Bereich der In-vitro-Diagnostik und umgeht gleichzeitig die Notwendigkeit einer kostspieligen, komplexen und umständlichen Instrumentierung. Eine solche Plattform bietet einen gewaltigen potenziellen Nutzen für den Einsatz in ressourcenbeschränkten Umgebungen und stellt einen bedeutenden Fortschritt bei feldtauglichen Diagnosewerkzeugen zur Erkennung und Quantifizierung von Krankheitserregern dar.

Diese Arbeit zeigt den Nutzen der Kombination von interdisziplinärem Wissen in Biologie, Chemie und Technik auf, um industrietaugliche Werkzeuge für Point-of-Care-Diagnoseanwendungen zu entwickeln, insbesondere für ressourcenbeschränkte Gebiete.

Acknowledgements IV

Abstract V

Table of contents IX

List of figures XII

List of tables XIX

Chapter 1

1.1. Microfluidic platform for pathogen detection 1

1.2. Microflow cytometry 6

1.2.1. Liquid handling 7

1.2.2. Microfluidic focusing technique

1.2.3. Pathogen detection in microflow cytometers 10

1.3. Droplet microfluidics 12

1.4. Nucleic acid amplification 15

1.4.1. PCR and digital PCR technique 15

1.4.2. Isothermal amplification methods

1.4.2.1. Loop-mediated isothermal amplification 20

1.5. Thesis overview 29

Chapter2 31

2.1. Flow Cytometry-Based method for pathogen detection 32

2.2. Materials & Methods 34

2.2.1. Automated and miniaturized sample preparation platform

2.2.2. Microfluidic device fabrication 37

2.2.3. Sampling procedure 38

2.2.4. Staining protocol 39

2.2.5. Flow cytometry measurements 39

2.2.6. Monitoring bacterial contamination 42

2.3. Results & Discussion 44

2.3.1. Assessment of dynamic range 45

2.3.2. Monitoring bacterial contamination

2.4. Conclusions 47

Chapter 3 49
3.1. Droplets: small, uniform, and high throughput 50
3.1.2. Droplet generation 52
3.1.2.1. Planar Shear-Induced droplet generation devices 52
3.1.2.2. Step emulsification 57
3.1.3. Applications of high throughput droplet generation 62
3.2. Material and methods 65
3.2.1. Device design and master mold fabrication 65
3.2.2. PDMS device fabrication 67
3.2.3. Step emulsification device development 68
3.2.4. Droplet production 72
3.2.4.1. Polyacrylamide beads production 72
3.2.4.2. Cell culture and single-cell encapsulation 73
3.2.4.3. PLGA production 74
3.3. Result and Discussion 75
3.3.1. Mixing process of the Tesla Micromixer 75
3.3.2. Polyacrylamide beads production 77
3.3.3. Cell culture and single-cell encapsulation 81
3.3.4. PLGA production 83
3.4. Conclusions 85

Chapter4 87
4.1. Nucleic acid amplification-based techniques for pathogen detection 89
4.2. Materials and Methods 92
4.2.1. Chemicals 92
4.2.2. Biological samples and reagents 92
4.2.3. Microfluidic device design and fabrication 95
4.2.4. Polyacrylamide hydrogel bead preparation 96
4.2.5. MRSA assay procedure 97
4.2.6. Selectivity study 98
4.3. Results and Discussion 99
4.3.1. PAA hydrogel characterization 99
4.3.2. H-LAMP characterization 104
4.3.3. DNA quantitation with H-LAMP 107

4.3.4. Bacterial lysate and selectivity testing 112
4.3.5. Stability of the hydrogel microbeads 113
4.4. Conclusions 116

Chapter5 118
5.1. Conclusions 119
5.2. Future research Directions 119

Abbreviations 121
Appendix A Supplementary to Chapter 2
References 125

List of figures

Figure 1.1. Schematic diagram of a flow cytometer composed of subsystems including microlfuidic sample manipulation, excitation and detection modules and a data processing unit. FL: fluorescence SSC: side scatter, FSC: forwared scatter, PD: photodiode, LD: laser…… 5

Figure 1.2. Microfluidic particle focusing strategies. (a) Schematic of microfluidic FCM, in which a spiral channel is used to create a Dean flow for high-throughput sheathless 3-D focusing[41].(b) Polystyrene microparticle and bioparticle focusing and separation using oscillatory viscoelastic microfluidics[50]. (c) Schematic of the experimental setup for focusing and side view images of microparticle flows. The images show the side view fluorescence images of particles before and after the SSAW is generated.[46]. (d) Schematic of continuous high-resolution dielectrophoresis-based cell sorting[49]…… 9

Figure 1.3. Droplet-based microfluidic platforms for pathogen detection (a) Schematic illustration of the detection of Salmonella based on a single-cell droplet-based microfluidic system. Quantification comprises three steps. (i) droplet generation and Salmonella single-cell encapsulation. (ii) droplet collection and cell culture. (iii) droplet counting based on the fluorescence presented by positive samples.[71]. (b) Encapsulation and culture of bacteria in agarose droplets showing (i) images and (ii) numerical simulations of droplet generation in a flow-focusing approach[72]. (c) Overview of a screening method for single-cell encapsulation inside agarose droplets. Single cells are encapsulated into monodisperse water-in-oil emulsion droplets. The aqueous solution also contains agarose that gelates upon cooling, so that solid gel beads form inside droplets. During incubation of the emulsion, cells grow into monoclonal microcolonies inside the beads. The latter are recovered from the emulsion and sorted by FACS [73]. (d) Integrated microfluidic platform design. After droplet formation and merging, droplets are arrested in a docking array for monitoring interactions among

macrophages and bacterial targets. The inset shows a droplet encapsulating *E. coli*, M1-WT, and M2-DS-Red-KI macrophages[75]……14

Figure 1.4. An overview of common PCR techniques. In conventional PCR, the amplification products are detected based using post-amplification gel electrophoresis. In qPCR, the amount of amplified DNA is measured at each cycle during the PCR reaction. In dPCR, the sample is partitioned into many compartments (in microwells, chambers, or droplets) such that each partition contains either one or no target sequences…… 17

Figure 1.5. Overview of different partitioning technologies for dPCR. (a) The Naica droplet-based sample partitioning chip (Stilla, France). (b) The Digital PCR (20K) Chip comprsies a microwell-based sample partitioning system (Thermo Fisher). (c) The channel-based sample partitioning system from Fluidigm [79]. (d) Inkjet printing-based sample partitioning[84, 85]…… 19

Figure 1.6. Schematic of the LAMP amplification technique. (1) The inner primer (FIP) binds to the single-stranded DNA followed by strand displacement and polymerization. (2) The binding of an outer primer (F3) take place followed by polymerization. (3) The newly synthesized strand displaces and forms a self-hybridizing loop structure. (4) The same process as described above is repeated on the opposite end of the target sequence through the binding of the inner primers (BIP) and (B3). (5) Short "dumbbell" loop structures are formed that can be amplified into dsDNA concatemers(Figure adopted from[96])…… 22

Figure 1.7. Microfluidic dLAMP devices. (a) A droplet-based microfluidic device for continuous flow digital LAMP, illustrating the three steps required for a complete analysis [99]. (b) A schematic illustration of the experimental workflow for digital LAMP in a droplet array[100]. (c) Schematic drawings and images showing the operation of a SlipChip for a two-step digital reverse transcription-loop-mediated isothermal amplification (dRT-LAMP)[101]. (d) Schematic illustration of the self-

transportation microfluidic device , upon coating PDMS surface with a hydrophilic film that allows for digital LAMP to be performed in a simple and robust manner [102]..... 26

Figure 2.1. Photograph (right) and schematic (left) of the fluidic sample preparation unit. The entire unit has dimensions of 5 x 5 x 20 cm and comprises a bi-directional syringe pump, a microfluidic device, a rotary valve with an integrated active magnetic mixer and a heating element..... 35

Figure 2.2. Schematic of the fluidic sample preparation unit. (a) Three-dimensional schematics of the rotary distribution valve and microfluidic device. (b) Top: Aerial view of the fluidic assembly, showing the microfluidic device, the chip holder and magnetic element. Bottom: Photograph of the assembled sample preparation module. All schematics are drawn to scale..... 36

Figure 2.3. Detailed schematic of the microfluidic device. *W* is connected to the water sample reservoir, *S* is connected to the SYBER Green I reservoir, *C* is connected to the glass capillary in the optical module, *B* is connected to the bleach (cleaning solution) reservoir and *R* is connected to the rinse solution, *O* is connected to a hermetically sealed waste reservoir..... 37

Figure 2.4. Photograph of the complete microfluidic device (scale bar 2mm)..... 38

Figure 2.5. Flow cytometric analysis of Nano Fluorescent Size Standard Kit beads, visualized by their normalized log-transformed signals in the side scatter and green (520 nm) fluorescence channels.40

Figure 2.6. Two-dimensional scatter plots of FL2 as a function of FL1 for a representative tap water sample. Gating within the scatter plot delineates small (LNA, green area) and large (HNA, blue area) sized bacteria and TCC (red dotted area)..... 41

Figure 2.7. Image of the complete flow cytometer assembly. (a) The sample preparation unit (b) is connected to the bNovate optical module..... 42

Figure 2.8. Schematic of the wash-in, wash-out and mixing reactor used for the detection of microbial contamination using FC. The setup included a stirred glass reactor, A peristaltic Pump (BT100-1L, Darwin Microfluidics, Paris, France) was used for wash-in and wash-out and spiking experiment…43

Figure 2.9. The cell concentration values for TCC over time for 6 sequential measurements (blue circles) of four different concentrations of an *E. coli* BioBall sample…… 44

Figure 2.10. Continuous analysis of water contamination by *E.coli* bacteria. (a) TCC measurements of three *E. coli* bacterial contamination experiments. (b)-(e) FL2 vs FL1 scatter plots showing the amount of bacteria at different stages of the experiment: (b) tap water sample, (c) *E coli* contaminated sample, (d) a partially washed contaminated sample and (e) return to tap water…... 46

Figure 2.11. Continuous analysis of water contamination by lake water. (a) TCC measurements of three lake water contamination experiments. (b)-(e) FL2 vs FL1 scatter plots showing the amount of bacteria at different stages of the experiment: (b) tap water sample, (c) lake water contaminated sample, (d) a partially washed contaminated sample and (e) return to tap water…….... 47

Figure 3.1. Schematic illustration of different types of emulsions. (a) a water-in-oil emulsion (w/o), (b) an oil-in-water emulsion (o/w) and (c) a water-in-oil-in-water (w/o/w) double emulsion…..... 52

Figure 3.2. Overview of the three most common planar shear-induced microfluidic droplet generation techniques. (a) T-junction, (b) Co-flow geometry and (c) Flow-focusing geometry. The aqueous (dispersed) phase is shown in blue and the oil (continuous) phase is shown in yellow…… 54

Figure 3.3. Parallelization and scaling out approaches for droplet generation. (a) A three-dimensional device made in PMMA, having 256 parallel droplet generators[188]. (b) A planar step emulsification device comprising 128 cross-junctions for the mass-production of monodisperse droplets[191]. (c) A three-dimensional monolithic elastomeric device containing 1000 parallel flow-focusing generators for large-scale droplet generation[187]. (d) A 3D printed parallelized microfluidic device containing radially organized stacks of microdroplet generator units[190]. (e) A multilayer

device consisting of parallel droplet-generators for high throughput cell encapsulation and synthetic microgel generation[189]…… 56

Figure 3.4. Evolution of the original Microfabricated Channel device. Droplet formation is realized using (a) A symmetric plate consisting of micro slots on both sides[196]. (b) An asymmetric plate with circular channels on the upstream side and slots on the downstream side[199] . (c) A symmetric plate consisting of several micronozzles[198]…… 58

Figure 3.5. (a) Image of droplet generation using a T-junction microfluidic device. Variation of input flow rates provides exceptional control over both droplet size and droplet payload. (b) Image of monodisperse droplets generated by the process step emulsification…… 60

Figure 3.6. Alternative fluid actuation methods for step emulsification. (a) Centrifugal-based step emulsification[208], (b) magnetic force-driven step emulsification[207], (c) Centrifugal-based step emulsification within an Eppendorf tube[209] and (d) Buoyancy-driven step emulsification[210]…… 61

Figure 3.7. Schematic of a typical droplet dPCR workflow. dPCR is performed according to following steps: master mix preparation, partitioning of the mix into a large number of discrete nanoliter or sub-nanoliter droplets, amplification through temperature cycling and image analysis…….. 64

Figure 3.8. Schematic depicting the master mold fabrication processes. First, the wafer is dehydrated, and spin coated with SU-8 photoresist. After the soft bake UV light and a photomask are used to transfer the pattern of the microfluidic features on to the surface. A post-exposure bake is followed by resist development. After the washing in isopropanol, the wafer is dried with air and hard baked…… 67

Figure 3.9. Step emulsification master molds: (a) Design a1 contains two separate oil channels, (b) Design a2 contains a modified channel geometry consisting of five oil microchannels (scale bar2mm)…… 69

Figure 3.10. A step emulsification device for single-cell encapsulation experiments (design a3). Here, an array of inlets (labelled cell inlets) is embedded inside the main nozzle array, which enables high throughput single cell encapsulation (scale bar2mm)..... 70

Figure 3.11. Master molds of step emulsification devices integrating micromixer units: (a) Design a4 consists of two inlets for the aqueous phase and a long microchannel for reagent mixing. (b) Design a5 design incorporates a custom tesla micromixer embedded before the aqueous channel (scale bar2mm)..... 71

Figure 3.12. The tesla-inspired passive micromixer integrated prior to the radial nozzle array, showing the design (upper image) and fluorescence analysis (lower images 1–5), scale bar 200 μm..... 76

Figure 3.13. Droplet formation in a step emulsification device (a) and zoomed image of neck formation in the nozzle (b). A sequence of the droplet formation process showing the droplet formation in step emulsification device..... 78

Figure 3.14. Optical microscopy images of droplet generated using design a4..... 78

Figure 3.15. Image of PAA microgels (a) freshly prepared and (b) after being stored for 120 days at 4°C prior to analysis. Scale bar 100 μm. (c) Histogram of the bead size distribution (CV~ 2.8 %).... 88

Figure 3.16. Optical microscopy images of single- CHO-K1 cells encapsulated in water-in-oil droplets, demonstrating the potential of the device producing monodisperse droplets and relatively good cell occupancy (scale bar 100μm) 82

Figure 3.17. (a) Optical microscopy images of PLGA droplet before polymerization (b) Histogram of the droplet size distribution demonstrating monodispersity with a CV of 3.5%, (c, d) monodisperse PLGA microgel particles (scale bar 100μm)..... 84

Figure 4.1. The custom-designed step emulsification device. (a) The master mold (SU8 on silicon). Scale bar 2 mm. (b) The tesla-inspired passive micromixer integrated prior to the radial nozzle array, showing the design (upper image) and fluorescence analysis (lower images 1–5). Scale bar 200 μm. (c) Bright field image of the nozzle array, showing the production of monodisperse droplets. Scale bar 100 μm..... 101

Figure 4.2. Image of PAA microgels (a) freshly prepared and (b) after being stored for 120 days at 4°C prior to analysis. Scale bar 100 μm. (c) Histogram of the bead size distribution..... 103

Figure 4.3. Agarose gel electropherogram, showing LAMP reaction products at different concentrations of the *mecA* gene (1, 10, 100, 1000 fg/μL), with a negative control (Ne-)..... 104

Figure 4.4. Fluorescence images of (a) positive (1000 pg/μL *mecA* sample) and (b) negative (0 pg/μL *mecA* sample) H-LAMP reaction, incubated at 60°C for 60 minutes. Scale bar 150 μm. c) Variation of fluorescence as a function of time for samples in (a) and (b)..... 106

Figure 4.5. Time-dependence fluorometric signal reactions with different concentrations of 0.001, 0.01, 0.1, 1, 10, 100, 1000 pg/μL mecA target..... 108

Figure 4.6. Fluorescence images of the bead monolayers in an observation channel for (a) the non-template control, and (b–h) the tested concentrations of 0.001, 0.01, 0.1, 1, 10, 100, 1000 pg/μL *mecA* target, respectively (representative cropped image sections). Scale bar 150 μm..... 109

Figure 4.7. Image analysis with CellProfiler. (a) Overview of CellProfiler pipeline used for analyzing beads images. (b) Original image. (c) Beads outlines..... 110

Figure 4.8. Bead intensity histogram generated by the "Density Plot" tool in CPA. Positive and negative beads can be clearly distinguished by using the threshold..... 111

Figure 4.9. (a) The calibration curve of the H-LAMP assay. b) An accuracy test comparing DNA amplification results (N = 3) of tube-based PCR tube and the H-LAMP system, detecting *mecA* in the range 1 to 100 pg/µL..... 129

Figure 4.10. (a) Selectivity study of H-LAMP. (b) Size stability test of the hydrogel beads over 120 days..... 130

List of Tables

Table 1.1. Overview of the literature relating to the detection of pathogens using microfluidic FCM technology..... 10

Table 1.2. LAMP vs PCR 23

Table 1.3. Overview of LAMP methods for pathogen detection implemented in microfluidic devices..... 27

Table 2.1: Overview of laser parameter values..... 38

Table 3.1. List of the geometrical features in design a5 of the step emulsification microfluidic device..... 72

Table 4.1. LAMP and PCR primers sets for *mecA* amplification..... 94

Table 4.2. The concentration of each components of LAMP method..... 95

Chapter 1 – Introduction

1.1. Platforms for pathogen detection

Pathogenic microorganisms refer to any microorganisms capable of causing human or animal diseases, including viruses, bacteria, fungi, protozoa and helminthes. Infectious agents may be transmitted from host to another organism through the atmosphere (inhaling the infectious agent in droplets emitted by sneezing or coughing), body fluids (e.g. sexual contact), food and contaminated water, causing disease. Such diseases are a leading cause of death worldwide, particularly in low-income countries that suffer from limited access to centralized labs for diagnostics and treatments[1]. According to the World Health Organization (WHO), around 600 million illnesses and 420,000 deaths in 2010 were attributed to diseases associated with various pathogens, particularly in food products[2].

Despite immense advances in sensor technologies and in the field of molecular diagnostics, pathogen detection is one of the most important challenges in contemporary life science research[3, 4].Standard methods for pathogen detection. such as bacterial culture (Standard Plate Count)[5], polymerase chain reaction (PCR)[6, 7], immunological methods (Enzyme-Linked ImmunoSorbent Assay (ELISA))[8, 9], flow cytometry (FC)[10] and mass spectrometry analysis (MS) [11] have been widely used due to their high selectivity and high sensitivity. Bacterial culture methods involve incubation of specimens in growth media with varying nutrients and antibiotics and nowadays constitute the majority of conventional tests for bacteria detection. Pathogen identification is determined visually based on the distinct growth patterns observed. The plate-culture technique is relatively simple in construction and provides a snapshot of the number of bacteria in the original sample at the time that it was

collected. However, it does have a number of drawbacks. To begin with, plating techniques utilize a significant amount of material, are tedious, labour intensive, and take a long time to provide results (depending on the species and the medium, the time required may range from overnight, to days or even weeks)[12]. In addition they are limited by low positive rates, and are inefficient at differentiating bacteria at the level of strain or species[13]. The inherent limitations of culture-based detection methodologies have resulted in interest in developing alternate pathogen detection and quantification methods.

Molecular-based diagnostic techniques for infectious diseases (e.g. PCR, rolling circle amplification (RCA), loop-mediated isothermal amplification (LAMP)) have been proven to show selectivity and reliability [14] to good effect and compared to bacterial culture methods, they provide more accurate identification of microorganisms and significantly reduce diagnosis time (between 1and 4 hours). The main reason for this is that direct detection of target microbial DNA in clinical samples eliminates the need for cultivation, drastically reducing the time to result. However, such tests typically require highly specialized laboratories and increased costs with respect to reagents, equipment, dedicated space, personnel training and labour[15]. In addition, due to the fact that molecular-based amplification methods are highly sensitive, contamination of the sample may produce misleading results in detecting the appropriate sequence.

Since PCR requires bespoke equipment, trained personnel and specialized workflows, it is normally only performed in dedicated laboratories and hospitals in both developed and developing countries[16]. Point-of-care (POC) tests by definition are performed in out-of-lab environments[17], such as emergency departments, an ICU or even in the home. That said,

there is a strong demand for low-cost molecular-based diagnostic tests with improved sensitivities and shorter response times. Indeed, to guide the development of diagnostic devices for use in low resource settings, the WHO compiled the ASSURED criterion, stating that devices should be Affordable, Sensitive, Specific, User-friendly, Rapid and robust, Equipment free and Deliverable to those in need[18]. Considering this guideline, microfluidic technologies hold immense promise for realizing rapid and low-cost diagnostic devices for pathogen detection in low-resource settings.

Microfluidics is a technology set that manipulates fluids within channels having dimensions that typically range from hundreds of nanometers to hundreds of microns[19, 20]. A key aspect of the development of microfluidic or “Lab-on-a-chip" (LoC) technologies is to transfer processes or operations performed on the benchtop to planar-based microdevices. The most compelling features of microfluidic devices include the ability to process small volumes of fluid, enhanced analytical performance, reduced instrumental footprints, exceptionally high analytical throughput, facile integration of functional processes and the capacity to exploit atypical fluid behaviour to control chemical and biological entities in one single device[21]. Such features allow experiments to be performed with on small sample volumes and on short timescales; metrics which are particularly important for rapid diagnosis and act to reduce hospitalization times and the mortality rates associated with infectious diseases[22]. In addition, it should not be forgotten that microfluidic devices can be cheap to produce, especially with exploiting low-cost materials such as paper or thermoplastic polymers, which can be mass-produced via technologies such as injection moulding[23].

As mentioned, the ability to precisely handle sub-nL volumes of reagents is a key feature of microfluidic devices that can be leveraged for pathogen detection purposes. Single cell detection and counting techniques are important for detecting the complete presence or absence of pathogens when diagnosing diseases. Unsurprisingly, some novel techniques have been developed in recent years, including droplet-based microfluidic systems for the detection of single microbial cells[24]. More generally, a wide range species can be encapsulated in droplets to perform a variety of biochemical assays at high throughput[25]. Due to the aforementioned features, microfluidic devices can in principle provide for superior performance when compared to macroscale systems for pathogen detection and analysis. Accordingly, we now review recent development in high throughput microfluidics, including microflow cytometry, pathogen encapsulation and detection in droplets and droplet-based approaches for nucleic acid amplification including PCR and LAMP.

1.2. Microfluidic flow cytometry

Flow cytometry (FC) is the most widely used analytical technique for the rapid enumeration and detection of cells suspended in a stream of fluid. FC in its most basic embodiment defines the “one-by-one” measurement of cells as they pass through a detection volume, enabling the analysis of cells of interest through their optical (fluorescence emission or scattering) signatures. Such an analysis yields a signal during the time-of-passage that is proportional to a particular parameter of interest. This technique allows the study of physical (e.g. size), morphological (e.g. shape, internal complexity) and biochemical properties (e.g. cell cycle distribution and DNA content) of a cellular population at the individual level. Thus, it is a powerful tool for analyzing pathogens in a high-throughput, and quantitative manner[26].

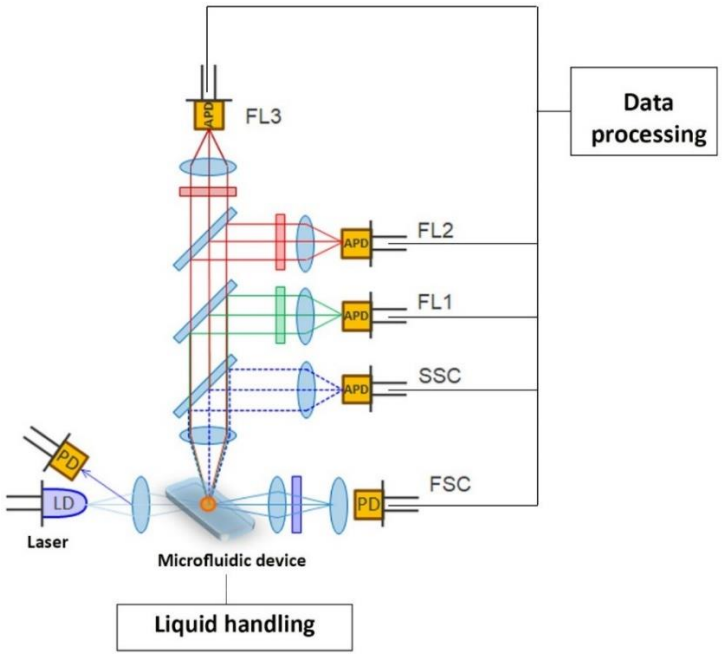

Figure 1.1. Schematic diagram of a flow cytometer composed of subsystems including microfluidic sample manipulation, excitation and detection modules and a data processing unit. FL: fluorescence SSC: side scatter, FSC: forward scatter, PD: photodiode, LD: laser

Although conventional FCM systems provide for rapid and reliable analytical capacities, they still are almost always bulky, expensive and mechanically complex. Moreover, operation normally requires highly trained personnel, multiple sample pre-treatment steps and the use of excessively high sample and reagent volumes. Indeed, one of the key reasons why the application of FCM in clinical microbiology is not widespread, is the lack of access to flow cytometry facilities. To this end, microfabricated cytometers integrating less expensive optical components are able to count cells in a rapid fashion and produce both sensitive and quantitative measurements at the single cell level. Indeed, such "microfluidic flow cytometers" provide a powerful tool for measuring the multiple properties of biological

samples. This emerging technology provides an opportunity to realize portable, accurate and sensitive diagnostic cytometers for pathogen detection (**Figure 1.1)**.

1.2.1. Liquid handling in microfluidic systems

Liquid handling is required to accomplish process such as sample delivery, sample loading, mixing, washing, and reagent disposal. In a conventional flow cytometer, sheath fluid and sample are delivered to the flow chamber via hydrodynamic pumping schemes. By using pressure or syringe pumps, a sheath flow is delivered at a high volumetric flow rate relative to the sample flow. This allows the sample stream to be hydrodynamically focused prior to detection, and ensures that cells are motivated in a single file manner. Since a uniform velocity through the interrogation volume is necessary for precise analysis, it is critical that the sample delivery method provides a pulse-free flow. Pulsatile flows result in varying transit times through the analysis volume, which reduces the measurement precision of the system[27].

Compared with conventional liquid handling systems, microfluidic systems allow the manipulation of small volume liquids with unprecedented control[28] and parallelism[29]. However, due to various fabrication and integration challenges, few handheld (self-contained) microfluidic systems capable of complex liquid handling exist on the market today; excluding capillary-driven microfluidics[30]. Most lab-on-a-chip systems still rely on bulky off-chip infrastructures such as pressure and syringe pumps to achieve their liquid manipulation functions, which severely limits the applicability of such systems for important applications such as PoC diagnostics or environmental monitoring. Other advantages of integrated liquid handling systems are the potential for modularity that ensures the system

can be integrated into other laboratory systems and protocols. An integrated liquid handling system is typically custom designed and/or built using off the-shelf components that are best suited to the smaller functions required. This includes the use of actuators such as pneumatic valves, solenoid valves, pressure sensors, flow sensors and data acquisition/control interface systems.

1.2.2. Microfluidic focusing techniques

One of the most critical aspects when developing a microfluidic flow cytometer is ensuring robust fluidics that will allow the efficient manipulation and positioning of cells in a flowing stream. Analysis of large numbers of single cells is achieved by utilizing the so-called "hydrodynamic focusing effect" inside micron-sized glass capillaries incorporated into the system. The sample stream, which contains the cells to be analyzed, is surrounded and squeezed by a sheath stream so that cells may be aligned in single file and pass through the optical detection volume one-by-one. Using this approach in a microfluidic system, cells can be focused in either two-dimensions (2D) or three-dimensions (3D)[31,32]. 3D focusing can be realized by fabricating multi-layer microfluidic devices, which confine cells in the vertical direction[33]. Other strategies have implemented multiple sheath flows to achieve 3D focusing of the sample stream[34]. The main drawbacks associated cell focusing in this way is the need for operation at high volumetric flow rates, with fluctuations in input flow-rates leading to disturbances in the focused sample stream, which may steer cells away from the detection plane. In addition, 3D focusing strategies require complex and costly fabrication procedures[35, 36].

Sheathless flow focusing methods, rely on a variety of forces, which may be externally imposed (termed as active focusing) or internally induced (termed as passive focusing). These forces have been demonstrated to directly manipulate particles for sheath-free focusing[37]. Passive focusing of cells relies on microfluidic architectures to cause vorticity and local disturbances in the flow in a passive manner. Inertial focusing of particles and cells provides an efficient and sheathless approach for controlling the position and spacing of cells, offering unique opportunities for the development of microfluidic flow cytometers[38]. Such passive manipulation of cells, without the use of external fields or sheath flows provides for uniform flow velocities and high-throughput single cell analysis[39,40], but it should be noted that the adoption of inertial focusing schemes necessitates operation at relatively high volumetric flow rates (**Figure 1.2 a**)[41]. Elasto-inertial focusing is an alternative passive cell manipulation technique[42,43], operating within a lower flow rate regime. Importantly, elasto-initial focusing is well suited for high resolution imaging FC since signal collection can be achieved using relatively long camera exposure times (**Figure 1.2 b**). Recent studies have demonstrated the utility of viscoelastic carrier fluids for enhanced elasto-inertial focusing of cells within straight, rectangular cross section microfluidic channels using low viscosity viscoelastic solutions[44].

3D particle focusing has also be achieved through the application of standing surface acoustic waves (SSAW) to particles and cells in flow, whereby pressure fields are used to drive species towards pressure nodes and antinodes[45]. Indeed, by carefully tuning the applied radio frequency signal, particles can be driven to the center of a microchannel[46]. An example of a SSAW-based system is shown in **Figure 1.2 c**, in which the interference of two identical surface acoustic waves is achieved using two parallel interdigital transducers (IDTs) on a

piezoelectric substrate[46]. However, it should be noted that such acoustofluidic methods rely on the application of an external force field, and thus require expensive, high speed electronics for operation. Dielectrophoresis (DEP)[47-49] is another active method for manipulation of cells. DEP focusing involves the translational motion of cells caused by forces exerted by a non-uniform electric field on electric dipoles. However, the strong dependence of the force on electrical conductivity of the medium and heat generation in conductive media, limits DEP as a universal approach for cell focusing. An example of DEP device for cell focusing is shown in **Figure 1.2 d**.

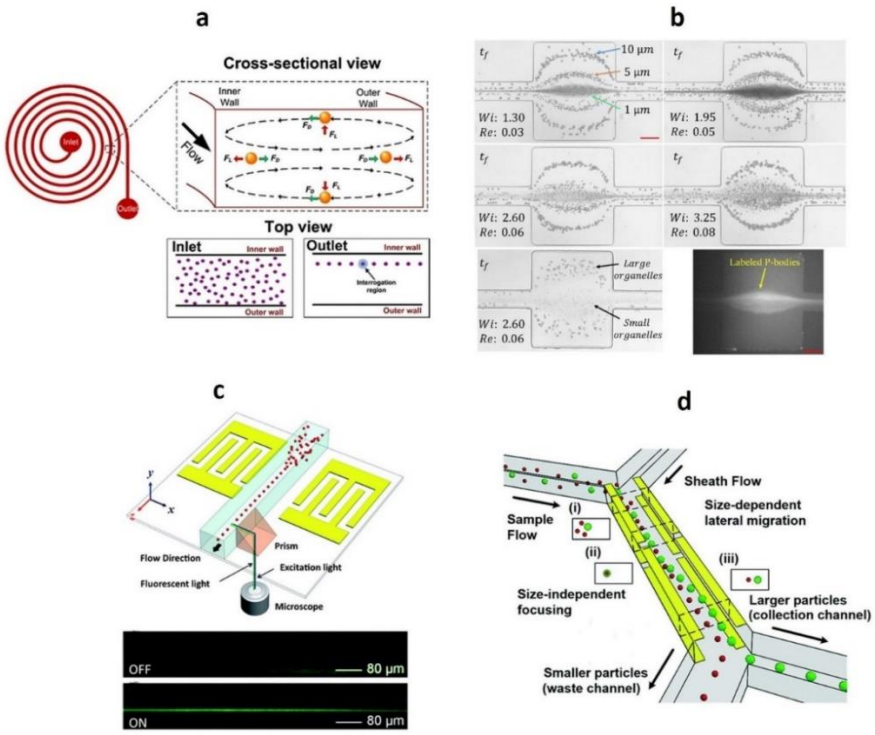

Figure 1.2. Microfluidic particle focusing strategies. (a) Schematic of microfluidic FCM, in which a spiral channel is used to create a Dean flow for high-throughput sheathless 3-D focusing[41].(b) Polystyrene microparticle and bioparticle focusing and separation using oscillatory viscoelastic microfluidics[50]. (c) Schematic of the experimental setup for focusing and side view images of

microparticle flows. The images show the side view fluorescence images of particles before and after the SSAW is generated[46]. (d) Schematic of continuous high-resolution dielectrophoresis-based cell sorting[49].

1.2.3. Pathogen detection in microflow cytometer

As noted, FC is a widely used tool to measure both physical and chemical characteristics of single cells. Unsurprisingly, this technology has multiple applications in life science research and diagnostics, including the rapid analysis of individual pathogen detection for food and water quality monitoring[51]. The technical demand in flow cytometry focuses on the detection and estimation of the concentration of pathogens of interest within clinical samples. An overview of the types of pathogen assayed using microfluidic cytometers is summarized in **Table 1.1**.

Table 1.1. Overview of the literature relating to the detection of pathogens using microfluidic FCM technology.

Microorganism	Approach	Volume processed	Time required	Limit of detection	Reference
F. tularensis *E. coli*	FC	Not reported	Not reported	≤0.99 μm size bacteria	Choi et al. [52]
Giardia lamblia	Smartphone based	10mL	1 hours	12 cysts per 10 mL	Koydemir et al.[53]
E. coli	μ-flow cytometer	Not reported	38 min	1×10^4 cells/mL	Golden et al.[54]
E. coli	FC	35 μL	45 mins	10^4 cells/mL	Yamaguchi et al.[55]
E. coli	Imaging cytometry	0.5 mL	10min	Not reported	Zordan et al.[56]
bacteria	Imaging cytometry	~200 μL	Not reported	500 ppm	Holzer et al.[44]
E. coli	μ-flow cytometry	Not reported	Not reported	10^6 cells/mL	Mu et al.[57]

E. coli	µ-flow cytometry	60µL	30 min	Not reported	Sakamoto et al.[58]
Marine bacterial	µ-flow cytometric	10 µL	19 min	Not reported	Gerdts et al.[59]
S. Typhimurium	nano-flow cytometer	100 µL	1.5 h	2×10^3 ells/mL	Mao et al.[60]
E. coli	nano-flow cytometer	200 µl	Not reported	1.0×10^2 cells/mL	Yang et al.[61]
Mixture of bacteria	nano-flow cytometer	40 mL	1h	$\sim10^2$ cells/mL	He et al. [62]
Diverse Bacteria	µ-flow cytometric	90 µL	Not reported	1×10^4 cells/mL	Shriver-Lake et al.[63]

While many microfluidic FC systems have been primarily designed to analyze mammalian cells, they have also been employed to quantify bacteria[58]. This is a difficult task since bacterial cells are typically 10-100 times smaller than mammalian cells, making them more difficult to confine to a single file. Consequently, there have also been efforts to develop cytometers specifically for bacterial cells. For example, Mao and co-workers developed a nano-flow cytometer for the rapid quantification of pathogenic *Salmonella Typhimurium (S. Typhimurium)* for use in food safety control[60]. Here the entire sampling process could be accomplished within 90 minutes, with a detection limit of 2×10^3 cells/mL and a specificity of 100% for *S. Typhimurium*. Such an approach could be readily applied to the simultaneous quantification of other pathogenic strains and bacteria through the use of specific surface binding antibodies. In addition, to detect weak bacterial autofluorescence a laboratory-built high-sensitivity flow cytometer has been shown to enable the individual analysis of nanoscale particles and quantify bacterial autofluorescence at the single-cell level [61]. Moreover, He and co-workers developed a label-free approach for total bacterial quantification in fruit juice. The detection method was based on the autofluorescence originated from small fluorophores in bacteria such as NADH and flavins. However such an

approach cannot provide accurate results, due to the large heterogeneity of bacterial autofluorescence within the same clone and also among strains[62].

To conclude, it is noted that whilst microfluidic flow cytometer devices have successfully incorporated miniaturized fluidic components, the miniaturization of the whole system, including the optical and signal acquisition units, requires additional fabrication procedures involving the construction of waveguides[42, 64].

1.3. Droplet-based microfluidic systems for pathogen encapsulation.

Droplet-based microfluidic systems have been considered as useful tools for high throughput screening. Low sample consumption, reduced reaction time, high throughput manipulation, fast mixing, and prevention of cross contamination at channel walls are just some of the benefits of droplet-based microfluidics[65, 66,67]. Droplets are ideal containers for biological materials, because they are encapsulated by an inert carrier fluid, which minimizes the opportunity for biomolecules to contact the channel walls and adsorb to device surfaces. Droplet-based microfluidic systems have also been widely used in cell-based assays. Indeed, several groups have encapsulated different types of cells (e.g. bacteria[68] and mammalian cells[69,70]) into microdroplets. One of the necessary key functions in exploiting droplet-based microfluidic systems for high throughput experimentation is the efficient encapsulation of single cells within individual droplets at high droplet generation rates. In the next paragraph we survey the most important droplet-based microfluidic platforms for pathogen detection.

For instance, An and co-workers presented a droplet-based microfluidic technique for encapsulating single Salmonella bacteria and their analysis after long term culturing[71].

(**Figure 1.3 a**). Here, the ratio of positive droplets (based on Poisson statistics) was used for quantitation, with a detection limit of 50 CFU/mL being achieved. Microbes are often encapsulated within microgel particles or droplets coated with extra protective layers in order to enhance their stability over time and during handling of emulsions. For example, Khater and co-workers used a microfluidic system to encapsulate microbes in agarose[72], assessing the impact of the capillary number, flow rate ratio of the dispersed to the continuous phase and agar concentration on the formation and size of droplets. This study provided guidelines for subsequent pathogen encapsulation studies aimed at high-throughput antibiotic susceptibility testing (**Figure 1.3 b**). In another study single-cell encapsulation of bacteria in droplets was combined with FACS for high-throughput screening applications[73] (**Figure 1.3 c**). Here, a droplet-based microfluidic device was used to encapsulate *E.* coli bacteria in agarose droplets. After incubation, monoclonal bacterial microcolonies containing phenotypically heterogeneous cells were FACS sorted to isolate members of a pBAD promoter library[74]. While most literature studies to date have focused on the encapsulation of single cells in microdroplets as a strategy to prevent crosstalk with neighbouring cells, Hondroulis and co-workers leveraged a droplet-based microfluidic approach to co-encapsulate polarized M1 and M2 macrophages with *E. coli bacteria,* through a passive merging scheme (**Figure 1.3 d**). The co-encapsulation of three types of cells into one droplet facilitated the monitoring of live-cell profiling of immune functions in situ and provided a quantitative analysis of macrophage heterogeneity[75].

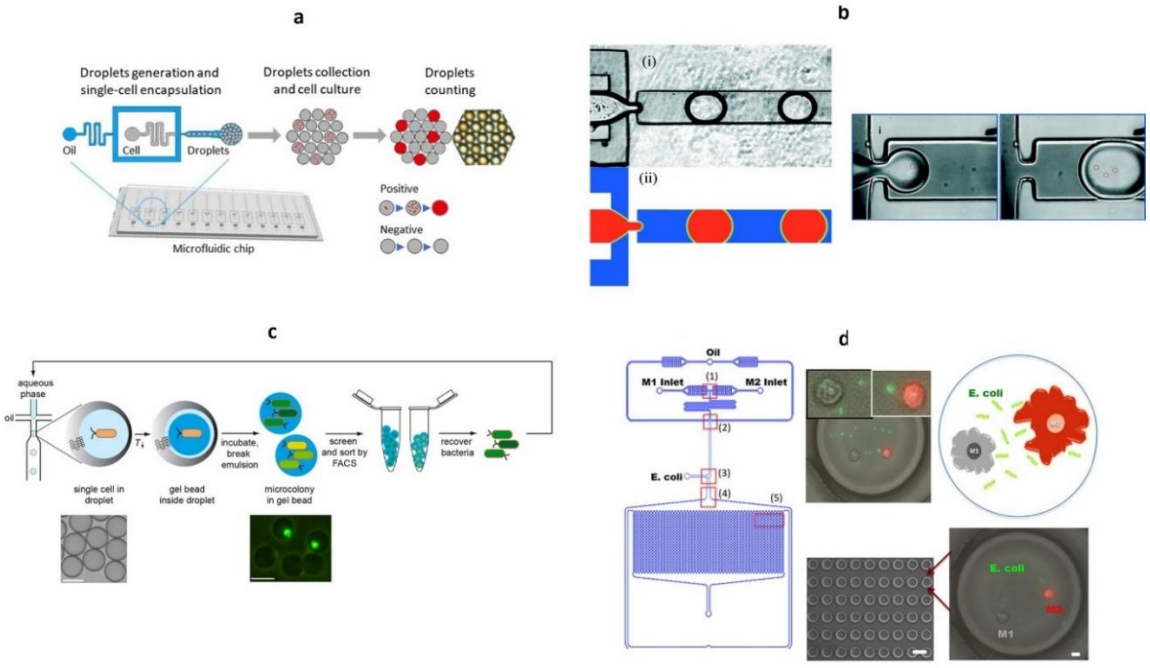

Figure 1.3. Droplet-based microfluidic platforms for pathogen detection (a) Schematic illustration of the detection of Salmonella based on a single-cell droplet-based microfluidic system. Quantification comprises three steps. (i) droplet generation and Salmonella single-cell encapsulation. (ii) droplet collection and cell culture. (iii) droplet counting based on the fluorescence presented by positive samples[71]. (b) Encapsulation and culture of bacteria in agarose droplets showing (i) images and (ii) numerical simulations of droplet generation in a flow-focusing approach[72]. (c) Overview of a screening method for single-cell encapsulation inside agarose droplets. Single cells are encapsulated into monodisperse water-in-oil emulsion droplets. The aqueous solution also contains agarose that gelates upon cooling, so that solid gel beads form inside droplets. During incubation of the emulsion, cells grow into monoclonal microcolonies inside the beads. The latter are recovered from the emulsion and sorted by FACS[73]. (d) Integrated microfluidic platform design. After droplet formation and merging, droplets are arrested in a docking array for monitoring interactions among macrophages and bacterial targets. The inset shows a droplet encapsulating *E. coli*, M1-WT, and M2-DS-Red-KI macrophages[75].

1.4. Nucleic acid amplification methods

1.4.1 PCR and digital PCR (dPCR)

Over the past decade researchers have begun to use nucleic acid amplification tests (NAATs) as versatile and rapid diagnostics, notably for infectious diseases. For instance, PCR has been recognized as the gold standard method to amplify a specific gene of interest for the detection of pathogens. Also methods including quantitative PCR (qPCR) and digital PCR (dPCR) systems[76] have been widely used for accurate quantification of nucleic acids with high precision.

Droplet-based microfluidic systems offer an outstanding technological platform for amplifying nucleic acids. In this regard, one the most compelling applications of droplet-based microfluidic systems has been digital droplet PCR (ddPCR), an extremely sensitive nucleic acid detection method, which operates at the single DNA copy level[77, 78]. In dPCR, the reaction mixture is compartmentalized uniformly into separate reaction chambers (governed by Poisson statistics), such that any reaction chamber will wither be empty or contain one target sequence. This is followed by the amplification process and subsequent real-time or endpoint detection (**Figure 1.4**). Since ddPCR is a digital method, dPCR allows for absolute quantification of the target DNA without the need for calibration standards.

The key difference between dPCR and qPCR lies in the way that amount of target sequence is quantified. In qPCR, the reaction is monitored throughout the whole amplification process and quantification is based on the analysis of a fluorescence signal during the exponential phase. The quantification of the target sequence in the sample is calculated by interpolation using a standard curve generated by a series of samples of known DNA

concentration, which are amplified together with the sample of unknown concentration. However, often this approach is imprecise since it requires the use of calibration standards with known concentrations. A standard curve is used to determine the efficiency, linear range, and reproducibility of a qPCR assay. In dPCR, once the reaction is finished, end point detection is performed and all compartments exhibiting increased fluorescence value can be assumed to have contained at least one DNA copy at the beginning. By counting the positive compartments, the number of DNA copies present in the original sample can be established without the need for calibration standards (as required in qPCR). This makes dPCR a precise method, especially at low target concentrations. Moreover, the fact that the analysis relies on an end point readout makes dPCR more resistant against inhibition than qPCR. Inhibition that slows down the reaction would therefore distort a qPCR measurement but is not relevant to dPCR as long as the reaction eventually yields a fluorescence signal above the threshold level.

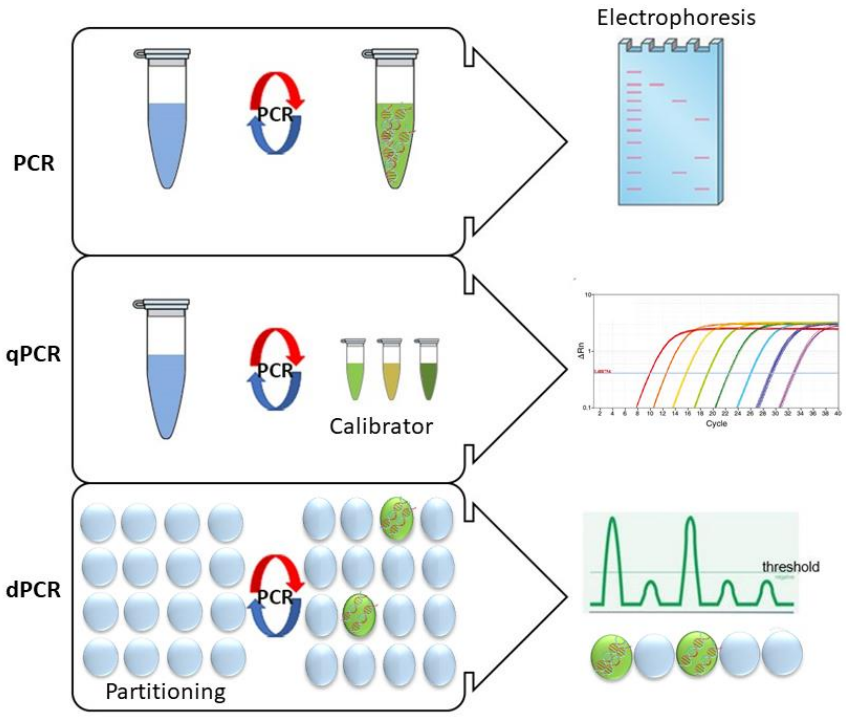

Figure 1.4. An overview of common PCR techniques. In conventional PCR, the amplification products are detected based using post-amplification gel electrophoresis. In qPCR, the amount of amplified DNA is measured at each cycle during the PCR reaction. In dPCR, the sample is partitioned into many compartments (in microwells, chambers, or droplets) such that each partition contains either one or no target sequences.

As mentioned previously, in dPCR the mix is separated into many aliquots (compartments) before the amplification begins. These compartments should be uniform in size (monodisperse) as the analysis procedure relies on the assumption that all compartments have the same volume. Apart from using droplets as containers, compartmentalization strategies can involve compartments with solid walls (e.g. as used by Fluidigm and Thermo Fisher) that are filled and then sealed mechanically (by valves or lids) or with immiscible fluids (such as oil[79]). For instance, the Naica system from Stilla Technologies uses a high throughput droplet generation approach, where the sample is flowed through a network of

microchannels and partitioned into a large array of individual droplets; a similar concept to step emulsification[80,81] (**Figure 1.5 a**). The microfluidic chip used in this system can accommodate up to eight samples, generating 14,000-16,000 droplets per sample. Interestingly, the Naica instrument has been used for SARS-CoV-2 detection[82,83] and demonstrated exceptional sensitivity and accuracy.

Droplet-based PCR methods require the use of biocompatible surfactants that maintain droplet stability at the elevated temperatures experienced during the thermocycling process.The issue of droplet instability at high temperatures can also be addressed by adopting a solid compartment approach to host many PCR reactions. Such an example is the high-density microwell array commercialized by Thermo Fisher (**Figure1.5 b**). This microarray contains 20,000 hexagonal wells, each one defining a 0.8–1 nL volume, and enables robust and high throughput sample partitioning. Twenty-four chips may be operated at one time, allowing thousands of data points to be analyzed per run. Compared to droplet dPCR, this method reduces the risk of cross-contamination that results from droplet merging. However, the production of the microfluidic devices involves a relatively complex procedure and a custom-built thermal cycler is also necessary to perform amplification. In a similar manner, Fluidigm recently launched a multilayer PDMS chip in which thousands of nL-volume chambers are separated by "microfluidic valves" (**Figure 1.5 c**)[79]. The chip integrates dynamic arrays of integrated fluidic circuits (IFCs), which contain thousands of interconnected channels and control valves that partition samples into approximately 800 reactions, with either 12 or 48 samples per chip.

Inkjet printing-based droplet generation for digital PCR [84, 85] allows for amplification and detection without any liquid transfer steps, thus avoiding cross-contamination and sample loss (**Figure 1.5 d**). Using inkjet printing, monodisperse droplets (800 pL) can be accurately generated and dispersed into a carrier oil phase, drastically simplifying the emulsification process.

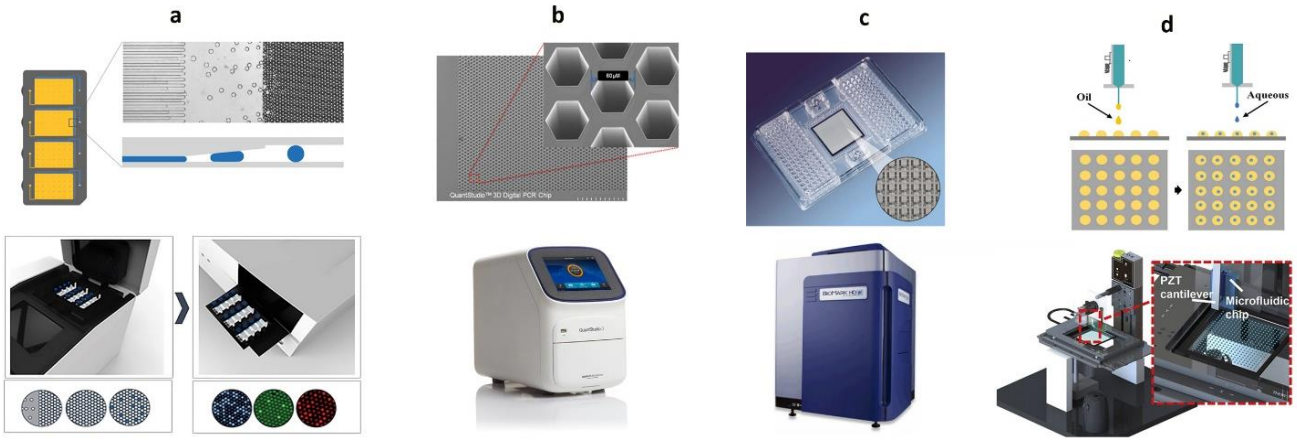

Figure 1.5. Overview of different partitioning technologies for dPCR. (a) The Naica droplet-based sample partitioning chip (Stilla, France). (b) The Digital PCR (20K) Chip comprises a microwell-based sample partitioning system (Thermo Fisher). (c) The channel-based sample partitioning system from Fluidigm [79]. (d) Inkjet printing-based sample partitioning[84, 85].

The past decade has shown how microfluidic techniques have transformed biomedical research, with digital PCR being an excellent example of a technology that has changed the way that biologists work (**Figure 1.5**). Today, many applications surrounding digital PCR are mounting. One of the main reasons for this increase is the fact that many dPCR devices have now been commercialized and thus reached wider accessibility since their use requires little knowledge of the involved microfluidic methods.

1.4.2. Isothermal amplification techniques

In addition to PCR, a number of nucleic acid amplification methods that operate at constant temperature have been developed. Since only one temperature is needed for the amplification, such methods are called “isothermal” amplification methods. Usually, double stranded DNA is separated by specific enzymes to allow primer annealing. A large variety of isothermal amplification methods are now available, with LAMP[86]and recombinase polymerase amplification (RPA)[87]being among the most frequently used[88].

For the purpose of quantifying DNA any amplification reaction can be used[89]. Indeed, isothermal methods such as droplet dRPA and droplet dLAMP are often less problematic than droplet dPCR with regard to droplet stability since the incubation temperature is lower and the incubation times shorter. Due to the fast analysis speed, dRPA and dLAMP are attractive candidates for the development of sample-to-digital-answer systems and highly desirable for potential PoC applications.

Over the past decade, significant effort has been put into refining isothermal techniques to overcome some of the limitation of PCR. In addition to LAMP and RPA, several other isothermal amplification techniques have also been developed including nucleic acid sequence-based amplification (NASBA), rolling circle amplification (RCA), strand displacement amplification (SDA), helicase dependent amplification (HDA) and single primer isothermal amplification (SPIA)[90]. However, in many cases primer design is more complex than for PCR, and there is a high degree of nonspecific amplification, which acts to raise background noise[91] Additionally, some isothermal methods require more enzyme than PCR, making them relatively costly[92].

1.4.2.1 Loop-mediated isothermal amplification (LAMP)

An isothermal amplification reaction that can be started (and maintained) by a thermal initiation step is advantageous in digital nucleic acid analysis. LAMP is an innovative gene amplification technology developed by Notomi and co-workers in 2000[64]. The target sequence is amplified at a constant temperature (between 60–65°C) using either two or three sets of primers and a *Bst* polymerase with a high strand displacement activity, thus eliminating the need for high-temperature DNA denaturation[93, 94]. Although LAMP is primarily applied for DNA amplification it can also be used for RNA if a reverse transcriptase is used[95]. LAMP uses four target-specific primers categorized as forward and backward inner primers (FIP and BIP) and forward and backward outer primers (F3 and B3) that anneal to unique sequences on the target gene (**Figure 1.6**). Loop forward and loop backward (LF and LB) are used to accelerate the reaction.

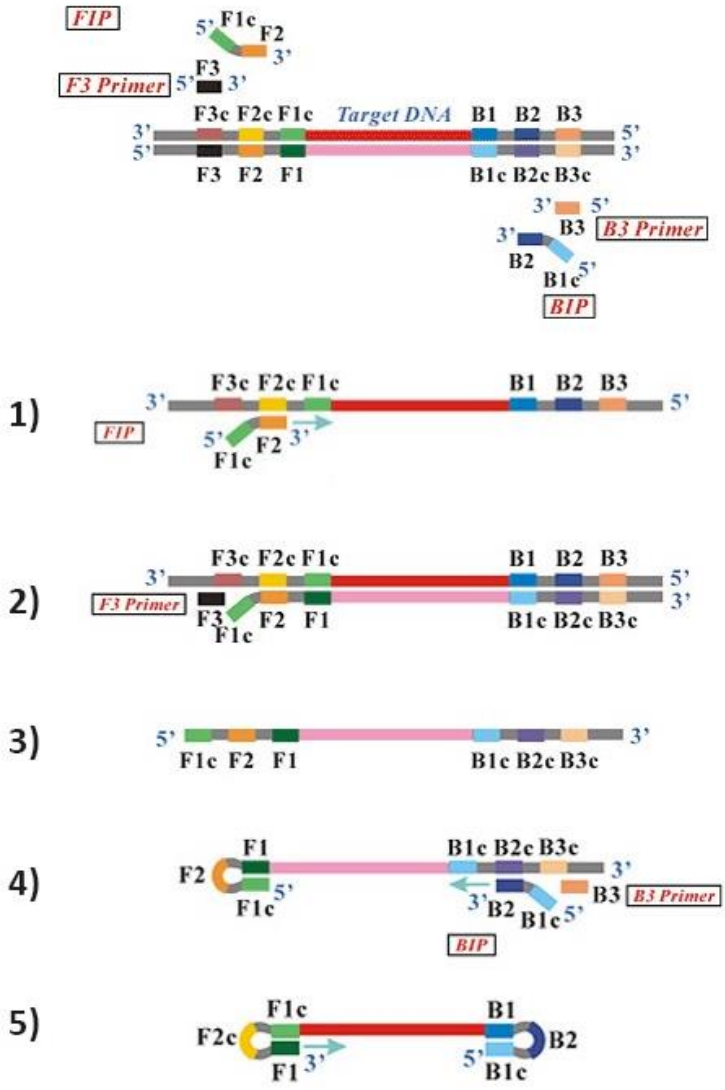

Figure 1.6. Schematic of the LAMP amplification technique. (1) The inner primer (FIP) binds to the single-stranded DNA followed by strand displacement and polymerization. (2) The binding of an outer primer (F3) take place followed by polymerization. (3) The newly synthesized strand displaces and forms a self-hybridizing loop structure. (4) The same process as described above is repeated on the opposite end of the target sequence through the binding of the inner primers (BIP) and (B3). (5) Short "dumbbell" loop structures are formed that can be amplified into dsDNA concatemers(Figure adopted from[96]).

As discussed, although PCR and LAMP are used for nucleic acid amplification they differ in many aspects. Some of these are listed in **Table 1.2**.

Table 1.2. LAMP vs PCR

	LAMP	**PCR**
Instrumental requirements	Isothermal (single temperature)	Requires temperature cycling
Specificity	Requires 6 primers	Requires 2 primers
Sensitivity	10 copies	10^1–10^2 copies
Instrumental requirements	Simple inexpensive instrument	Requires a thermocycler (heating and cooling)
Tolerance	Tolerant to sample matrix inhibitors	Sensitive to sample matrix inhibitors
Multiplexing capability	Difficult to multiplex	Can be multiplexed
Speed	Rapid, typically 30 minutes	Slow, >1 hour
Operation steps	Streamlined protocol (similar for all targets) with minimal steps	Varied protocols and run conditions (depending on target)
Amplification efficiency	10^6–10^9	10^7–10^{10}
Result evaluation	Amenable for visual detection, such as Turbidity or colorimetry	Not amenable for visual detection. High equipment requirements, such as electrophoresis and gel imaging system
Maturity of the Technology	New applications being explored	A well-established technique

LAMP amplification proceeds at moderate temperatures and is fast amplification, yielding 10^6–10^9 copies of target DNA within 30 to 60 minutes. This makes LAMP an interesting candidate for isothermal digital droplet amplification in POC platforms (e.g. paper-based

microfluidics, droplet microfluidics and digital microfluidics). Microfluidic dLAMP can compartmentalize LAMP mixtures into thousands of compartments, enabling nucleic acids to be quantified with the improved sensitivity and dynamic range of digital amplification methods. Unlike chamber-based microfluidic dLAMP, the droplet dLAMP technique compartmentalizes LAMP mixtures by emulsifying droplets inside the device via simple structures and avoiding the complicated fabrication of microwells. In addition, the compartment number can be adjusted on demand by simply varying the flow rate of the oil and aqueous phases; this ease of tunability typically leads to a larger number of compartments and hence enhanced detection sensitivity and dynamic range[89, 97]. In addition, compared to the microfluidic devices used in chamber-based dLAMP, compartmentalizing the LAMP reagents using oil enables higher heat transfer efficiency. With these advantages, droplet-based microfluidic dLAMP is gradually becoming a robust tool for nucleic acid quantification[98]. For example, Rane and co-workers developed an integrated droplet-based dLAMP platform that consisted of a single nozzle droplet generator, an incubation chamber and a fluorescence detection region (**Figure 1.7 a**). Such a system provided a high degree of integration and miniaturization for the detection of Neisseria gonorrhoeae with a LOD of 600 copies/μL[99]. However, droplet LAMP methods can suffer from droplets instability when droplets are densely packed at high temperature. To address this issue, Ma and co-workers developed a novel device capable of droplet generation, sorting droplets and executing LAMP across 240 trapped and separated droplets (each having a volume of 220 pL) over 40 minutes at 56°C (**Figure 1.7 b**)[100]. In this manner nucleic acids could be accurately quantified, with a dynamic range of 50 to 2.5×10^3 DNA copies per μL. Using this approach, droplets can be easily separated from each other in a spatially defined droplet array to eliminate droplet-

to-droplet coalescence during the reaction process. Another approach uses a Slip Chip, which consists of 1,280 cavities of 3 nL volume to perform digital droplet reverse transcription LAMP[101]. Such a system uses two glass plates with elongated cavities. The cavities on both plates are overlapping, so when the two plates are placed on top of each other with oil in between, they form channels that are connected to the inlets and outlets. These channels are filled with the LAMP solution and afterwards, the two glass plates are slid sideways over each other. The connectivity between the cavities is thereby lost, generating discrete compartments (**Figure 1.7 c**).

Microwell self-driven dLAMP has also been realized through the utilisation of capillary forces[102] in PDMS devices coated with a hydrophilic film, as shown in **Figure 1.7 d**. Due to the hydrophilic properties of such a device, a master mix solution was able to migrate through the microwells via capillary forces, where amplification of a gene-specific to a vancomycin-resistant Enterococcus strain was performed. This high-sensitivity, self-driven and portable microfluidic system yielded a limit of detection only 11 copies using only 30 μL of sample.

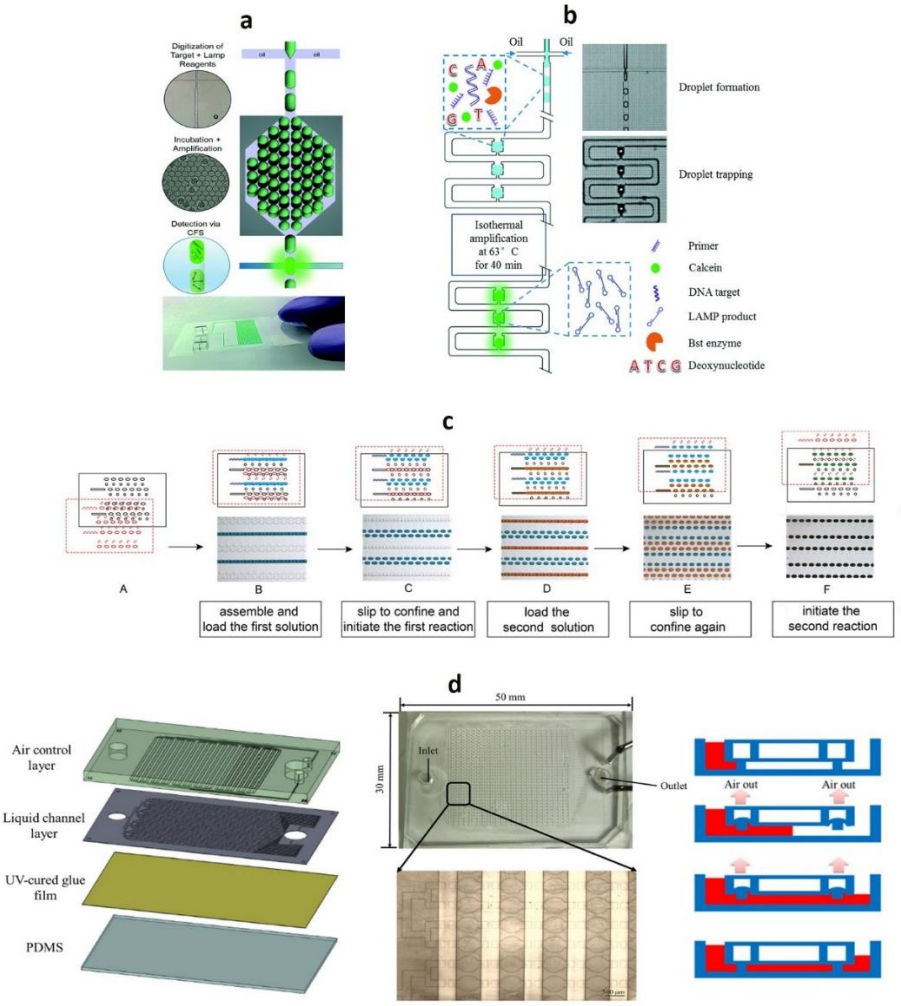

Figure 1.7. Microfluidic dLAMP devices. (a) A droplet-based microfluidic device for continuous flow digital LAMP, illustrating the three steps required for a complete analysis[99]. (b) A schematic illustration of the experimental workflow for digital LAMP in a droplet array[100]. (c) Schematic drawings and images showing the operation of a SlipChip for a two-step digital reverse transcription-loop-mediated isothermal amplification (dRT-LAMP)[101]. (d) Schematic illustration of the self-transportation microfluidic device , upon coating PDMS surface with a hydrophilic film that allows for digital LAMP to be performed in a simple and robust manner[102].

As is evident from the previous examples, droplet-based microfluidic dLAMP is a robust tool in nucleic acid quantification. However, there are still some disadvantages associated with droplet-based microfluidic dLAMP, which are linked to the massive number of droplets generated during each experiment. To this end, a high-throughput detection and analysis tool such as flow cytometry is often required. Nevertheless, owing to its instrumental simplicity, high specificity, and strong tolerance to inhibitors in the nucleic acid samples, LAMP within microfluidic systems is now regarded as a simple and accurate technique to quantify pathogenic nucleic acids (**Table 1.3**).

Table 1.3. Overview of LAMP methods for pathogen detection implemented in microfluidic devices.

Pathogen	Sample	Time required	Limit of detection	Amplification	Reference
Neisseria gonorrhoeae	Blood	110 min	~600 copies/μL	dLAMP	Rane at al.[99]
vancomycin-resistant Enterococcus (VRE)		30min	11 copies of the genome	dLAMP	Ma et al.[102]
ZIKA virus	oral samples	40min	5PFU	RT-LAMP	Song et al.[103]
HIV-1	Spiked saliva sample		10 HIV particles	RT-LAMP	Liu et al.[104]
Nervous necrosis virus (NNV)	Grouper larvae	1 h	10 fg of cDNA	RT-LAMP	Wang et al.[105]
Salmonella	milk	70min	1.7×10^2 CFU/mL	LAMP	Trinh et al.[106]
Pseudorabies virus (PRV)	Synthetic	1 h	10 fg DNA/ μL	LAMP	Fang et al.[107]
E. coli	serum	70 min	3 copies/μL	gLAMP	Chen et al.[108]
E. coli Salmonella spp Vibrio cholerae	chicken meat	60 min	3×10^{-5} ng/μL	LAMP	Seyed et al.[109]
Vibrio parahemolyticus	shrimp	60 min	1×10^3 CFU/mL	CMD-LAMP	Pang et al.[110]

VRE bacteria		40 min	one copy of DNA	dLAMP	Ma et al.[100]
Salmonella	milk	30min	5×10^5 CFU/mL	dLAMP	Azizi et al.[111]
Listeria monocytogenes, E. coli, Salmonella		60 min	10^5 CFU/mL	dLAMP	Duarte et al.[112]
Salmonella Typhimurium, Vibrio parahaemolyticus	water or milk	80 min	50 CFU	LAMP	Park et al.[113]
E. coli, Salmonella typhimurium, Vibrio parahaemolyticus	food samples	60min	500 copy level	LAMP	Seo et al.[114]
E. coli		60 min	15.2 copies/μL	centrifugal LAMP	Oh et al.[115]
Salmonella	food samples	70 min	5×10^{-3} ng/lL	LAMP	Sayad et al.[116]
Vibrio parahaemolyticus		60min	7.2 copies/μL	LAMP	Xia et al.[117]
Salmonella	food samples	62 min	2.5×10^{-3} ng/μL	LAMP	Uddin et al.[118]
Staphylococcus aureus		45 min	10 copies/1.45 μL	LAMP	Huang et al.[119]
SARS-CoV		20–25 min	a few target RNA	LAMP	Kim et al.[120]
MS2 virus	Wastewater sample	40 min	11 copies/μL	RT-LAMP	Lin et al.[121]
Zika Chikungunya Dengue viruses	blood	35min	$1.56e^5$ PFU/mL	RT-LAMP	Ganguli et al.[122]
HIV	blood	40min	10 fg/ μL	RT-LAMP	Safavieh et al.[123]
Zika virus	tap water, urine, plasma	15min	1 copy/μL	RT-LAMP LAMP	Kaarj et al.[124]

As shown in **Table 1.3**, a wide range of LAMP amplification applications have been realized within microfluidic devices. Interestingly, the dead volume for most of these systems is rarely reported, with most suffering from a low degree of integration and requiring multiple

manual handling steps. Indeed, normally the emulsification, amplification and readout steps are performed separately in different machines. Such low degrees of integration almost always leads to relatively high dead volumes, with much of the dispersed phase being lost in channels and tubing during the compartmentalization process. This can be problematic if only small amounts of the sample are available or if the sample is expensive. Accordingly, digital amplification systems are needed that are easy to use, involve few manual handling steps, possess small dead volumes and reliably produce large numbers of monodisperse compartments. To this end, a platform possessing these characteristics for the detection of pathogenic nucleic acid is described in Chapter 4.

1.5. Thesis overview

This thesis aims to develop robust and high-throughput microfluidic platforms integrated with existing technologies (such as FCM and nucleic acid amplification techniques) for highly sensitive pathogen detection. The thesis is divided into 5 chapters.

In **Chapter 1**, the field of pathogen detection has been introduced and general concepts relating to flow cytometry and droplet-based microfluidics for nucleic acid amplification summarized. This discussion was supplemented by a comparison of different methods for nucleic acid amplification.

Chapter 2 presents a novel sample preparation unit that when coupled to the optical module of a commercial flow cytometer is able to perform fully automated and high throughput analysis of microbial species in drinking and lake water samples. Specifically, the developed system is able to assay *E. coli* in water over a wide concentration range (between 10^3 and

10^6 cells/mL) and with a relative standard deviation of less than 6%. The utility of the platform as a valuable tool in the water treatment industry is further confirmed through the quantitative analysis of contaminated lake water samples on timescales less than 30 minutes.

Chapter 3 describes the engineering of a droplet-based microfluidic system leveraging step emulsification to generate and process droplets in a high throughput manner. As a proof-of-concept, the developed devices were used to generate either water-in-oil or oil-in-water emulsions and polyacrylamide (PAA) and PLGA microgel particles.

Chapter 4 describes the synthesis of PAA beads using a robust step-emulsification device. Such a system allows the rapid synthesis of large numbers of stable hydrogel microbeads, at a throughput of up to 15 mL/h. The microbeads are then used for particle-templated emulsification of LAMP reaction components, thus achieving micro-compartmentalization of the reaction. Such an assay is successful in detecting MRSA (methicillin-resistant Staphylococcus aureus) within 30 minutes, with a limit-of-detection of 1 fg/µL (10^3 copies/µL) and a linear range of 10^{-1} to 10^2 copies/µL ($R2 = 0.997$), with excellent selectivity and accuracy with respect to PCR-based methods (t-value $= 0.70$, $<$ t-critical $= 1.85$). The novel method enables the direct translation of technical advances in droplet-based microfluidics to the IVD field, whilst circumventing the need for costly and/or cumbersome instrumentation.

Chapter 5 presents the conclusions of the work presented in this thesis and a research outlook.

Chapter 2

Miniaturization of fluid sample preparation platform for automated flow cytometry

We present a novel sample preparation unit that when coupled to the optical module of a commercial flow cytometer is able to perform fully automated and high throughput analysis of microbial species in drinking and lake water samples. Specifically, the developed system is able to assay *E. coli* in water over a wide concentration range (between 10^3 and 10^6 cells/mL) and with a relative standard deviation of less than 6%. The utility of the platform as a valuable tool in the water treatment industry is further confirmed through the quantitative analysis of contaminated lake water samples on timescales less than 30 minutes.

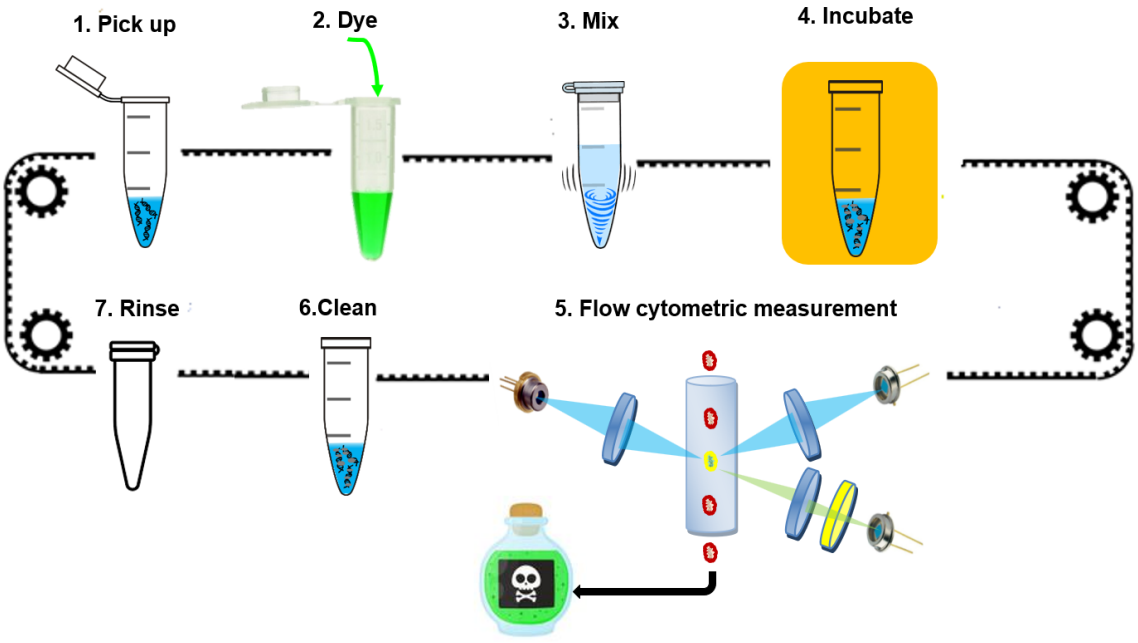

Introduction

2.1. Flow Cytometry-Based method for pathogen detection

The routine assessment of the microbiological quality of water is traditionally performed via the heterotrophic plate count (HPC) method, which involves quantification of heterotrophic bacteria cultured on semi-solid, nutrient rich media (such as agar) and under defined incubation conditions [125-127], Unfortunately, operational limits for HPC are highly regulated by drinking water legislation and vary from country to country. For example, in the USA, drinking water must have an HPC value of no more than 500 colonies/mL to ensure compliance with the National Primary Drinking Water Regulations (NPDWR)[128], whilst in countries such as Switzerland an HPC of no more than 20 colonies/mL is acceptable for treated drinking water[129]. Additionally, the UK and France recently replaced defined maximum values with guidelines stating that counting of bacterial colonies should not "show any sudden increase as well as no significant rising trend over time"[130]. Such a lack of global agreement on standard HPC values when assessing the general microbiological quality of water presents a significant global public health risk.

As an analytical method, HPC is time consuming and labour intensive, typically requiring between 2 to 7 days to complete[126].Additionally, only a small fraction of bacteria in drinking water are cultivable in HPC, making it difficult to assess the level of contamination caused by bacteria type[131,132]. Indeed, the biological information provided by HPC is normally unrepresentative of the entire bacterial community, and its utility in studying microbial dynamics in drinking water distribution systems remains questionable. More generally, since HPC methods are currently unable to quantify the abundance and composition of

bacteria in water, the definition of global HPC standards for water contamination is simply not possible[133-135].

Recent developments in microbial species analysis have highlighted the potential of optical microscopy[136], flow cytometry (FC)[137], next generation sequencing (NGS)[138,139]and other cultivation-independent methods for the detection and identification of pathogens[140]. For example, NGS can provide deep insights into microbial community composition (i.e. the microbiome)[141] and pathogen diagnostics, however its implementation in diverse out-of-lab settings is compromised by significant infrastructural requirements, bioinformatics challenges and the difficulties associated with detecting short sequence read lengths[142]. Put simply, further developments are required for quantification of various types bacteria in drinking water in out-of-laboratory settings.

Flow cytometric detection of (fluorescently-labelled) cells of interest is the gold-standard method for the quantification and characterization of various types bacteria in drinking water samples, due to its ability to precisely and rapidly detect total microbial cell counts[143-146], with fluorescent staining allowing for the direct differentiation of viable and non-viable cells. The use of FC in microbial analysis has been an important recent development in microbiological research[44,147], since multiple features and properties of tens of thousands of individuals cells can be measured within a few tens of seconds. Population statistics obtained from flow cytometry data may reveal important biological information, such as cell heterogeneity and the presence of distinct cellular sub-populations[147], which are inaccessible to HPC methods. Accordingly, FC can in principle be used as a high-throughput water monitoring technique, able to provide detailed insights about microbial dynamics within water distribution systems. Indeed, the potential benefits of fully automated, portable

FC platforms able to extract microbiological information in an online fashion are without doubt[148-151].To this end, we now describe the development and evaluation of a microfluidic sample preparation platform that performs automated fluorescent staining of bacteria within a portable flow cytometer. The integration of a microfluidic module for the preparation of fluorescently stained bacteria enables efficient, low-cost and automated sample pre-treatment, which in turn engenders operation in a range of out-of-laboratory environments. To evaluate the efficacy of the microfluidic platform as a sample treatment module for FC we assess the stability, accuracy and measurement range, through analysis of total cell count (TCC) in tap water samples contaminated with *E. coli* bacteria and unprocessed lake water samples. Such measurements confirm the first successful integration of a microfluidic sample preparation module with a commercial optical module for water monitoring.

2.2. Materials & Methods

2.2.1. Automated and miniaturized sample preparation platform

The microfluidic sample preparation platform was designed to conduct multiple unit operations, including sample filtering, reagent delivery, reagent mixing and reaction incubation. Specifically, the module consists of a bidirectional miniaturized syringe pump, a temperature-controlled heating element, a microfluidic device, a rotary valve driven by a stepper motor and an incubation chamber in contact with the valve (**Figure 2.1**).

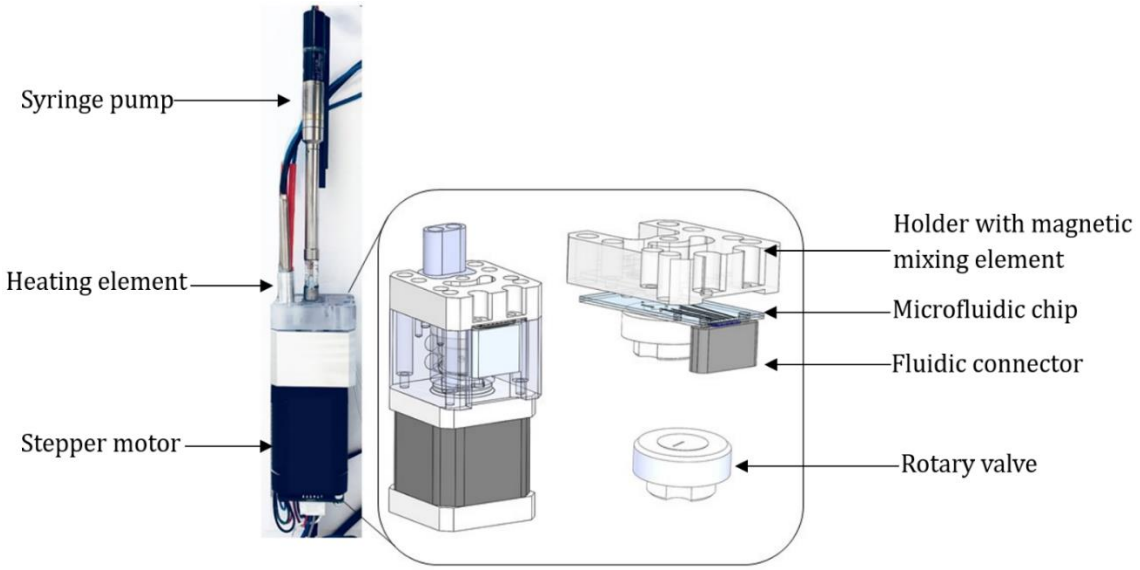

Figure 2.1. Photograph (right) and schematic (left) of the fluidic sample preparation unit. The entire unit has dimensions of 5 x 5 x 20 cm and comprises a bi-directional syringe pump, a microfluidic device, a rotary valve with an integrated active magnetic mixer and a heating element.

A miniaturized bi-directional syringe pump (SBP-100G-LL, Takasago, Nagoya, Japan) was used to load reagent into the microfluidic device and placed directly onto the rotary distribution valve. The rotary distribution valve comprises a central inlet port that connects to several outlet ports of the microfluidic device (**Figure 2.2**).

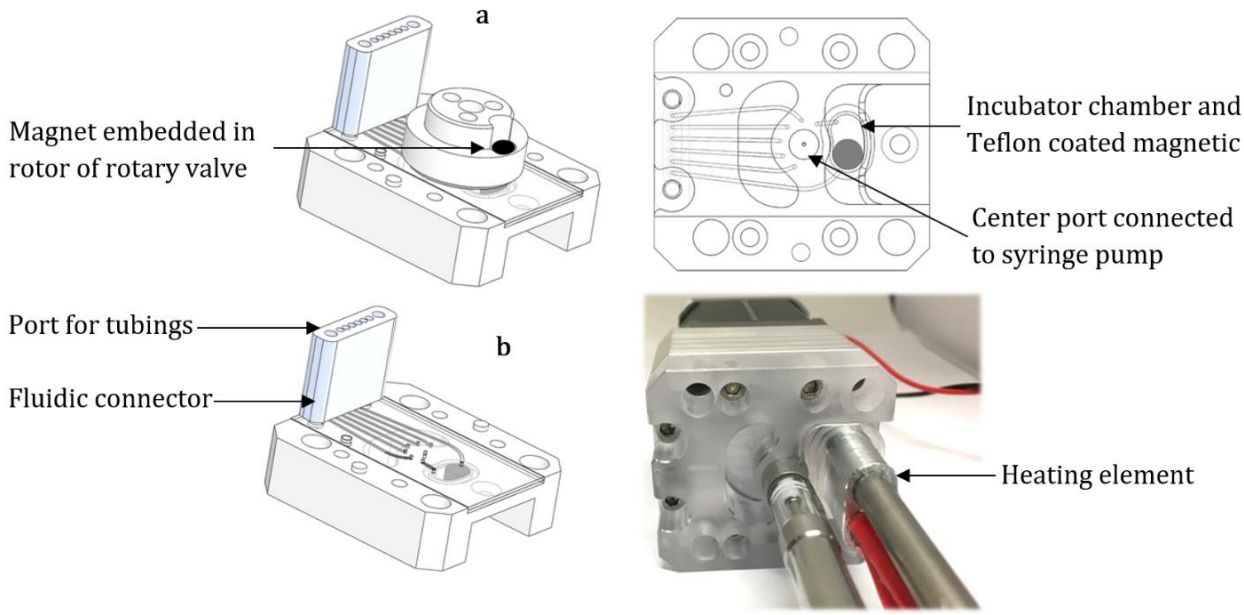

Figure 2.2. Schematic of the fluidic sample preparation unit. (a) Three-dimensional schematics of the rotary distribution valve and microfluidic device. (b) Top: Aerial view of the fluidic assembly, showing the microfluidic device, the chip holder and magnetic element. Bottom: Photograph of the assembled sample preparation module. All schematics are drawn to scale.

Significantly, the distribution valve serves both as a mixer and flow distributor (into the incubation chamber). When the stepper motor drives the rotary distribution valve, the Teflon coated magnetic element located within the incubation chamber was driven back and forth leading to efficient reagent mixing (**Figure 2.3**). A heating element located above the incubation chamber ensures maintenance of an optimal temperature of 39°C for bacterial staining.

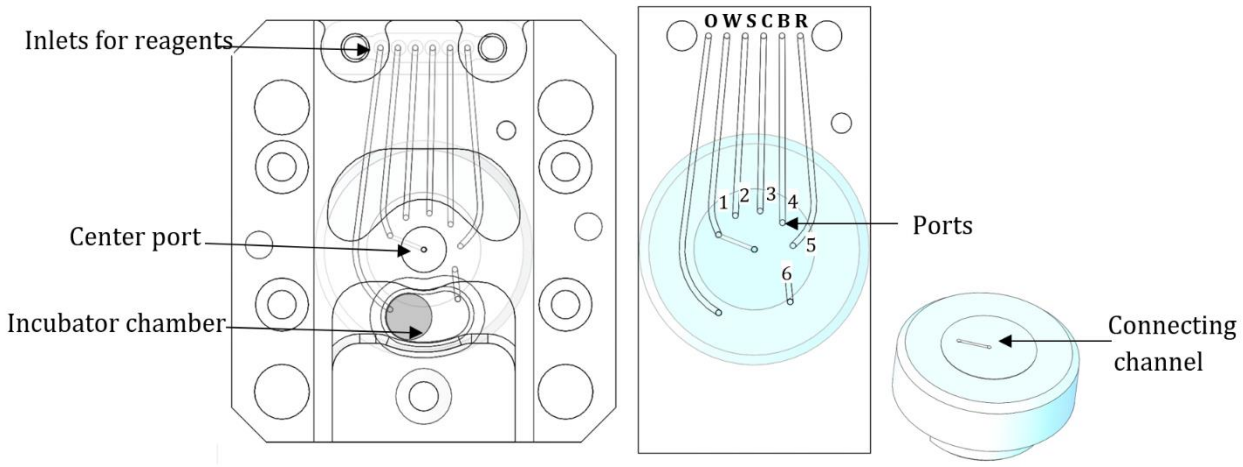

Figure 2.3. Detailed schematic of the microfluidic device. *W* is connected to the water sample reservoir, *S* is connected to the SYBER Green I reservoir, *C* is connected to the glass capillary in the optical module, *B* is connected to the bleach (cleaning solution) reservoir and *R* is connected to the rinse solution, *O* is connected to a hermetically sealed waste reservoir.

2.2.2. Microfluidic device fabrication

A 355 nm UV laser marking system (TruMark 5000, Trumpf, Barr, Switzerland), operating at a pulse repetition frequency of 100 kHz was used to ablate microchannels on the surface of borosilicate glass wafers (Borofloat 33, Schott AG, Switzerland). The ablation threshold for the material/wavelength combination was determined via empirical ablation models[152, 153]. After ablation, the glass substrates were sonicated in acetone and ethanol solutions, activated in a piranha solution (consisting of sulfuric acid and hydrogen peroxide in a 1:1 ratio), dried at room temperature for 6 hours and finally bonded in a bonder aligner (AWB 04 Wafer Bonder, AML, Didcot, UK) at 550°C for 30 minutes and at a pressure of 200N/cm^2. This resulted in a hermetically sealed glass device as shown in **Figure 2.4**. Additional technical details regarding the fabrication process are provided in **Table 2.1**.

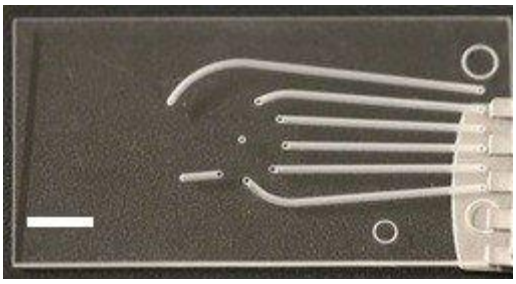

Figure 2.4. Photograph of the complete microfluidic device (scale bar 2mm).

Table 2.1: Overview of laser parameter values.

Laser source	TruMark 5000 (TRUMPF)
wavelength	355 (nm)
pulse duration	15 (ns)
focal length	101-160 (mm)
beam focus diameter	25 (µm)
repetition rate	100 (kHz)

2.2.3. Sampling procedure

As shown in **Figure 2.3**, the microfluidic device consists of a manifold containing several microchannels that connected to specific reagent reservoirs. Reagents were stored in sealed off-chip reservoirs and connected via PFA tubing (450HP, Zeus, Dublin, Ireland) to a 6-port custom-built aluminium fluidic connector, with water samples being initially filtered through a 36 µm pore nylon mesh (Thomas Scientific, New Jersey, United States). The sampling procedure comprises the following unit operations. First rotation of the rotary distribution valve to "position 1" allows 90 µL of pre-filtered water to be transferred from microchannel *W* and stored in the syringe reservoir. The valve was then rotated sequentially to "position 2" to collect 10 µL of dye solution from microchannel *S*, and then to "position 6"

to inject 100 µL of sample from the syringe pump reservoir into the incubator chamber. When the incubation chamber was filled with sample and dye solution, efficient mixing was achieved (as described) through rotation of the magnetic element, with sample subsequently being incubated for 10 minutes at 39°C. Next, the sample was aspirated from "position 6" and injected at a flow rate (20µL/min) into the flow cytometer capillary via microchannel *C*. After use, cleaning reagent (a mixture of 5% bleach and 1% of carbonate-bicarbonate buffer in ultra-pure water) was injected into the incubator to remove any sample residue prior to further use. The same procedure was used to rinse the incubation chamber and FC capillary via microchannel *R*. Finally, microchannel *O* was connected to atmosphere to remove any residual air bubbles inside the incubation chamber. All preparation steps involving light sensitive materials (e.g., fluorescence labelling) were performed in a light protective case.

2.2.4. Staining protocol

Water samples were stained according to a standardized protocol for water analysis[154, 155].Briefly, pre-filtered water samples were stained with 10 µL of dye solution and incubated in the dark for 15 minutes at 39˚C (± 2°C). The dye solution comprising SYBR Green I (Invitrogen, Basel, Switzerland) in DMSO was diluted in pre-filtered (10 mM, pH 8) sterile Tris-EDTA buffer (Sigma Aldrich, Buchs, Switzerland) to a final concentration relative to the stock solution of 1:10,000.

2.2.5. Flow cytometry measurements

Flow cytometry experiments were performed using the optical unit of a Bactosense flow cytometer (bNovate, Ecublens, Switzerland), equipped with a laser diode emitting at a 488 nm and two photodiodes. Fluorescence emission originating from flowing bacteria (at 20

µL/min) was detected at two wavelengths: 520 nm (using a 525/45 bandpass filter) and 715 nm (using a 715 LP longpass filter) (Chroma Technology Corporation, Bellows Falls, USA). Side scatter signals were detected using a 488/10 bandpass filter. The performance of the flow cytometer was evaluated prior to each experiment using a NFPPS-52-4K Nano Fluorescent Size Standard Kit (Spherotech, Zug, Switzerland), as illustrated in **Figure 2.5**. This contains four types of polymer microspheres, with average diameters of 0.1-0.3 µm, 0.4-0.6 µm, 0.7-0.9 µm and 1.0-1.9 µm. 25 µL of each bead suspension was mixed with 1900 µL of ultrapure water (Sigma Aldrich, Buchs, Switzerland) and flow cytometry analysis performed on 50 µL of the mixture. **Figure 2.5** clearly verified flow cytometer's ability to distinguish small beads from instrument noise and debris. These polymer microspheres can also be used to evaluate the laser fluctuation or obstructions in the flow cell.

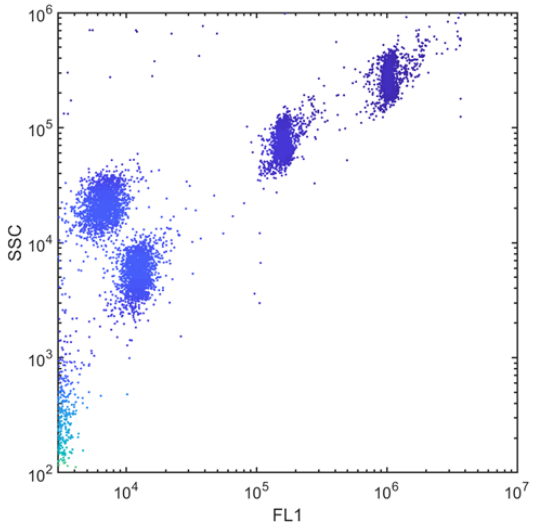

Figure 2.5. Flow cytometric analysis of Nano Fluorescent Size Standard Kit beads, visualized by their normalized log-transformed signals in the side scatter and green (520 nm) fluorescence channels.

Data acquisition and analysis were enabled through custom software written in LabVIEW (National Instruments, Baden, Switzerland). Flow cytometric parameters (FL1, FL2 and SSC) were collected and automatically stored as FCS data files. Collected FCS data files were then analysed using in-house Matlab code (MathWorks, Novi, USA). Appropriate gating values were used to separate bacteria from background signals and to distinguish between high nucleic acid content (HNA) and low nucleic acid content (LNA) bacteria, as described previously[i] and as shown in **Figure 2.6**.

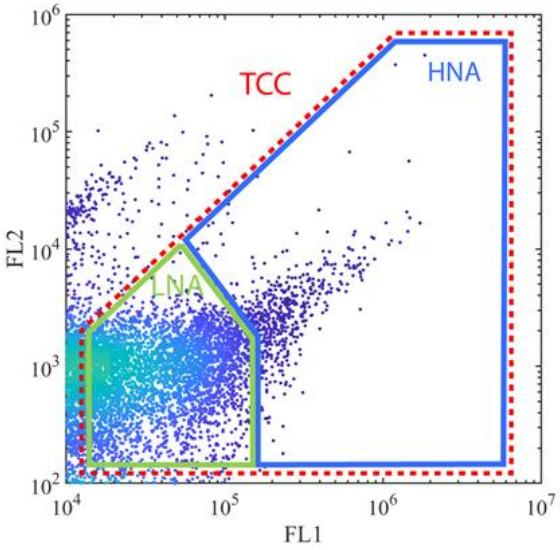

Figure 2.6. Two-dimensional scatter plots of FL2 as a function of FL1 for a representative tap water sample. Gating within the scatter plot delineates small (LNA, green area) and large (HNA, blue area) sized bacteria and TCC (red dotted area).

The complete flow cytometry platform, including both the sample preparation and optical module are shown in **Figure 2.7**.

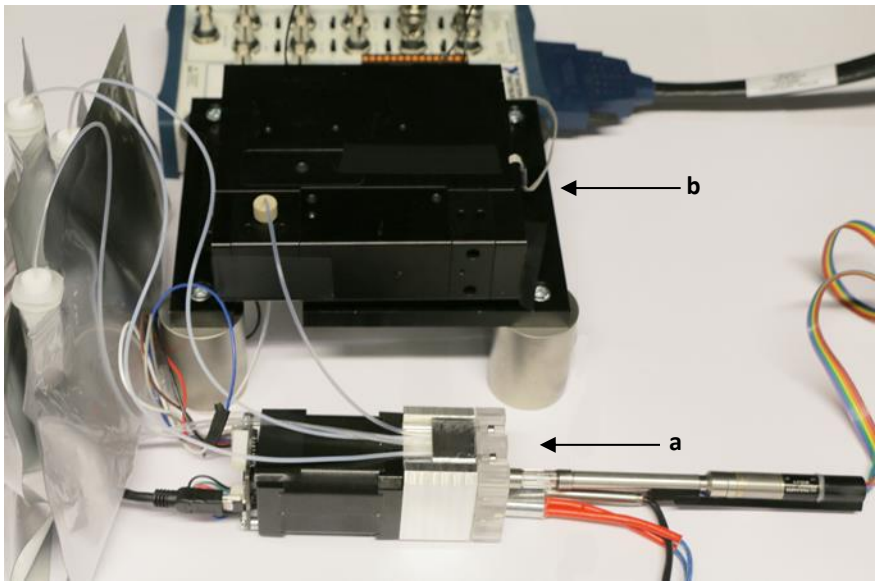

Figure 2.7. Image of the complete flow cytometer assembly. (a) The sample preparation unit (b) is connected to the bNovate optical module.

2.2.6. Monitoring bacterial contamination

E. coli BioBalls (bioMérieux, Marcy l´Etoile, France) were initially used to artificially contaminate water samples, due to the fact that they contain a precise number of viable bacteria with a known number of colony forming units (CFU); here 2×10^6 CFU/mL. Specifically, a 60 mL glass reactor was used as a bioreactor (in a wash-in/wash-out/mixing mode) and continuously fed with tap water (pH = 8.1, chlorine = 0 mg/L). **Figure 2.8** presents a schematic of the system.

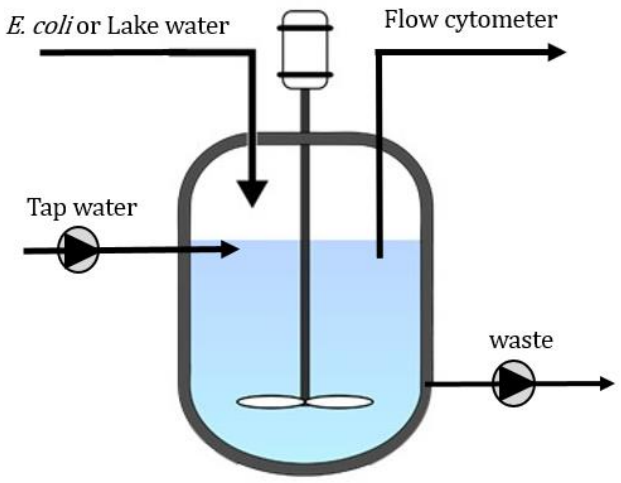

Figure 2.8. Schematic of the wash-in, wash-out and mixing reactor used for the detection of microbial contamination using FC. The setup included a stirred glass reactor, A peristaltic Pump (BT100-1L, Darwin Microfluidics, Paris, France) was used for wash-in and wash-out and spiking experiment.

Baseline FC measurements were acquired every 5 minutes for a period of 30 minutes by manual sampling. Subsequently, the sample flow was terminated and 1.1 mL of an *E. coli* BioBall solution (2×10^6 CFU/mL) added to the reactor over a period of 1 minute, simulating a sudden contamination event. The reactor contents were then mixed for a period of 20 minutes (with 100 mL volume samples being analysed by FC every five minutes). Next, the water flow was re-established, with fresh tap water being delivered at a rate of 5 mL/min, allowing *E. coli* to be washed from the reactor. Again, 100 mL volume water samples were withdrawn every 5 minutes and analysed by FC, to extract TCC and the percentage of HNA cells as quantitative indicators of microbial contamination. The entire measurement sequence was repeated three times. A second set of experiments was performed in an identical manner, except with the *E. coli* BioBall solution being replaced by 8 mL water sourced from Lake Lucerne (Switzerland).

2.3. Results & Discussion

2.3.1. Assessment of dynamic range

Any flow cytometry workflow for water quality monitoring must be able to accurately quantify a broad range of bacterial concentrations[156-158].To this end, the performance of the optical and integrated fluidic sample preparation module was initially assessed by analysing four different dilutions of the *E. coli* Bioball sample. The previously described staining protocol and gating strategy were used in all experiments. *E. coli* concentrations ranged from $3x10^3$ to $3x10^6$ cells/mL, with each sample being analysed six times over a period 90 minutes. As shown in **Figure 2.9**, bacterial concentrations could be assayed in a precise and accurate manner over the entire concentration range, with RSD values varying between 6% (for the $3x10^3$ cells/mL sample) and 5% for (for the $3x10^6$ cells/mL sample).

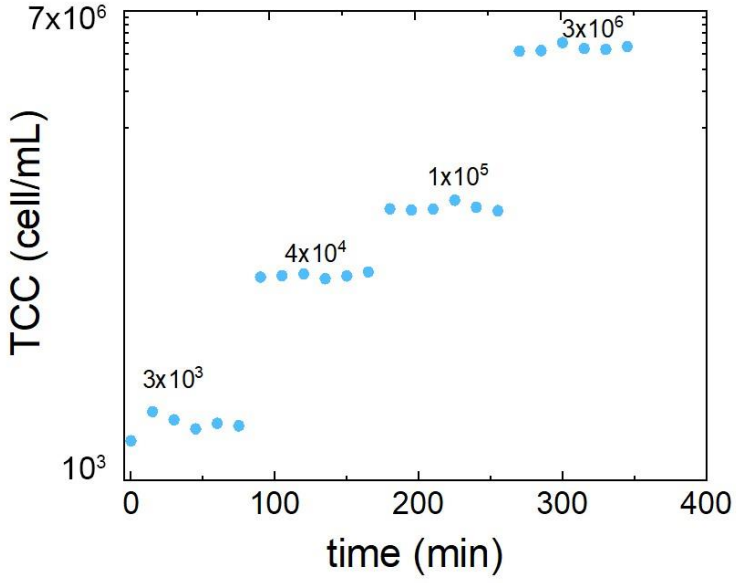

Figure 2.9. The cell concentration values for TCC over time for 6 sequential measurements (blue circles) of four different concentrations of an *E. coli* BioBall sample.

It should be noted that in general, bacterial concentrations will vary as a function of water quality. For example, clean ground water can contain as little as a 10^3–10^4 cells/mL[159],whilst lake water is typically characterized by concentrations in excess of a few million cells/mL[160, 161].Moreover, an increase in both total cell count (TCC) and HNA can be used as a robust indicator of bacterial contamination.

2.3.2. Monitoring bacterial contamination

The degree of water contamination is ideally assessed by quantifying changes in both the TCC and the percentage of HNA cells. **Figure 2.10** presents the continuous analysis of a drinking water sample spiked with a 1.1 mL of *E. coli* (at 2×10^6 CFU/mL) in a flow-through reactor, as described previously. After spiking *E. coli* bacteria, the cell concentrations reached an average maximum of $1.3x10^6$ cells/mL, with the percentage of the HNA cells increasing to an average maximum of 80.7%. The substantial increase in both HNA content bacteria and TCC can be immediately seen in the two-dimensional density plots of FL2 as a function of FL1 (**Figure 2.10 c and d; Supplementary Movie 2**).

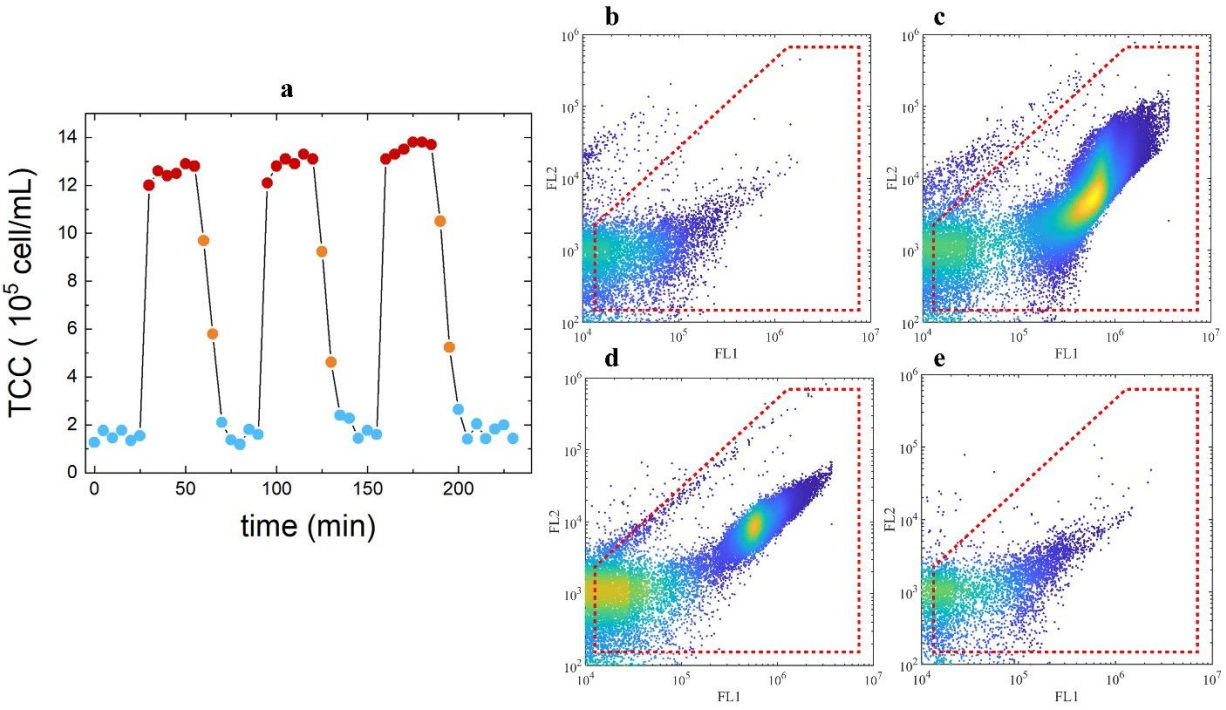

Figure 2.10. Continuous analysis of water contamination by *E.coli* bacteria. (a) TCC measurements of three *E. coli* bacterial contamination experiments. (b)-(e) FL2 vs FL1 scatter plots showing the amount of bacteria at different stages of the experiment: (b) tap water sample, (c) *E coli* contaminated sample, (d) a partially washed contaminated sample and (e) return to tap water.

Analysis of tap water samples spiked with lake water (**Figure 2.11**) shows the same trend as in the case of **Figure 2.11 a** demonstrating the efficacy of our approach to detect low levels of contamination in a "real natural contaminant" sample from Lake water. This is highly relevant in the case of a small volume of concentrated contamination when mixed with a larger volume of drinking water due to backflow or cross-connections in pipelines. Indeed, the sensitivity and high temporal resolution of our approach can be adopted for the detection of small water contamination levels in water pipping systems.

A strong inorganic or/and organic component of lake water typically contributes to this background signal shown with black gate in the density plots of FL2 vs FL1 in **Figure 2.11 c**.

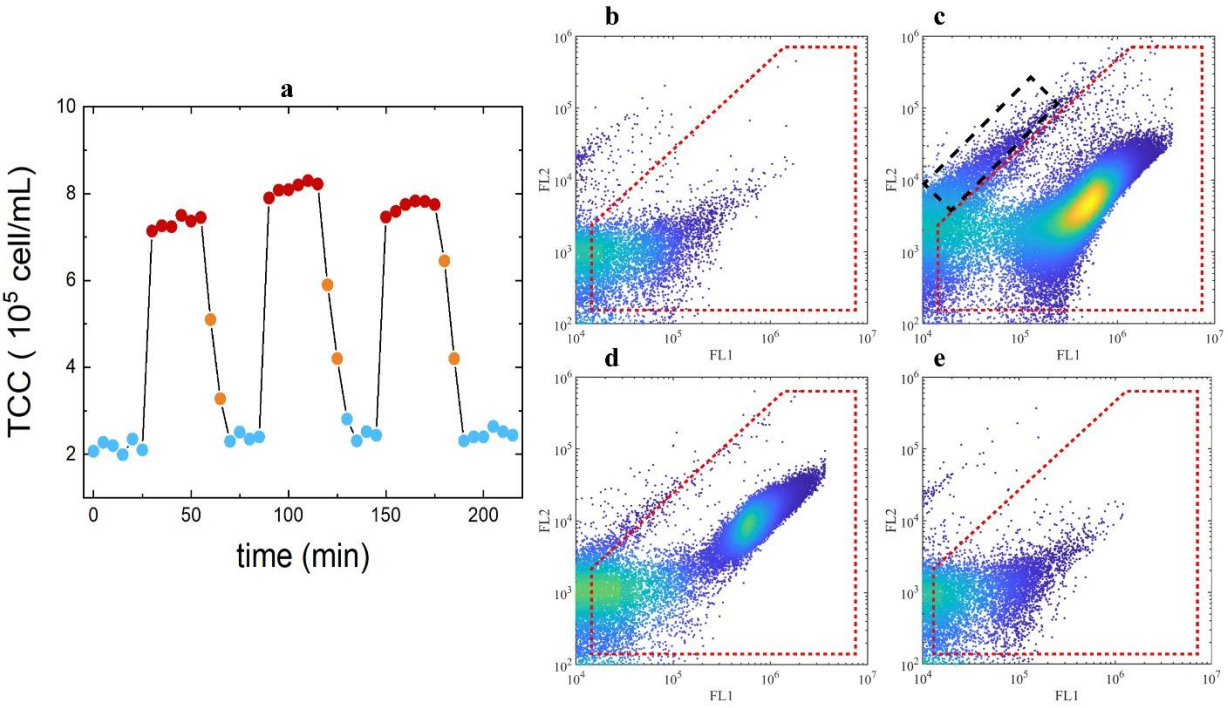

Figure 2.11. Continuous analysis of water contamination by lake water. (a) TCC measurements of three lake water contamination experiments. (b)-(e) FL2 vs FL1 scatter plots showing the amount of bacteria at different stages of the experiment:(b) tap water sample, (c) lake water contaminated sample, (d) a partially washed contaminated sample and (e) return to tap water.

2.4. Conclusions

Herein, we have presented a fully automated and miniaturized sample preparation module, which engendered the development of a low-cost and portable flow cytometer for the analysis of microbial properties of drinking water. The developed microfluidic device has a dead volume of only 20 μL which originates from the need to avoid cross-contamination. The module allows analysis of sample volumes as low as 100 μL, with the waste generated from each complete measurement being less than 500μL. This contrasts with commercially available flow cytometers, where minimum sample volumes are typically above 1mL, with several mLs of waste being generated per measurement, due to the use of sheath fluids. In

addition, the compact and fully enclosed design of the module obviates the contamination risks associated with manual sample preparation. The integrated distribution valve in conjunction with the microfluidic device provides for rapid and contamination-free switching between different fluidic reservoirs, which is essential for the sample preparation when monitoring microbial drinking water quality. Combining both fluid distribution and reagent mixing within a single microfluidic device affords several benefits. These include, significantly reduced manufacturing costs, reduced system complexity and lower power consumption. In contrast to passive mixing schemes, the use of an active (magnetically actuated) mixer enables rapid mixing, even when using high-volume ratios between the reagent and the water sample. Importantly, the developed workflow can be extended to the detection of pathogenic organisms (such as *Legionella pneumophila* and *Salmonella),* or integrated with warning systems and automatic disinfection actions to address sudden contamination events[162].

To conclude, we have developed a novel microfluidic sample preparation module that allows for the automated flow cytometric analysis of bacterial populations in drinking water. The analytical method involves reproducible staining and analysis of bacteria with a common nucleic acid stain to obtain the TCC values over a wide concentration range and provides for quantitative tracking of contamination events on short timescales.

Appendix A. Supplementary data

A patent application for Microfluidic distribution valve has been filed (WO2020035366).

A patent application for fluid dosing system has been filed (EP 3751241A1)[163].

Chapter 3.

High-Throughput droplet generation using a step emulsification device

The ability to perform laboratory processes on small scales using miniaturized devices provides numerous benefits for the experimentalist, including vastly reduced reagent and waste volumes, enhanced analytical performance, system portability and improved assay control. Most common laboratory operations involve sample and reagents components in the condensed phase and as a result, process miniaturization can be accomplished via the use of water-in-oil droplets. Such droplet-based microfluidic systems allow for assays to be performed in a high-throughput and high-information content manner. In this chapter, we describe important technical aspects related to the engineering of droplet-based microfluidic systems, and present a novel step emulsification device that is adept at generating and processing droplets in a high throughput manner.

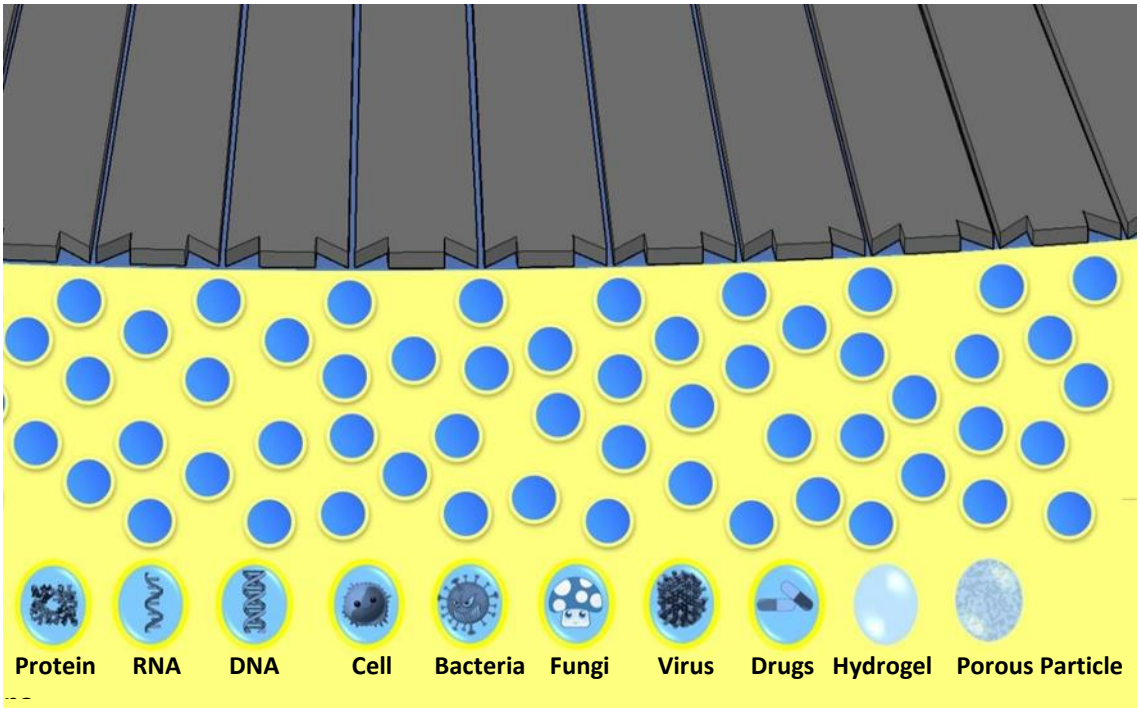

Chapter 3 - Introduction

3.1. Droplets: small, uniform, and high throughput

In recent years, microfluidic technologies have emerged as powerful high throughput platforms for performing a variety of chemical and biological experiments. Microfluidic systems are able to process small volumes of fluid using channels and features with characteristic dimensions that range from hundreds of nanometers to hundreds of microns[164]. Such systems offer numerous advantages over conventional analytical instrumentation, including rapid analysis times, superior analytical performance, reduced sample/reagent consumption, compact instrumental footprints, portability and the facile integration of functional components[65].

Droplet-based microfluidic devices are increasingly used in biological research since bioassays can be performed in a rapid, controlled and efficient manner[165]. Such devices utilize flow instabilities between immiscible fluids in microfluidic channels to most commonly create monodisperse water-in-oil (w/o) microdroplets. To prevent droplets from coalescing and minimize molecular transport between droplets, surfactants are normally added to the continuous phase to stabilize the oil-droplet interface. These molecules consist of hydrophobic and hydrophilic groups, and are chosen to be compatible with the chemical nature of both the discrete phase and the carrier oil. In this way, droplet-based microfluidic systems offer precise control over droplet size, droplet payload, whilst ensuring minimal cross-contamination and sample loss over the timescale of the experiment[19, 166].

Droplet-based microfluidic platforms are ideally suited to performing a range of biological studies. For example, droplets with pL volumes provide ideal environments for single cell

studies, where single (or small numbers) of cells may be encapsulated and subsequently processed in rapid and controllable manner[167, 168]. In addition, droplet-based microfluidic platforms enable chemical and biochemical assays to be processed in a high-throughput manner, enabling a range of large-scale applications especially in the pharmaceutical, chemical and biotechnology industries[169, 170].

At a basic level, emulsions are metastable colloids containing a minimum two immiscible fluids. One of these fluids is dispersed in the other by applying a shear force, in the presence of a surfactant. As noted, aqueous droplets formed within an oil-based carrier fluid are termed water-in-oil emulsions (w/o), whilst oil-in-water (o/w) emulsions are produced when the aqueous fluid acts as the continuous phase (**Figure 3.1 a, b)**. Higher-order emulsions, where multiple droplets are contained inside a larger droplet, can also be formed in a direct manner and are commonly termed multiple emulsions. Double emulsions, the most common multiple emulsion, consist of a water-based core surrounded by an oil shell (stabilized by a surfactant) and a water outer phase. Such a structure is shown schematically in **Figure 3.1 c**. Double emulsions have shown significant utility in many consumer applications; most notably in the food, cosmetic, agriculture, and pharmaceutical industries[171].

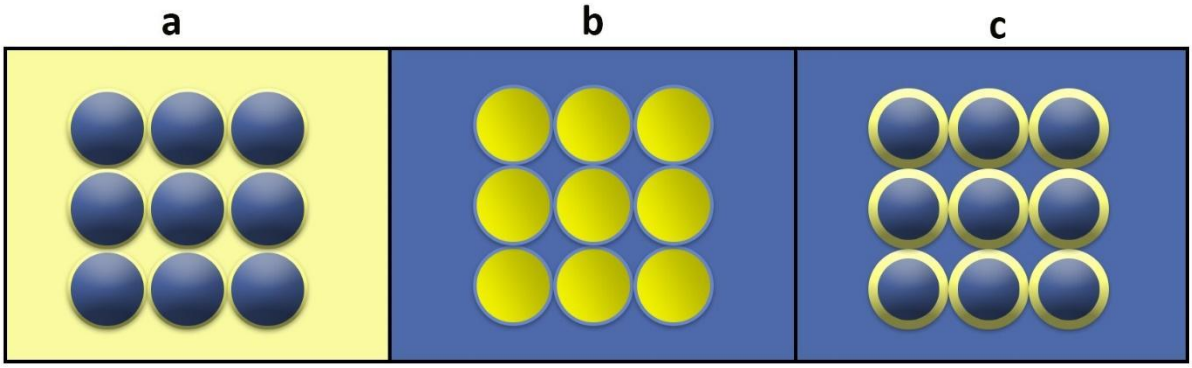

Figure 3.1. Schematic illustration of different types of emulsions. (a) a water-in-oil emulsion (w/o), (b) an oil-in-water emulsion (o/w) and (c) a water-in-oil-in-water (w/o/w) double emulsion.

Emulsions can be produced using a variety of techniques, such as agitation or mechanical mixing using rotor-stator systems[172, 173]. However, such emulsification techniques lead to unacceptably broad distributions in droplet size, since the main physical parameters that control drop formation (e.g. shear) are not homogeneous. For applications where emulsion droplets are to be used as templates, such as in the creation of monodisperse polymer particles[174, 175] , droplet size variations should be a small as possible. Fortunately, droplet-based microfluidic systems provided a direct route to the creation of monodisperse droplet populations, where both the average droplet size and payload may be controlled by the user.

3.1.2. Droplet generation

3.1.2.1. Planar Shear-Induced droplet generation devices

Various kinds of single nozzle droplet generators can be used for microfluidic droplet formation, including T-junctions[176], co-flow[177] and flow-focusing geometries[178] or glass nozzles[179] (**Figure 3.2**). In these approaches, two immiscible liquids meet at an intersection

or nozzle, with droplet pinch-off (formation) being driven by shearing (T-junction) or squeezing (flow focusing) of the oil phase[180].

The first report of a T-junction device was made by Thorsen and co-workers in 2001. In this device, an aqueous flow and oil flow were injected at right angles to each other, with droplets being formed as a result of shear forces created at the intersection of the water and oil phase (**Figure 3.2 a**). Importantly, droplet size could be tuned by altering the channel width, the relative flow rates of the water and oil phases or the interfacial tension of fluids. In such a device, pressure fluctuations are generated in the continuous and dispersed phases, with consistent droplets of relatively high monodispersity being formed.

In the case of co-flow droplet formation, the dispersed phase is injected through a small capillary centered within a larger diameter parallel capillary, as illustrated in **Figure 3.2 b** [181]. Here, droplets are generated by viscous shear of the continuous phase over the dispersed phase, with the droplet formation mechanism being controlled by viscous shear and surface tension.

In the flow-focusing approach, the dispersed phase is introduced via a central channel, with the continuous phase being delivered via flanking channels. In a simple sense, the oil phase is used to push, elongate and neck the aqueous phase with a microchannel constriction (**Figure 3.2 c**). The integration of such a constriction constrains the aqueous phase and drives pinch off from the primary flow. In flow-focusing geometries, the size of the formed droplet is controlled by the size of the orifice as well as the relative flow rates between the oil and water phases[178].

In general, the mechanism by which monodisperse drops are formed, will depend on the relative strengths of viscous forces and surface tension. In this regard, the capillary number (Ca) is a useful figure of merit. The capillary number is defined as:

$$Ca = \frac{viscous\ force}{surface\ tension} = \frac{\mu V}{\gamma} \quad (3.1)$$

Where μ is the dynamic viscosity, V the characteristic velocity, and γ the interfacial tension. When $Ca < 0.5$ (dripping regime), droplet breakup can be controlled by the interfacial tension, whilst when $Ca > 0.5$ (squeezing regime), droplets are produced through a process that depends primarily on viscous drag and interfacial tension determined by the viscous forces resulting in more elongated droplet that pinch off due to Rayleigh instabilities[182]. In both the dripping and the squeezing regimes, droplet size is controlled by the relative flow rates of the continuous and the dispersed fluids. Since droplet generation in flow-focusing units depends strongly on flow rates[183], closed feedback loop systems have been used to generate stable monodispersed droplets for a long period. For example, fast-response, pressure-driven pumps can be used to control flow rates, with image-based feedback loop systems enabling drift correction, whilst monitoring droplet sizes in real-time[184].

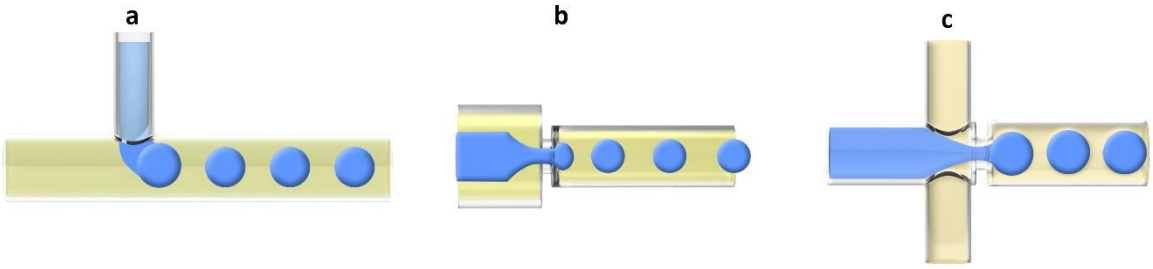

Figure 3.2. Overview of the three most common planar shear-induced microfluidic droplet generation techniques. (a) T-junction, (b) Co-flow geometry and (c) Flow-focusing geometry. The aqueous (dispersed) phase is shown in blue and the oil (continuous) phase is shown in yellow.

In all the aforementioned single nozzle droplet generators, a variety of factors such as the flow rates of aqueous and oil phase, their viscosities, interfacial tension and channel geometry will affect the droplet generation mechanism. In addition, the establishment of stable droplet generation requires some period of time before equilibration. Such issues increase the consumption of expensive and precious reagents, which can be a critical issue when performing biological assays that involve bespoke or non-commercial proteins[185, 186]. Furthermore, since the size of droplets produced in single nozzle droplet generators is highly sensitive to fluctuations in flow, high-cost precision pumps are typically required. Finally, the low volume throughput associated with single nozzle droplet generators also hinders their adoption applications where large-scale droplet populations are required.

An obvious strategy to increase the droplet throughput is via parallelization, which involves numbering up individual droplet generators with shared inputs. To date, there have been several reports of parallelization as a tool to scale out the production of chip-based single-phase emulsions. Parallelization geometries may involve various design strategies, including tree-like branched distribution geometries (**Figure 3.3 a, b**)[187, 188] and parallel droplet generators[189], either fabricated via multilayer soft lithography (**Figure 3.3 c, e**) or through the use of additive (**Figure 3.3 d)**[190].

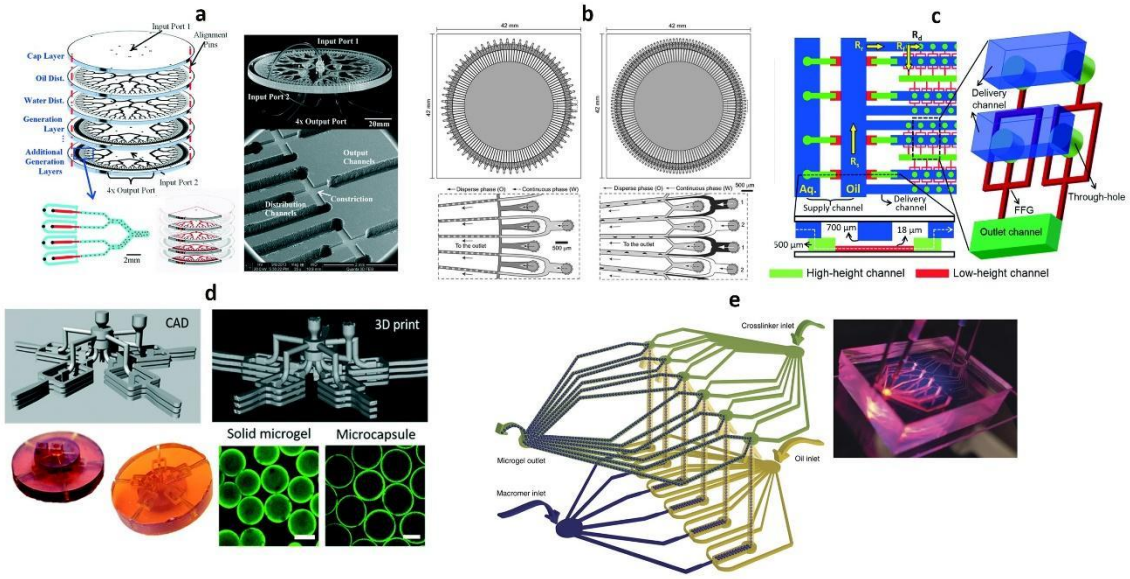

Figure 3.3. Parallelization and scaling out approaches for droplet generation. (a) A three-dimensional device made in PMMA, having 256 parallel droplet generators[188]. (b) A planar step emulsification device comprising 128 cross-junctions for the mass-production of monodisperse droplets[191]. (c) A three-dimensional monolithic elastomeric device containing 1000 parallel flow-focusing generators for large-scale droplet generation[187]. (d) A 3D printed parallelized microfluidic device containing radially organized stacks of microdroplet generator units[190]. (e) A multilayer device consisting of parallel droplet-generators for high throughput cell encapsulation and synthetic microgel generation[189].

However, it is important to note that many of the parallelization approaches described require highly precise manufacturing, which prohibits mass production of the device. In addition, most reported approaches require a uniform flow distribution amongst all channels; a daunting task for those not expert in microfluidics. Indeed, attaining a high degree of monodispersity in parallelized systems is far from simple, since individual drop makers, necessarily placed close to each other because of limited space availability, can

interact and develop new dynamical regimes producing droplets of uncontrollable size[191, 192].

3.1.2.2. Step emulsification: an approach for large-scale droplet production.

A promising approach that simplifies microfluidic design and circumvents issues of polydispersity involves the concept of step emulsification. Generating uniform droplets through step emulsification[193] provides an attractive route towards large-scale droplet production. In such a scenario, the formation of droplets is exclusively controlled by the geometry of the microfluidic channels and is independent of the flow rates of fluids when in the dripping regime[194]. In addition, droplet throughput can be enhanced by simply adjusting the droplet velocity or the number of droplet generators. Such advantages make step emulsification the method of choice when attempting to produce large number of monodisperse droplets is short periods of time.

The concept of step emulsification (also called micro channel emulsification(MCE)) was originally developed by Mitsutoshi and co-workers[80], with early devices incorporating a sudden expansion within a microchannel to trigger droplet formation. Such devices were fabricated by photolithography and deep reactive ion etching (DRIE) on a 5-inch silicon substrate to create symmetric and uniformly arranged wafer-through holes (**Figure 3.4 a**)[195]. To enhance the performance of the original MC device with respect to droplet monodispersity, Kobayashi and co-workers developed an asymmetric design (**Figure 3.4 b**), with each device having a 10 μm diameter micron-sized hole on the upstream side and 70 μm depth slots on the downstream side[81, 196]. The two input phases are delivered into the high aspect ratio channel, which suppresses interfacial tension and induces instabilities. The

stream of the soon to be dispersed phase abruptly breaks up into droplets at the step where the upstream channel ends. Such an asymmetric microchannel structure improves the droplet detachment process and the resulting monodispersity of droplets[196, 197]. Sugiura and co-workers further refined the MC device by incorporating nozzles and modifying the surface of the device to improve both throughput and droplet monodispersity (**Figure 3.4 c**)[198]. This device enables encapsulation of living cells with CV less than 15%.

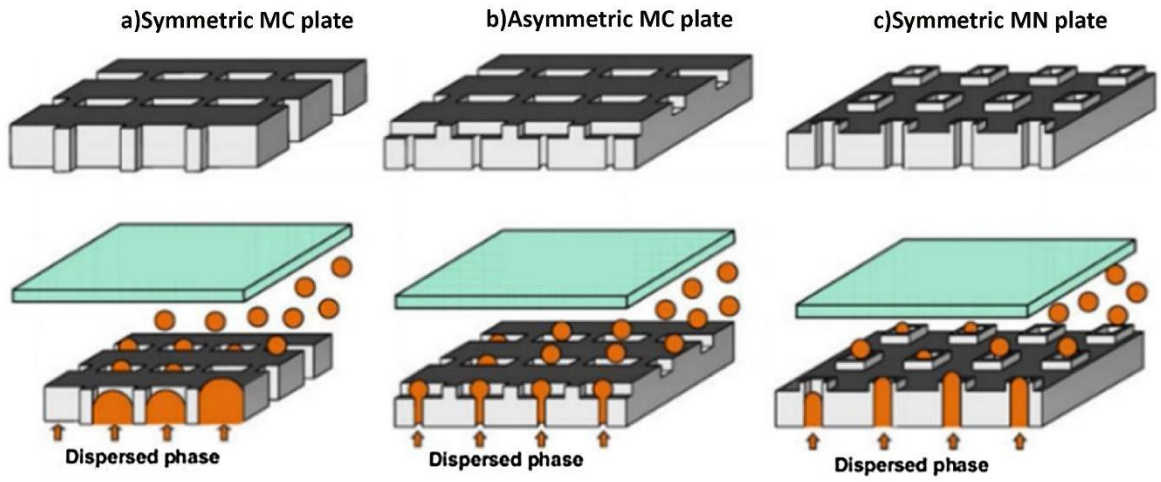

Figure 3.4. Evolution of the original Microfabricated Channel device. Droplet formation is realized using (a) A symmetric plate consisting of micro slots on both sides[196]. (b) An asymmetric plate with circular channels on the upstream side and slots on the downstream side[199] . (c) A symmetric plate consisting of several micronozzles[198].

Although Nakaima's MC device was a game-changer in the emulsion production field, it has significant drawbacks with respect to the complexity of fabrication and operational robustness. The device was made by photolithography and deep reactive ion etching. This is a complex procedure and not widely available. This prevented MC arrays being broadly adopted by end-users. Interestingly, other researchers inspired by the MC device fabricated

devices consisting of arrays of nozzles (or orifices) that could be used as parallel step-emulsifiers[193, 198]. The work of Kobayashi and co-workers nicely illustrates this approach[199]. Here, soybean oil droplets with diameters between 31 and 32 μm (and a CV of <10%) were produced in a silicon straight-through microchannel plate containing 211,248 channels, and with a throughput of up to 20-30 ml/h. More recently, the same group presented a 60 × 60-mm micro channel emulsification (MCE) chip in single-crystal silicon, containing 14 microchannel arrays and 1.2×10^4 microchannels. Such a device was successful in mass-producing 10 μm diameter droplets of soybean oil at a throughput of 1.5 ml/h[200]. Similarly, van Dijke and co-workers reported three parallelized edge-based droplet generation systems able to form 7.5 μm diameter droplets with a CV below 10%[201]. However, a drawback of step emulsification is the relatively low droplet production rate per single droplet maker. Accordingly, highly parallelized devices comprising many hundreds of droplet makers are needed to realize throughputs in excess of those achieved using flow focusing geometries (5K).

Recent studies on highly parallelized step-emulsification devices fabricated in polydimethylsiloxane[202] and glass[203] have shown the scalability of step emulsification through parallelization, whilst maintaining droplet monodispersity due to the insensitivity of droplet size on volumetric flow rates. A section of a typical step emulsification device with parallel nozzles, designed and fabricated during my PhD work, is illustrated in **Figure 3.5 b**. Although powerful, such a device has some drawbacks compared to more common flow-focusing or T-junctions geometries. The device comprises two layers and is thus more difficult to make than single layer droplet-production devices. Second, there is a limitation of control over the individual droplet size and payload. [47,50]. In addition, the " structure" of

step-emulsification chips does not favor the preparation of complex droplets of controllable composition[191]. Since shear-induced droplet generators offer a higher degree of control over droplet payloads (**Figure 3.5 a**), they may be used to excellent effect in high-throughput single cell studies[204], directed evolution of novel proteins, enzyme kinetic studies[205] and the study of protein crystallization[206].

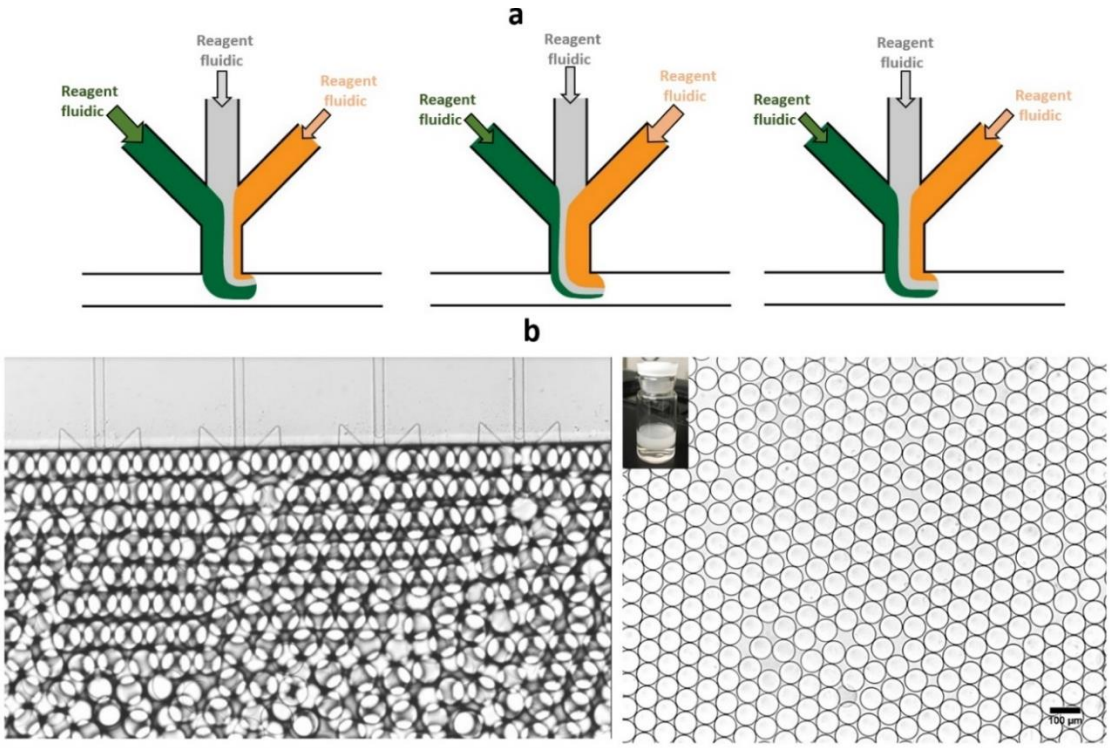

Figure 3.5. (a) Image of droplet generation using a T-junction microfluidic device. Variation of input flow rates provides exceptional control over both droplet size and droplet payload. (b) Image of monodisperse droplets generated by the process step emulsification.

In contrast to shear-induced droplet generators, the size of droplets produced by step emulsification is defined simply by the geometry of the nozzle and is independent of the input flow rates, viscosity and interfacial tension of the component fluids. Furthermore, and in contrast to both T-junctions and flow focusing geometries, step emulsification systems

require no "run-in time" to stabilize flows. The monodispersity of droplets is improved compare to those of T-junction and flow-focusing systems, making step emulsification an attractive system for massive production of monodisperse emulsions.

In the light of the aforementioned advantages, a few select studies have utilized step emulsification for droplet generation, but with fluid manipulation schemes based on magnetic[207]or centrifugal forces[208,209], rather than syringe pumps (**Figure 3.6)**. Such methods greatly reduce infrastructure costs and significantly demonstrate the potential of step emulsification as a robust and scalable platform in out-of-laboratory environments.

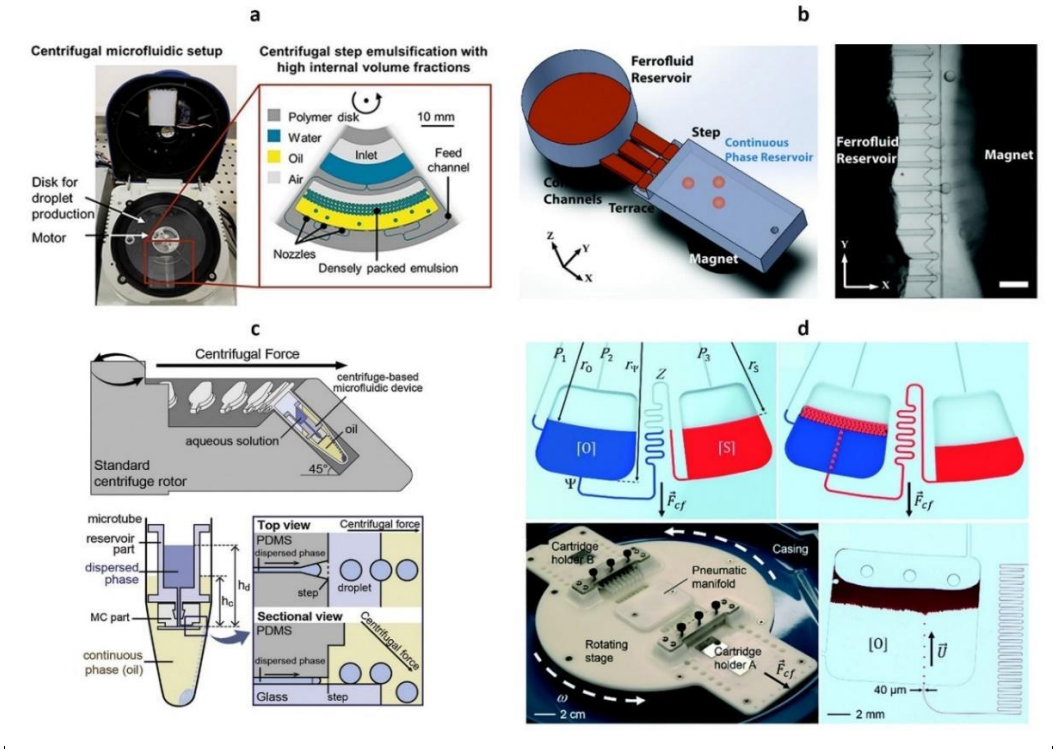

Figure 3.6. Alternative fluid actuation methods for step emulsification. (a) Centrifugal-based step emulsification[208], (b) magnetic force-driven step emulsification[207], (c) Centrifugal-based step emulsification within an Eppendorf tube[209] and (d) Buoyancy-driven step emulsification[210].

3.1.3. Applications of high throughput droplet generation

Hydrogels: solid and stable reaction vessels

Polymer microspheres are widely used in bio-pharmaceutical[211, 212]and drug delivery[212] applications, For example, poly (lactic-co-glycolic acid) (PLGA) is a biodegradable polymer commonly used as a carrier in drug encapsulation and drug delivery applications[213, 214]. To ensure a high degree of control over drug release profiles and timescales, monodisperse microparticles are a necessity. Conventional emulsion methods for PLGA particle synthesis employ high shear force mixing to generate particles[215]. Unfortunately, microparticles produced in this way are typically large, with populations exhibiting wide variations in size and shape. On the other hand, droplet–based microfluidic reactors can precisely control the entire material fabrication process and thus be employed for the production of large numbers of monodisperse PLGA microbeads[216]. In general, droplet-based microfluidic systems are highly adept in precise microparticle manufacturing, especially when the formed droplets are used as templates to prepare microparticles with various morphologies[217]. An interesting application of hydrogel microbeads is their use as templates for the formation of monodisperse droplets for performing biochemical reactions in the resultant droplets. Indeed, by vortexing a mixture of hydrogel particles and sample solution, encapsulation of the sample within monodisperse emulsions can be accomplished without the need for advanced microfluidic systems[218]. An example of such an application is described in Chapter 4 of this thesis.

Nucleic acid amplification

Compartmentalization plays a key role in digital PCR (dPCR). Here DNA and other biomolecules are encapsulated into compartments (separated into many aliquots) and isolated from the surrounding environment prior to amplification. DNA encapsulation into droplets normally occurs in a random manner, where the average DNA occupancy depends on the concentration of DNA molecules in the dispersed phase prior to droplet generation. Successful operation of such a scheme relies on the assumption that all compartments are of the same volume. In this respect, droplet-based microfluidic have obvious utility, due to the ease with which both the number and size of droplets may be controlled. To ensure that the vast majority of droplets contain either one or no DNA target molecules, the solution is diluted so that the number of droplets is higher than the number of DNA targets in the PCR mixture. After partitioning is complete, the DNA targets within the droplets can be amplified via thermal cycling. Amplification is normally monitored through the use of a fluorescent intercalating dye or probe[219]. Consequently, droplets containing the amplified DNA product will be fluorescent, whilst empty droplets will be dark. After the reaction is complete, all fluorescence droplets can eb assumed to have originated from a single DNA copy and are therefore counted as "1" (positive), whereas all droplets are assumed to be empty and counted as "0" (negative). An illustration of the ddPCR workflow is given in **Figure 3.7**.

The distribution of DNA molecules over the droplets is described by Poisson statistics, with each droplet having the same probability of containing a target DNA sequence. However, the number of positive droplets may underestimate the amount of template DNA since there will be a small but finite probability that some events might be associated with multiple DNA

template molecules encapsulated within a single droplet. In such a situation, the number of DNA molecules can be calculated using the following formula:

$$\lambda = -\ln(1 - P) \quad (3.2)$$

where λ is the average number of DNA templates per droplet, and P is the fraction of positive droplets measured experimentally[220]. From the λ value, the volume of each PCR replicate and the total number of replicates, an estimate of the absolute target DNA concentration, can be calculated.

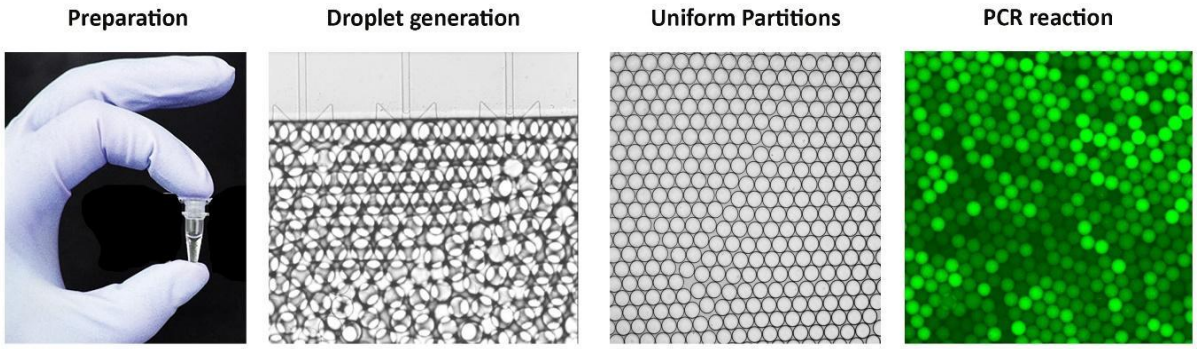

Figure 3.7. Schematic of a typical droplet dPCR workflow. dPCR is performed according to following steps: master mix preparation, partitioning of the mix into a large number of discrete nanoliter or sub-nanoliter droplets, amplification through temperature cycling and image analysis.

Step emulsification is an excellent candidate for creating monodisperse compartments in dPCR, since only one phase needs to be moving for the droplet generation, with the flow rate not influencing the droplet size. Significantly, such a platform can form the basis of a range of easy-to-use digital nucleic acid analysis systems, incorporating amplification processes such as PCR, LAMP, RCA.

Cell encapsulation

Over the past decade, droplet-based microfluidic systems have become increasingly popular due to their utility in high-throughput biological and chemical assays[221]. One of the key functions in this respect is the encapsulation of single cells within individual droplets. The ability to compartmentalize cells within pL-volume droplets has enabled the extraction of information at genomic[222], transcriptomic[223], proteomic[224] and metabolomic levels[225] from large numbers of individual cells.

To enable the performance of uniform and high-throughput biochemical reactions in droplets, numerous studies have addressed two key issues, namely increasing the rate of single encapsulation (i.e. the number of droplets that encapsulate only a single cell) and generating monodisperse droplets. Droplet-based microfluidic technologies also offer the advantages of confining individual cells with user-defined reagents and preventing dilution of species when performing single cell assays[226]. As discussed, step emulsification can be leveraged as a high throughput platform for cell encapsulation through modifications in nozzle geometry.

3.2. Material and methods

3.2.1. Device design and master mold fabrication

Microfluidic channel patterns were designed using AutoCAD 2017 (Autodesk, San Rafael, CA, USA) and printed onto a 177 μm thick fine grain transparency film (Micro Lithography Services Ltd, Chelmsford, UK). Master molds were fabricated using standard photolithography techniques illustrated in **Figure 3.8**. In the current work, step

emulsification devices consist of two layers: the nozzle layer being approximately 20 μm thick and the step layer being approximately 250 μm thick.

Initially, a 100 mm silicon wafer (Siegert Wafer GmbH, Aachen, Germany) was dehydrated for 30 minutes at 200°C. This step facilitates the adhesion of the SU-8 photoresist to the surface of the silicon wafer. Then, one layer of GM1060 photoresist (Gersteltec, Pully, Switzerland) was spin-coated onto the silicon wafer. Spin speeds were varied to control the final photoresist coating thickness according to manufacturer's specifications. After spin-coating, the wafer was placed on a hotplate at 65°C for five minutes, followed by curing at 95°C on a hotplate for 10 minutes. The photolithography mask was then used to transfer the microfluidic channel pattern to the photoresist layer by exposure to ultra-violet light. To fabricate the step channel, two layers of GM1070 (Gersteltec, Pully, Switzerland) photoresist were spin-coated, yielding a total layer height of 250 μm. A post-exposure bake at 95°C was performed to induce thermally-activated cross-linking of the exposed SU-8 photoresist. Subsequently, the mold was developed in poly(ethylene glycol) methacrylate (Sigma, Buchs, Switzerland) for 15 minutes and cleaned in isopropanol for a further 5 minutes. The mold was hard-baked at 150°C for 10 minutes. Finally, it was treated with chlorotrimethylsilane (Sigma Aldrich, Buchs, Switzerland) vapor in a vacuum desiccator to make the surface of the mold hydrophobic and prevent adhesion of PDMS during molding and demolding. Images of the completed master mold are shown in **Figures 3.9, 3.10** and **3.11.**

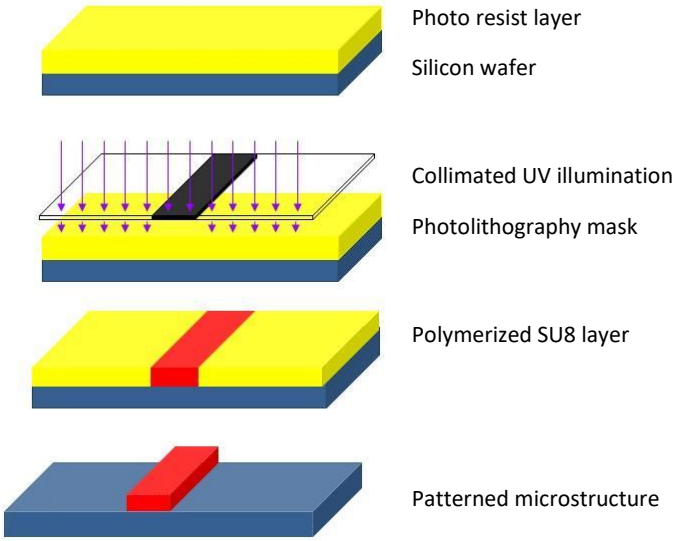

Figure 3.8. Schematic depicting the master mold fabrication processes. First, the wafer is dehydrated, and spin coated with SU-8 photoresist. After the soft bake UV light and a photomask are used to transfer the pattern of the microfluidic features on to the surface. A post-exposure bake is followed by resist development. After the washing in isopropanol, the wafer is dried with air and hard baked.

3.2.2. PDMS device fabrication

A degassed 10:1 mixture of PDMS monomer and curing agent (Sylgard 184, Dow Corning, Midland, MI, USA) was poured over the master mold and peeled off after polymerization at 70°C for 4 hours. Inlet and outlet ports were created using a hole-puncher (Technical Innovations, West Palm Beach, USA). Afterwards, the structured PDMS substrate was bonded to a 1mm thick glass substrate (Menzel-Glaser, Manheim am Rhein, Germany) after treating both surfaces in an oxygen plasma (EMITECH K1000X, Quorum Technologies, UK) for 60 seconds. The step emulsification channel was also treated with an HFE 7500-based solution containing 1% (v/v) trichloro-(1H,1H,2H,2H-perfluorooctyl) silane for 10 minutes and then rinsed with 100 µL of the HFE 7500 oil. This procedure generates a stable

hydrophobic surface. At this point, the step emulsification device is ready to use for water-in-oil droplet formation.

3.2.3. Step emulsification device development

Initially, water-in-oil droplets were formed using the design a1 (**Figure 3.9**), where two separate inlets are used for the oil phase. Whilst this device was able to generate monodisperse droplet populations, the device was found to be prone to droplet jamming in front of the nozzles and additionally required the use of two syringe pumps simultaneously delivering two oil streams into the device. Accordingly, a second device was designed to incorporate a single oil inlet. This device consisted of one main inlet that acts to distribute the oil phase to five channels (**Figure 3.9**). Such an approach yielded a uniform and steady oil phase flow in the main radial channel where emulsions were formed. This improved design was used for PLGA microparticle production experiments.

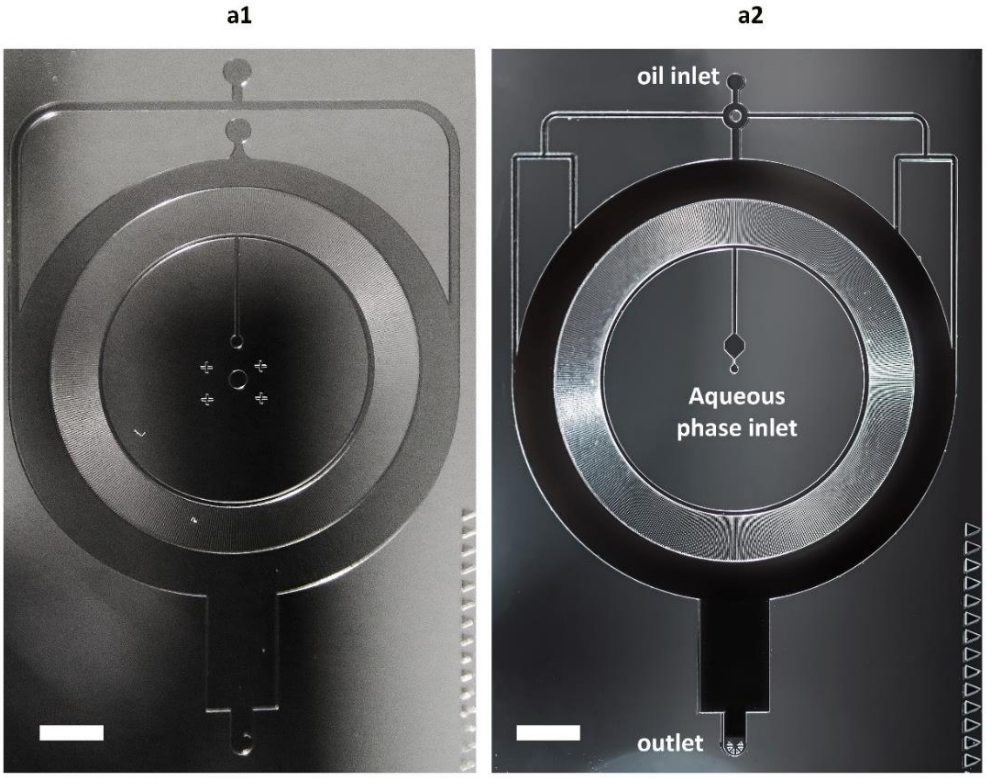

Figure 3.9. Step emulsification master molds: (a) Design a1 contains two separate oil channels, (b) Design a2 contains a modified channel geometry consisting of five oil microchannels (scale bar2mm).

For the single-cell encapsulation experiments, an array of inlets was embedded inside the nozzle array structure of design a2 to form design a3. This modification enabled the injection of cells into the nozzles, as shown **Figure 3.10**.

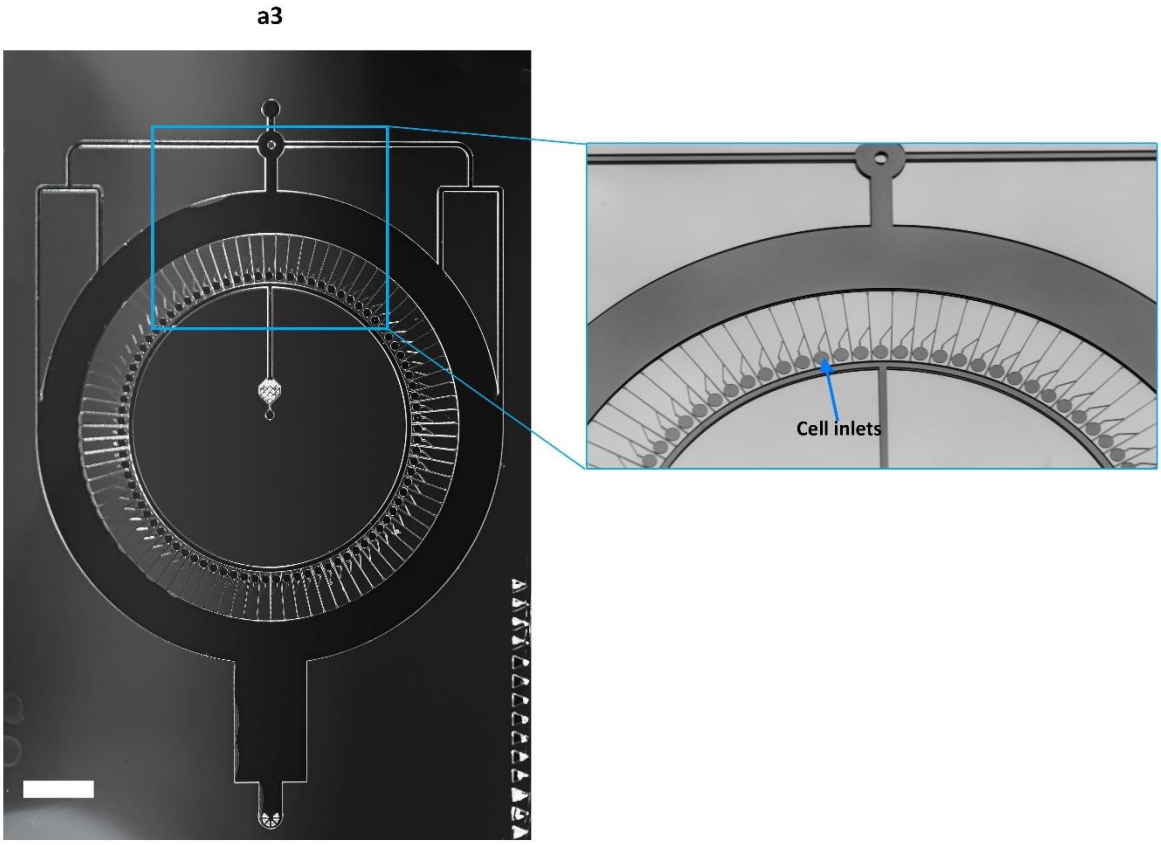

Figure 3.10. A step emulsification device for single-cell encapsulation experiments (design a3). Here, an array of inlets (labelled cell inlets) is embedded inside the main nozzle array, which enables high throughput single cell encapsulation (scale bar2mm).

A novel feature of the step emulsification device was a mixing unit embedded before the main aqueous channel. Such a mixing unit was integrated to ensure efficient mixing of all reagents (i.e. monomers, initiator and buffer) required for the polymerization of the aqueous phase. For instance, in the synthesis of PAA beads, the monomers and initiators were placed in separate glass syringes to avoid pre-polymerization of the PAA and clogging of the syringes.

Initially, a long-looped channel (30 mm in length) was designed to mix the monomer and the initiator (**Figure 3.11,** design a4). However, in this geometry the mixing process is governed

by molecular diffusion which can be insufficient to mix monomers and initiators on short timescale. Therefore, to ensure efficient mixing at low Reynolds numbers, the looped channel was replaced by a tesla-inspired micromixer (**Figure 3.11,** design a5) for the PAAmicroparticle production. Details of this geometry are provided in Table **3.1.**

Figure 3.11. Master molds of step emulsification devices integrating micromixer units: (a) Design a4 consists of two inlets for the aqueous phase and a long microchannel for reagent mixing. (b) Design a5 design incorporates a custom tesla micromixer embedded before the aqueous channel (scale bar2mm).

Table 3.1. List of the geometrical features in design a5 of the step emulsification microfluidic device.

Description	Value
Depth oil channel	250± 10 µm
Width oil channel	47 µm
Length oil channel	10 mm
Depth micromixer	250 µm
Number of mixing stages	7
Depth nozzle	20 ± 3 µm
Width nozzle	20 ± 0.5µm
Length nozzle	3068 µm
Number of nozzles	203
Depth outlet channel	250 µm
Width outlet channel	1600 µm

A single outlet was used to collect the generated emulsions in all of designs. All PDMS devices were fabricated using multilayer lithography to generate a "step" channel (250 µm high) bonded directly to a glass slide.

3.2.4. Droplet production

3.2.4.1. Polyacrylamide bead production

The acrylamide precursor solution was prepared according to the protocol developed by Hatori and co-workers[218]. Briefly, a solution containing 7% acrylamide, 0.2% N,N′-methylenebis(acrylamide) and 0.3% ammonium persulfate (Sigma Aldrich, Buch, Switzerland) was mixed using a Tesla micromixer and used as the aqueous phase. HFE-7500 oil (3M, St. Paul, MN, USA) containing 2% (w/w) PFPE-PEG surfactant (Ran biotechnologies,

Beverly, USA) and supplemented with 1% TEMED (Sigma Aldrich, Buch, Switzerland) was used as the oil phase. Low-pressure dosing modules (neMESYS, Cetoni GmbH, Korbussen, Germany) were used to feed solutions from 1 mL gastight syringes (Hamilton Bonaduz AG, Bonaduz, Switzerland) through 0.33 mm i.d. Tygon tubing (Cole Palmer, Hanwell, UK) to the inlets of the microfluidic device (design a5). Water-in-oil droplets with diameters of approximately 75 μm were generated and monitored via bright-field microscopy. Droplets were collected and incubated on a heat block at 65°C for 12 hours to allow the polymerization process to occur. Excess oil from the bottom of the emulsion reservoir was extracted and replaced with an equal volume of perfluoro-1-octanol (Sigma Aldrich, Buchs, Switzerland) to dissolve the surfactant layer. Subsequently, the monodisperse PAA microgels were washed several times with washing buffer, according to the procedure of Hatori and co-workers[218, 227], and finally redispersed in 0.5% Triton-X100, DNase/RNase free water (Invitrogen, California, USA). PAA hydrogels were stored at 4 °C until further use.

3.2.4.2. Cell culture and single-cell encapsulation procedures

A Chinese hamster ovary CHO-K1 (ECACC catalog no. 85051005) line was obtained from Sigma-Aldrich (Sigma-Aldrich, Buch, Switzerland). Cells were cultured in a vertical T-75 flask filled with 12 mL of the complete growth medium: F-12 Ham (Sigma-Aldrich, Buch, Switzerland) supplemented with fetal bovine serum 10% v/v (FBS, Thermo Fisher Scientific, Basel, Switzerland) L-glutamine 10% v/v (Thermo Fisher Scientific, Basel, Switzerland)). This solution was kept in an incubator (Thermo Fisher Scientific, Basel, Switzerland) which provides sterile conditions at 37°C within a 5% carbon dioxide atmosphere. CHO-K1 cells were inoculated in fresh growth medium at an initial concentration of 10^5 cells/mL. To

acquire enough (approximately 1 mL) cell suspension, two flasks of cells were cultured for four days simultaneously, then spun down and suspended in fresh medium at the desired cell density and before viability drops below 95%.

For cell encapsulation experiments, Novec 7500 Engineered fluid (3M, St. Paul, USA) was mixed with 2% (w/w) PFPE-PEG surfactant (Ran Biotechnologies, Beverly, USA) and injected into the main oil inlet at a flow rate of 40 µL/min, while the aqueous phase (0.22 µm filtered deionized water) was introduced at a flow rate of 10 µL/min. CHO-K1 cells suspended in culture medium with 1% OptiPrep (Sigma-Aldrich, Buchs, Switzerland) were injected through the cell inlets. All fluids were delivered using two neMESYS syringe pumps (Cetoni GmbH, Korbussen, Germany) into the step emulsification device a3 (**Figure 3.10**) to generate cell-encapsulated microdroplets. Fluorinated ethylene propylene (FEP) tubing, with an inner diameter of 0.5 mm, was used to connect the syringes to the microfluidic device inlets.

3.2.4.3. PLGA production

For oil-in-water droplet generation, a poly (vinyl alcohol) (PVA) surface treatment was applied to the channels to make surfaces hydrophilic. Briefly, a 1% aqueous solution of PVA (Sigma-Aldrich, Buch, Switzerland), was injected into the microchannels and incubated for at least five minutes at room temperature. This is long enough for the PVA to self-assemble onto the microchannel surface. The PVA solution was then removed from the channel under vacuum, and the device was incubated at 100°C for 5 minutes and 120°C for five hours to thermally anneal the PVA.

Oil-in-water emulsions were produced using the step emulsification device a2. The continuous phase contained 2 wt. % PVA (Mw 31,000–50,000, 98%–99% hydrolyzed, Sigma-Aldrich) that acts as a surfactant when dissolved in water. The dispersed phase, containing Poly (D, L-lactide-co-glycolide) (PLGA, Mw 40,000–75,000, 65:35, Sigma-Aldrich, Buchs, Switzerland) (0.5 wt.%) dissolved in dichloromethane (Sigma-Aldrich, Buchs, Switzerland), was injected into the nozzle array and oil-in-water droplets were generated and collected in a glass vial. To obtain microparticles, droplets were kept under magnetic stirring conditions at room temperature for 24 hours to evaporate residual organic solvent. Particles were collected by centrifugation (4500 rpm for 5 minutes) and then washed twice with distilled water to eliminate any excess surfactant. Finally, washed particles were stored at room temperature inside glass vials.

3.3. Results and Discussion

3.3.1. Mixing process of the Tesla micromixer

The design of the mixing unit is based on a tesla micromixer reported by Wang and co-workers, where the asymmetric shape enhances the mixing efficiency at low Capillary and low Reynold numbers[228, 229]. Here, the asymmetric shape enhances mixing efficiencies at low Capillary and low Reynold numbers. The specific structure of the mixer causes chaotic flow by collision of the fluid streams on redirection, which significantly improves mixing. The mixing performance of the micromixer was assessed by dilution of 100 μM fluorescein isothiocyanate (FITC) in Dulbecco's phosphate-buffered saline, with mixing being monitored by fluorescence microscopy. FITC was injected into the central inlet, and water through the two out inlets. Immediately after the inlet junction, the fluorescence signal exhibits a step

function, with the maximum intensity in the center of the channel where the fluorescent FITC stream flows in a laminar manner between the non-fluorescent water streams, **Figure 3.12 a** (1). As the solution flows through the micromixer, fluorescence deceases at the center of the channel and increases at the edges, as the FITC is diluted into the water. Here, the solution interfaces increase in an exponential fashion (Figure **3.12 a** (2–4)). Mixing can be judged as 100% if the transverse fluorescence profile across the channel is essentially flat. After the fifth mixing unit, mixing performance was estimated to be 90% (**Figure 3.12 a** (5)), which was deemed to be sufficient in the current device.

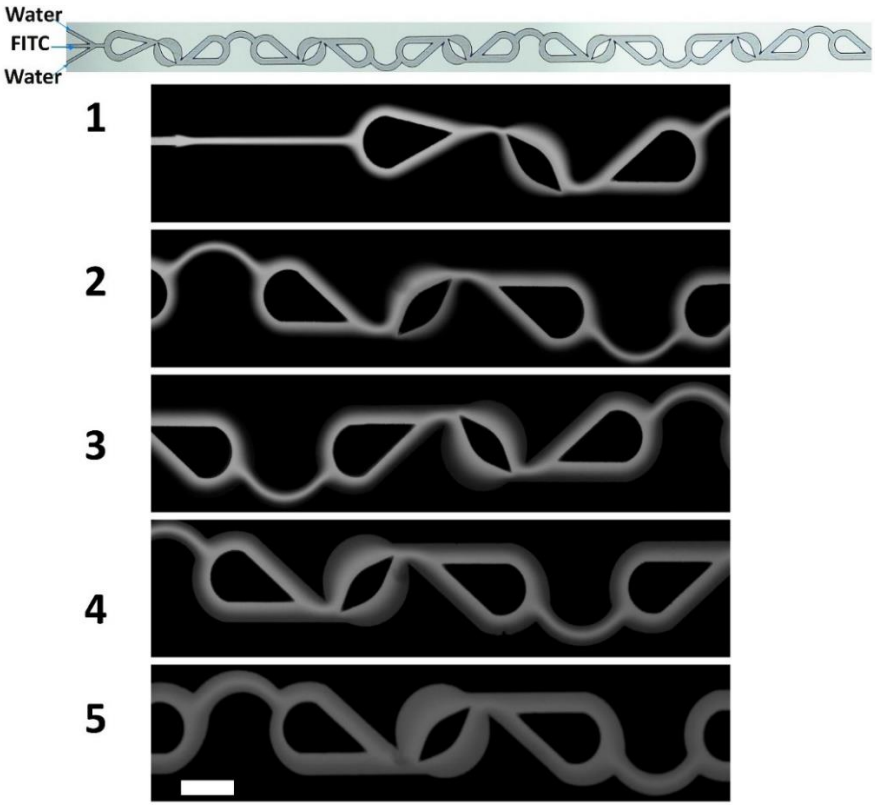

Figure 3.12. The tesla-inspired passive micromixer integrated prior to the radial nozzle array, showing the design (upper image) and fluorescence analysis (lower images 1–5), scale bar 200 μm.

3.3.2. Polyacrylamide bead production

PDMS devices fabricated from master mold a5 (**Figure 3.13 a**) were used for high-throughput droplet generation. Oil was injected into the main channel at a flow rate of 80 µL/min. To produce PAA beads, the aqueous phase containing the acrylamide monomer (7% w/v) and N,N′-methylenebis(acrylamide)(0.2% w/v) was injected into one of the aqueous inlets (**Figure 3.13 b**). Ammonium persulfate (at 0.30% w/v) with Tris buffer (10 mM) was injected into the second aqueous inlet A flow rate of 30 µL/min was used for both inlet flows.

The breakup of the aqueous fluid into droplets, is illustrated in **Figure 3.13**. Droplets are formed by injecting the aqueous phase through a nozzle and into an oil reservoir that contains the oil phase. Initially, the aqueous fluid forms a neck inside the nozzle as shown in **Figure 3.13 b**. Once the neck is formed and reaches the end of the nozzle, it expands into the oil reservoir forming a symmetrical bulb (**Figure 3.13 d, e, f)**. Initially, the bulb remains connected to the main thread in the nozzle (**Figure 3.13 g**) Hence, the bulb grows and the pressure gradient increases, Rayleigh-Plateau instability triggers the break-up of the bulb from the remaining dispersed phase in the nozzle and a droplet forms (**Figure 3.13 h)**. Indeed, the instability is determined by the shape of the nozzle at the outlet and the droplet size is independent of dispersed phase flow rate. The flow rate independence of the droplet size in step emulsification device makes it possible to scale up an array of droplet makers while keeping size monodispersity.

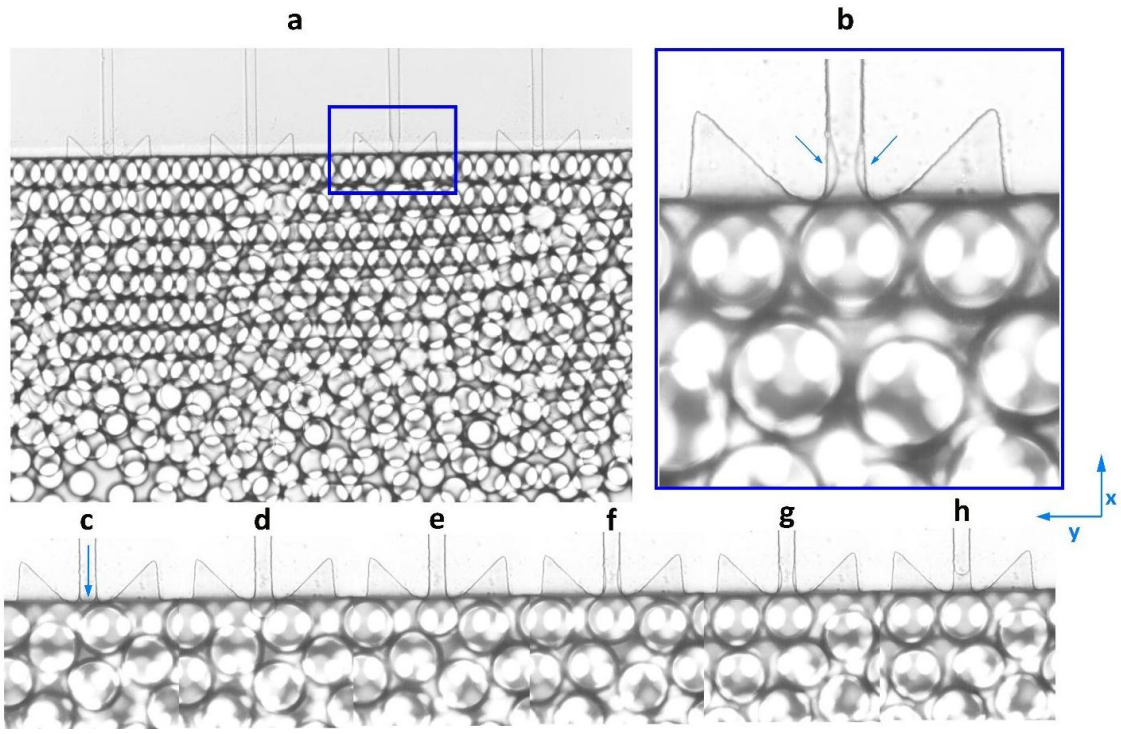

Figure 3.13. Droplet formation in a step emulsification device (a) and zoomed image of neck formation in the nozzle (b). A sequence of the droplet formation process showing the droplet formation in step emulsification device.

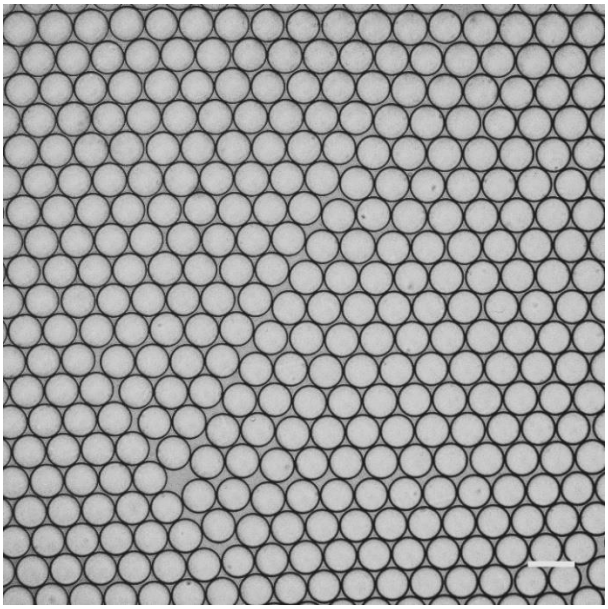

Figure 3.14. Optical microscopy images of droplet generated using design a4, scale bar 100 μm.

Incubation of the pre-polymer droplets at 60°C for 12 hours yielded the PAA beads. Excess monomer, precursor and oil were removed by multiple washings and centrifugations. The obtained hydrogel beads are shown in **Figure 3.15 a and** were highly monodisperse (CV of 2.8%), with an average size of 72 $\pm$ 4.5 μm (**Figure 3.15 b**). The droplet size is determined by the smallest channel dimension (nozzle height here ca ~ 20 μm) and is independent of flow rates. In other to tune the size of droplets, new devices with different nozzle heights need to be fabricated.

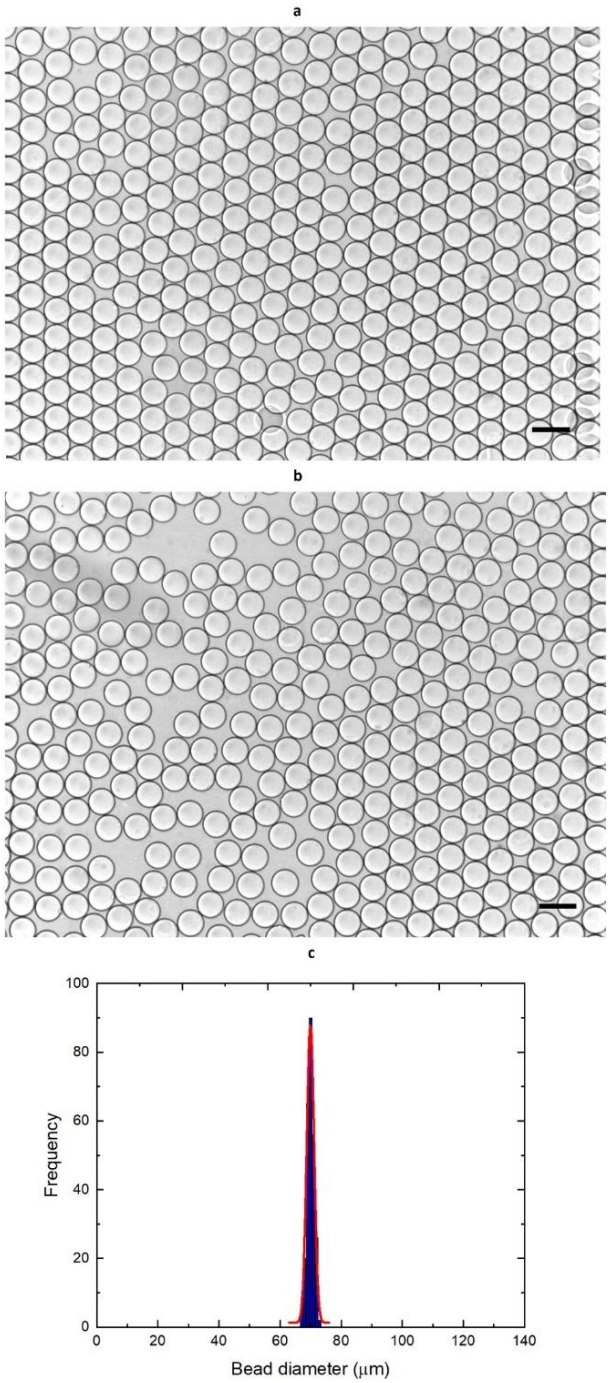

Figure 3.15. Image of PAA microgels (a) freshly prepared and (b) after being stored for 120 days at 4°C prior to analysis. Scale bar 100 μm. (c) Histogram of the bead size distribution (CV~ 2.8 %).

For almost all real-world applications, it is critical that the PAA hydrogel microbeads are stable for long periods before use. Accordingly, we assessed the stability of the hydrogel beads over a period of 120 days at 4°C in the washing buffer. **Figure 3.15 a** show that there was no significant change in the mean bead diameter and size distribution over the testing period, showing high storage stability. This observation is agreement with Hatori and co-workers who showed that their hydrogel particles could be stored for up to a year without any change in particle integrity[226]. The aforementioned device can also be used for the synthesis of complex polymer particles consisting of a mixture of more than one polymer.

3.3.3. Cell encapsulation

As previously noted, existing single-cell encapsulation microfluidic approaches typically yield relatively low single cell occupancies (i.e few droplets which contain a single cell). Accordingly, the ability to mitigate the low single-cell occupancies is to produce droplets at a high throughput. To address this limitation to some degree, we leverage the high throughput droplet generation nature of step emulsification a for single-cell encapsulation studies, with a view to creating large numbers of droplets that contain single cells. Since the proposed single cell encapsulation method is independent of the aqueous phase flow rate, this device can be easily integrated with a 3D printed inlet holder as a "world to chip" connector.

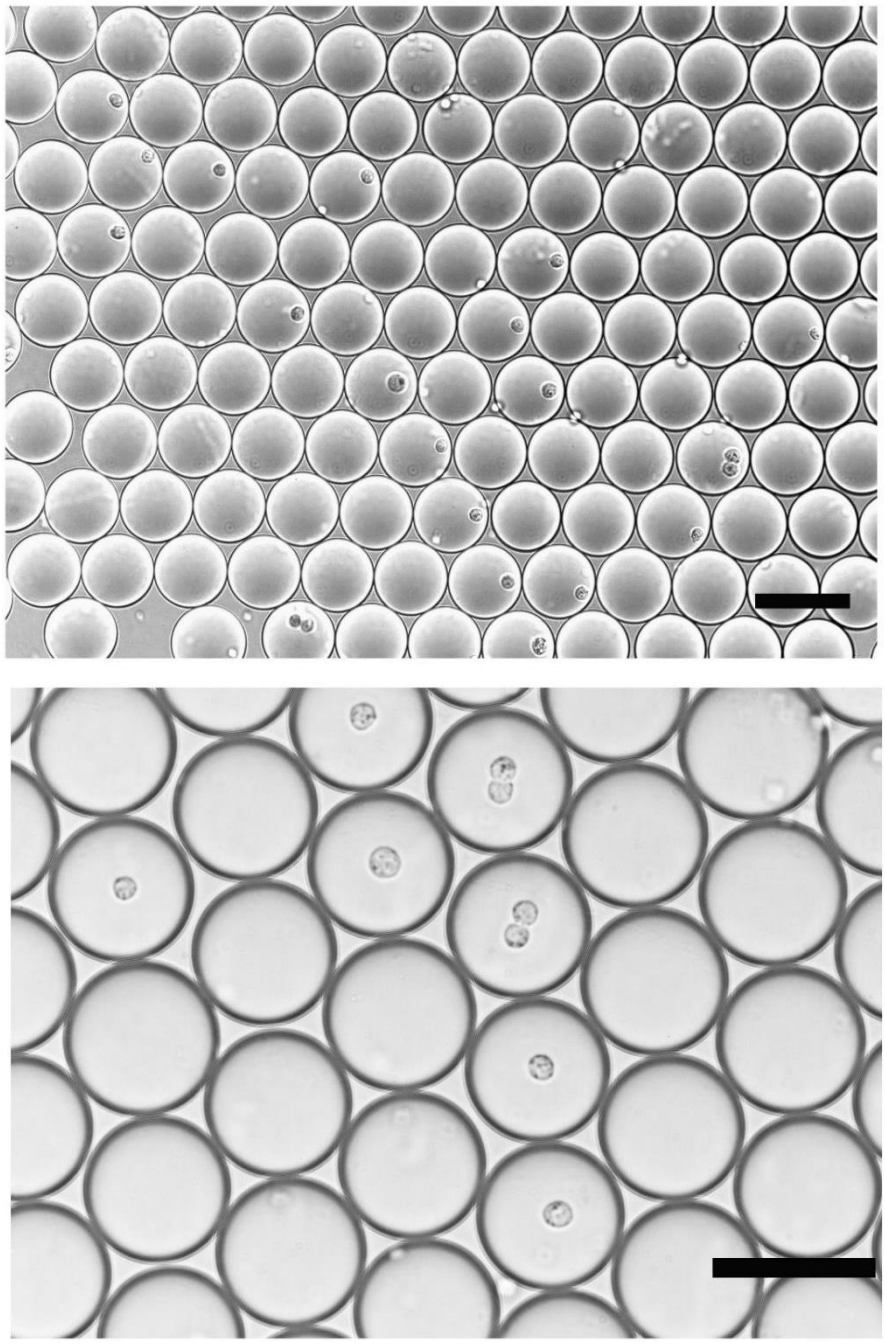

Figure 3.16. Optical microscopy images of single- CHO-K1 cells encapsulated in water-in-oil droplets, demonstrating the potential of the device producing monodisperse droplets and relatively good cell occupancy (scale bar 100μm).

A notable feature of directly injecting cells inside the nozzle is that high-efficiency single-cell encapsulation experiments can be performed at relatively low cell concentrations. For example, single-cell occupancy of approximately 30% ±5 was achieved for CHO-K1 cells as shown in **Figure 3.16**. This value is lower than single cell occupancy percentages achieved in flow focusing devices. This can be justified by the fact since cells can adhere to each other (before the encapsulation process), thus the efficiency of the single cell encapsulation single-cell occupancy droplets to some extent.

3.4.4. PLGA microparticle production

To demonstrate the capability of the current step emulsification device (design a2) for the production of oil-in-water emulsions, PLGA particles were synthesized according to the procedure reported by Perez and co-workers[81]. To prepare polymer microparticles, the polymer is first dissolved in an organic solvent to form the discrete phase. This phase is then mixed with an aqueous continuous phase to form an oil-in-water emulsion. As a final step, the emulsion droplets are solidified to form polymer microparticles. To solidify droplets, the organic solvent must be removed. In the current case, spherical microparticles were successfully formed by solvent elimination due to the combined effects of high solvent volatility and polymer precipitation (**Figure 3.17**). Specifically, monodisperse microparticles PLGA particles having a mean size of 89 μm and a CV of 3.5% were obtained (**Figure 3.17**) compared to the size distribution of particles obtained by conventional methods (e.g. bulk material mixing). For instance, Kirby and co-workers reported the production of protein loaded PLGA microparticles with a mean diameter of 97.85 μm and standard deviation of ± 30.06[230]. However, after solvent evaporation, we observed that the surface of the solidified

PLGA microparticles becomes porous (**Figure 3.17 d**). One possible explanation for this, is that during solvent evaporation droplet shrinkage occurs and the precipitating polymer shell breaks to form a characteristic porous surface. However, despite these surface artifacts, the PLGA microparticles kept their round shape and integrity after solvent evaporation.

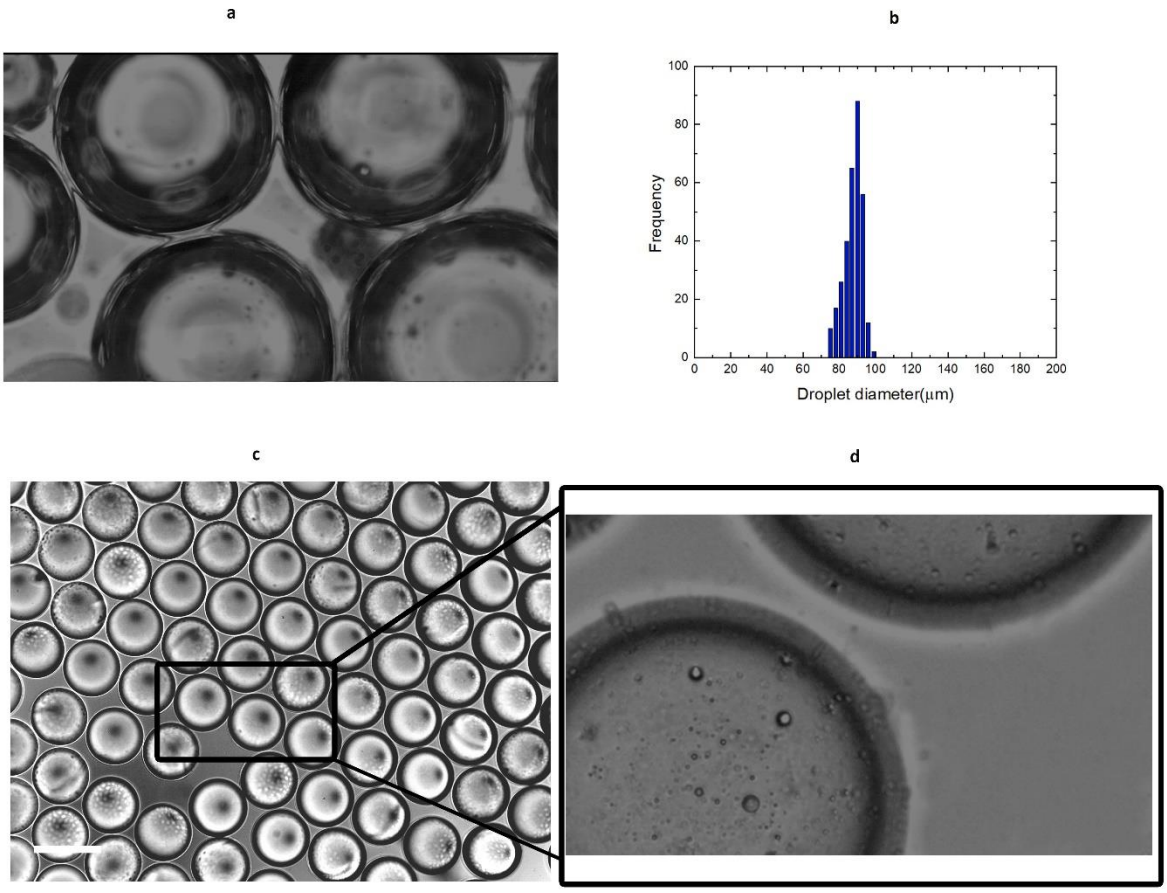

Figure 3.17. (a) Optical microscopy images of PLGA droplet before polymerization (b) Histogram of the droplet size distribution demonstrating monodispersity with a CV of 3.5%, (c, d) monodisperse PLGA microgel particles (scale bar 100μm).

It is worth noting that for oil-in-water droplet generation, the PVA hydrophilic surface treatment of the device was stable for only 20 minutes, with the device periodically clogging due to the precipitation of PLGA monomer in the nozzle channels. Additionally, although

dichloromethane was used as an organic solvent for PLGA production, the use of dimethyl carbonate is likely to be a superior alternative, since it is considerably less toxic and has a higher vapour pressure.

Herein, we have demonstrated the high throughput production of monodisperse PLGA microparticles that have significant utility as drug delivery systems.

3.4. Conclusions

In this chapter the design and the fabrication of a variety of step emulsification devices capable of producing monodisperse droplets at high throughput has been described. Such devices contain large numbers of nozzles, with each nozzle slowing down the fluid flow and establishing the quasistatic conditions that are required to create the static instability that leads to droplet formation. Since this instability depends only on the nozzle geometry, droplet size is independent of flow rates making this type of device simple to use in a range of settings. As a proof-of-concept, the devices were used to generate either water- in-oil or oil-in-water emulsions, and subsequently PAA and PLGA microgel particles. Such examples illustrate the wide range of applications that can benefit from this microfluidic technology.

Since droplet production via step emulsification is not influenced by the flow rates of both aqueous and oil phases, long-term monodisperse droplet production at high flow rates is enabled. For example, design a5 was operated with an aqueous phase flow rate of up to 15 mL/h producing water-in-oil droplets with an average diameter of 72 ± 4.5 μm. Such performance metrics are far too superior to the low throughput and unreliable long-term droplet production nature of single nozzle droplet generators.

The high throughput and robust nature of droplet production in step emulsification devices are highly attractive for a range of industrial applications. The added value of monodispersity for pharmaceutical, diagnostics, and biomedical applications is evident. We hope to see further development on step emulsification for

Considering the flow rate insensitivity of the size of droplets, low-cost syringe pump or even a handheld pump can be used for liquid manipulation. Indeed, in resource-limited settings, "equipment-free'' droplet-based microfluidic devices based on the step emulsification should result in a variety of field-deployable instruments. Moreover, the step emulsification devices described in this chapter could be employed to produce hydrogel microparticles for use in clinical practice and medical research. For instance, PAA beads can be used for dPCR[227], and polyethylene glycol (PEG) hydrogel beads can be used for both dPCR and single cell phenotyping[231].

Chapter 4
Hydrogel LAMP for highly sensitive drug-resistance bacteria diagnostics

Application of droplet-based nucleic acid detection assays for point-of-care disease diagnostics in resource-limited settings is enabled by decoupling the relatively complex droplet synthesis steps from the diagnostic assay itself. To this end, we have developed a new micro-compartmentalized nucleic acid quantification assay based on hydrogel microparticles that are synthesized in batch and stored before later application in a loop-mediated isothermal amplification (LAMP)-based procedure. We targeted the detection of Methicillin-resistant *Staphylococcus aureus* (MRSA) as a model system. Polyacrylamide-hydrogel beads were synthesized using a robust and reproducible step-emulsification route, which allows rapid synthesis of large numbers of stable hydrogel microbeads (at a throughput of up to 15 mL/h). In the hydrogel LAMP assay (termed H-LAMP), the microbeads were used for particle-templated emulsification of LAMP reaction components, thus achieving micro-compartmentalization of the reaction. The assay was successful in detecting MRSA within 30 minutes, with a limit-of-detection of 1 fg/μL (10^3 copies/μL) and a linear range of 10^{-1} to 10^2 copies/μL ($R^2 = 0.997$), with excellent selectivity and accuracy with respect to polymerase chain reaction (PCR)-based methods (t-value = 0.70, < t-critical = 1.85). Overall, this approach enables the direct translation of technical advances in droplet microfluidics to the IVD field whilst circumventing the need for costly and/or cumbersome instrumentation.

This chapter is adapted from a manuscript entitled “Hydrogel LAMP Development for Highly Sensitive Drug-Resistance Bacteria Detection", authored by Akkapol Suea-Ngam, Zahra A. Halvorsen, Vincent Revol, Stavros Stavrakis, Philip D. Howes and Andrew J. deMello. In preparation.

Note: This project was conducted by Akkapol Suea-Ngam (ASN) and Zahra Halvorsen (ZH), with an equal contribution from both. ASN designed and developed the LAMP part and provided all biological resources for the project, including gene analysis, LAMP primer design, LAMP system design, LAMP optimization in bulk, LAMP data analysis, analytical method design and development, bacterial sample preparation, polymerase chain reaction design and data investigation, and

original draft preparation. ZH designed and prepared the microfluidic device for hydrogel bead fabrication, including microfluidic device optimization, micromixer optimization, micromixer simulation, hydrogel optimization and preparation, LAMP and hydrogel bead investigation in bulk and microfluidic platforms, LAMP solution to microfluidic device protocol optimization, fluorometry setup, data analysis, and original draft preparation.

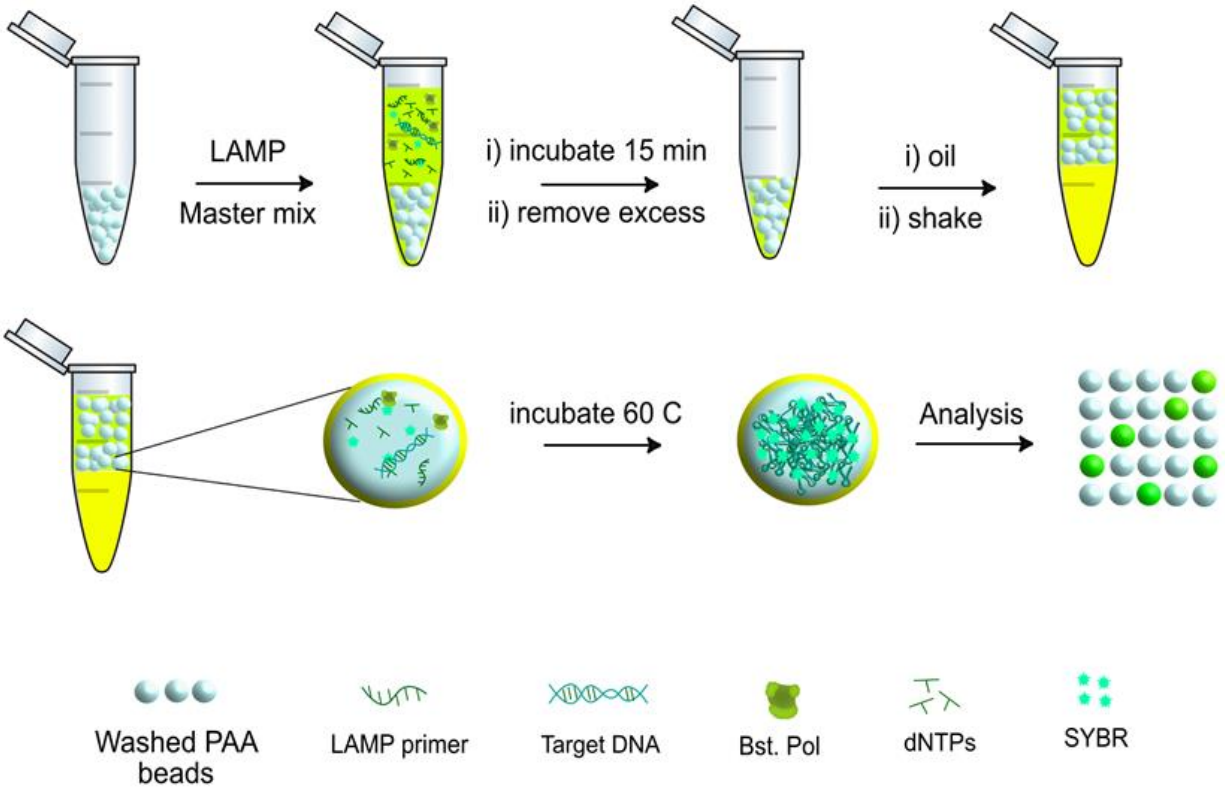

Scheme 4. 1. Schematic illustrates HD-LAMP protocol using droplet hydrogel platform that absorbs LAMP master mix and target gene for MRSA analysis

Chapter 4 – Introduction

4.1. Nucleic acid amplification-based techniques for pathogen detection

The compartmentalization of reactions into many isolated units can be of significant utility in experimental science, a key example being in droplet-based nucleic acid (NA) quantification assays[232]. Micro-compartmentalization of nucleic acid amplification tests (NAATs) is one of the standout applications of microfluidic technologies to date[233-235]. It allows highly sensitive analysis without the need for a calibration curve (based on droplet counting and Poisson statistics[236, 237]). Further, the approach reduces device complexity, since only an end-point reading is required, which can be achieved using a smartphone, for example[238, 239]. Accordingly, this methodology is an attractive option for in vitro diagnostics (IVDs) that intend to move testing away from specialized labs and towards point-of-care or field settings[76, 240, 241].

Unfortunately, current droplet-based NAAT systems typically possess several important disadvantages. First, creating monodisperse, robust and consistent droplets is a specialized task in itself, requiring dedicated equipment (e.g. pumps, microfluidic chips) that significantly add to the complexity of any system that incorporates them in its workflow[242]. Second, in the case of droplet PCR (dPCR), long term incubation of droplets at raised cycling temperatures (up to 95°C) commonly leads to droplet instability[243]. Third, droplet-generating microfluidic systems can suffer operational difficulties, such as clogging, and are generally relatively low throughput, which limits the number of samples that can be analyzed[244]. Further, they require careful cleaning or replacement which is expensive and

time-consuming[245]. Finally, material exchange and cross contamination between droplets can be significant, which is highly problematic for accurate quantitation[246].

Due to the above difficulties, and in the context of IVDs, it is preferable to decouple the complexity of the droplet synthesis from the IVD device itself, thus opening up the possibility of cheap but high-performance assays/devices that can be deployed at the point-of-care or in resource-limited settings. The work presented in this chapter directly addresses this challenge.

Recently, the Abate group reported a microfluidic-free technique using hydrogel particles to perform dPCR and cell culture[218]. By generating hydrogel beads and removing excess solution, DNA templates or cells could diffuse into the hydrogel structure, before being encapsulated within an oil phase prior to incubation. For NAATs, the limit of (template DNA) detection achieved was 10^2 copies/μL. However, despite the fact that detection of yeast and Lamda virus DNA was achieved, the approach is expensive (requiring Taqman probes), requires a dedicated thermocycler and requires at least 2 hours of operation time, which limits field deployability. To address these problems, we leveraged polyacrylamide hydrogels generated via step-emulsification[194, 247, 248]. Such an approach results in millions of monodisperse and stable hydrogel beads formed by cross-linking. These beads exhibit excellent stability over time and during handling, and importantly can be readily be used to run several reactions in parallel (in multiple wells and/or with multiple reporter dyes), which is very challenging in systems incoprorating 'live' droplet generation. Furthermore, such hydrogel beads can be readily imaged after the amplification process via single-colour fluorescence imaging, or even using a smartphone camera[239].

In the development of the assay reported in this chapter, we targeted the detection of Methicillin-resistant *Staphylococcus aureus* (MRSA) as a model system. Antimicrobial resistance (AMR) in bacterial infections kills more than seven hundred thousand people per year; a number predicted to rise to ten million by 2050[249]. Thus, rapid, simple, and effective detection, in particular in hospitals and health centers, is necessary[250]. The World Health Organization (WHO) has emphasized the importance of controlling infections on the front line through the provision of appropriate IVDs for rapid AMR detection[251]. Motivated by this importance, we chose to target methicillin-resistant *Staphylococcus aureus* (MRSA), the most prevalent AMR pathogen, which poses a formidable risk with persistently high morbidity and mortality[252-254].

Bacterial cell culture is the current gold-standard method to detect AMR[255]. However, this process is laborious and time-consuming, typically requiring days from sampling to result[256]. Moroever, contamination with exogenous bacteria is common, the true-positive rate is low and differentiation of bacteria at the level of strains and species is poor[13]. In contrast, targeting the direct detection of the bacterial genetic material in clinical samples using NAATs can facilitate the development of rapid and versatile IVDs that can be readily adapted to new targets[9, 233, 257].

Herein, we report a hydrogel microparticle-templated NAAT system for the detection of MRSA using loop-mediated isothermal amplification (LAMP), an isothermal NAAT that is commonly leveraged for point-of-care diagnostics[89]. LAMP is known to offer highly robust, sensitive and specific amplification of target NAs, and benefits from an isothermal and energy-efficient assay procedure. Although LAMP has been developed in a number of a

droplet-based platforms (dLAMP)[111, 258], it has yet to be successfully demonstrated in hydrogel bead-based assays. We term our assay H-LAMP, and demonstrate that it can detect the *mecA* gene of MRSA down to 1000 copies/µL within 30 minutes. Further, the developed system I s shown to be highly selective for MRSA against MSSA and other common bacteria.

4.2. Materials and Methods

4.2.1. Chemicals

All chemicals were analytical grade and used as received. Acrylamide, N,N′-methylenebis(acrylamide), ammonium persulfate, trichloro-(1H,1H,2H,2H-perfluorooctyl) silane, Triton-X100, perfluoro-1-octanol, NaCl, Ethylenediaminetetraacetic acid (EDTA), KCl, Tris-buffer (pH 8.0), tetramethylethylenediamine, Novel Juice dye, Dulbecco's phosphate-buffered saline (DPBS, 1x) and SYBR Green I (10'000x) were purchased from Sigma Aldrich (Buchs, Switzerland). Diamond dye was purchased from Promega (Dübendorf, Switzerland). PFPE-PEG surfactant (008-Fluorosurfactant) was purchased from Ran Biotechnologies (Beverly, USA) and used with Novec HFE-7500 fluorinated oil (St. Paul, USA). Fluorescein isothiocyanate (FITC) was purchased from Thermo Fisher Scientific (Basel, Switzerland). All aqueous-based solutions except LAMP solution were prepared using ultrapure water from a Millipore Synergy water purification system 18 Ω (Darmstadt, Germany).

4.2.2. Biological samples and reagents

For LAMP, the *mecA* gene—located in the SCCmec region found in all MRSA strains—was chosen as the target[259]. LAMP and PCR primers were designed based on a 685 bp *mecA* gene sequence, obtained from the NCBI database and analyzed using the program MEGA 7.0.26.

The *mecA* sequence used in this work was amplified from the MRSA Newman strain using PCR primers, as shown in **Table 4.1**. The PCR products were quantified using a Nanodrop 2000 (Thermo Fisher Scientific, Reinach, Switzerland).

The LAMP reaction was performed following a standard methodology[260], which required 0.8 µM of the two outer primers (F3 and B3) for strand displacement during the non-cyclic step, and 1.6 µM of the inner primers (FIB and BIP) for both the sense and the antisense sequence, which helps in loop formation. Further, two additional primers (LF and LB) were added (to 1.6 µM) to accelerate the reaction, thus reducing the required incubation time. All LAMP solutions were prepared using DNase and RNase free water (Thermo Fisher Scientific, Reinach, Switzerland). Optimal concentrations of Bst polymerase, $MgSO_4$, betaine, and dNTPs were found to be 100 U/mL (5 units per reaction), 10 mM, 1 M, and 1 mM, respectively. To obtain quantitative results from the tube-based LAMP reaction (at 58 °C), C_T values (time at which the amplification curve reaches one-third of its maximum value), were plotted against the obtained signal to acquire the calibration curve, using a QuantStudio™ 5 Real-Time PCR System (Thermo Fisher Scientific, Reinach, Switzerland). The PCR reaction was carried out as follows: 12.5 µL Go Taq® Hot Start Green Master Mix, 2.5 µL of both the LF and LB primers, 1 µL of MRSA lysate, and 6.5 µL RNase/DNase free water. The amplification process was initiated by heating at 95°C for 2 minutes, followed by 30 cycles of denaturation at 95°C for 30 seconds, annealing at 55°C for 30 seconds, and extension at 72°C for 1 minute. The final extension was applied at 72°C for 5 minutes before storing at 4°C. For assay development, the PCR product was used as the target, as it contains the *mecA* gene sequence. For bacterial lysate testing, H-LAMP responding to the native *mecA*

sequence in the bacterial genome. The following sequences were used for the H-LAMP and PCR assay (**Table 4.1**) and concentration of each components of LAMP assay (**Table 4.2**).

Table 4.1. LAMP and PCR primers sets for *mecA* amplification.

Reaction	Name	Oligonucleotide
	FIB	5' ACCTAATAGATGTGAAGTCGCTTTTTTCATCTTACAACTAATGAAACAGAA 3'
	BIP	5' TATGTTGGTCCCATTAACTCTGAAGTCCCTTTTTACCAATAACTGCA 3'
LAMP	LF	5' TTCTAGAGGATAGTTACGACT 3'
	LB	5' CAAAAAGAATATAAAGGCTATAA 3'
	F3	5' GATGAATATTTAAGWGATTTCGC 3'
	B3	5' TGGAGCTT TTTATCGTAAAGTT 3'
PCR	Forward	5' AGATTGGGATCATAGCGTCAT 3'
	Backward	5' TTGAGGGTGGATAGCAGTACC 3'

Table 4.2. The concentration of each components of LAMP method

Components	Final amount for 3 reactions
FIP and BIP (20 mM)	2 µL each
F3 and B3 (10 mM)	1 µL each
LF and LB (20 mM)	1.5 µL each
Betaine	5 µL
dNTPs (10 mM)	4 µL
Polymerase buffer (5X)	3 µL
SYBR green (1/5000)	1 µL
DNase/RNase free water	2 µL
Target DNA	4 µL
Bst Polymerase (8,000 unit/mL)	1 µL
Total	30 µL

4.2.3. Microfluidic device design and fabrication

Microfluidic channel patterns were designed using AutoCAD 2017 (Autodesk, San Rafael, CA, USA) and printed onto a 177 µm thick fine grain transparency film (Micro Lithography Services Ltd, Chelmsford, UK). Master molds were fabricated using standard photolithography techniques. Our step emulsification device consists of two layers: the nozzle layer being approximately of 20 µm thick, and a step layer approximately 250 µm thick. A degassed 10:1 mixture of polydimethylsiloxane (PDMS) monomer and curing agent (Sylgard 184, Dow Corning, Midland, MI, USA) was poured over the master mold and peeled off after polymerization at 70°C for 4 hours. Inlet and outlet ports were created using a hole-puncher (Technical Innovations, West Palm Beach, FL, USA). The structured PDMS substrate

was bonded to a 1 mm thick glass substrate (Menzel-Glaser, Manheim am Rhein, Germany) after treating both surfaces in an oxygen plasma (EMITECH K1000X, Quorum Technologies, Lewes, UK) for 60 seconds. The step emulsification channel was also treated with an HFE 7500-based solution containing 1% (v/v) trichloro-(1H,1H,2H,2H-perfluorooctyl) silane for 10 minutes, and then rinsed with 100 µL of the HFE 7500 oil. This procedure generates a stable hydrophobic surface. At this point, the step emulsification device was ready to use for water-in-oil droplet formation.

4.2.4. Polyacrylamide hydrogel bead preparation

The acrylamide precursor solution was prepared according to the protocol developed by Hatori and co-workers[218]. Briefly, a solution containing 7% acrylamide, 0.2% N,N′-methylenebis(acrylamide) and 0.3% ammonium persulfate was mixed in a micromixer and used as the aqueous phase. The HFE-7500 oil containing 2% (w/w) PFPE-PEG surfactant, and supplemented with 1% TEMED was used as the oil phase. Low-pressure dosing modules (neMESYS, Cetoni GmbH, Korbussen, Germany) were used to feed in precursor solutions from 1 mL gastight syringes (Hamilton Bonaduz AG, Bonaduz, Switzerland) through 0.33 mm i.d. Tygon tubing (Cole Palmer, Hanwell, UK) and into the inlets of the microfluidic device (**Figure 4.1**). Water-in-oil droplets with mean diameter of approximately 75 µm were generated and monitored via bright-field microscopy. Droplets were collected and incubated on a heat block at 65°C for 12 hours to allow the polymerization process to proceed. Excess oil from the bottom of the emulsion reservoir was extracted and replaced with an equal volume of perfluoro-1-octanol to solubilize the surfactant layer. Subsequently, the monodisperse polyacrylamide (PAA) hydrogel microbeads were washed several times with

washing buffer, according to procedure of Abate and co-workers[218, 244], and finally redispersed in 0.5% Triton-X100,DNase/RNase free water (Invitrogen, California, USA). They were stored for at 4°C until further use.

4.2.5. MRSA assay procedure

A 30 µL solution containing pelleted PAA particles was mixed with 30 µL of LAMP master mix (making a total volume of 60 µL), then incubated at room temperature for 15 minutes to allow the LAMP reagents to diffuse into the PAA beads. Excess solution was carefully removed from the upper layer. To compartmentalize the LAMP-primed PAA beads in oil, 100 µL of HFE-7500 oil containing 5% (w/w) PFPE-PEG surfactant was added into the tube containing the hydrogel microbeads, and the whole mixture was vortexed. The microbeads were then incubated at 60°C for 60 minutes (and monitored in a real time-PCR machine when required), then 20 µL of the solution was pipetted onto a glass side in order to obtain a monolayer of well-ordered beads. The slides were then imaged by fluorescence microscopy using an inverted Eclipse Ti-E microscope (Nikon, Zürich, Switzerland) equipped with an IDT high-speed camera (Motion Pro Y5.1, Niederoenz, Switzerland) and an ORCA-flash 4.0 CMOS camera (Hamamatsu, Solothurn, Switzerland). Fluorescence imaging was performed using two different objective lenses, i.e. a 20x 0.45 NA, and Plano N 10x NA. Collected images were then analyzed using ImageJ (U.S. National Institutes of Health, Bethesda, MD, USA), by counting bright beads as the positive and dim beads as negative, to quantify the *mecA* target. Bright-field imaging of the hydrogel beads was performed using the high-speed camera, with plasma light source illumination (HPLS200 series Thorlabs, Newton, NJ, USA) and a 20x 0.45

NA S Plan Fluor objective (Nikon, Zürich, Switzerland). 0.25 objective (Olympus, Tokyo, Japan).

4.2.5. Selectivity study

MRSA (*Staphylococcus aureus* USA300 JE2; source: Annelies Zinkernagel, Division of Infectious Diseases and Hospital Epidemiology, University Hospital Zurich, University of Zurich, Zurich, Switzerland; properties: methicillin-resistant *S. aureus*), E. coli (*Escherichia coli* JM109; source: Stratagene, San Diego, CA, USA; properties: *E. coli* lab strain, non-pathogenic), *E. faecalis* (*Enterococcus faecalis* ATCC 19433; source: ATCC 19433; properties: type strain), *L. monocytogenes* (*Listeria monocytogenes* Scott A; source: Weihenstephan Listeria Collection; properties: clinical isolate, serovar 4b), *S. epidermidis* (*Staphylococcus epidermidis* MP04; source: Max Paape, ARS, USDA, Beltsville, MD, USA; properties: bovine mastitis isolate) and methicillin-sensitive *S. aureus* (MSSA)(*Staphylococcus aureus* Newman; source: NCTC 8178, Annelies Zinkernagel, Division of Infectious Diseases and Hospital Epidemiology, University Hospital Zurich, University of Zurich, Zurich, Switzerland) were obtained from Institute of Food, Nutrition and Health, ETH Zurich, Switzerland. Bacterial colonies were collected and lysed in TE buffer (Fischer Scientific, Reinach, Switzerland) at 95°C for 5 minutes. Then 1 µL of the lysate was added to the hydrogel with the LAMP master mix, before proceeding with the amplification reaction and readout.

4.3. Results and Discussion

4.3.1. PAA hydrogel characterization

We chose to synthesize the hydrogel microbeads using an acrylamide monomer. These are known to be excellent hosts for the compartmentalization of biochemical reactions[261,27], and demonstrate exceptional stability compared to standard droplets, which tend to rupture or coalesce under either mechanical shear or thermal instability.

To perform high-throughput droplet generation, a radial nozzle array consisting of 200 channels was employed (**Figure 4.1 a**). Oil was flowed into the main channel at a flow rate of 80 µL/min, and the aqueous solution at 60 µL/min, into the mixing channel (**Figure 4.1 b**). The microfluidic step emulsification device enables production of monodisperse emulsions at a throughput of up to 15 mL/h. In the synthesis of PAA hydrogel beads, the monomers and initiators were prepared in separate glass syringes to avoid pre-polymerization of the PAA and clogging of the syringes. Due to the low Reynolds number environment within the microfluidic channels, it can be challenging to mix monomers and initiators on short timescales[262, 263]. Accordingly, we included a dedicated micromixer section in the microfluidic path. This is highly beneficial, as it provides not only excellent mixing but also allows efficient heat transfer, preventing polymerization within the micromixer.

The micromixer design was based on a tesla micromixer reported by Wang and co-workers[228, 229]. Here, the asymmetric shape enhances mixing efficiencies at low Capillary and low Reynold numbers. The specific structure of the mixer causes chaotic flow by collision of the fluid streams on redirection, which significantly improves mixing. The mixing performance of the micromixer was assessed by dilution of 100 µM fluorescein

isothiocyanate (FITC) in Dulbecco's phosphate-buffered saline, with mixing being monitored by fluorescence microscopy. FITC was injected into the central inlet, and water through the two out inlets (**Figure 4.1 b**). Immediately after the inlet junction, the fluorescence signal exhibits a step function, with the maximum intensity in the center of the channel where the fluorescent FITC stream flows in a laminar manner between the non-fluorescent water streams, **Figure 4.1 b(1)**. As the solution flows through the micromixer, fluorescence deceases at the center of the channel and increases at the edges, as the FITC is diluted into the water. Here, the solution interfaces increase in an exponential fashion (**Figure 4.1 b(2–4)**). Mixing can be judged as 100% if the transverse fluorescence profile across the channel is essentially flat. After the fifth mixing unit, mixing performance was estimated to be 90% (**Figure 4.1 b(5)**), which was deemed to be sufficient in the current device.

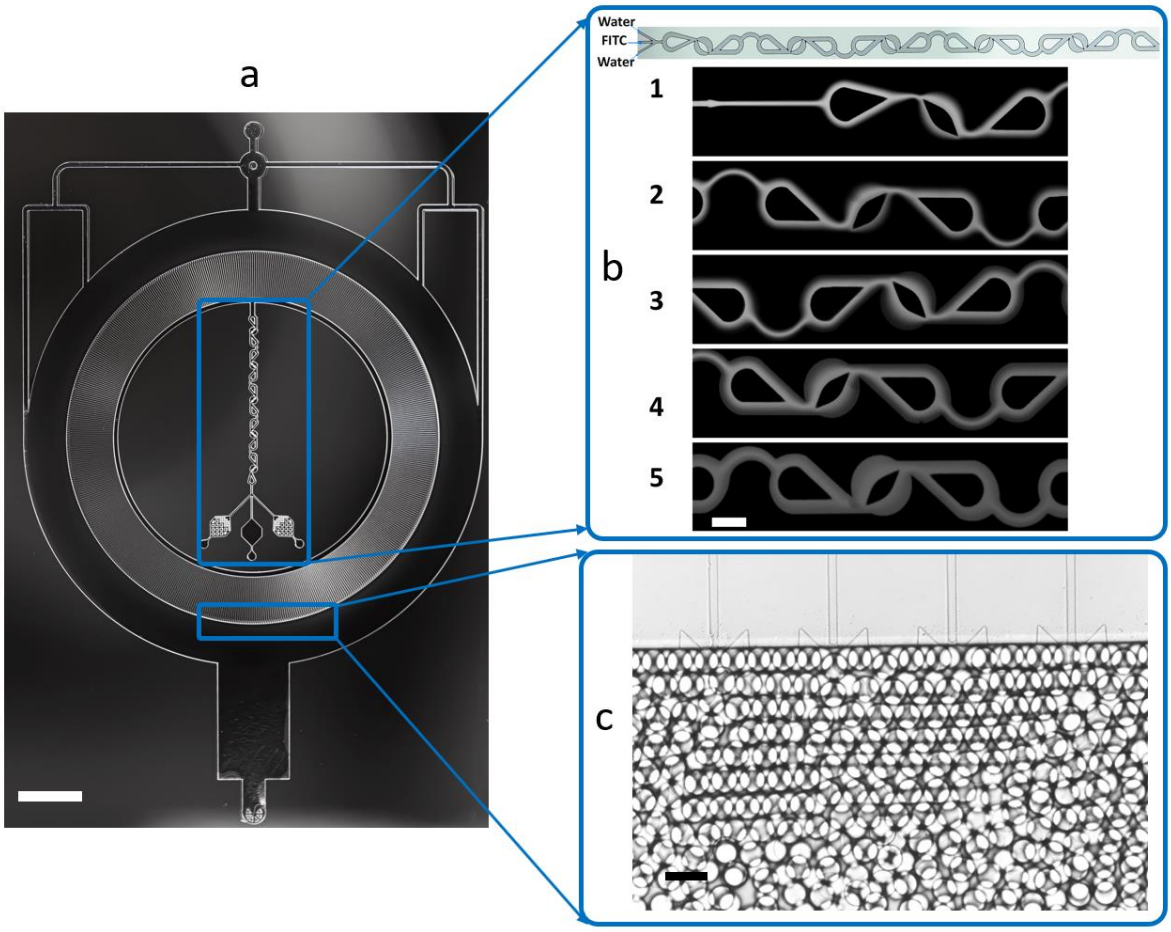

Figure 4.1. The custom-designed step emulsification device. (a) The master mold (SU8 on silicon). Scale bar 2 mm. (b) The tesla-inspired passive micromixer integrated prior to the radial nozzle array, showing the design (upper image) and fluorescence analysis (lower images 1–5). Scale bar 200 µm. (c) Bright field image of the nozzle array, showing the production of monodisperse droplets. Scale bar 100 µm.

After exiting the micromixer, the mixed monomer solution then flowed along the main aqueous channel toward the nozzles, rapidly generating droplets of the pre-polymer solution. Through use of step-emulsification, monodisperse water-in-oil droplets were obtained. The aqueous droplets were collected and incubated on a heat block at 65°C for 12 hours for the polymerization process to proceed. Excess oil was removed by three cycles of

centrifugation, washing with buffer (following the protocol of Demaree and co-workers[244]), and the obtained polymerized beads were stored at 4 °C before use. The beads were highly stable under storage. **Figure 4.2** shows the beads imaged by bright field microscopy, when freshly prepared (**Figure 4.2 a**) and after 120 days in storage (**Figure 4.2 b**). The freshly prepared beads were measured to have a mean diameter of 72 ± 4.5 μm ($n = 400$), with a very narrow size distribution (**Figure 4.2 c**), demonstrating their high stability and low polydispersity. Uniformity of microbead size is crucial for application in NAATs, and we show here that our step emulsification approach provides an excellent means of producing such beads via high-throughput droplet generation.

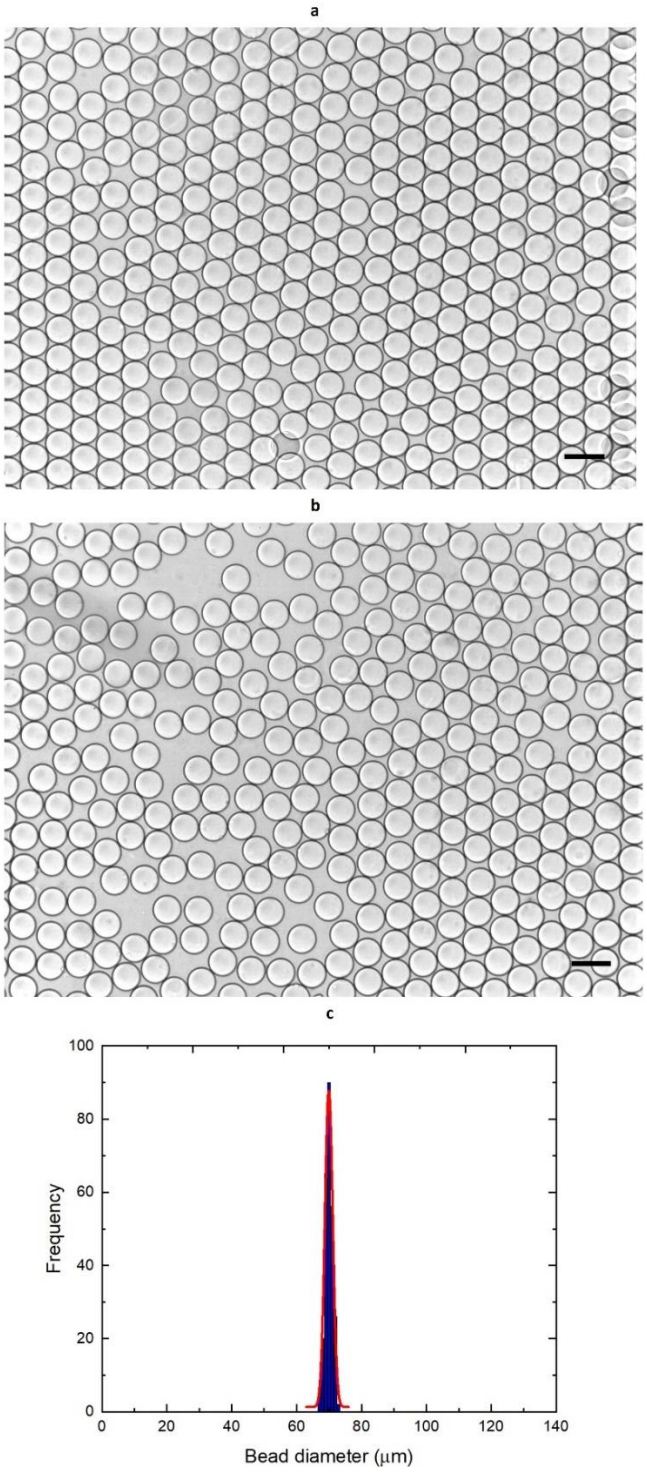

Figure 4.2. Image of PAA microgels (a) freshly prepared and (b) after being stored for 120 days at 4°C prior to analysis. Scale bar 100 μm. (c) Histogram of the bead size distribution.

4.3.2. H-LAMP characterization

LAMP reagents and primers were used as detailed in the work of Suea-Ngam and co-workers[260]. Briefly, to test the system and provide a reference reaction for H-LAMP development, we performed a tube-based LAMP reaction for the detection of *mecA*, with incubation at 60°C for 30 minutes. Next, the amplified LAMP products were mixed with Novel Juice dye, before loading into a 2% agarose gel with Diamond dye, to allow visual product monitoring. **Figure 4.3** shows an electropherogram of the LAMP reaction products, which confirmed successful and sensitive amplification of *mecA*, and showed that the designed LAMP protocol was able to detect *mecA* down to 1 fg/µL within 30 minutes, additionally demonstrating the ultra-sensitive detection capability of our LAMP assay in its bulk form.

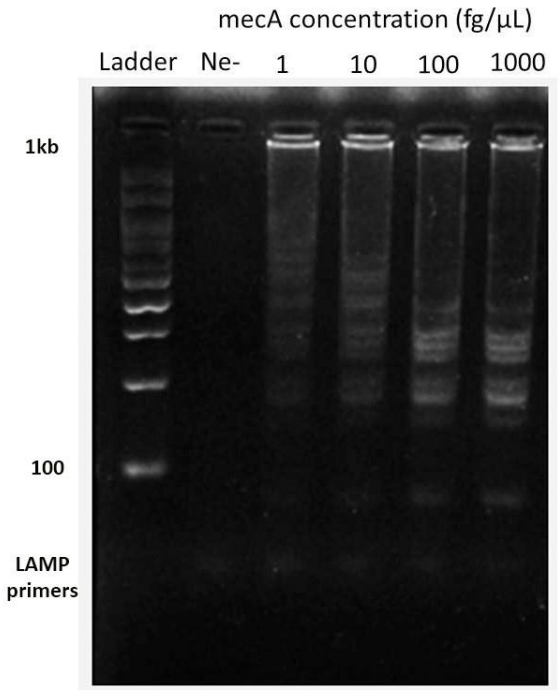

Figure 4.3. Agarose gel electropherogram, showing LAMP reaction products at different concentrations of the *mecA* gene (1, 10, 100, 1000 fg/µL), with a negative control (Ne-).

Next, we tested the LAMP reaction with the previously synthesized PAA microbeads. Here, 30 µL of washed microbeads were added into 27 µL of the LAMP master mix, containing 1 µL of DNA template. This was incubated for 15 minutes, before adding 1 µL of 1x SYBR green and 1 µL of the polymerase. Then the solution was compartmentalized by adding 100 µL of the HFE-7500 oil with 5% PFPE-PEG surfactant, and then vortexed for 30 seconds. For the negative control, the DNA template solution was replaced by DNase/RNase free water. After vortexing, the compartmentalized PAA beads were incubated in either a real-time PCR machine, or on a hot plate at 60°C to allow the LAMP reaction to proceed. A fluorescence image of the beads after incubation with a 1000 pg/µL *mecA* sample is shown in **Figure 4.4a**. The brightly fluorescent beads indicate that in these particles, amplification of the dsDNA target by LAMP has been successful, and that the SYBR green dye has bound to the reaction product, yielding the fluorescent signal. Conversely, in the negative control (**Figure 4.4 b**), the beads remained non-fluorescent, indicating that amplification had not occurred in the absence of *mecA*. The corresponding real-time amplification curves are shown in **Figure 4.4 c**.

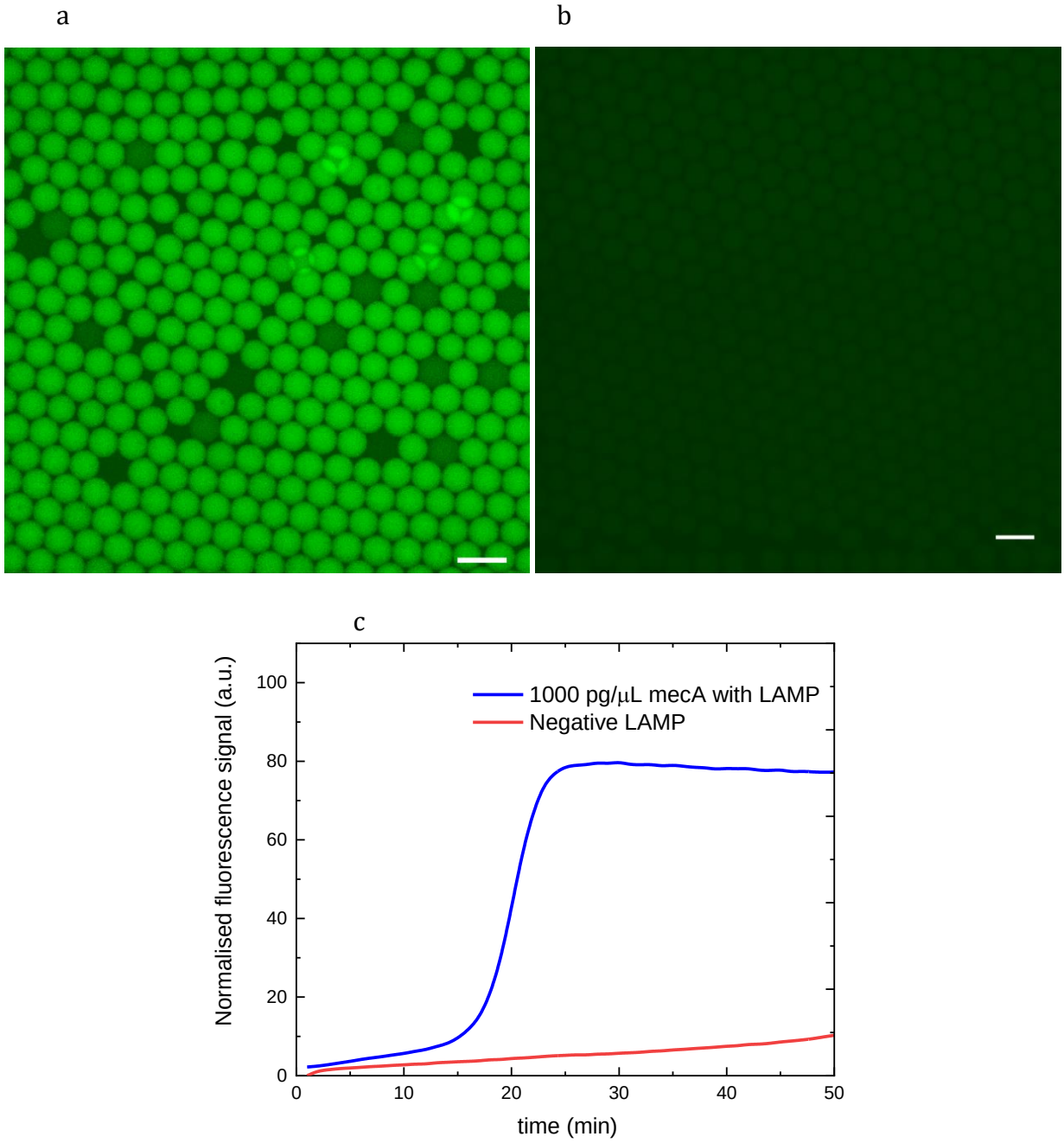

Figure 4.4. Fluorescence images of (a) positive (1000 pg/µL *mecA* sample) and (b) negative (0 pg/µL *mecA* sample) H-LAMP reaction, incubated at 60°C for 60 minutes. Scale bar 150 µm. c) Variation of fluorescence as a function of time for samples in (a) and (b).

4.3.3. DNA quantitation with H-LAMP

The primary aim of the current study was to enable rapid and simple droplet-based LAMP (dLAMP) by removing the microfluidic system as part of the assay process; as required in other digital droplet approaches. Instead, the PAA hydrogel beads can be made in large batches and stored for long periods of time prior to use. To demonstrate this possibility, we incubated different concentrations of our target molecule (from 10^{-3} to 10^{3} pg/μL *mecA* gene) with the microbeads and compartmentalized them with oil. Just as in standard microfluidic dLAMP, increasing the target concentration increases the relative number of fluorescent droplets. Accordingly, the ratio of 'on' to 'off' beads can be related to the concentration of target in the sample.

Real-time fluorescence monitoring was used to analyze the H-LAMP reaction with varying target concentrations (**Figure 4.5**). After encapsulation of the LAMP mastermix and *mecA* target in the PAA hydrogel beads, samples were placed in a real-time PCR machine. The C_T value of the LAMP amplicon production (the time taken for the fluorescent signal to cross the one-third threshold of the final plateau value) was plotted against the *mecA* concentration in order to derive a calibration curve. **Figure 4.5 a** shows that the reaction ran successfully. A significant fluorescence signal developed for the samples in the range 1–1000 pg/μL within 30 minutes, but the lower concentration samples required a longer incubation time. Accordingly, a final assay time of 70 minutes was chosen for the H-LAMP assay.

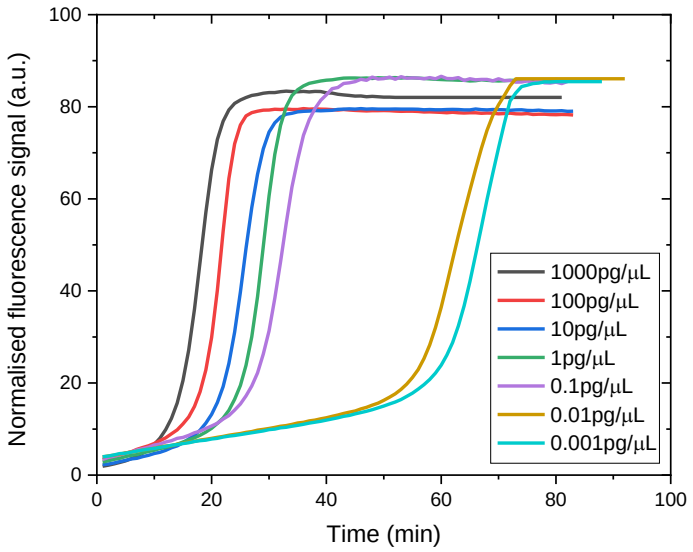

Figure 4.5. Time-dependence fluorometric signal reactions with different concentrations of 0.001, 0.01, 0.1, 1, 10, 100, 1000 pg/μL mecA target.

Next, we analyzed the fluorescence images of the H-LAMP beads of different *mecA* sample concentrations in order to derive a calibration curve directly from the on/off bead counting process. **Figure 4.6** shows the images of bead monolayers resulting from eight different concentrations of the *mecA* gene (10^{-3}–10^{3} pg/μL), after encapsulation in the PAA beads and amplification by LAMP. It can be observed that an increasing concentration of target leads to an increasing proportion of bright beads. To relate this proportion to the amplicon concentration, positive beads were counted and compared to the total number of beads in one frame, using the following equation:

$$R_B(\%) = N_B / N_T \times 100\% \quad (4.1)$$

where R_B is the proportion of positive versus negative beads, N_B is the number of positive beads per image (i.e. those containing LAMP product), and N_T is the total number of beads per image.

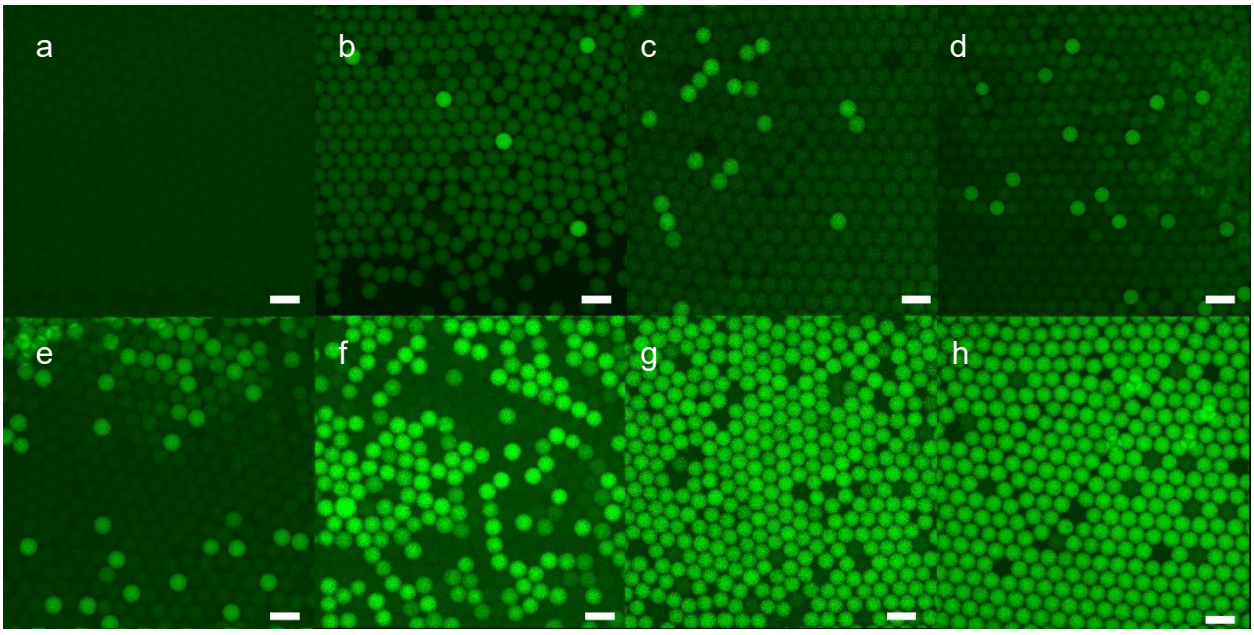

Figure 4.6. Fluorescence images of the bead monolayers in an observation channel for (a) the non-template control, and (b–h) the tested concentrations of 0.001, 0.01, 0.1, 1, 10, 100, 1000 pg/μL *mecA* target, respectively (representative cropped image sections). Scale bar 150 μm.

We analyzed droplets using the open-source Cell Profiler (CP) software and its companion Cell Profiler Analyst (CPA)[264]. CP is used to identify droplets or beads and measure their relative fluorescence intensity, and well-suited to the analysis of quantitative data from digital droplet assays comprising many thousands of droplets. We imported hydrogel bead images in TIF format into the CP "Images" module. Next, we used the "IdentifyPrimaryObject" module to find objects of interest (in this case hydrogel beads) within the images. All features with diameters exceeding a user-defined threshold (100 μm in most experiments) or touching the border of the image are discarded. Then the "MeasureObjectIntensity" module is used to measure the pixel intensity of the selected objects, with "positive" beads being those having an intensity above a user-defined threshold. The image analysis pipeline, along with raw and processed images are presented in **Figure 4.7**. As can be seen in **Figure 4.7c**, all the beads with a fluorescence intensity value above the threshold have markings around

them. Those that are within the correct diameter range are marked with a green outline, with beads having a yellow outline being discarded.

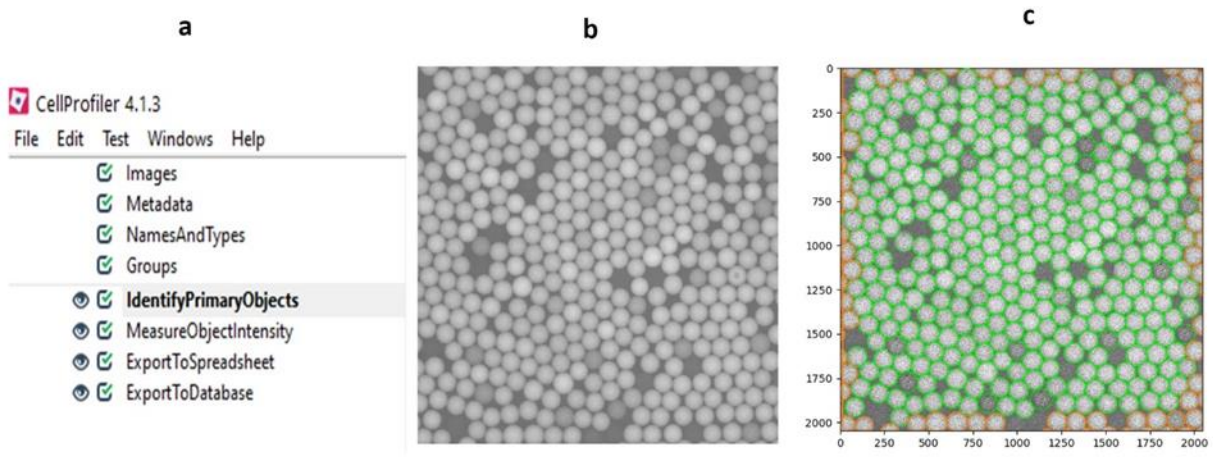

Figure 4.7. Image analysis with CellProfiler. (a) Overview of CellProfiler pipeline used for analyzing beads images. (b) Original image. (c) Beads outlines.

The data are then exported as a csv file to allow additional analysis in Matlab using the "ExportToSpreadsheet" module. The SQLite database was used to visualize the mean fluorescence intensity units of beads via the CPA histogram tool (**Figure 4.8**), with the data generated by the CP pipeline being used to calculate the number of positive fluorescent beads.

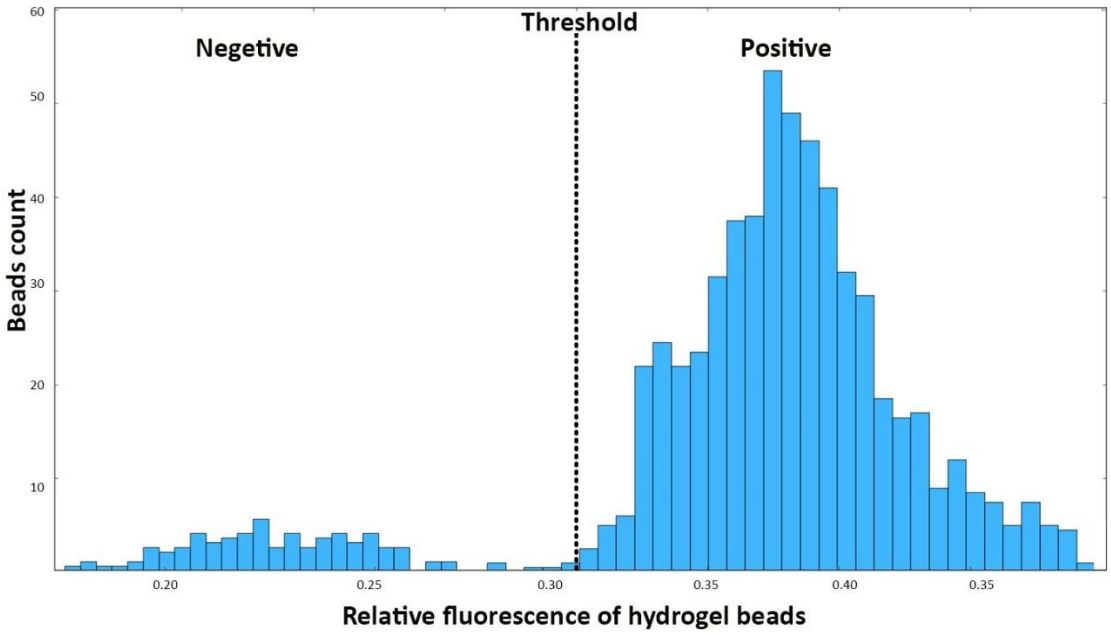

Figure 4.8. Bead intensity histogram generated by the "Density Plot" tool in CPA. Positive and negative beads can be clearly distinguished by using the threshold.

Figure 4.9 a shows a calibration curve of R_B versus *mecA* concentration (10^{-3} and 10^{4} pg/µL), with linearity between 10^{-1} to 10^{2} pg/µL (R^2= 0.983). The limit of detection (LOD) was determined (based on serial dilution experiment) to be 1 fg/µL (~1000 copies/µL) of *mecA* (at ca. 700 bp), which exhibits R_B value of 5%.

To validate the accuracy of the H-LAMP method, the gold-standard method (PCR) was used as a comparison. A concentration series of the *mecA* target (1 to 10^{2} pg/µL) was assessed using each method (N=3), yielding a coefficient of determination (R^2) of 0.979 when plotted against one-another (**Figure 4.9 b**). There was no significant difference between the two methods (t-value = 0.70, < t-critical = 1.85, α= 0.05, 95% confidence, N = 9), suggesting excellent agreement between H-LAMP and PCR.

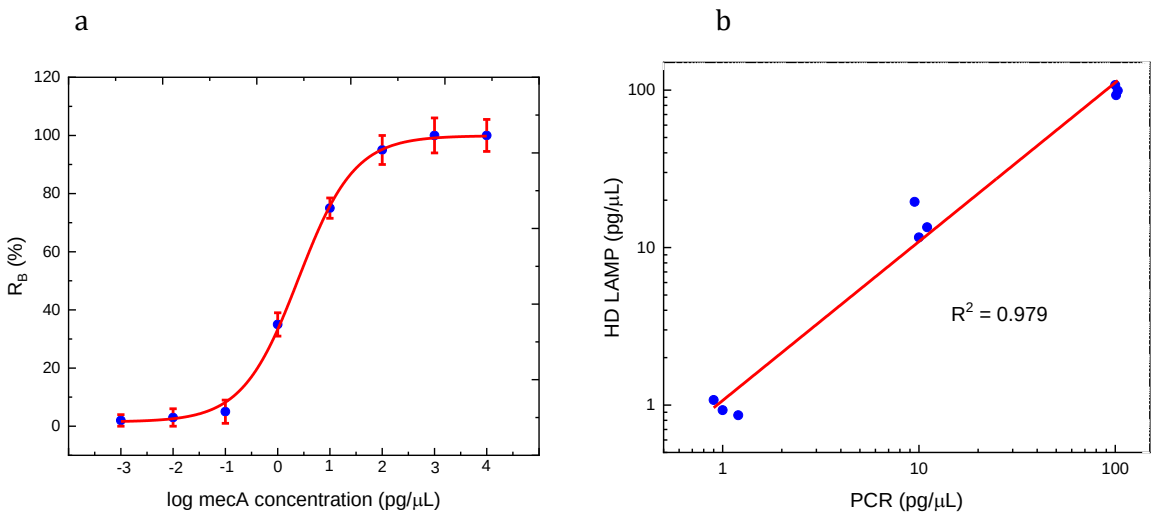

Figure 4.9. (a) The calibration curve of the H-LAMP assay. b) An accuracy test comparing DNA amplification results (N = 3) of tube-based PCR tube and the H-LAMP system, detecting *mecA* in the range 1 to 100 pg/μL.

4.3.4. Bacterial lysate and selectivity testing

Next, we conducted experiments to determine if the assay would work with a complex sample, such as a bacterial lysate, and could directly detect the native *mecA* gene in the MRSA genome. Accordingly, the LAMP master mix was used to detect MRSA (USA-300) bacteria against other common bacteria, including *E. coli*, *E. faecalis*, *L. monocytogenes*, *S. epidermidis* and *S. aureus* (see Materials and Methods for details). To obtain the lysates, bacterial colonies were collected and lysed in TE buffer at 95°C for 5 minutes. Then 1 μL of the lysate was added to the LAMP-hydrogel working solution before proceeding with the amplification reaction and readout. Results revealed excellent selectivity for the target *mecA* gene (**Figure 4.10 a**), with a positive result for MRSA, and a negative result for all other bacteria. In summary, we observed that H-LAMP can be applied for gene detection in real bacterial lysate samples, and that it achieves an excellent level of specificity.

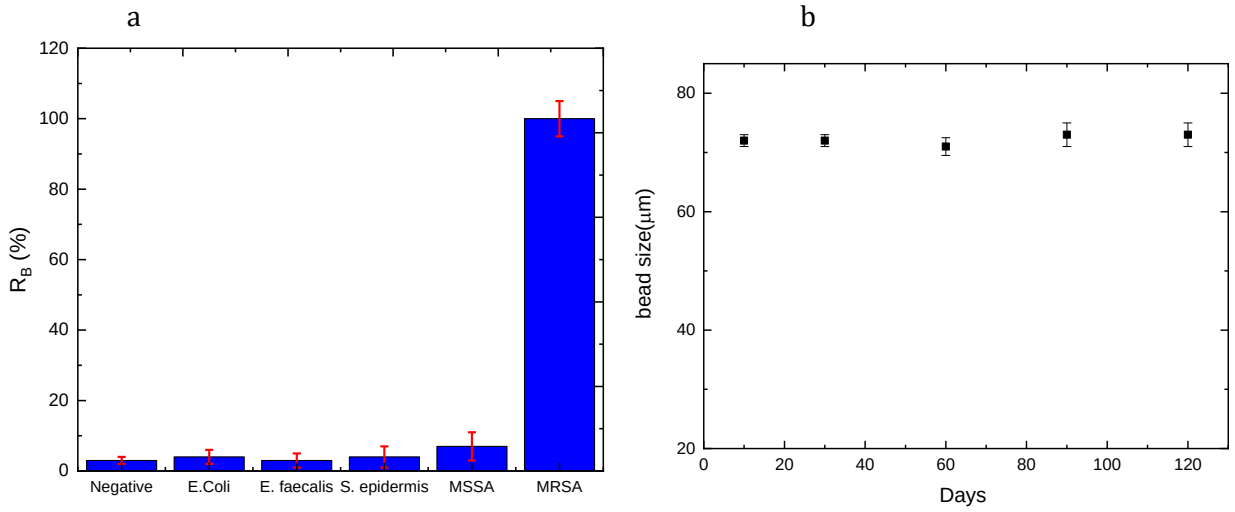

Figure 4.10. (a) Selectivity study of H-LAMP. (b) Size stability test of the hydrogel beads over 120 days.

4.3.5. Stability of the hydrogel microbeads

For almost all real-world applications, it is critical that the PAA hydrogel microbeads are stable for long periods before use. Accordingly, we assessed the stability of the hydrogel beads during storage over a period of 120 days at 4°C in washing buffer. **Figure 4.10 b** shows that there was no significant change in the mean bead diameter and size distribution over the testing period, confirming high storage stability. This observation is agreement with Hatori and co-workers [244], who showed that their hydrogel particles could be stored for up to a year without any change in particle integrity. We therefore note the promise of these PAA hydrogel beads for deployment in real healthcare applications, for example in field-deployable diagnostics.

4.4. Conclusions

Loop-mediated isothermal amplification was successfully conducted using a PAA hydrogel microbead-based compartmentalization approach (H-LAMP) to detect the antibiotic-resistant bacteria MRSA. A microfluidic device, that included a custom-designed micromixer for rapid mixing, was used to form droplets by step emulsification. High-throughput was achieved by step-emulsification generation of monodispersed droplets (up to 15 mL/h), and finally PAA hydrogel microbeads after cross-linking polymerization of polyacrylamide. These beads were then used to compartmentalize a LAMP reaction by simple vortexing of the master mix with the beads in oil. Target quantification was demonstrated by simple counting of fluorescent versus non-fluorescent beads using fluorescence imaging. The process yielded linearity between 10^{-1} and 10^{2} pg/μL ($R^2 = 0.997$), with a limit of detection down to 1 fg/μL (1000 copies/μL). Our H-LAMP technique showed excellent selectivity in the detection of MRSA versus other common bacteria, including *E. coli*, *E. faecalis*, *L. monocytogenes*, *S. epidermidis*, and *S. aureus*. Finally, comparison with PCR showed no significant difference for quantification of the *mecA* gene.

The ultimate goal of the work performed herein was to provide a system whereby PAA hydrogel beads could be stored and then supplied to an end user to use in their own NAAT assay. We have proved that such a concept works in conjunction with LAMP, which confers the significant benefit of high sensitivity, selectivity, and isothermal temperature. The relatively large size of the hydrogel beads synthesized in this work (72 ± 4.5 μm) ultimately proved a limitation in sensitivity. However, we believe that in future work it would be possible to synthesize smaller hydrogel beads, which should decrease the limit of detection

and possibly allow single-molecule-per-bead detection, and therefore true digital NAAT assays.

Overall, we believe we have successfully demonstrated the utility of step-emulsification for producing hydrogel microbeads for use in NAATs. Our developed H-LAMP assay is simple, low-cost, and easily disposable, and possesses the potential to run several reactions in parallel using multiple sample reservoirs and/or dyes. It is likely to provide an excellent platform to allow end-users to run 'microfluidic' LAMP assays without the expertise or equipment requirements of traditional droplet-based NAAT approaches. We feel that, by combining this development with the merging area of 'mobile health' (m-Health), a truly impactful assay for point-of-care or resource-limited settings could be produced in the near future.

Chapter 5

5.1. Conclusions and perspectives

The overarching goal of this thesaural work was to develop novel and powerful microfluidic platforms for the accurate detection and analysis of pathogens. More specifically, studies focused on developing a microfluidic sample preparation module for high-throughput flow cytometric detection of bacteria in water sample and the implementation of a field deployable nucleic acid amplification system that leverages the unique features of droplet-based microfluidics.

The first part of the thesis describes the creation of a miniaturized and automated sample preparation platform that seamlessly interfaces with the optical module of a portable commercial flow cytometer. The integrated system is able, for the first time, to perform fully automated and high-throughput analysis of microbial species in drinking and lake water samples. The utility of the platform as a valuable tool in the water treatment industry is confirmed through the quantitative analysis of contaminated lake water samples on timescales of less than 30 minutes. Compare to plating techniques that utilize a significant amount of material, are tedious, labour intensive, and take a long time to provide results, our method provides fast and precise analysis of bacterial populations in drinking water.

The second part of the thesis describes the development of a microfabricated step emulsification device for the high-throughput generation of monodisperse droplet populations that can be used as templates for the production of functional microparticles and as vehicles for single cell encapsulation experiments. As a proof-of-concept, we used this system to produce large quantities of monodisperse PAA hydrogel and PLGA microparticles

on short timescales. Importantly, the high-throughput production of microparticles with high level of structural control was made possible by exploiting of a micromixer integrated within in the microfluidic device (which facilitated efficient mixing of reagents required for as specific reaction) prior to droplet formation. Moreover, since the microfluidic device is able to create both water-in-oil or oil-in-water emulsions, it can be used in the production of a broad variety of polymer microparticles that in turn can be applied to relevant problems in the fields of macromolecular delivery, food processing and hazardous material handling.

Effective diagnostic tools that are quantitative and operate in out-of-laboratory environments are urgently needed to treat and limit the spread of infectious diseases. In this regard, the ability to target the genetic material of pathogens in clinical samples using nucleic acid amplification tests enables the development of adaptable diagnostic tools that can be repurposed for user-defined targets; for example, during epidemics and pandemics. Indeed, the global COVID-19 pandemic crisis has recently motivated the development of point-of-care diagnostic tools based on digital amplification assays for early diagnosis and absolute quantification of the target samples. In this regard, there is much potential to combine efficient isothermal DNA or RNA amplification methods with high sensitivity optical and electrochemical detection technologies within microfluidic platforms to realize rapid and sensitive pathogen detection. Accordingly, the final part of this thesis describes the development of a novel micro-compartmentalized nucleic acid quantification assay based on hydrogel microparticles that can be batch synthesized in large numbers and stored for subsequent application in loop-mediated isothermal amplification (LAMP)-based procedures. Specifically, we targeted the detection of Methicillin-resistant Staphylococcus aureus (MRSA), the most prevalent AMR pathogen. In our hydrogel LAMP assay (which we

term H-LAMP), monodisperse polyacrylamide microbeads were used for particle-templated emulsification of LAMP reaction components, thus achieving micro-compartmentalization of the reaction. The assay was successful in detecting MRSA within 30 minutes, with a limit-of-detection of 1 fg/μL (10^3 copies/μL). Overall, this new approach enables the direct translation of technical advances in droplet-based microfluidics to the in vitro diagnostics field, whilst circumventing the need for costly, complex and cumbersome instrumentation. Our proof-of-principle studies confirm that the amplification simple to implement, incorporates few manual handling steps, involves minimal sample dead volumes, reliably produces compartments with a low CV and is able to generate a large and scalable number of compartments. We believe that hydrogel LAMP can become a valuable component within the nucleic acid amplification test toolbox and allow the establishment of point-of-care devices for pathogen control and clinical diagnosis in resource-limited environments.

5.2. Future Research Directions

5.2.1. FCM project

In chapter 2 we demonstrated the utility of an automated flow cytometer for monitoring the microbiological quality of water, we were able to quantify TCC (total cell count), HNA and LNA (High nucleic acid content cell and Low nucleic acid content cell respectively). However, I strongly believe system can be improved by modification of optical module and a double staining protocol ((SYBR Green I) SG and propidium iodide (PI)) to determine intact cell concentration (ICC). Ideally, both measurements (TCC and ICC) are performed in parallel to maximize information gathered. In addition, the developed workflow can be extended to the

detection of a range of pathogenic organisms, including Legionella pneumophila and Salmonella).

5.2.2. Step emulsification project

Step emulsification is widely used for production of functional polymeric microparticles; However, several future developments can be envisioned on the use of step emulsification for single cell encapsulation. Further optimization is required to show the full potential of our design for higher single cell occupancy as it is currently limited by the its performance.

Possible other applications that can be investigated would be library preparation for sequencing, digital immunoassays and digital counting of bacteria and cells. Thus, the development of step emulsification for biological methods are hopefully only the base for many successive applications.

5.2.3. H-LAMP project

The relatively large size of the hydrogel beads synthesized in this work (72 ± 4.5 μm) ultimately proved a limitation in sensitivity. However, we believe that in future work it would be possible to synthesize smaller hydrogel beads, using very small nozzles in the range of a few micrometers, which should decrease the limit of detection and possibly allow single-molecule-per-bead detection, and more precise quantification results.

I strongly believe that for a truly field deployable NAAT assays, it would be a big asset to develop a handheld smartphone-based detection platform. The smartphone-based data acquisition and analysis system can be used in combination of an app and should be able to obtain full-field fluorescence image at one time and simply output the results. Such a

portable and inexpensive handheld device has a great potential in a broad range of POC applications such as infactious diseases detection, clinical diagnostics, and the quality monitoring of water and food in resource-limited areas.

Abbreviation

AM	additive manufacturing
BIP	Backward inner primer
BF	Bright field
BSA	Bovine serum albumin
bp	base pairs
CFU	Colony forming units
cq	Quantification cycle
CV	Coefficient of variation
CMD-LAMP	on-chip mixed-dye-based LAMP
DNA	Deoxyribonucleic acid
DMSO	Dimethylsulfoxide
dPCR	Digital polymerase chain reaction
dLAMP	Digital loop-mediated isothermal amplification
dsDNA	Double-stranded deoxyribonucleic acid
dNTP	deoxynucleotide
DEP	Dielectrophoresis
EXPAR	exponential amplification reaction
EDTA	Ethylenediaminetetraacetic acid
ELISA	Enzyme-linked immunosorbent assay
E. coli	Escherichia coli
FAFC	fluorescence-activated flow cytometry
FACS	fluorescence-activated cell sorter

FBS	Fetal bovine serum
FC-40:	3M Fluorinated Electronic Liquid FC-40
FCS	Flow cytometry standard
FCM	Flow cytometry
FSC	Forward scatter
FIP	Forward inner primer
g-LAMP	in-gel loop-mediated isothermal amplification
HIV	human immunodeficiency virus
HFE-7100	Fluorinated solvent
HFE-7500	Fluorinated solvent
HNA	High nucleic acid content (events)
HBV	hepatitis B virus
HPC	Heterotrophic plate count
LAMP	Loop-mediated isothermal amplification
ICEO	Induced charge electroosmosis
LED	Light-emitting diode
LoopB	Backward loop primer
LoopF	Forward loop primer
LED	Light-emitting diode
LOC	Lab-on-chip
LOD	Limit of detection
LCR	Ligase Chain reaction
LNA	Low nucleic acid content (events)
MRSA	methicillin-resistant Staphylococcus aureus

μPADs	paper-based microfluidic analytical devices
MS	mass spectrometry
NASBA	Nucleic acid sequence-based amplification
NAATs	Nucleic acid amplification tests
nFCM	nano-flow cytometer
O/W	Oil in water emulsion
PA	Photoacoustic
PBS	Phosphate buffered saline
PCR	polymerase chain reaction
PEG	Polyethylene glycol
PFU	plaque-forming units
PVA	Polyvinyl alcohol
PAA	Polyacrylamide
PLGA	Poly(lactic-co-glycolic acid)
PDMS	Polydimethylsiloxane
POS	positive compartments
PS	Polystyrene
PTFE	Polytetrafluoroethylene
POC	Point-of-care
PMMA	Poly(methyl methacrylate)
PRV	Pseudorabies virus
qPCR	quantitative PCR
RT-LAMP	reverse-transcription loop-mediated isothermal amplification
RP	rapid prototyping

RT-PCR	reverse-transcription
RNA	Ribonucleic acid
RCS	rolling circle amplification
RDTs	Rapid diagnostic tests
SDA	strand displacement amplification
SAW	surface acoustic wave
SD	Standard deviation
SLMB	Schweizerisches Lebensmittelbuch (Swiss Food Book)
SSC	Sideward scatter
ssDNA	Single-stranded deoxyribonucleic acid
SYBR Green I	N',N'-dimethyl-N-[4-[(E)-(3-methyl-1,3-benzothiazol-2-ylidene)methyl]-1-phenylquinolin-1-ium-2-yl]-N-propylpropane-1,3-diamine
TCC	Total cell counts
TL	Thermal lens
TB	Mycobacterium tuberculosis
UV	Ultraviolet
US transducer	Ultrasonic transducer
VP	Vibrio parahaemolyticus
VRE	vancomycin-resistant Enterococcus
WTW	Water treatment works
W/O	Water in oil emulsion
W/O/W	Water in oil in water double emulsion
WHO	World Health organization

(12) INTERNATIONAL APPLICATION PUBLISHED UNDER THE PATENT COOPERATION TREATY (PCT)

(19) World Intellectual Property Organization
International Bureau

(43) International Publication Date
20 February 2020 (20.02.2020)

WIPO | PCT

(10) International Publication Number
WO 2020/035366 A1

(51) International Patent Classification:
F16K 99/00 (2006.01) *B01F 13/08* (2006.01)
B01F 13/00 (2006.01) *BOIL 3/00* (2006.01)

(21) International Application Number:
PCT/EP2019/071210

(22) International Filing Date:
07 August 2019 (07.08.2019)

(25) Filing Language: English

(26) Publication Language: English

(30) Priority Data:
18188767.0 13 August 2018 (13.08.2018) EP

(71) Applicant: CSEM CENTRE SUISSE D'ELECTRONIQUE ET DE MICROTECHNIQUE SA - RECHERCHE ET DÉVELOPPEMENT [CH/CH]; Rue Jaquet-Droz 1, 2002 Neuchatel (CH).

(72) Inventors: SCHMID, Noa; Alpenstrasse 10, 6010 Kriens (CH). GRAF, Siegfried; Ober-Kuonimattweg 18, 6010 Kriens (CH). HALVORSEN, Zahra, Alsadat; Effinger-strasse 3, 8002 Zurich (CH).

(74) Agent: E-PATENT S.A.; Saint-Honore 1 Case postale 2510, 2001 Neuchatel (CH).

(81) Designated States *(unless otherwise indicated, for every kind of national protection available)*: AE, AG, AL, AM, AO, AT, AU, AZ, BA, BB, BG, BH, BN, BR, BW, BY, BZ, CA, CH, CL, CN, CO, CR, CU, CZ, DE, DJ, DK, DM, DO, DZ, EC, EE, EG, ES, FI, GB, GD, GE, GH, GM, GT, HN, HR, HU, ID, IL, IN, IR, IS, JO, JP, KE, KG, KH, KN, KP, KR, KW, KZ, LA, LC, LK, LR, LS, LU, LY, MA, MD, ME, MG, MK, MN, MW, MX, MY, MZ, NA, NG, NI, NO, NZ,

(54) Title: MICROFLUIDIC DISTRIBUTION VALVE

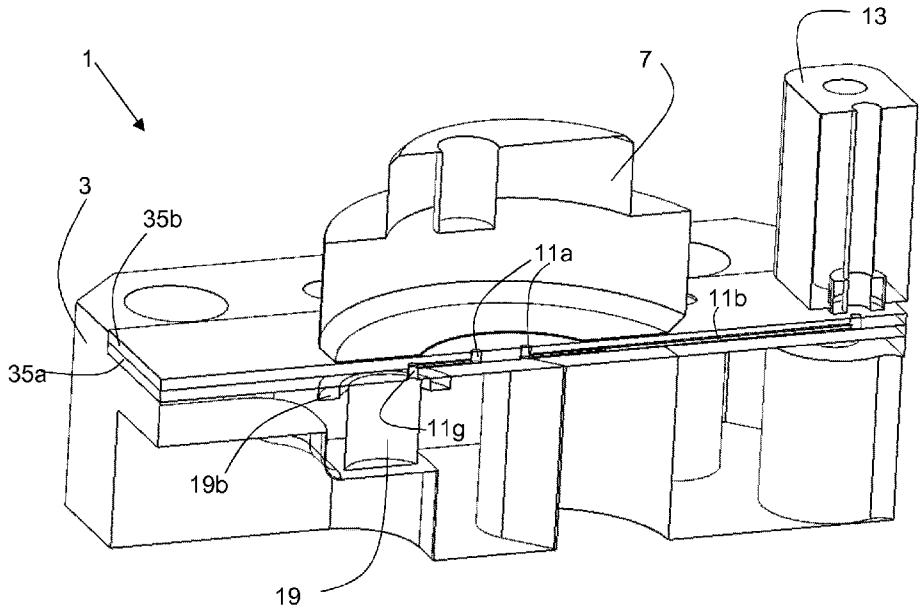

Figure 6

(57) Abstract: Distribution valve (1) comprising: - a stationary element (3) comprising a first valve bearing surface (5), said stationary element (3) comprising a plurality of first fluid ports (11a) and at least one second fluid port (11c), each of said fluid ports (11a, 11c) emerging at said first valve bearing surface (5) and being in fluidic communication with a corresponding conduit (lib, lid) provided in said stationary element (3); - a movable element (7) comprising a second valve bearing surface (9) in contact with said first bearing surface (5), said movable element (7) being arranged to be movable with respect to said stationary element (3) and being arranged to bring at least one of said first ports (11a) into fluidic communication with said second port (11c) in function of the relative position of said movable element (7) with respect to said stationary element (3); characterised in that: - said stationary element (3) comprises a mixing chamber (19) in fluidic communication with one of said first fluid ports (11a). In another embodiment, the mixing chamber

WO 2020/035366 A1

[Continued on next page]

OM, PA, PE, PG, PH, PL, PT, QA, RO, RS, RU, RW, SA, SC, SD, SE, SG, SK, SL, SM, ST, SV, SY, TH, TJ, TM, TN, TR, TT, TZ, UA, UG, US, UZ, VC, VN, ZA, ZM, ZW.

(84) Designated States *(unless otherwise indicated, for every kind of regional protection available)*: ARIPO (BW, GH, GM, KE, LR, LS, MW, MZ, NA, RW, SD, SL, ST, SZ, TZ, UG, ZM, ZW), Eurasian (AM, AZ, BY, KG, KZ, RU, TJ, TM), European (AL, AT, BE, BG, CH, CY, CZ, DE, DK, EE, ES, FI, FR, GB, GR, HR, HU, IE, IS, IT, LT, LU, LV, MC, MK, MT, NL, NO, PL, PT, RO, RS, SE, SI, SK, SM, TR), OAPI (BF, BJ, CF, CG, Cl, CM, GA, GN, GQ, GW, KM, ML, MR, NE, SN, TD, TG).

Published:

— *with international search report (Art. 21(3))*

(19) can be provided in the movable element (7) rather than in the stationary element (3).

Description

MICROFLUIDIC DISTRIBUTION VALVE

Technical Field

[0001] The present invention relates to the technical field of distribution valves. More particularly, it relates to a microfluidic distribution valves suitable for laboratory use.

State of the art

[0002] WO2017/037072 describes a rotary microfluidic distribution valve particularly suited for use in an automated flow cytometer. This valve comprises a stator having a plurality of peripheral ports, and a central port connected to a syringe-type pump. A rotor mounted pivotally on the stator comprises at least one conduit which can be used to connect any of the peripheral ports to the central port, depending on the relative angular position between the rotor and the stator. As a result, various fluids can be drawn from the peripheral ports into the syringe-type pump, from where they can subsequently be output to another of the peripheral ports. It is also possible to draw several different fluids into the syringe-type pump, e.g. for carrying out a biological or chemical reaction.

[0003] However, when several fluids are drawn into the syringe-type pump simultaneously, it is difficult to ensure that they are well-mixed in order to carry out a biological or chemical reaction under homogeneous conditions. Better mixing would require attaching an external mixing chamber to a fluid port, which is bulky, expensive and will result in long fluid transit distances through the connecting conduits, which is particularly problematic in the case of very small samples. In such a case, long conduits lead to fluid losses and complications with cleaning and/or sterilisation.

[0004] An aim of the present invention is hence to at least partially overcome the above-mentioned drawbacks.

Disclosure of the invention

[0005] More specifically, according to a first aspect, the invention relates to a distribution valve as defined in claim 1. This valve comprises:

[0006] - a stationary element intended to be immovably fixed on a support, this element comprising a first valve bearing surface, a plurality of first fluid ports and at least one second fluid port, each of said fluid ports emerging (i.e. opening) at said first valve bearing surface and being in fluidic communication with a corresponding conduit provided in said stationary element. These conduits may be distinct from the ports and in fluidic communication therewith, or may be formed simply by the extension of the port from its opening. Said second fluid port may e.g. be arranged to be in selective or permanent fluidic communication with a pump such as a syringe-type pump, membrane pump or similar, or may simply lead to a further conduit;

[0007] - a movable element comprising a second valve bearing surface in contact with said first bearing surface, said movable element being arranged to be movable with respect to said stationary element and being arranged to bring at least one of said first ports into fluidic communication with said second port in function of the relative position of said movable element with respect to said stationary element. This fluidic communication may be achieved e.g. by means of a connecting conduit provided in or adjacent to the second valve bearing surface. By implication, the first and second valve bearing surfaces cooperate with each other so as to be sealed one to the other with the exception of where fluidic communication with said ports is desired, in function of the relative position of the two elements. The valve bearing surfaces may be planar, or may be cylindrical or partially cylindrical.

[0008] According to the invention, the said stationary element comprises a mixing chamber in fluidic communication with one of said first fluid ports. In other words, this chamber is enclosed within the structure of the stationary element.

[0009] As a result, mixing can take place within the valve structure itself, rather than in a pump or in an external mixing chamber. The mixing can take place by

creating turbulence in the chamber by operating the pump, or by means of at least one mixing element (see below). The system is thus compact, and the conduits leading to the mixing chamber are kept as short as possible. This latter aspect helps with cleaning, minimises wastage of samples, and so on, and reduces (or even eliminates) dead volume.

[0010] According to a second aspect, the distribution valve comprises:

[001 1] - a stationary element comprising a first valve bearing surface, said stationary element comprising a plurality of first fluid ports and at least one second fluid port, each of said fluid ports emerging (i.e. opening) at said first valve bearing surface and being in fluidic communication with a corresponding conduit provided in said stationary element. These conduits may be distinct from the ports and in fluidic communication therewith, or may be formed simply by the extension of the port from its opening. Said at least one second fluid port may, for instance, be arranged to be in permanent or selective fluidic communication with a pump such as a syringe-type pump, membrane pump or similar, or may simply lead to a further conduit;

[0012] - a movable element comprising a second valve bearing surface in contact with said first bearing surface, said movable element being arranged to be movable with respect to said stationary element and being arranged to bring at least one of said first ports into fluidic communication with said second port in function of the relative position of said movable element with respect to said stationary element. This fluidic communication may be achieved e.g. by means of a connecting conduit provided in or adjacent to the second valve bearing surface. By implication, the first and second valve bearing surfaces cooperate with each other so as to be sealed one to the other with the exception of where fluidic communication with said ports is desired, in function of the relative position of the two elements. The valve bearing surfaces may be planar, or may be cylindrical.

[0013] According to this aspect of the invention, said movable element comprises a mixing chamber in (permanent or selective) fluidic communication with said at least one second port and arranged to be brought into fluidic communication with at least one of said first ports. In other words, the mixing

chamber is formed within the structure of the movable element such that it can be made to connect the second port to at least one of the first ports. The movable element may comprise a further connecting conduit arranged to fluidically connect the second port to one of the first ports, but in its absence, such fluidic communication can simply pass through the mixing chamber.

[0014] Again, mixing can take place within the valve structure itself, rather than in a pump or in an external mixing chamber. The mixing can take place by creating turbulence in the chamber by operating the pump, or by means of at least one mixing element (see below). The system is thus compact, and the conduits leading to the mixing chamber are kept as short as possible. This latter aspect helps with cleaning, minimises wastage of samples, reduces or eliminates dead volume, and so on.

[0015] Advantageously, said mixing chamber had a cross-sectional area at least five times as large as the cross-sectional area of one of said conduits. This provides enough volume and cross-sectional area to enable sufficient mixing to take place.

[0016] Advantageously, at least one mixing element is positioned inside said mixing chamber. This mixing element can e.g. be a mechanical agitator such as a plunger-type stirrer, at least one magnetically-attractable pellet or bead (e.g. made of a ferromagnetic or ferrimagnetic material, and optionally encapsulated e.g. in a polymer such as PTFE). The use of such an active mixing element permits good mixing of even relatively viscous fluids, and/or of mixtures with a very high volume ratio difference (i.e. a large proportion of one component and a small proportion of a second component). It also permits fast mixing, and a reduction of reagent volume.

[0017] In the case in which the at least one mixing element is at least one magnetically-attractable pellet or bead, the one of the stationary element and the movable element which does not contain the mixing chamber comprising a magnet or an electromagnet arranged to magnetically couple with said at least one magnetically-attractable pellet or bead. In other words, if the mixing chamber is in the stationary element, the (electro)magnet is in the movable element, and if the mixing chamber is in the movable element, the

(electro)magnet is in the stationary element. Hence, by simply moving the movable element with respect to the stationary element while the (electro)magnet is mechanically coupled with the magnetically-attractable pellet or bead, this latter can be moved within the mixing chamber and create turbulence to "stir" the fluid therein. Alternatively, one or more electromagnets may be situated adjacent to the mixing chamber, so as to be able to move the mixing element by magnetic coupling. Typically, the magnet or electromagnet is fixed in relation to the element in which it is incorporated (whether it be the stationary element or the movable element according to the case in question), but it can also be movable with respect thereto.

[0018] Advantageously, the movable element may be arranged to rotate with respect to said stationary element, or may be arranged to translate with respect thereto, along one or more translational axes.

[0019] Advantageously, a heating element may be arranged adjacent to at least one wall of said mixing chamber, so as to be able to use the mixing chamber for incubating samples while a chemical or biological reaction takes place.

[0020] Advantageously, an adaptor for attaching a plurality of hoses may be positioned on said stationary element and is arranged such that at least some of said hoses are in fluidic communication with corresponding first ports.

[0021] Advantageously, and notably in the case in which the valve bearing surfaces are planar, at least part of the volume of said mixing chamber, preferably at least 25% of its volume, preferably at least 50% of its volume, preferably at least 75% of its volume, preferably substantially all of its volume is situated within a locus defined by extending the outer peripheral wall of said movable element through the thickness of the stationary element. In the case in which the movable element translates, the minimum percentage can hold in all translational positions, or only in certain positions, whereas in the case in which the movable element rotates about an axis, this will typically hold at all times unless the movable element is non-cylindrical (e.g. cut away on one or more sides), in which case the same considerations as for a translational

element may apply. In any case, this allows a particularly compact construction.

Brief description of the drawings

[0022] Further details of the invention will appear more clearly upon reading the description below, in connection with the following figures which illustrate:

- Figure 1: an isometric view of a distribution valve 1 according to a first embodiment of the invention, viewed from its upper side ("upper" referring to the orientation of figure 1);
- Figure 2: an isometric view of the underside of the valve of figure 1;
- Figure 3: a partially exploded isometric view of the distribution valve of figure 1, showing the valve bearing surfaces on each component;
- Figure 4: an isometric, partially-transparent cross-sectional view parallel to the plane of the first valve bearing surface, this section passing through the ports in said surface;
- Figure 5: an isometric, partially-transparent cross-sectional view parallel to the plane of the first valve bearing surface, this section passing beneath the conduits visible in figure 4;
- Figure 6: an isometric, partially-transparent cross-sectional view perpendicular to the plane of the first valve bearing surface, this section passing through the mixing chamber and the port leading into it;
- Figures 7 and 8: isometric views from different angles of the upper side of the stationary component, the valve plates having been removed in order to expose the mixing chamber;
- Figure 9: a schematic view of an alternative mixing element;
- Figures 10 and 11: schematic views of alternative arrangements of mixing chamber and mixing element;
- Figure 12: a schematic transparent plan view of an alternative embodiment of the valve of the invention, in which the movable part is arranged to slide rather than rotate;

- Figure 13: a schematic cross-sectional view of the embodiment of figure 12, the section passing through the ports;
- Figure 14: a schematic cross-sectional view of a further embodiment of a valve according to the invention;
- Figure 15: a schematic transparent plan view of the embodiment of figure 14; and
- Figure 16 is a schematic cross-sectional view of a mixing chamber with adjacent heating element.

Embodiments of the invention

[0023] Figures 1-8 illustrate a microfluidic distribution valve 1 according to an embodiment of the invention. This microfluidic distribution valve 1 is suitable for laboratory use, e.g. for carrying out assays, chemical reactions, biological reactions, for flow cytometry and so on. The fluid in question is typically a liquid, but the system can also be used with gases, gels and so on.

[0024] The valve 1 comprises a first, stationary, element 3, intended to be attached to a support by means of bolts or similar. A plurality mounting holes, lugs or similar may be provided to this effect, if required. The stationary element 3 comprises a first valve bearing surface 5 on a first surface thereof, illustrated here as being the upper surface. A second, movable, element 7 is provided, which comprises a second valve bearing surface 9 in contact with this first valve bearing surface 5, the materials used for these surfaces being chosen and finished to such a degree that they are sealed one to the other except where required to enable fluidic communication (see below). For instance, the first valve bearing surface 5 should ideally be polished, and is ideally made from a relatively hard material such as glass, silicon, silica, ceramic, glass-ceramic, stainless steel or similar, or from a softer material with a relatively hard coating like diamond-like carbon, alumina, silica or similar. The second valve bearing surface 9 is ideally made of a softer, relatively low-friction material such as PTFE, PEEK, nylon or similar, or can be a harder material as mentioned above coated with PTFE, PEEK, nylon or similar. Or, these materials can be reversed, the harder materials forming the second

valve bearing surface 9 and the softer materials forming the first valve bearing surface 5. In both cases, the first and second valve bearing surfaces 5, 9 will then seal to each other aside from where ports interface with each other, without requiring further sealing means. However, other materials are possible, and conventional seal arrangements can be used.

[0025] In the illustrated embodiment of figures 1-8, the movable element 7 is a rotor, arranged to be supported by any convenient means (not illustrated) such that it rotates about its central axis 7a under manual or automatic control. This rotation can be powered by hand, or by a motor such as a stepper motor (not illustrated), under the command of a suitable controller. However, other arrangements will be discussed below. In the illustrated embodiment, the movable element 7 is provided on an upper face of the stationary element 3, however different orientations are possible.

[0026] First valve bearing surface 5 comprises a plurality of fluid ports 11a, 11c which emerge at corresponding openings provided in said surface 5. These ports 11 are of two types: a first type 11a, a number of which lead to conduits 11b which are each in fluid connection with a corresponding channel of an adaptor 13 arranged to permit the attachment of hoses to the first ports 11a (see figures 6 and 14), and a second type of port 11c, which is a central, common port in the present embodiment, but can be one or more second ports 11c offset from the centre as desired and as mentioned above. The diameter of the ports is typically in the range of 50µm to 2mm, more particularly around 100-800pm, however larger or smaller ports are possible. The conduits 11b typically have a cross-sectional diameter (or width and depth) in the range of 50µm to 1mm, more particularly around 100-300pm.

[0027] The second valve bearing surface 9 of the movable part 7 comprises a connecting conduit 15 arranged to be able to connect any of the first ports 11a to the second port 11c, depending on the position of the movable element 7 with respect to the stationary element 3. Since in the illustrated embodiment the movable element 7 is adapted to rotate about its central axis 7a with respect to the stationary element 3, the connecting conduit 15 is simply a radial groove extending from the centre of rotation with sufficient

length so as to be able to interface with any of the first ports 11a (see figure 3). Alternatively, the connecting conduit 15 may be embedded in the movable element 7, emerging at the second valve bearing surface 9 at corresponding ports at its two extremities. In any case, the connecting conduit fluidically connects the first port 11a in question with the second port 11c simultaneously, thereby providing a continuous and contiguous flowpath therebetween. This is clearly distinct from a situation in which a movable conduit is used to "shuttle" aliquots of fluid from one port to the next as is the case in document US2009/1 29981 . In this latter case, there is no continuous flowpath between the two ports at any time.

[0028] When the angular position of the movable element 7 with respect to the stationary element 3 causes the connecting conduit 15 to overlap a first port 11a, this latter is then fluidically connected with the second port 11c, and fluid can be drawn from that first port 11a, through the connecting conduit 15, and into the second port 11c, or vice-versa. This second port 11c itself forms a short, axial conduit 11m, which opens into an interface 17 adapted to be connected to a bi-directional pump 31 such as a syringe-type pump or any other convenient type of pump (see figure 14, in which a syringe-type pump 31 in fluidic communication with the interface is illustrated schematically, although other types of pump are possible, such as a membrane pump, a peristaltic pump, a gear pump, a vane pump, a displacement pump actuated pneumatically, or any other form of bi-directional pump). In the illustrated embodiment, this interface 17 is provided in the opposite side of the stationary element 3 to the first valve bearing surface 5, but it is also possible to provide a corresponding conduit leading from the second port 11c to emerge in any convenient position on the stationary element 3. It should also be noted that the pump 31 is not necessary, and the second port 11c may just open into a further conduit leading to the adaptor 13 or elsewhere. Also, as mentioned above, further second ports 11c can be provided, e.g. arranged at one or more radii and at various angular positions considered from the axis of rotation 7a, one or more connecting conduits 15 being arranged as required to connect one or more second ports 11c to one or more first ports

11a depending on the position of the movable element 7 with respect to the stationary element 3. In such a case, typically none of the second ports 11c would be situated on the axis of rotation 7a, but it is not excluded that one such second port 11c might be positioned there. These variations apply equally to all of the embodiments of the invention, mutatis mutandis.

[0029] According to this embodiment of the invention, at least one of the first ports 11a is connected to the corresponding channel of the adaptor 13 via a mixing chamber 19, visible in figures 5 and 6.

[0030] Mixing chamber 19 is formed as a cavity in the stationary element 3, and is in fluidic communication with one of the first ports 11a via a first conduit 11d, and with the adaptor 13 by means of a further conduit 11f. Each of these conduits 11d, 11f emerges proximate to a respective, opposite, end of the mixing chamber 19 via a corresponding port 11g, which does not emerge at the first valve bearing surface 5 but simply causes the corresponding conduit 11d, 11f to open into the mixing chamber 19. Mixing chamber 19 has a cross-sectional area at least five times, preferably at least 10 times, as great as the conduit 11d leading to it, considered in any of its median planes and compared with the lateral cross-sectional area of the conduit 11d. Mixing chamber 19 typically has a volume of between 0.01 ml_ and 1ml_, preferably between 0.05ml_ and 0.5ml_. Ideally, the mixing chamber 19 is contained entirely within the footprint of the movable element 7, i.e. is entirely overlapped by this latter. In other words, if one were to define a locus extending the outer peripheral wall of the movable element 7 through the thickness of the stationary element 3, the mixing chamber is ideally entirely contained within this cylindrical locus, which is particularly compact. Different shapes of movable element 7 will, of course, result in differently-shaped loci. However, it is also possible that the mixing chamber 19 is only partially within this locus (e.g. at least 25%, preferably at least 50%, further preferably at least 75% of its volume is situated within the locus). This same principle can also apply to a translational movable element 7 (see the description of figures 12-13 below), in which case it may hold in all positions of the movable element 7 or only in some positions. These arrangements are distinct from

the mixing chamber being situated in a separate element and connected to a first port 11a by a further conduit, or situated within the stationary element 3 but displaced laterally with respect to the movable element 7 and outside of its footprint. This latter situation is not to be construed as excluded, but is not preferred.

[0031] It should further be noted that, rather than having a conduit 11d fluidically connecting one of the first ports 11a to the mixing chamber 19, said first port 11a can open directly into the chamber 19, which applies equally to the embodiment of figures 12-13 below. In such a case, said first port 11a itself forms the conduit leading from the opening of the port in the first valve bearing surface 5 into the mixing chamber 19.

[0032] By pivoting the movable element 7 so as to align its connecting conduit 15 with a particular first port 11a, fluid can be drawn into a pump connected to the interface 17 from an external source fluidically connected to the corresponding channel in the adaptor 13. The movable element 7 can then be rotated so as to align its connecting conduit 15 with the first port 11a leading to the mixing chamber 19, and the fluid can then be injected into the mixing chamber 19. In other words, depending on the relative angular position of the movable element 7 with respect to the stationary element 3, a first port 11a can be selected and brought into fluidic communication with the second port 11b.

[0033] By working the pump in both directions, turbulence can be created in the mixing chamber 19, thereby mixing the fluid therein. Several different fluids from different first ports 11a can be injected sequentially into the mixing chamber 9, and then mixed by generating turbulence as described above. Alternatively, several different fluids from different first ports 11a can be aspirated sequentially into the pump 31 and then injected into the mixing chamber 19 in one operation after placing the movable element 7 in the correct orientation with respect to the stationary element 3 so as to cause the second port 11c to communicate fluidically with the mixing chamber 19.

[0034] In order to avoid having to operate the pump backwards and forwards to mix the fluid in the chamber 19, one or more mixing elements 21 can be provided

therein. As illustrated, this mixing element is a single magnetically-attractable pellet fitted loosely into the chamber 19, but multiple, smaller pellets or beads are also possible. The magnetically-attractable pellet may for instance be steel or another ferromagnetic metal, a ferrimagnetic ceramic, or other magnetically-attractable material. The pellet may be encapsulated in an inert substance such as glass, a ceramic, or a polymer such as PTFE. In the illustrated embodiment, the pellet is cylindrical, with its longitudinal axis parallel to the axis 7a of the movable element 7 (see figure 1), but other shapes such as spheres, polyhedral, or irregular forms are also possible.

[0035] A magnet 23 (see figure 1) is provided in the movable element 7, and is preferably fixed therein. Alternatively, magnet 23 may be movably mounted in the movable element 7. This magnet 7 permits manipulation of the mixing element 21 in the chamber 19. Since the mixing element 21 is loosely fitted in the chamber 19 with play between itself and the wall of the chamber 19, when the mixing element 21 is moved back and forth turbulence is created in the fluid contained therein, which causes mixing to take place. Ideally, when the magnet 23 overlaps the mixing chamber 19, none of the first ports 11a are in fluidic communication with the connecting conduit 15, to prevent undesired transfer of small quantities of fluid from one port to another. Alternatively, the magnet 23 may be placed in a separate element on the opposite side of the stationary element 3 to the movable element 7, or on a sidewall thereof, in sufficient proximity to magnetically-couple with the pellet 21. Further alternatively, multiple electromagnets could be placed at different locations adjacent to the mixing chamber 19, such as adjacent to the two ends thereof, sequential activation of these electromagnets causing the mixing element 21 to move back and forth. Alternatively, the pellet 21 could be electrostatically-attractable, and a pair of electrical conductors (e.g. conducting plates) could be arranged adjacent to the mixing chamber 19 on opposite sides thereof, such that an application of a suitable varying voltage to said conductors causes the pellet 21 to move by electrostatic attraction / repulsion.

[0036] As illustrated, the chamber 19 extends along an arc of a circle centred on the axis 7a, but it can also extend along a straight line, can be cylindrical, have a square or rectangular cross-section in the plane of the stationary element 3, or have any other convenient shape.

[0037] Alternatively, the mixing element 21 may be mechanically actuated, e.g. a plunger-type agitator arrangement passing through a sidewall or the underside of the stationary element 3, as illustrated in figure 9. In such a case, sufficient sealing between the stem 21a of the plunger and the stationary element 3 should be provided, e.g. by suitable choices of materials and surface finishes, or by the provision of suitable seals (e.g. sealing rings) between the stem 21a and the walls of the passageway in which it is fitted. The head of the plunger is sized and shaped so as to permit fluid to pass through and/or around the head as it is moved back and forth, and to this end the head of the plunger may comprise fluid passageways through its thickness, being made e.g. from gauze, a perforated sheet or similar.

[0038] In each case, the mixing element 21 has several advantages. It improves the speed of mixing, permits a reduction of reagent volume, permits mixing liquids with several components in which one component is present in a very small proportion with respect to the other (e.g. one component being <10%, <5% or even <1% by volume of the total liquid present), and permits mixing of even relatively viscous liquids.

[0039] Figure 10 illustrates a further variant, in side view, in which the mixing chamber 19 is divided into two by a permeable wall 19a substantially parallel to the plane of the first valve bearing surface 5, which may e.g. be a gauze, a sieve-like structure (i.e. a wall comprising a plurality of holes in a regular or irregular pattern), a membrane comprising microchannels or similar. The mixing element 21 is illustrated as being situated in the chamber 19 on the side of the wall 19a facing the ports 11g, however it may also be on the side facing away from said ports. Figure 11 illustrates, in plan view, a further arrangement in which the wall 19a is substantially perpendicular to the plane of the first valve bearing surface 5, the ports 11g emerge on a first side thereof, and the mixing element 21 is situated on the same side of the wall

19a as the ports 11g. Alternatively, the mixing element 21 may be on the opposite side of the wall to the ports 11g.

[0040] In all of these variations, the permeable wall 19a serves to improve turbulence in the fluid in the chamber 19, and thereby to improve mixing and the homogeneity of the fluid once mixed.

[0041] Figures 12 and 13 illustrate schematically a further variant of a valve 1 according to the invention, respectively in transparent plan view and in cross-section along the line of ports 11a, 11g. In figure 12, the movable element 7 and its features are illustrated with dotted lines in order to distinguish them from the stationary element 3 (solid lines) and the conduits 11b, 11d, 11f (dashed lines) which are embedded in the body of the stationary element 3.

[0042] In this variant, the movable element 7 is arranged to slide, i.e. translate, along a longitudinal axis with respect to the stationary element 3, and to this end the first ports 11a are arranged in a straight line extending parallel to this longitudinal axis. The second port 11b is formed as a slot also extending along a direction parallel to this longitudinal axis of displacement, and the connecting port 15 provided in the movable element 7 is arranged to be able to bring any of the first ports 11a in fluidic connection with the second port 11b. Again, one of the first ports 11a leads to a mixing chamber 19, which may be of any of the forms discussed above. Again, a mixing element 21 may be provided therein (not illustrated in figures 12 and 13), which may be of any type disclosed above. Also, a magnet may be provided in the movable element 7 as before, such that sliding the movable element 7 along its axis of motion while the magnet is magnetically coupled with the mixing element 21 will assist in mixing the fluid in the chamber 19. The conduits 11b, 11f extend laterally, and interface with an adaptor 13 provided on a sidewall of the stationary element 3, however an arrangement similar to that of figures 1-8 is also possible. Furthermore, the interface 17 for a pump is also arranged on a sidewall of the stationary element 3, and is fluidically connected with the second port 11b by a further conduit 11h. Ideally, the movable element 7 should be sized such that none of the first or second ports 11a, 11b are

opened to the air when the movable element is in one of its extreme positions.

[0043] The other features of the valve 1 are as before, and need not be described further.

[0044] Figures 14 and 15 illustrate yet another embodiment of the invention, conduits buried in the material of an element again being represented by thick dashed lines. In this embodiment, which is similar to that of figure 1, the mixing chamber 19 is provided in the movable element 7 rather than in the stationary element 3. As illustrated, the chamber 19 is connected to a central port 11j of the movable element 7, which is in permanent fluidic communication with the second port 11c of the stationary element 3. Towards its side remote from the central port 11j, the chamber is in fluidic communication with a further port 11k positioned so as to be able to be brought into fluidic communication with one of the first ports 11a according to the relative angular position of the movable element 7 with respect to the stationary element 3. Further port 11k may open directly into the mixing chamber 19 (itself hence forming a conduit), or may be fluidically connected thereto by means of a further conduit.

[0045] Furthermore, a conventional connecting conduit 15 is provided as in figure 1, extending from the central port 11j to a further port 11m, again positioned so as to be able to be brought into fluidic communication with one of the first ports 11a. As illustrated, this connecting conduit extends in an opposite radial direction to the chamber 19 (although other directions are possible), and the first ports 11a are positioned such that it is not possible that both of the further ports 11k, 11m overlap different first ports 11a at the same time. This prevents undesired fluid flows between ports. However, it should be noted that the connecting conduit 15 is not required in this embodiment, and if it is omitted, all fluid communication between the second port 11c and one of the first ports 11a is carried out via the mixing chamber 19.

[0046] As before, the chamber 19 may contain a mixing element 21 of any convenient type (not illustrated in figures 14 and 15), and in the case of a magnetically-manipulatable mixing element 21, a magnet may be provided at

a convenient location in the stationary element 3, and may be fixed or movably mounted therein. Equally, one or more electromagnets can be provided as an alternative to a permanent magnet.

[0047] The same principle of locating the mixing chamber 19 in the movable element 7 can also be applied to the embodiment of figures 12 and 13.

[0048] Figure 16 illustrates schematically an arrangement in which a heating element 33 such as an electric heating element, a conduit for warm water or similar, is provided adjacent to at least one wall of the mixing chamber 19. This enables the chamber 19 to be heated and therefore be used as an incubation chamber or to carry out reactions at higher than ambient temperatures. Although this has been illustrated in the context of a chamber 19 provided in the stationary element 3, it is equally applicable to a chamber provided in the movable element 7 as in figures 14 and 15.

[0049] In terms of the construction of the stationary element 3, this can be produced as a unitary, monolithic part, e.g. by additive manufacturing (3D printing, stereolithography, or similar), thereby incorporating all cavities, conduits and ports into a single, unitary construction. Suitable materials are polymers such as acrylic (PMMA), nylon, epoxy, PEEK but also ceramics, glasses, glass-ceramics, stainless steel and so on, and surfaces may be post-machined and coated with a layer of another substance such as PTFE, Parylene or DLC (diamond-like carbon).

[0050] However, the embodiment as illustrated in figures 1-8 has been designed with multi-part manufacturing in mind, in order to simplify manufacture by conventional methods. As can particularly be seen in figures 7 and 8, the main body of the stationary element 3 is provided with the mixing chamber 19 and with part of the conduit leading from the second port 11c to the interface 17. A first plate 35a is situated on the upper surface of the main body of the stationary element 3, and closes the mixing chamber 19. A groove 19b may be provided in the upper surface of said main body, and may contain a sealing ring, as is generally known, in order to guarantee the sealing of the periphery of the mixing chamber 19. However, if the first plate is e.g. laser

welded or glued around the upper face of the mixing chamber 19, this joint can be omitted. First plate 35a comprises openings for the ports 11g and 11c. Ports 11g, 11c can be formed e.g. by conventional drilling, by laser ablation or similar.

[0051] A second plate 35b is provided upon the first plate 35a, this second plate 35b comprising first ports 11a and the corresponding conduits 11b, 11d, 11f, together with a through-hole for second port 11c. Second plate 35b hence comprises the first valve bearing surface 5. Since the conduits 11b, 11d, 11f extend parallel to the surface of the plate, they can be formed e.g. by irradiation of a transparent material such as a suitable glass by the intersection of two or more lasers, followed by chemical etching of the irradiated channel. This technique is known as laser-induced deep etching (LIDE) or laser-assisted etching, and typically uses a femtosecond laser. Alternatively, the conduits 11b, 11d, 11f can be formed in situ in the case in which the plate is formed by additive manufacturing (3D printing, such as SLM, SLS, stereolithography or similar). Or, the second plate 35b can be formed by two sub-plates in which half of each conduit is machined, etched or laser-ablated as a groove, with the conduit being formed once the two sub-plates are unified by friction welding, laser welding, gluing or similar. The same principle can be applied to a single groove in one plate, the other plate having a flat surface facing the groove. This flat plate could alternatively, for instance, be formed as an adhesive tape bonded to the grooved plate. Both of the first and second plates 35a, 35b are fixed together and to the main body of the stationary element 3, e.g. by gluing, laser welding, friction welding, clamping or similar. The two plates 35a, 35b are constructed such that they are sealed one to the other aside from where fluid pathways are intentionally provided.

[0052] Although the invention has been described with reference to specific embodiments, variations thereto are foreseeable without departing from the scope of the invention as defined in the appended claims.

[0053] For instance, the valve bearing surfaces 5, 9 do not have to be planar, and can be cylindrical or shaped as a partial cylinder. In such a case, the first ports 11a are distributed circumferentially, and the second port 11b can be arranged as required, e.g. extending parallel to, or even along, the axis of said cylinder. Furthermore, it is also possible to provide multiple mixing chambers 19 in any given distribution valve 1, for instance for dilution purposes or for carrying out multiple different reactions in different chambers simultaneously.

Claims

1. Distribution valve (1) comprising:

- a stationary element (3) comprising a first valve bearing surface (5), said stationary element (3) comprising a plurality of first fluid ports (11a) and at least one second fluid port (11c), each of said fluid ports (11a, 11c) emerging at said first valve bearing surface (5) and being in fluidic communication with a corresponding conduit (11b, 11d, 11m) provided in said stationary element (3);

- a movable element (7) comprising a second valve bearing surface (9) in contact with said first bearing surface (5), said movable element (7) being arranged to be movable with respect to said stationary element (3) and being arranged to bring at least one of said first ports (11a) into fluidic communication with said second port (11c) in function of the relative position of said movable element (7) with respect to said stationary element (3);

characterised in that:

- said stationary element (3) comprises a mixing chamber (19) in fluidic communication with one of said first fluid ports (11a).

2. Distribution valve (1) comprising:

- a stationary element (3) comprising a first valve bearing surface (5), said stationary element (3) comprising a plurality of first fluid ports (11a) and at least one second fluid port (11c), each of said fluid ports (11a, 11c) emerging at said first valve bearing surface (5) and being in fluidic communication with a corresponding conduit (11b, 11d, 11m) provided in said stationary element (3);

- a movable element (7) comprising a second valve bearing surface (9) in contact with said first bearing surface (5), said movable element (7) being arranged to be movable with respect to said stationary element (3) and being arranged to bring at least one of said first ports (11a) into fluidic communication with said second port (11c) in function of the relative position of said movable element (7) with respect to said stationary element (3);

characterised in that:

- said movable element (7) comprises a mixing chamber (19) in fluidic communication with said second port (11c) and arranged to be brought into fluidic communication with at least one of said first ports (11a).

3. Distribution valve (1) according to any preceding claim, wherein said mixing chamber (19) had a cross-sectional area at least five times as large as the cross-sectional area of one of said conduits (11b, 11d, 11m).

4. Distribution valve (1) according to any preceding claim, wherein at least one mixing element (21) is positioned inside said mixing chamber.

5. Distribution valve (1) according to the preceding claim, wherein said mixing element (21) is at least one of:
- a mechanical agitator;
- a magnetically-attractable element, pellet or bead.
- an electrostatically-attractable element, pellet or bead.

6. Distribution valve (1) according to any preceding claim, wherein said mixing element (21) is at least one magnetically-attractable pellet or bead, the one of the stationary element (3) and the movable element (7) which does not contain the mixing chamber (19) comprising a magnet (23) or an electromagnet arranged to magnetically couple with said at least one magnetically-attractable pellet or bead.

7. Distribution valve (1) according to claim 6, wherein said magnet (23) or electromagnet is fixed with respect to the element (3; 7) which does not contain the mixing chamber.

8. Distribution valve (1) according to any preceding claim, wherein said movable element (7) is arranged to rotate with respect to said stationary element (3).

9. Distribution valve (1) according to one of claims 1-7, wherein said movable element (7) is arranged to translate with respect to said stationary element (3).

10. Distribution valve (1) according to any preceding claim, wherein a heating element (33) is arranged adjacent to at least one wall of said mixing chamber (19).

11. Distribution valve (1) according to any preceding claim, wherein an adaptor (13) for attaching a plurality of hoses is positioned on said stationary element (3) and is arranged such that at least some of said hoses are in fluidic communication with corresponding first ports (11a).

12. Distribution valve (1) according to any preceding claim, wherein each of said first and second valve bearing surfaces (5, 9) is planar, cylindrical, or partially cylindrical.

13. Distribution valve according to any preceding claim, wherein at least part, preferably at least 25%, preferably at least 50%, preferably at least 75%, preferably substantially all of the volume of said mixing chamber is situated within a locus defined by extending the outer peripheral wall of said movable element (7) through the thickness of the stationary element (3).

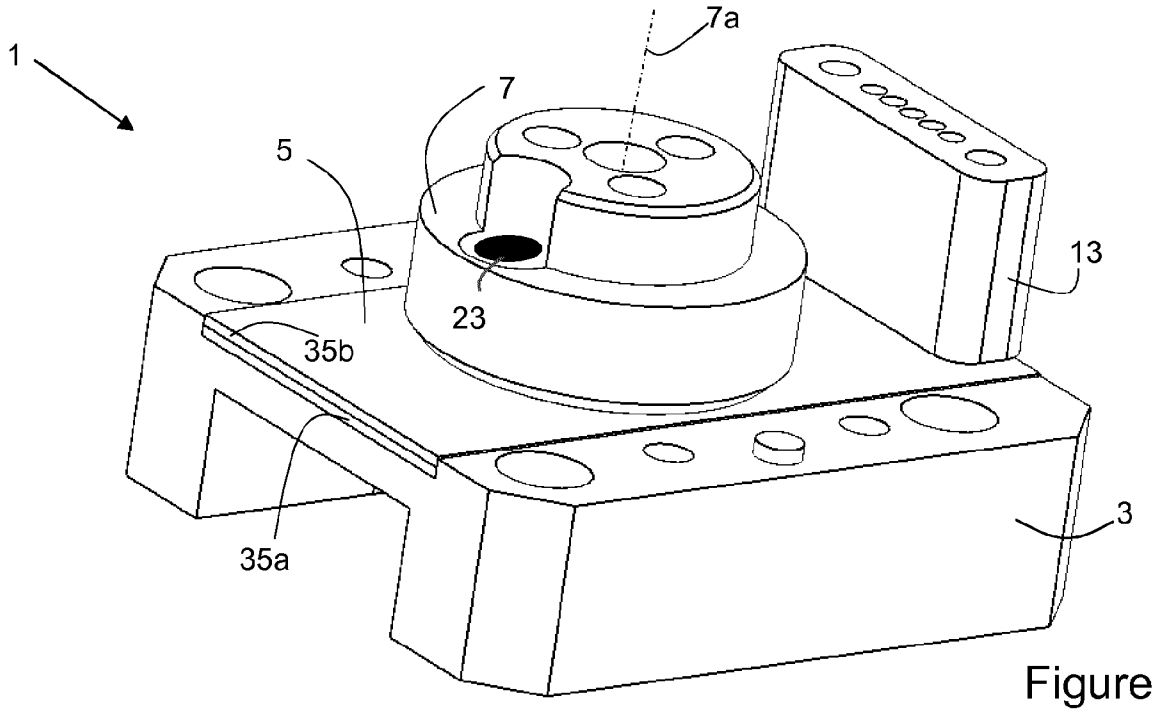

Figure 1

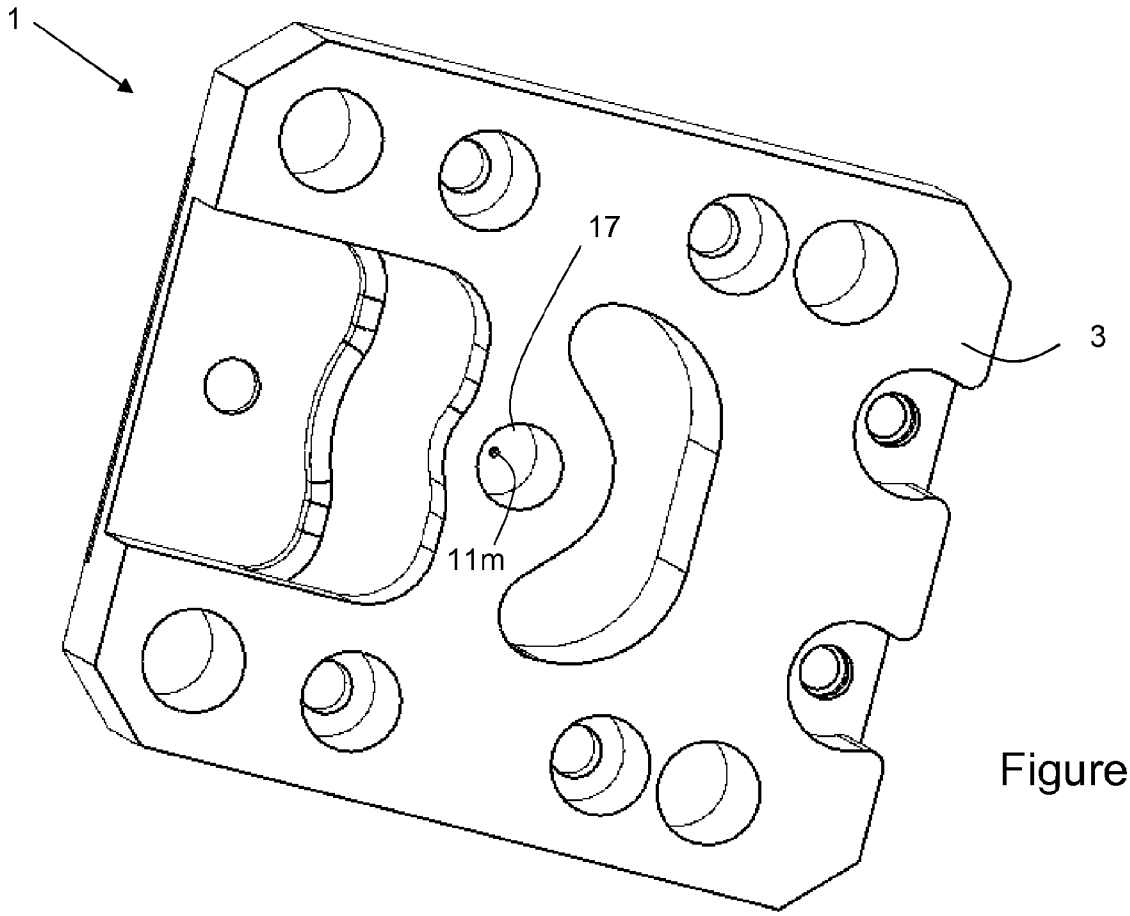

Figure 2

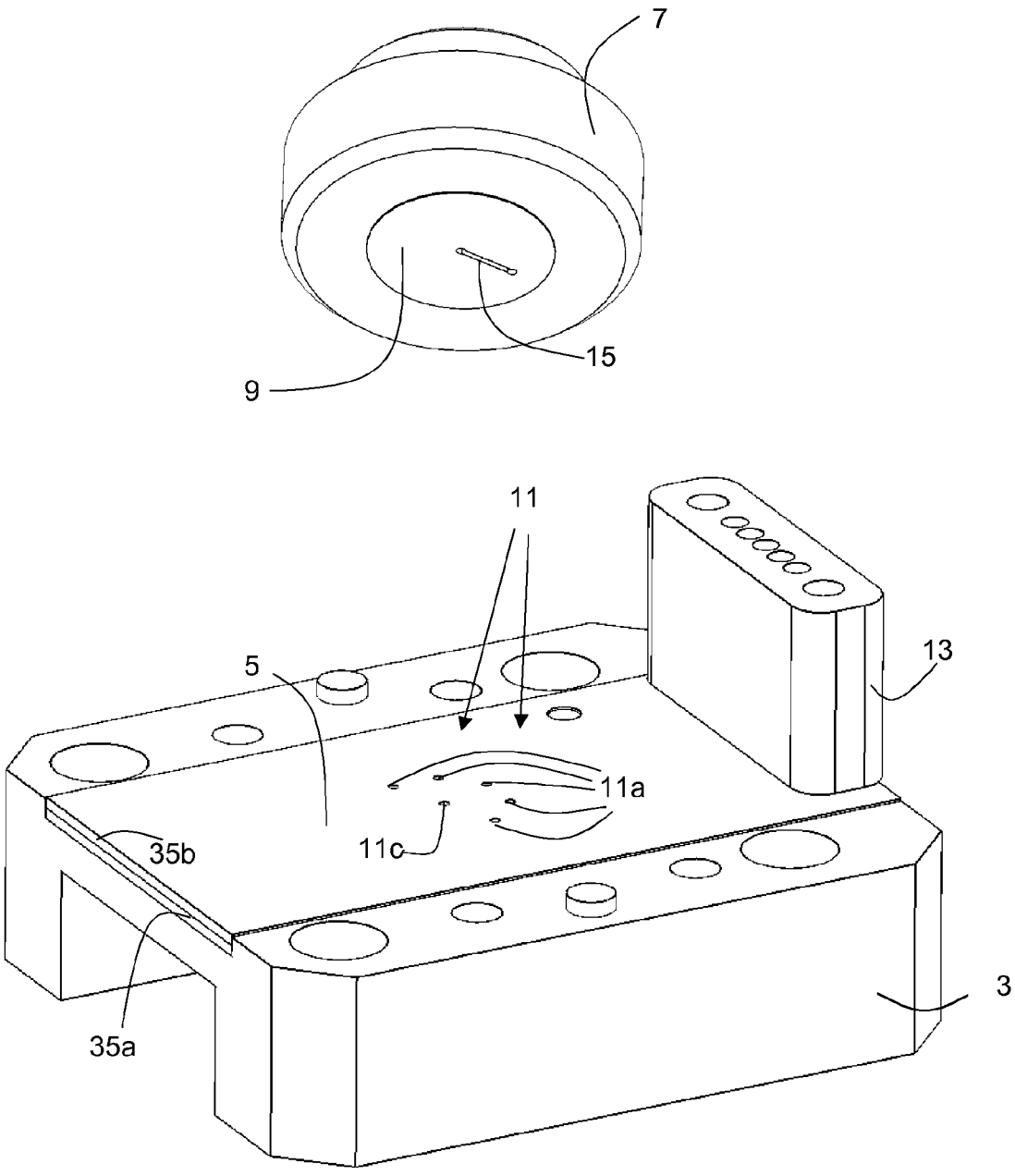

Figure 3

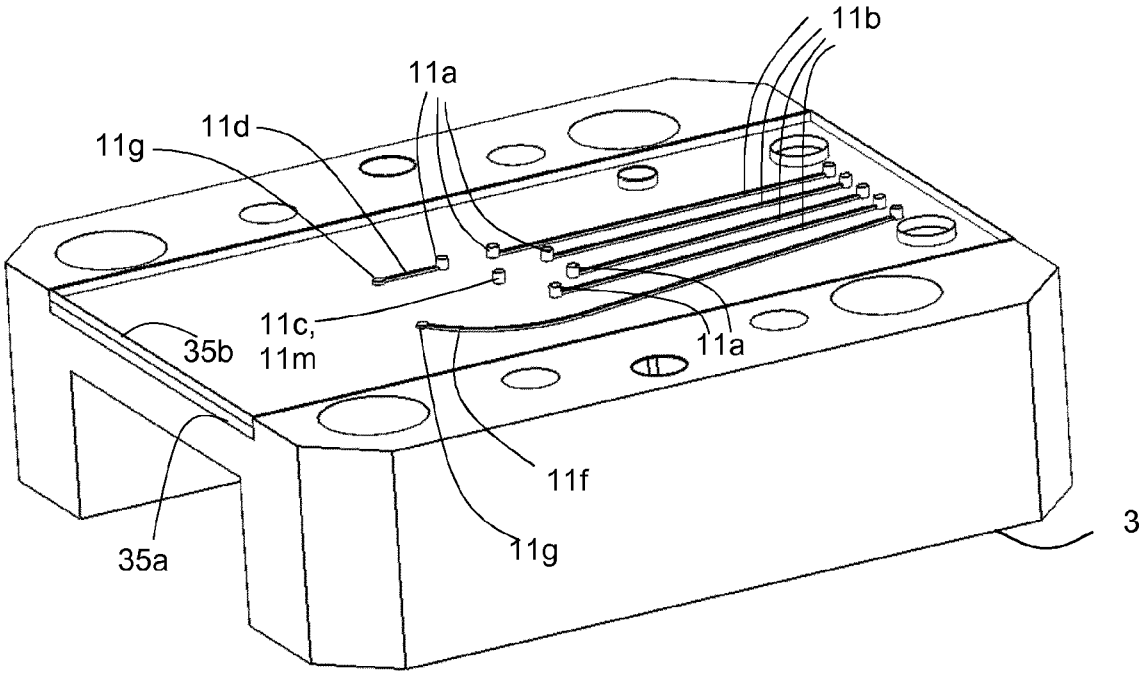

Figure 4

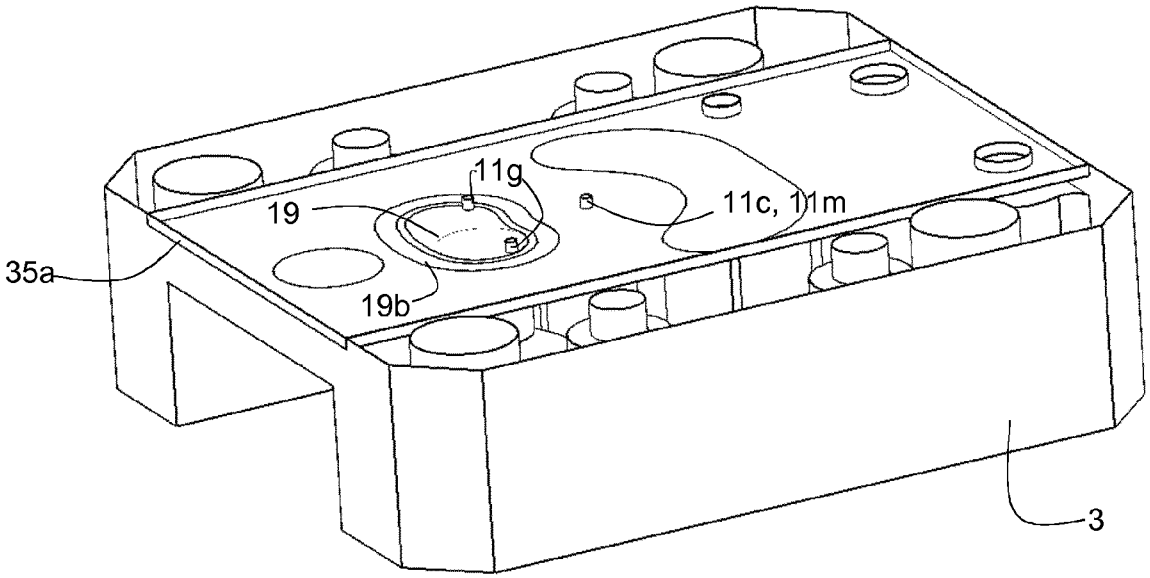

Figure 5

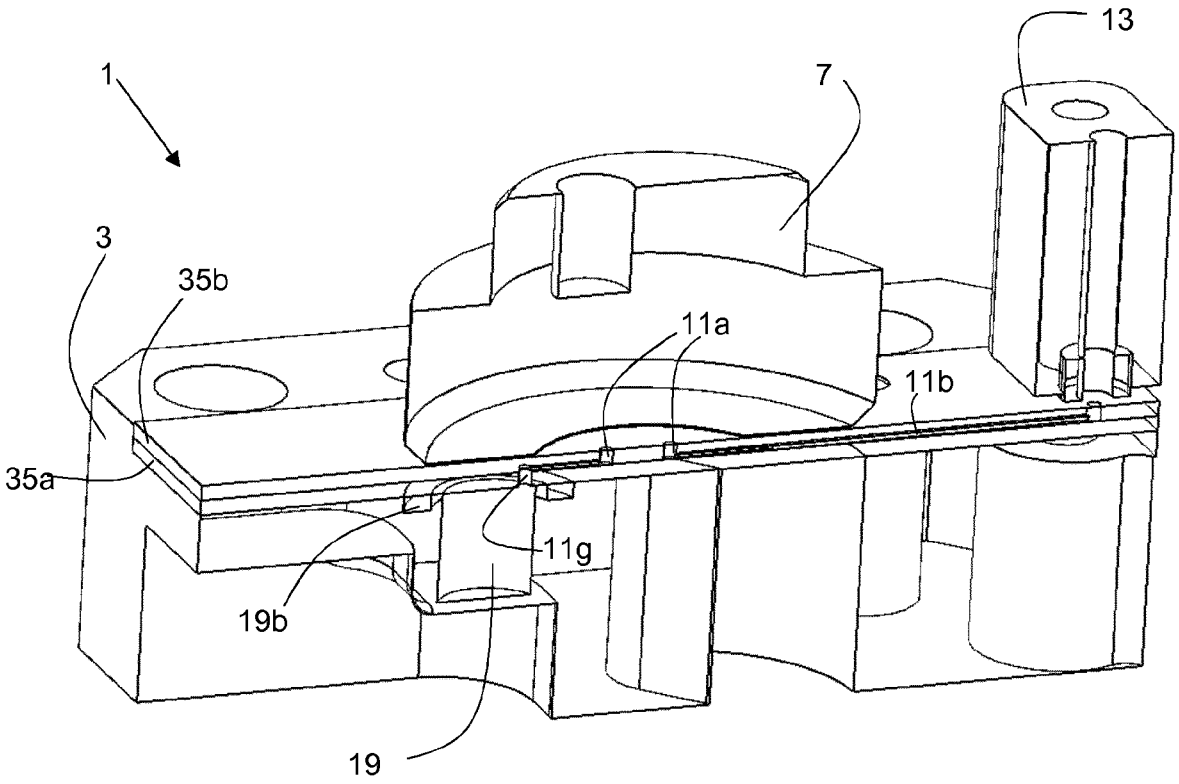

Figure 6

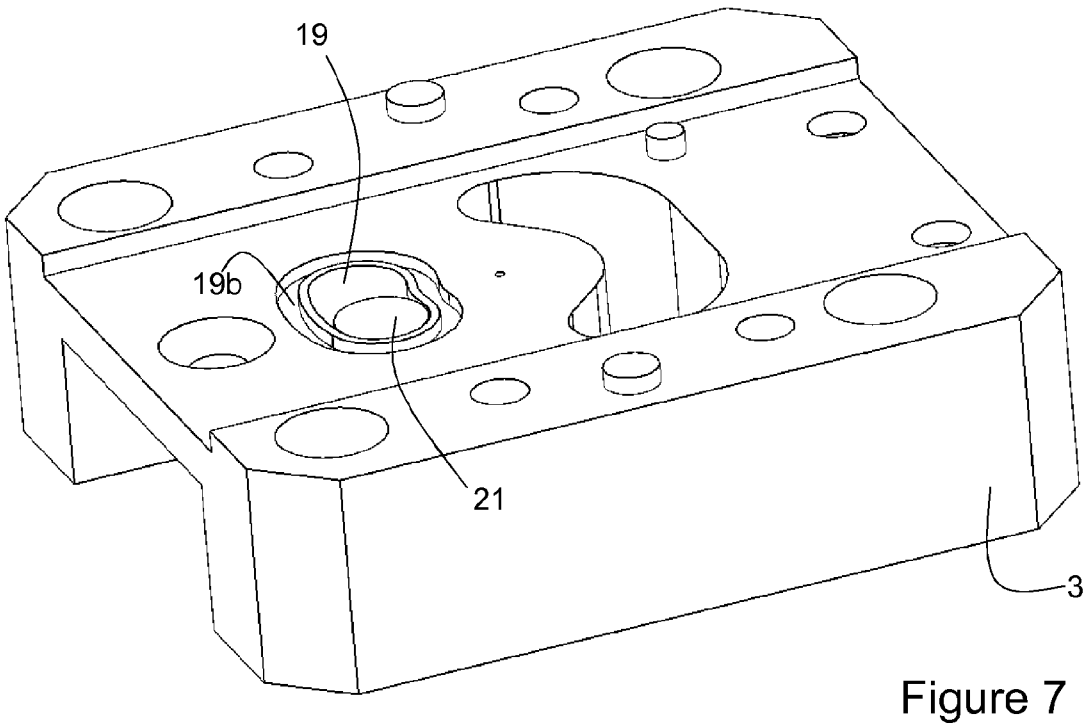

Figure 7

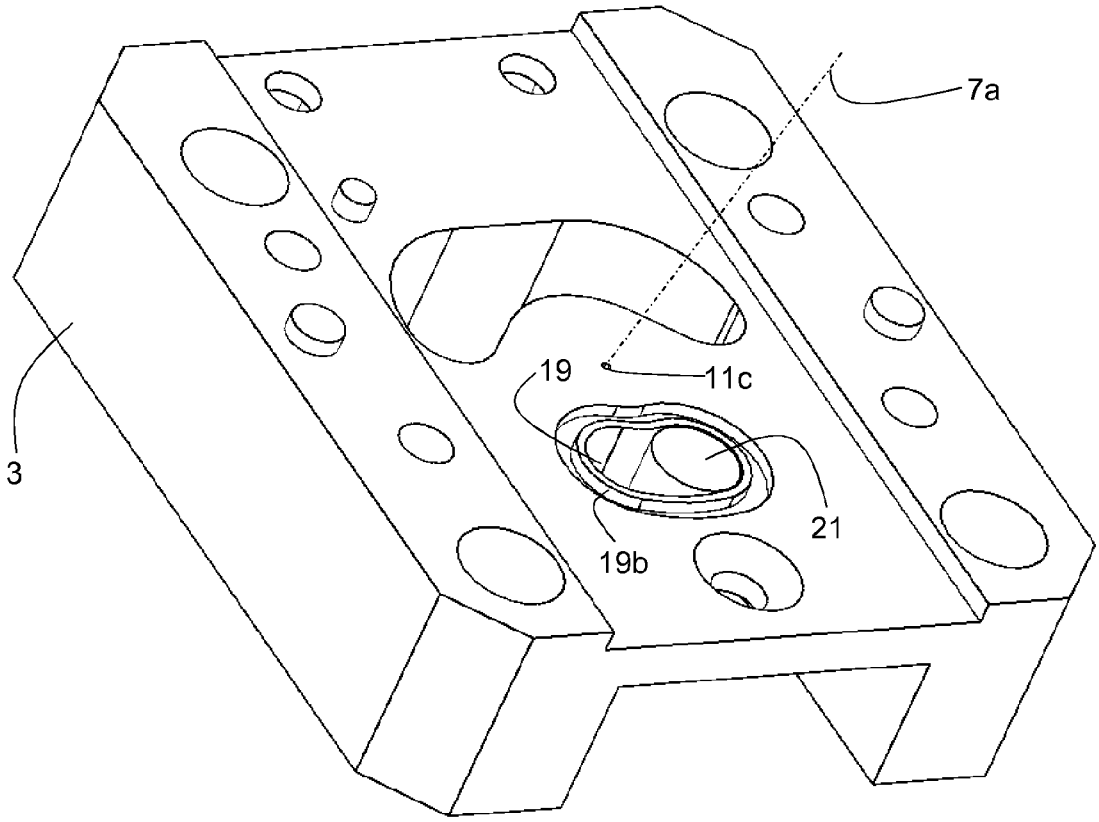

Figure 8

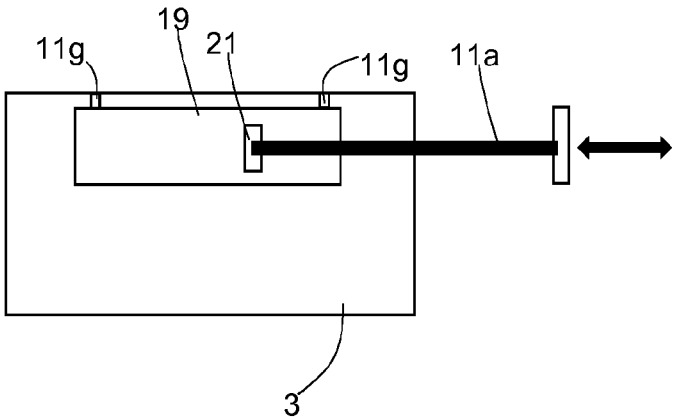

Figure 9

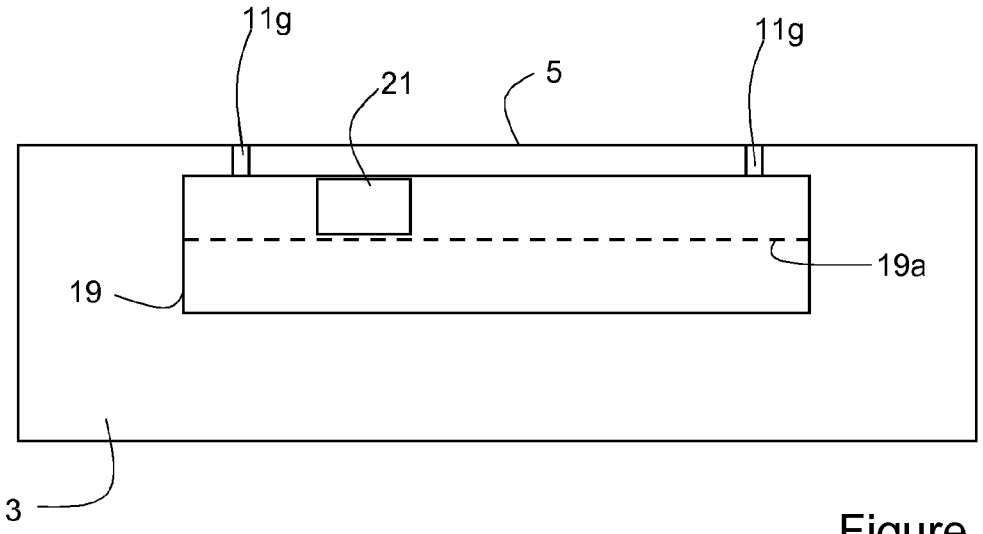

Figure 10

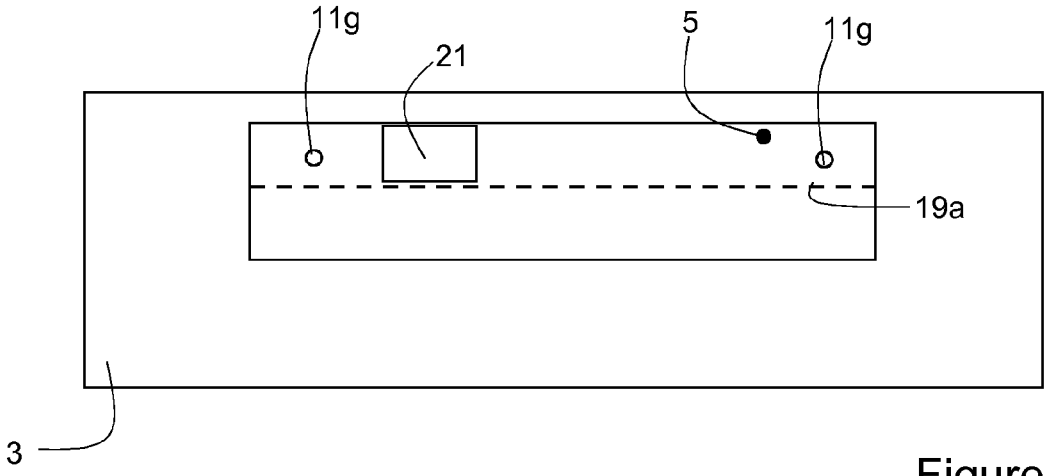

Figure 11

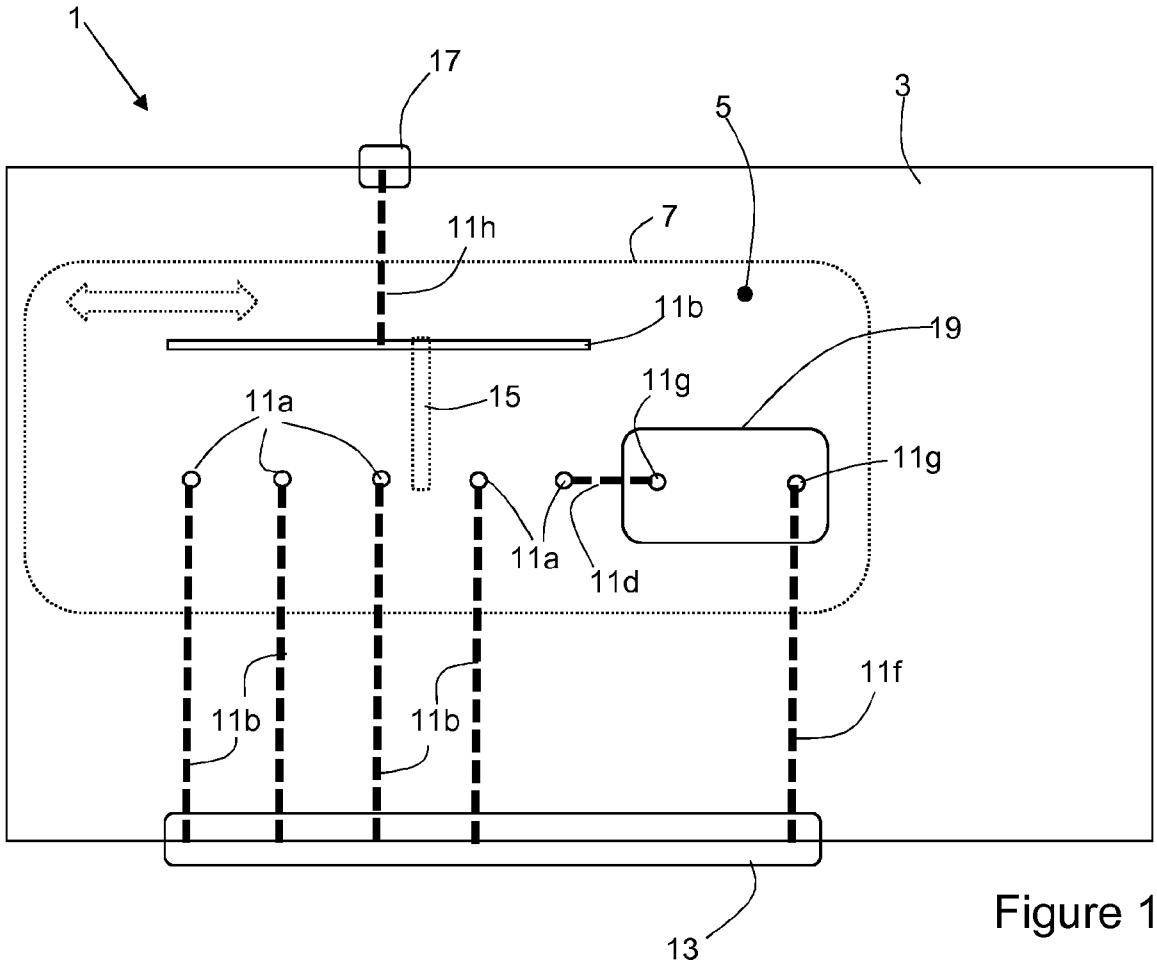

Figure 12

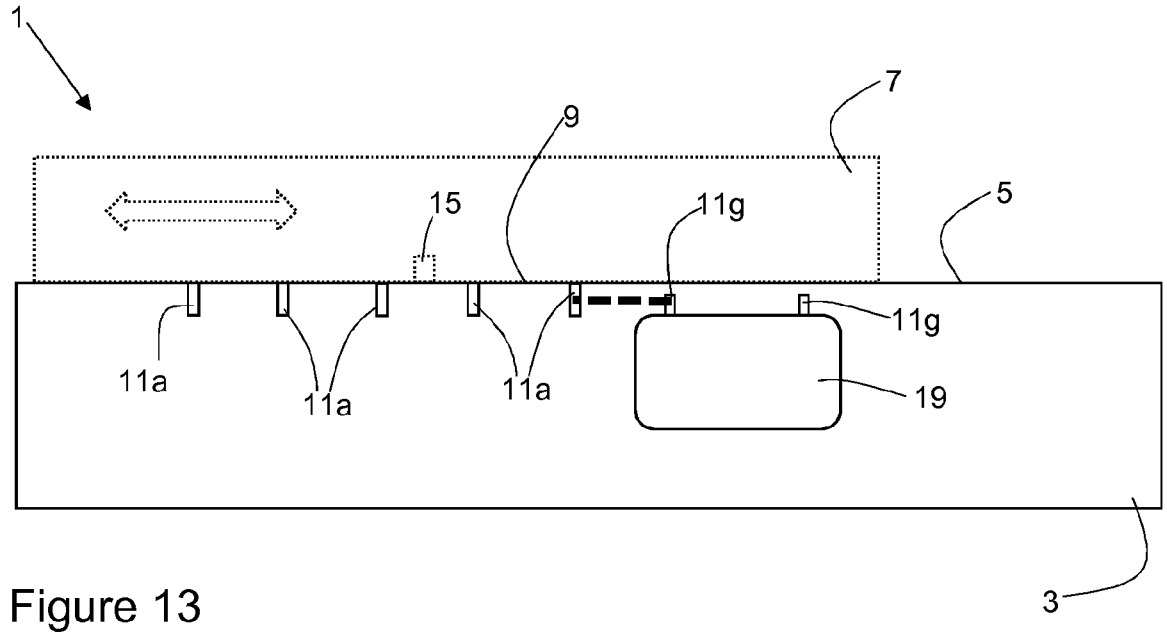

Figure 13

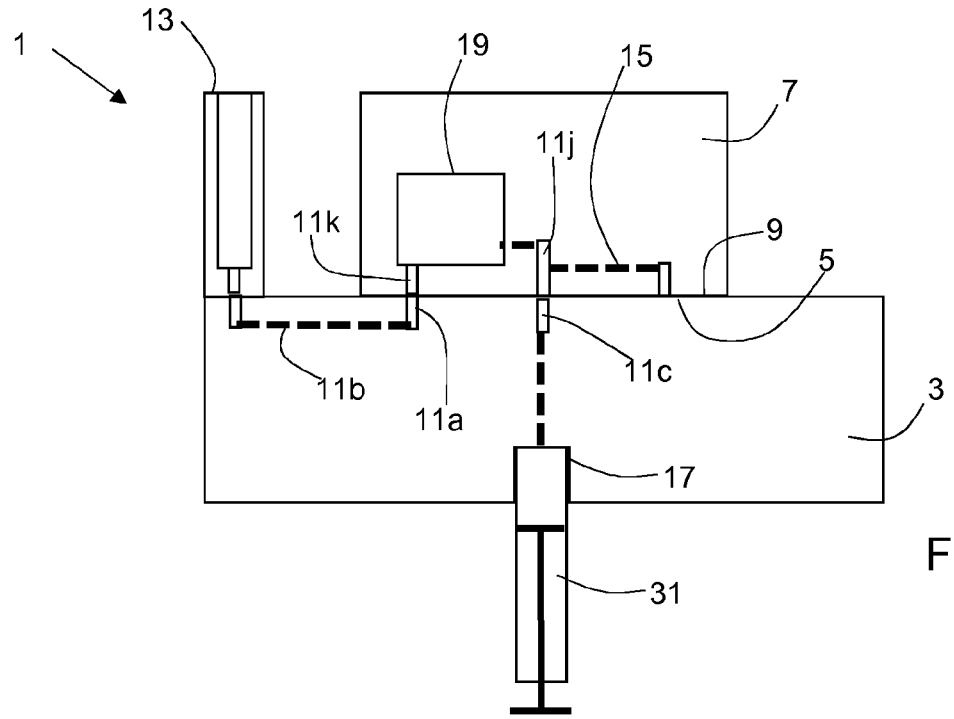

Figure 14

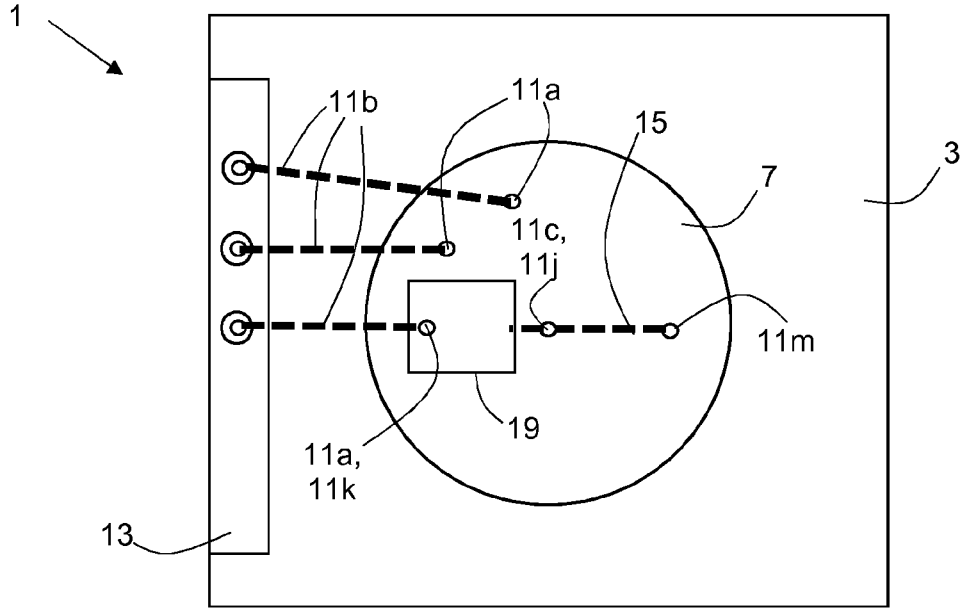

Figure 15

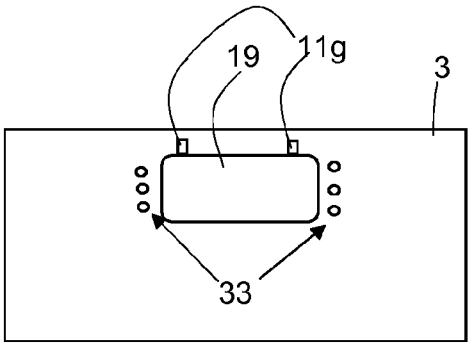

Figure 16

INTERNATIONAL SEARCH REPORT

International application No
PCT/EP2019/07 1210

A. CLASSIFICATION OF SUBJECT MATTER
INV. F16K99/00 B01F13/00 B01F13/08 B01L3/00
ADD.

According to International Patent Classification (IPC) or to both national classification and IPC

B. FIELDS SEARCHED

Minimum documentation searched (classification system followed by classification symbols)
F16K B01F B01L

Documentation searched other than minimum documentation to the extent that such documents are included in the fields searched

Electronic data base consulted during the international search (name of data base and, where practicable, search terms used)
EPO-Internal , WPI Data

C. DOCUMENTS CONSIDERED TO BE RELEVANT

Category*	Citation of document, with indication, where appropriate, of the relevant passages	Relevant to claim No.
X Y	US 2017/144155 A1 (BOHM SEBASTIAN [US] ET AL) 25 May 2017 (2017-05-25) paragraph [0100] - paragraph [0101] -----	1-3,8, 10-13 4-7
Y A	US 5 490 971 A (GIFFORD MICHAEL M [US] ET AL) 13 February 1996 (1996-02-13) column 6, line 45 - line 59; figure 3 -----	4-7 1,2,9,12
X	US 2011/318774 A1 (LARSEN ULRIK DARLING [DK]) 29 December 2011 (2011-12-29) paragraph [0105] - paragraph [0156]; figures -----	1,3-5,8, 11-13
X	US 2016/346782 A1 (DOTHIE PAMELA ANN [GB] ET AL) 1 December 2016 (2016-12-01) paragraph [0186] - paragraph [0285]; figures -----	1,3-5,8, 12,13
	-/--	

[X] Further documents are listed in the continuation of Box C.

[X] See patent family annex.

* Special categories of cited documents :

"A" document defining the general state of the art which is not considered to be of particular relevance

"E" earlier application or patent but published on or after the international filing date

"L" document which may throw doubts on priority claim(s) orwhich is cited to establish the publication date of another citation or other special reason (as specified)

"O" document referring to an oral disclosure, use, exhibition or other means

"P" document published prior to the international filing date but later than the priority date claimed

"T" later document published after the international filing date or priority date and not in conflict with the application but cited to understand the principle or theory underlying the invention

"X" document of particular relevance; the claimed invention cannot be considered novel or cannot be considered to involve an inventive step when the document is taken alone

"Y" document of particular relevance; the claimed invention cannot be considered to involve an inventive step when the document is combined with one or more other such documents, such combination being obvious to a person skilled in the art

"&" document member of the same patent family

Date of the actual completion of the international search	Date of mailing of the international search report
9 October 2019	23/10/2019

Name and mailing address of the ISA/	Authorized officer
European Patent Office, P.B. 5818 Patentlaan 2 NL - 2280 HV Rijswijk Tel. (+31-70) 340-2040, Fax: (+31-70) 340-3016	Lanel, François

1

Form PCT/ISA/210 (second sheet) (April 2005)

C(Continuation). DOCUMENTS CONSIDERED TO BE RELEVANT

Category*	Citation of document, with indication, where appropriate, of the relevant passages	Relevant to claim No.
X	US 2017/328924 A1 (JONES RONALD [US] ET AL) 16 November 2017 (2017-11-16) paragraph [0007]; figures ----- US 2009/129981 A1 (TOKITA TOSHINOBU [JP] ET AL) 21 May 2009 (2009-05-21) paragraph [0058] - paragraph [0059]; figures 1a-8d -----	1,3-5,8, 11-13
X		1,3,9, 10,12,13

INTERNATIONAL SEARCH REPORT

Information on patent family members

International application No
PCT/EP2019/07 1210

Patent document cited in search report	Publication date	Patent family member(s)	Publication date
US 2017144155 A1	25-05-2017	AU 2015269684 A1	15-12-2016
		CA 2950335 A1	10-12-2015
		CN 106573241 A	19-04-2017
		EP 3151964 A2	12-04-2017
		JP 2017522546 A	10-08-2017
		KR 20170015974 A	10-02-2017
		RU 2019114034 A	14-06-2019
		US 2017144155 A1	25-05-2017
		WO 2015187868 A2	10-12-2015
US 5490971 A	13-02-1996	AU 3956295 A	15-05-1996
		US 5490971 A	13-02-1996
		WO 9612561 A1	02-05-1996
US 2011318774 A1	29-12-2011	AU 2006212607 A1	17-08-2006
		CA 2597496 A1	17-08-2006
		EP 1891413 A1	27-02-2008
		JP 5096170 B2	12-12-2012
		JP 2008530539 A	07-08-2008
		US 2011318774 A1	29-12-2011
		WO 2006084472 A1	17-08-2006
US 2016346782 A1	01-12-2016	CN 104344864 A	11-02-2015
		CN 108917874 A	30-11-2018
		EP 2842628 A1	04-03-2015
		US 2015044696 A1	12-02-2015
		US 2016346782 A1	01-12-2016
US 2017328924 A1	16-11-2017	NONE	
US 2009129981 A1	21-05-2009	JP 2009128037 A	11-06-2009
		US 2009129981 A1	21-05-2009

(19) Europäisches Patentamt
European Patent Office
Office européen des brevets

(11) EP 3 751 241 A1

(12) EUROPEAN PATENT APPLICATION

(43) Date of publication:
16.12.2020 Bulletin 2020/51

(51) Int Cl.:
G01F 11/08 *(2006.01)* ***G01F 15/16*** *(2006.01)*

(21) Application number: **19179741.4**

(22) Date of filing: **12.06.2019**

(84) Designated Contracting States:
AL AT BE BG CH CY CZ DE DK EE ES FI FR GB GR HR HU IE IS IT LI LT LU LV MC MK MT NL NO PL PT RO RS SE SI SK SM TR
Designated Extension States:
BA ME
Designated Validation States:
KH MA MD TN

(71) Applicant: **CSEM**
Centre Suisse d'Electronique et de Microtechnique SA
2002 Neuchâtel (CH)

(72) Inventors:
- **SCHMID, Noa**
  6010 Kriens (CH)
- **GRAF, Siegfried**
  6010 Kriens (CH)
- **HALVORSEN, Zahra Alsadat**
  8002 Zürich (CH)

(74) Representative: **e-Patent SA**
Rue Saint-Honoré 1
Boîte Postale CP 2510
2001 Neuchâtel (CH)

(54) FLUID DOSING SYSTEM

(57) Fluid dosing system (1) comprising:
- a dosing chamber (3) divided in a fluid-tight manner by means of a displaceable membrane (5) into:
a) a dosing compartment (3a); and
b) a working fluid compartment (3b) filled with a working fluid having a bulk modulus of at least 1GPa;

- a first fluid port (3c) in fluidic communication with said dosing compartment (3a);
- a second fluid port (3d) in fluidic communication with said working fluid compartment (3b);
- an expansion reservoir (9) in fluidic communication with said fluid second port (3d) and filled with said working fluid;
- a bidirectional pump (7) in fluidic communication with said second port (3d) and said expansion reservoir (9) so as to be able to pump said working fluid bidirectionally between said working fluid compartment (3b) and said expansion reservoir (9);
- a flow sensor (13) arranged to measure flow of said working fluid based on displacement of at least part of said expansion reservoir (9).

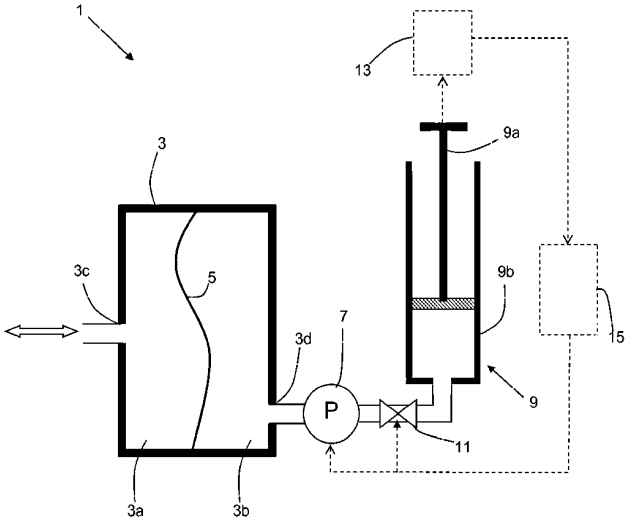

Figure 1

EP 3 751 241 A1

Description

Technical Field

[0001] The present invention relates to the technical field of pumps. More particularly, it relates to a fluid metering system which is capable of substantially pulse-free operation.

State of the art

[0002] Syringe pumps are well known in the art, and are little more than a conventional syringe in which the piston is actuated by a motor via a rack- and-pinion, gearwheel or screw arrangement so as to dispense and/or aspirate a sample, typically a liquid sample. Such actuation results in the flow of the sample being pulsatory, and requires a significantly bulky apparatus. Furthermore, the sliding fit of the piston results in stick-slip during actuation, leading to inaccuracy, and is subject to wear. In respect of this latter point, due to the sliding seal formed between the piston and the cylinder of the syringe, particles can be sloughed off the piston head, contaminating the liquid. Also, contaminants on the dry sidewalls of the syringe can be introduced into the liquid if the piston head rides over them, which is a major issue in the case in which the sterility of the liquid to be dispensed must be maintained.

[0003] Syringe pumps are sometimes combined with flow volume and/or flow rate sensors, which have to be placed in contact with the fluid being dosed. This presents a further contamination risk, particularly in the case of biological samples which need to be kept sterile, requiring the sensor remain scrupulously clean and sterile, which is difficult to achieve.

[0004] US 6419462 describes various embodiments of positive displacement liquid delivery apparatuses, which avoid such a sliding seal in contact with the liquid to be dispensed. Figure 1 of this document will be briefly described in the following. This apparatus comprises a housing defining a cavity which is divided into two compartments by a flexible membrane. The first compartment is filled with the liquid to be metered and delivered, and is in fluidic communication with a reservoir thereof via a corresponding valve (the input valve). It is likewise in fluidic communication with an output port by means of a second (output) valve. The second compartment is filled with a substantially incompressible working fluid such as water, silicone oil or similar, and is in communication with a working fluid reservoir via a constant flow pump. A bypass valve enables the working fluid compartment to be drained to the working fluid reservoir.

[0005] To operate the apparatus, a quantity of liquid to be dispensed is introduced into the first compartment by closing the output valve, opening the input valve, and forcing the liquid to be dispensed to enter into the first compartment by gas pressure. At the same time, the bypass valve is opened so as to allow the working fluid displaced by the movement of the flexible membrane to drain into the working fluid reservoir.

[0006] Subsequently, the input valve is closed, and the output valve is opened. The bypass valve is likewise closed, and the constant flow pump is operated. The volume of fluid delivered corresponds to the volume of working fluid pumped, which can be determined by e.g. counting the number of turns or part turns of the pump actuator.

[0007] However, such an arrangement is complicated and requires three valves for its operation. Furthermore, since it relies on predetermination of the volume of working fluid pumped in function of the operation of the pump, errors can occur due to non-correlation between the nominal flow rate of the pump and the actual flow rate.

[0008] An aim of the present invention is hence to at least partially overcome the above-mentioned disadvantages of the prior art.

Disclosure of the invention

[0009] The invention hence relates to a fluid dosing system as described in claim 1. This fluid dosing system comprises:

- a dosing chamber divided in a fluid-tight manner by a displaceable membrane into:

  a) a dosing compartment, which may contain a liquid to be dispensed or a gas such as air intended to aspirate and dispense a liquid as generally known in pipetting; and
  b) a working fluid compartment filled with a working fluid having a bulk modulus of at least 1GPa, which is hence substantially incompressible. This working fluid can be e.g. water, hydraulic fluid, mineral oil, silicone oil or similar.

- a first fluid port in fluidic communication with said dosing compartment, which hence permits gas or liquid to enter and leave the dosing compartment;
- a second fluid port in fluidic communication with said working fluid compartment;
- an expansion reservoir in indirect fluidic communication with said second port and filled with said working fluid;
- a bidirectional pump in fluidic communication with said second port and said expansion reservoir so as to be able to pump said working fluid bidirectionally between said working fluid compartment and said expansion reservoir. In other words, the pump is interposed between the second port and the expansion reservoir;
- a flow sensor arranged to measure flow of said working fluid based on displacement of said expansion reservoir, and thereby to determine the volume which has flowed and/or its flow rate.

[0010] This displacement can be measured directly,

e.g. by measuring the displacement of a piston or the end face of a bellows, or may be indirect, e.g. by measuring displacement of air caused by expansion and contraction of the expansion reservoir in an air-filled enclosure.

[0011] As a result, accurate measurement of the volume and/or flow rate of fluid aspirated or dosed is possible, without placing a sensor in contact with the fluid itself, and without relying on the calibration of a constant volume pump. Hence other types of pumps such as viscous flow pumps can be used, which do not have a precise relationship between their mechanical actuation and the volume pumped. Since the fluid pumped is substantially incompressible, precise measurement can be obtained (which is not possible with e.g. pneumatic actuation without having a sensor in contact with the fluid being pumped), while avoiding the inaccuracies associated with pump-related stick-slip, gear backlash or similar of a syringe pump. Furthermore, the system can be made extremely compact, and is hence suitable for microfluidic applications.

[0012] In an embodiment, the expansion reservoir comprises a cylinder in which a piston is slidingly mounted, said flow sensor being arranged to measure displacement of said piston.

[0013] In a different embodiment, said expansion reservoir comprises an expandable bellows.

[0014] Advantageously, said expansion reservoir comprises an expandable enclosure filled with said working fluid and situated in a gas filled chamber, said gas filled chamber having a gas port situated therein, and said flow sensor being arranged to measure the flow volume and/or the flow rate of said gas through said gas port. The expansion and contraction of the expandable enclosure displaces air through the gas port, this flow of air corresponding to the flow of fluid being aspirated or dispensed from the dosing compartment. Such an arrangement can be made extremely compact, and comprises no sliding seals which may be subject to wear. The expandable enclosure may, for instance, be a balloon, an expandable bellows, or a compartment in the gas filled chamber delimited by a displaceable membrane.

[0015] In respect of the pump, this can advantageously be a gear pump or a viscous drag pump. In the latter case, a controllable valve may be situated in the fluid pathway between the working fluid compartment and the expansion reservoir, either between the working fluid compartment and the pump, or between the pump and the expansion reservoir. This valve prevents movement of the working fluid when the viscous drag pump is not being operated. Preferably, this valve is arranged to be controlled by a controller on the basis of an output of said flow sensor.

[0016] Advantageously, the pump is arranged to be controlled by a controller on the basis of an output of said flow sensor. Such feedback control permits very precise dosing of predetermined quantities of fluid.

[0017] A fluid dosing system as described above can, for instance, be integrated into a pipetting system, a flow cytometry system, a microfluidic chip or similar.

Brief description of the drawings

[0018] Further details of the invention will appear more clearly upon reading the description below, in connection with the following figures which illustrate:

- Figure 1: a schematic view of a first embodiment of the invention;
- Figure 2: a schematic view of a second embodiment of the invention;
- Figure 3: a schematic view of a third embodiment of the invention;
- Figure 4: a schematic view of a fourth embodiment of the invention; and
- Figure 5: a schematic view of a pipetting system incorporating a fluid dosing system according to the invention.

Embodiments of the invention

[0019] Figure 1 illustrates a first embodiment of a fluid dosing system 1 according to the invention. In the figures, dashed lines illustrate functional relationships transmitting information or commands, for instance by electronics, optics, mechanics or other means, as appropriate in each case.

[0020] This system comprises a hollow dosing chamber 3 divided into a dosing compartment 3a and a working fluid compartment 3b by means of a movable membrane 5.

[0021] Membrane 5 is sealingly fixed to the walls of the chamber 3, and may be for instance a simple membrane made of an elastic material such as a polymer or an elastomer, may be a substantially inelastic material arranged with slack such that the mid-part membrane can displace, may be metallic or polymer bellows-type arrangement (similar to that used in a traditional aneroid capsule) or any other convenient arrangement. Suitable materials are metals, PTFE, polymers, elastomers, and so on, which are impermeable to the fluids with which it is in contact.

[0022] Dosing compartment 3a can be filled either with the fluid to be dosed, or a gas such as air, nitrogen or argon, and has a first fluid port 3c arranged in a sidewall thereof, in order to allow said fluid to enter and leave the dosing compartment 3a. Depending on the manner in which the system 1 is being used, a pipette tip and/or a suitable conduit may be directly or indirectly connected to the first fluid port 3c in fluidic communication therewith. In the case in which dosing compartment 3a is filled with a gas, a liquid sample can be aspirated into and dispensed from the pipette tip and/or conduit as is generally known, and hence need not be described in detail.

[0023] Working fluid compartment 3b is filled with a

working fluid such as water, hydraulic fluid, mineral oil, silicone oil or similar, substantially incompressible fluid, defined in context of the present invention as exhibiting a bulk modulus of greater than 1 GPa, preferably at least 1.5 GPa, further preferably at least 2 GPa.

[0024] Working fluid compartment 3b is provided with a second fluid port 3d in a sidewall thereof. In order to cause the working fluid to enter and leave the working fluid compartment 3b, a bidirectional pump 7 is provided in fluidic communication therewith, and is arranged to pump said working fluid between said working fluid compartment 3b and an expansion reservoir 9, to which end it is likewise in fluidic communication therewith, and which will be described in further detail below.

[0025] Pump 7 is advantageously of the viscous drag type, such as described in EP2208891. Such a pump is not only bidirectional, but it is entirely pulsation-free. However, when such a pump is stopped, it exhibits internal leakage, in which case a controllable valve 11 is provided in the fluid pathway between the working fluid compartment 3b and the expansion reservoir 9. In the illustrated embodiment, this is situated between the pump 7 and the expansion reservoir 9, however this can alternatively be situated between the pump 7 and the working fluid compartment 3b. It should also be noted that the pump 7 can be integrated into the sidewall of the working fluid compartment 3b, and/or the valve 7 may be integrated with the pump 7. In the case of such a pump, the pressure which can be produced is proportional to the viscosity of the working fluid, which is typically higher than that of water (e.g. hydraulic fluid, silicone oil or similar).

[0026] Other types of bidirectional pump are also possible, such as a gear pump which is substantially (but not entirely) pulsation free. Since such gear pumps typically do not exhibit significant internal leakage, the valve 7 may be optional in such cases. Due to the inertia of the working fluid and the membrane 5, the small residual pulsation is essentially filtered out and is reduced to insignificance, and hence such pumps are suitable for use with the invention.

[0027] Hence, by pumping working fluid into or out of the working fluid compartment 3b, its volume can be changed. This causes at least part of the membrane 5 to displace, which modifies the volume of the dosing compartment 3a to the same extent, due to the incompressibility of the working fluid.

[0028] As a result, by measuring the change in volume of the expansion reservoir 9, the volume and/or flow rate of fluid entering into or leaving the dosing chamber 3a can be precisely measured, without interacting directly therewith, and without a sliding seal being present in contact with the fluid in the dosing chamber 3a.

[0029] In the embodiment of figure 1, the expansion reservoir 9 is a syringe-type arrangement, with a piston 9a slidably arranged in a cylinder 9b as is generally known. The sliding seal between the piston 9a and the cylinder 9b is arranged to present as little resistance as possible, such that the volume of working fluid in the expansion chamber 9 can vary without overworking the pump 7.

[0030] The displacement of the piston 9a can be determined by a measuring device 13, which may for instance comprise a mechanical measurement system comprising for instance a toothed rack attached to the piston 9a and a pinion or gear wheel meshing therewith such that its rotation can be measured e.g. by means of a rotary encoder. Alternatively, nonmechanical measurement can be carried out, e.g. by means of ultrasonic or laser measurement of the position of the piston 9a, optical reading of a Vernier scale, a capacitive or inductive sensing system, or similar, as is generally known.

[0031] This measuring device 13 is in operational connection with a controller 15, which determines the volume of working fluid pumped, and / or its flow rate. Controller 15 may also control the pump 7, e.g. by a Proportional-Integral-Differential (PID) controller, simple feedback control, or similar, in order to pump a predetermined quantity of working fluid and thereby to aspirate or dispense a predetermined quantity of a sample. At the same time, controller 15 may command valve 11 (if present) to open and close as appropriate.

[0032] The embodiment of figure 2 differs from that of figure 1 in that the expansion reservoir 9 comprises a flexible balloon 9c defining an expandable enclosure situated inside a substantially rigid chamber 9d. This latter is filled with a gas such as air, and comprises an outlet port 9f in fluidic communication with a flow meter 17 which forms part of measuring device 13 and is arranged to measure the volumetric flow and / or flow rate of said gas into and out of the rigid chamber 9d. Any convenient type of flow meter 17 can be used, such as a differential pressure flow meter comprising a flow restriction, an anemometer-type flow meter, a Coriolis flow meter, or similar. The other side of the flow meter can vent to atmosphere or to a yet further reservoir (not illustrated). In other words, displacement of the surface of the balloon 9c hence causes the volume of the air-filled portion of the rigid chamber 9d to change, displacing air through the outlet port 9f, this displaced air having substantially the same volume as the fluid aspirated / dispensed. The flow meter 17 thereby indirectly measures this volume based on displacement of the surface of the balloon 9c during aspiration / dispensing as working fluid enters or leaves it.

[0033] As before, measuring device 13 is in operational connection with a controller 15.

[0034] Alternatively, the expansion reservoir 9 may comprise an expandable bellows (not illustrated) or other expandable enclosure instead of a balloon 9c, the system functioning otherwise in the same manner.

[0035] The embodiment of figure 3 differs from that of figure 1 in that an expandable bellows 9g, the expansion of which is measured mechanically, optically or by ultrasound on the basis of the displacement of its end face.

[0036] Finally, the embodiment of figure 4 differs from that of figure 2 in that the expansion chamber 9 comprises

a membrane 9h similar to the membrane 5 of the dosing chamber, which functions in the same manner, and for which the same considerations apply. This membrane 9h delimits one side of an expandable enclosure 9j formed between the sidewalls of the chamber 9d and the membrane 9h. Displacement of the membrane 9h can alternatively be measured ultrasonically, magnetically (e.g. by fixing a magnet to the membrane 9h and measuring its displacement by means of a magnetic sensor such as a Hall probe), capacitively or optically rather than by use of the flow meter 17.

[0037] In all of the above embodiments, since the measurement of the volume of fluid aspirated or dispensed takes place remotely from said fluid, all risk of contamination by sliding seals or flow meters in contact therewith is removed, while retaining excellent measurement accuracy.

[0038] It should be noted that the system 1 of the invention is particularly suited for aspiring and dosing relatively small quantities of fluid, particularly under 10mL, more particularly under 1mL, and provides accuracy down to approximately 0.01μL. Typical flow rates can be as large as 2 mL/s, or as small as 1 μL per minute, depending on the dimensions of the system 1 and the type of pump 7 used. As a result, the system 1 is particularly suited to laboratory automation products for e.g. pipetting, titration or other applications such as flow cytometry, but it can also be applied in any liquid metering applications or microfluidics in general due to the fact that it can be constructed in a very compact manner.

[0039] To this end, figure 5 illustrates schematically a pipetting system 100 comprising one or more fluid dosing systems 1 according to the invention, the first fluid port 3a of each being in fluidic communication with a conduit 21 leading to a pipetting tip 2, which likewise has a conduit passing through it axially, as is generally known. As mentioned above, the entire conduit 21 and dosing compartment 3a may be filled with the liquid to be pipetted, or they may be filled with air, the liquid to be pipetted only being aspirated a certain distance along the conduit 21 as is generally known.

[0040] Alternatively, the system 100 may be a flow cytometry system or a microfluidic chip. It is not necessary to illustrate these other possibilities explicitly, since the application of one or more fluid dosing system 1 therein is clear to the skilled person.

[0041] Although the invention has been described in terms of specific embodiments, variations thereto are possible without departing from the scope of the invention as defined in the appended claims.

Claims

1. Fluid dosing system (1) comprising:

   - a dosing chamber (3) divided in a fluid-tight manner by means of a displaceable membrane (5) into:

     a) a dosing compartment (3a); and
     b) a working fluid compartment (3b) filled with a working fluid having a bulk modulus of at least 1GPa;

   - a first fluid port (3c) in fluidic communication with said dosing compartment (3a);
   - a second fluid port (3d) in fluidic communication with said working fluid compartment (3b);
   - an expansion reservoir (9) in fluidic communication with said fluid second port (3d) and filled with said working fluid;
   - a bidirectional pump (7) in fluidic communication with said second port (3d) and said expansion reservoir (9) so as to be able to pump said working fluid bidirectionally between said working fluid compartment (3b) and said expansion reservoir (9);
   - a flow sensor (13) arranged to measure flow of said working fluid based on displacement of at least part of said expansion reservoir (9).

2. Fluid dosing system (1) according to claim 1, wherein said expansion reservoir (9) comprises a cylinder (9b) in which a piston (9a) is slidingly mounted, said flow sensor being arranged to measure displacement of said piston (9a).

3. Fluid dosing system (1) according to claim 1, wherein said expansion reservoir (9) comprises an expandable bellows (9g).

4. Fluid dosing system (1) according to claim 1, wherein said expansion reservoir (9) comprises an expandable enclosure (9c; 9j); filled with said working fluid and situated in a gas filled chamber (9d), said gas filled chamber (9d) having a gas port (9f) situated therein, and said flow sensor (13) being arranged to measure flow of said gas through said gas port (9f).

5. Fluid dosing system (1) according to claim 4, wherein said expandable enclosure is a balloon (9c) or an expandable bellows or is at least partially delimited by a displaceable membrane (9h).

6. Fluid dosing system (1) according to any preceding claim, wherein said dosing compartment (3a) is filled with a gas

7. Fluid dosing system (1) according to one of claims 1-5, wherein said dosing compartment (3a) is filled with a liquid, preferably a liquid to be dispensed by the system.

8. Fluid dosing system (1) according to any preceding claim, wherein said pump (7) is a gear pump.

9. Fluid dosing system (1) according to one of claims 1-7, wherein said pump (7) is a viscous drag pump.

10. Fluid dosing system (1) according to the preceding claim, further comprising a controllable valve (11) situated between said expansion reservoir (9) and said working fluid compartment (3b).

11. Fluid dosing system (1) according to claim 10, wherein said valve (11) is arranged to be controlled by a controller (15) on the basis of an output of said flow sensor (13).

12. Fluid dosing system (1) according to any preceding claim, wherein said pump (7) is arranged to be controlled by a controller (15) on the basis of an output of said flow sensor (13).

13. Pipetting system (100) comprising at least one fluid dosing system (1) according to any preceding claim.

14. Flow cytometry system comprising at least one fluid dosing system (1) according to any of claims 1-12.

15. Microfluidic chip comprising at least one fluid dosing system (1) according to any of claims 1-12.

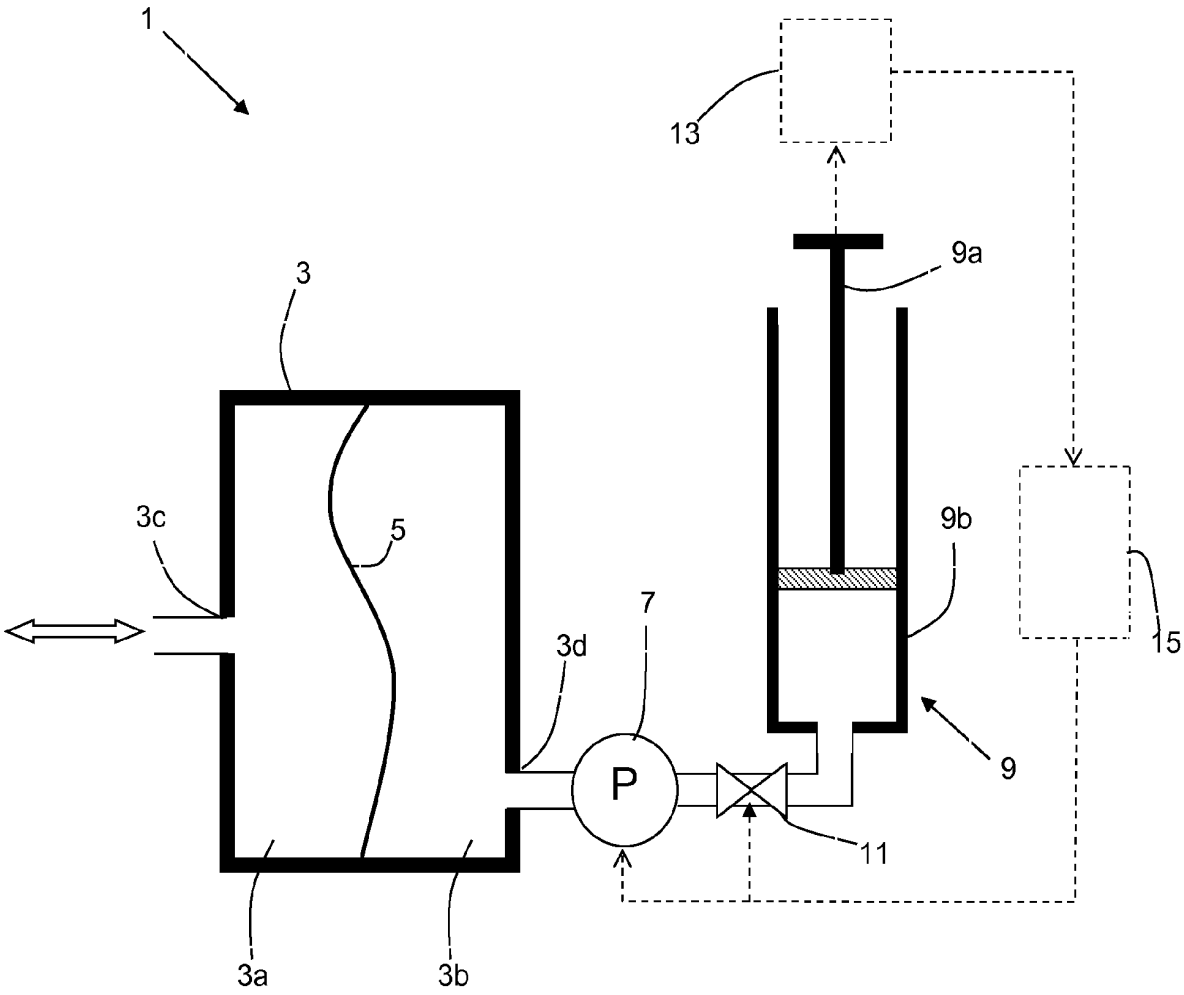

Figure 1

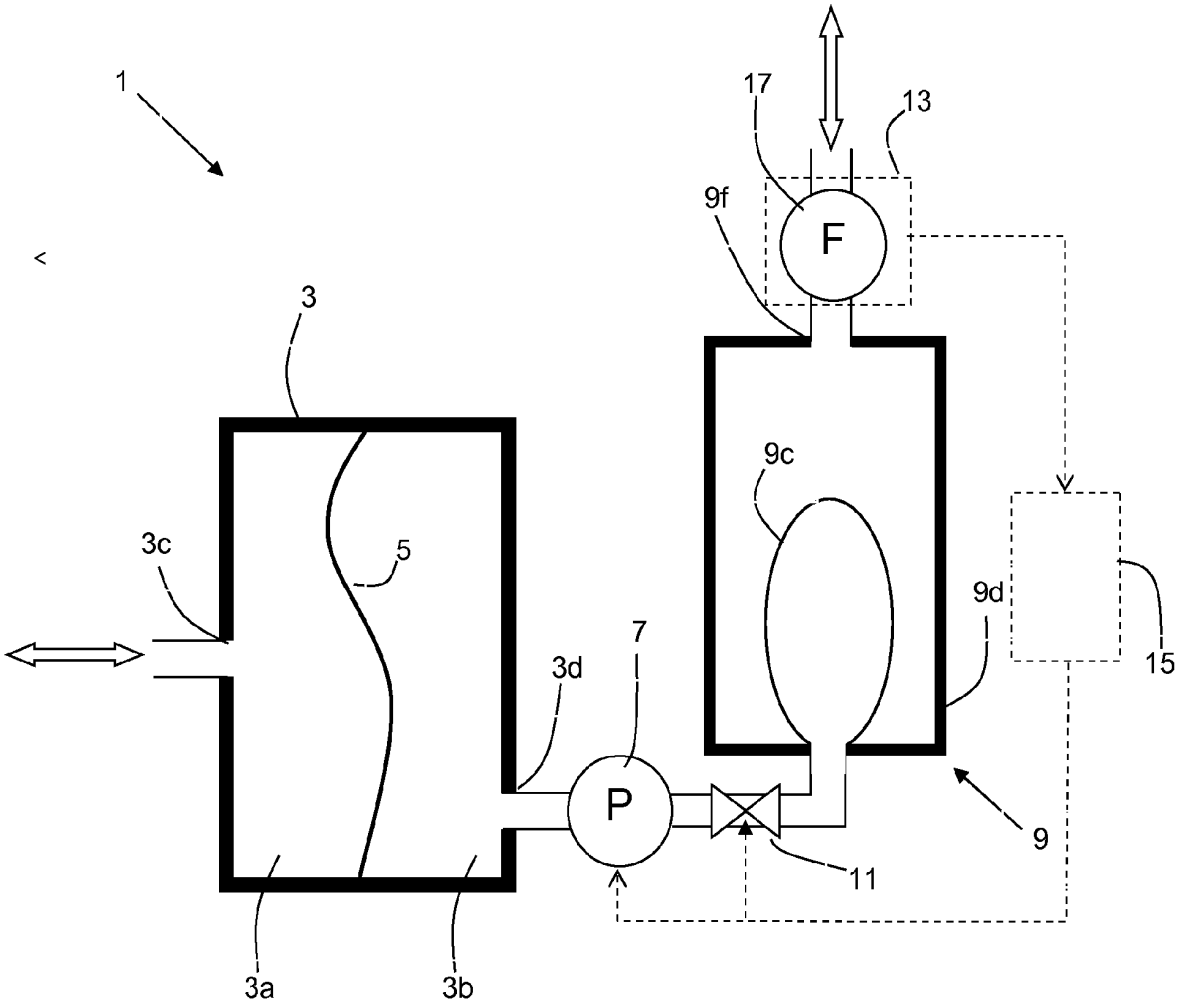

Figure 2

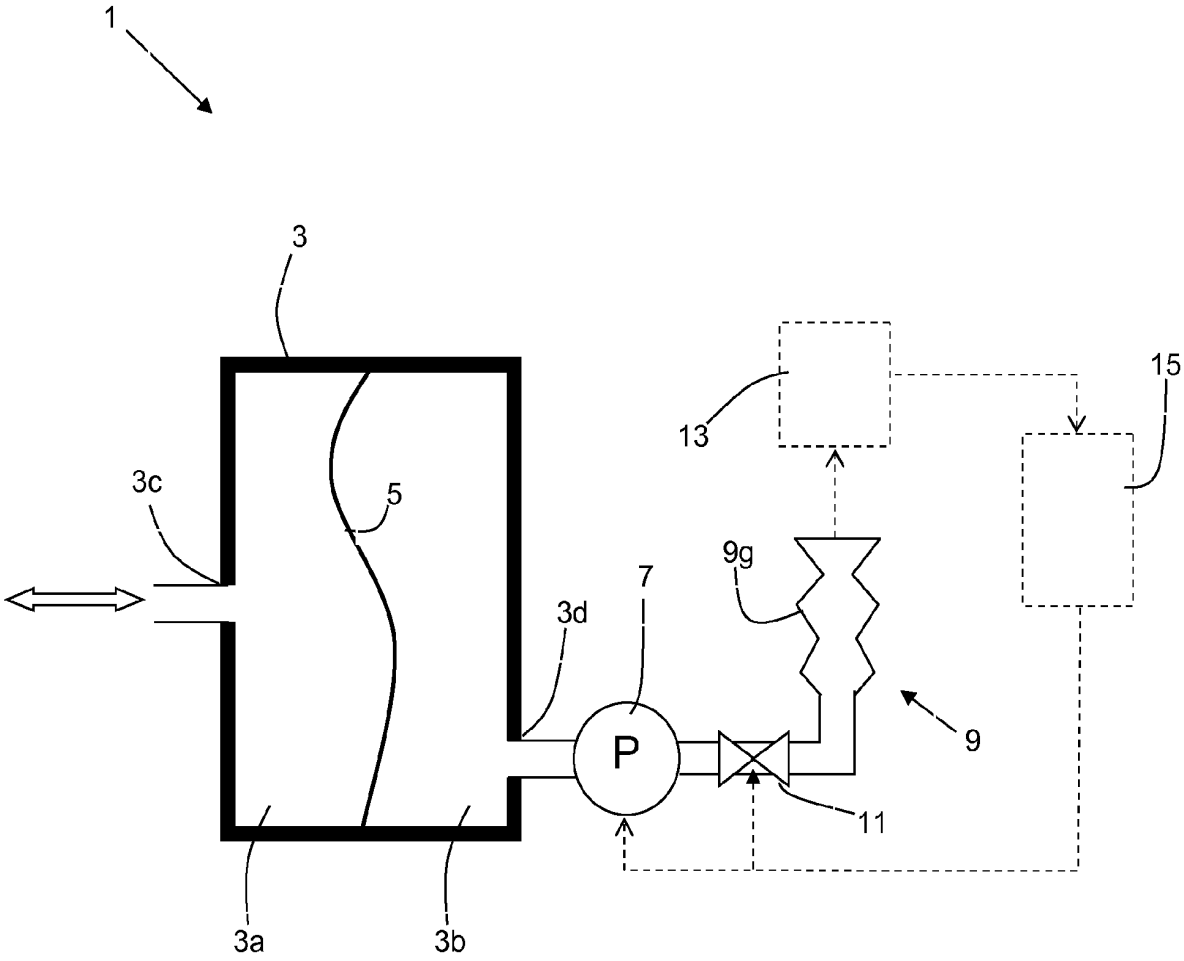

Figure 3

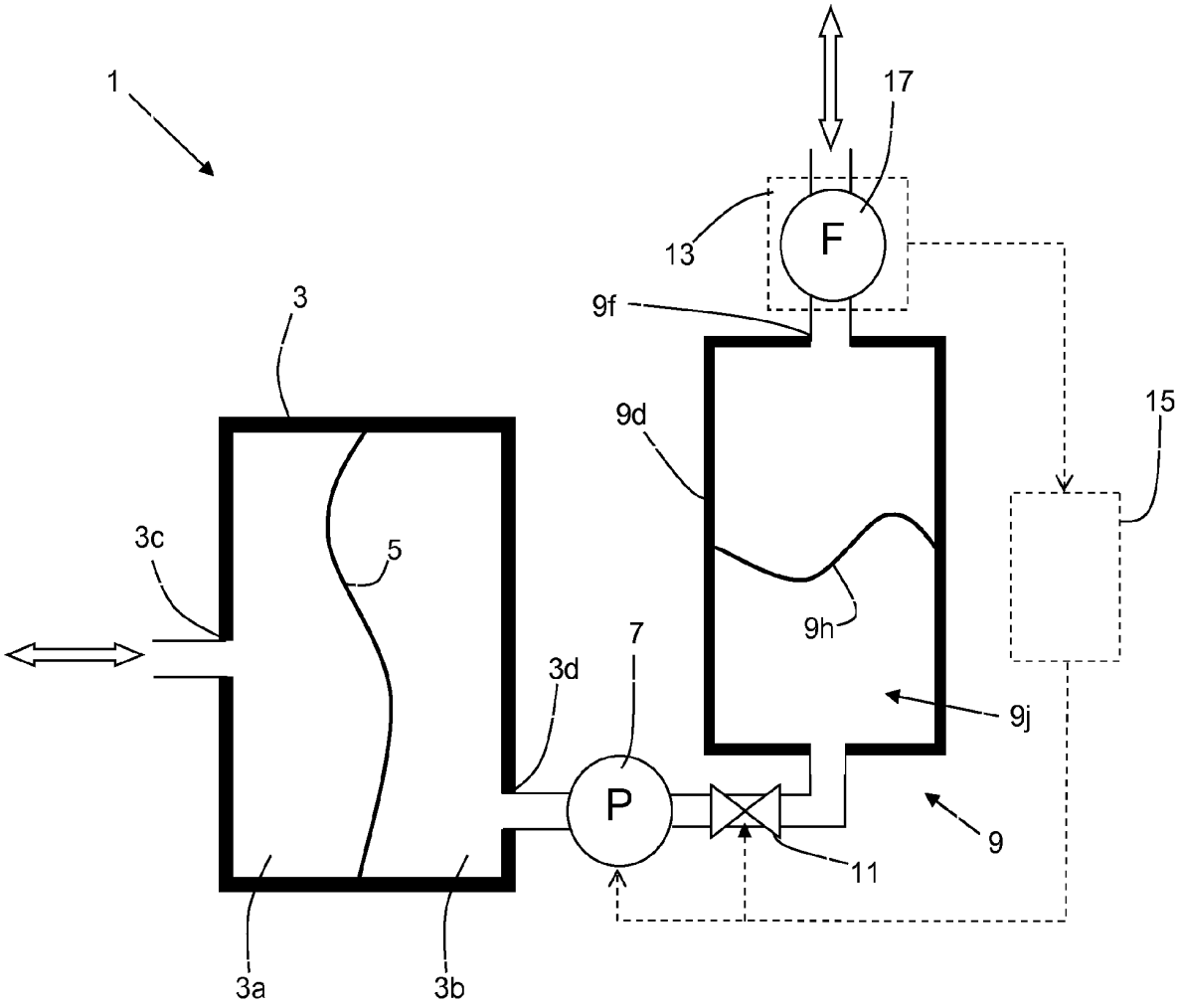

Figure 4

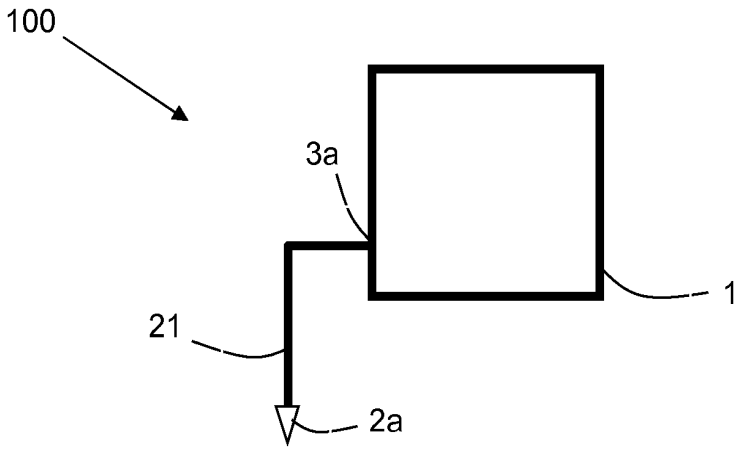

Figure 5

Europäisches Patentamt
European Patent Office
Office européen des brevets

EUROPEAN SEARCH REPORT

Application Number
EP 19 17 9741

DOCUMENTS CONSIDERED TO BE RELEVANT

Category	Citation of document with indication, where appropriate, of relevant passages	Relevant to claim	CLASSIFICATION OF THE APPLICATION (IPC)
X Y	US 2004/265179 A1 (NELSON IAN [US] ET AL) 30 December 2004 (2004-12-30) * figure 2 * * [0033]-[0036],[0061] *	1,3-14 2	INV. G01F11/08 G01F15/16
Y	WO 2009/013447 A1 (EQUINE HEALTHCARE LTD [GB]; BULBROOK LEE [GB]) 29 January 2009 (2009-01-29) * figures 2,3 *	2	
A	US 2007/144233 A1 (KUDO TETSUJI [JP] ET AL) 28 June 2007 (2007-06-28) * figure 1 *	1-15	

TECHNICAL FIELDS SEARCHED (IPC)

G01F
F04B

The present search report has been drawn up for all claims

Place of search	Date of completion of the search	Examiner
The Hague	15 November 2019	Stitou, Adel

CATEGORY OF CITED DOCUMENTS

X : particularly relevant if taken alone
Y : particularly relevant if combined with another document of the same category
A : technological background
O : non-written disclosure
P : intermediate document

T : theory or principle underlying the invention
E : earlier patent document, but published on, or after the filing date
D : document cited in the application
L : document cited for other reasons

& : member of the same patent family, corresponding document

EPO FORM 1503 03.82 (P04C01)

ANNEX TO THE EUROPEAN SEARCH REPORT ON EUROPEAN PATENT APPLICATION NO. EP 19 17 9741

This annex lists the patent family members relating to the patent documents cited in the above-mentioned European search report. The members are as contained in the European Patent Office EDP file on
The European Patent Office is in no way liable for these particulars which are merely given for the purpose of information.

15-11-2019

Patent document cited in search report	Publication date	Patent family member(s)	Publication date
US 2004265179 A1	30-12-2004	AU 2004206229 A1	05-08-2004
		CA 2509799 A1	05-08-2004
		EP 1583979 A1	12-10-2005
		JP 2006516317 A	29-06-2006
		KR 20050092417 A	21-09-2005
		US 2004265179 A1	30-12-2004
		WO 2004065974 A1	05-08-2004
WO 2009013447 A1	29-01-2009	GB 2451135 A	21-01-2009
		WO 2009013447 A1	29-01-2009
US 2007144233 A1	28-06-2007	DE 102006000430 A1	21-06-2007
		JP 4822106 B2	24-11-2011
		JP 2007163152 A	28-06-2007
		US 2007144233 A1	28-06-2007

EPO FORM P0459

For more details about this annex : see Official Journal of the European Patent Office, No. 12/82

REFERENCES CITED IN THE DESCRIPTION

This list of references cited by the applicant is for the reader's convenience only. It does not form part of the European patent document. Even though great care has been taken in compiling the references, errors or omissions cannot be excluded and the EPO disclaims all liability in this regard.

Patent documents cited in the description

- US 6419462 B **[0004]**
- EP 2208891 A **[0025]**

References

1. Miller, J. M.; Binnicker, M. J.; Campbell, S.; Carroll, K. C.; Chapin, K. C.; Gilligan, P. H.; Gonzalez, M. D.; Jerris, R. C.; Kehl, S. C.; Patel, R., A guide to utilization of the microbiology laboratory for diagnosis of infectious diseases: 2018 update by the Infectious Diseases Society of America and the American Society for Microbiology. *Clinical Infectious Diseases* **2018,** *67* (6), e1-e94.
2. Organization, W. H., Guidance on mainstreaming biodiversity for nutrition and health. **2020**.
3. Zeng, D.; Chen, Z.; Jiang, Y.; Xue, F.; Li, B., Advances and challenges in viability detection of foodborne pathogens. *Frontiers in microbiology* **2016,** *7*, 1833.
4. Cho, I.-H.; Ku, S., Current technical approaches for the early detection of foodborne pathogens: challenges and opportunities. *International journal of molecular sciences* **2017,** *18* (10), 2078.
5. Granzow, H.; Weiland, F.; Fichtner, D.; Enzmann, P., Studies of the ultrastructure and morphogenesis of fish pathogenic viruses grown in cell culture. *Journal of Fish Diseases* **1997,** *20* (1), 1-10.
6. Tschiedel, E.; Goralski, A.; Steinmann, J.; Rath, P.-M.; Olivier, M.; Mellies, U.; Kottmann, T.; Stehling, F., Multiplex PCR of bronchoalveolar lavage fluid in children enhances the rate of pathogen detection. *BMC pulmonary medicine* **2019,** *19* (1), 132.
7. Fernández-Carballo, B. L.; McGuiness, I.; McBeth, C.; Kalashnikov, M.; Borrós, S.; Sharon, A.; Sauer-Budge, A. F., Low-cost, real-time, continuous flow PCR system for pathogen detection. *Biomedical microdevices* **2016,** *18* (2), 34.
8. Khater, M.; de la Escosura-Muñiz, A.; Merkoçi, A., Biosensors for plant pathogen detection. *Biosensors and Bioelectronics* **2017,** *93*, 72-86.
9. Alahi, M. E. E.; Mukhopadhyay, S. C., Detection methodologies for pathogen and toxins: a review. *Sensors* **2017,** *17* (8), 1885.
10. Kennedy, D.; Wilkinson, M. G., Application of flow cytometry to the detection of pathogenic bacteria. *Curr Issues Mol Biol* **2017,** *23*, 21-38.
11. Wang, K.; Li, S.; Petersen, M.; Wang, S.; Lu, X., Detection and characterization of antibiotic-resistant bacteria using surface-enhanced raman spectroscopy. *Nanomaterials* **2018,** *8* (10), 762.
12. Simoska, O.; Stevenson, K. J., Electrochemical sensors for rapid diagnosis of pathogens in real time. *Analyst* **2019,** *144* (22), 6461-6478.
13. Chen, Y.; Wang, Z.; Liu, Y.; Wang, X.; Li, Y.; Ma, P.; Gu, B.; Li, H., Recent advances in rapid pathogen detection method based on biosensors. *European Journal of Clinical Microbiology & Infectious Diseases* **2018,** *37* (6), 1021-1037.
14. Váradi, L.; Luo, J. L.; Hibbs, D. E.; Perry, J. D.; Anderson, R. J.; Orenga, S.; Groundwater, P. W., Methods for the detection and identification of pathogenic bacteria: past, present, and future. *Chemical Society Reviews* **2017,** *46* (16), 4818-4832.
15. Goluch, E. D., Microbial identification using electrochemical detection of metabolites. *Trends in biotechnology* **2017,** *35* (12), 1125-1128.
16. Usdin, M.; Guillerm, M.; Calmy, A., Patient needs and point-of-care requirements for HIV load testing in resource-limited settings. *Journal of infectious diseases* **2010,** *201* (Supplement_1), S73-S77.
17. Weigl, B.; Boyle, D.; Santos, T. d. l.; Peck, R.; Steele, M., Simplicity of use: a critical feature for widespread adoption of diagnostic technologies in low-resource settings. *Expert Review of Medical Devices* **2009,** *6* (5), 461-464.
18. Urdea, M.; Penny, L. A.; Olmsted, S. S.; Giovanni, M. Y.; Kaspar, P.; Shepherd, A.; Wilson, P.; Dahl, C. A.; Buchsbaum, S.; Moeller, G., Requirements for high impact diagnostics in the developing world. *Nature* **2006,** *444* (1), 73-79.
19. Whitesides, G. M., The origins and the future of microfluidics. *Nature* **2006,** *442* (7101), 368-373.

20. McFarlin, B. K.; Bowman, E. M., Advanced flow cytometry techniques for clinical detection. *Methods (San Diego, Calif.)* **2018,** *134*, 1.
21. Demello, A. J., Control and detection of chemical reactions in microfluidic systems. *Nature* **2006,** *442* (7101), 394-402.
22. Wang, Y.; Yu, L.; Kong, X.; Sun, L., Application of nanodiagnostics in point-of-care tests for infectious diseases. *International journal of nanomedicine* **2017,** *12*, 4789.
23. Dressler, O. J.; Casadevall i Solvas, X.; DeMello, A. J., Chemical and biological dynamics using droplet-based microfluidics. *Annual Review of Analytical Chemistry* **2017,** *10*, 1-24.
24. Lagus, T. P.; Edd, J. F., A review of the theory, methods and recent applications of high-throughput single-cell droplet microfluidics. *Journal of Physics D: Applied Physics* **2013,** *46* (11), 114005.
25. i Solvas, X. C.; DeMello, A., Droplet microfluidics: recent developments and future applications. *Chemical Communications* **2011,** *47* (7), 1936-1942.
26. Darzynkiewicz, Z.; Juan, G.; Li, X.; Gorczyca, W.; Murakami, T.; Traganos, F., Cytometry in cell necrobiology: analysis of apoptosis and accidental cell death (necrosis). *Cytometry: The Journal of the International Society for Analytical Cytology* **1997,** *27* (1), 1-20.
27. Xiang, J.; Cai, Z.; Zhang, Y.; Wang, W., A micro-cam actuated linear peristaltic pump for microfluidic applications. *Sensors and Actuators A: Physical* **2016,** *251*, 20-25.
28. Rissin, D. M.; Walt, D. R., Digital concentration readout of single enzyme molecules using femtoliter arrays and Poisson statistics. *Nano letters* **2006,** *6* (3), 520-523.
29. White, J. A.; Streets, A. M., Controller for microfluidic large-scale integration. *HardwareX* **2018,** *3*, 135-145.
30. Di Nardo, F.; Alladio, E.; Baggiani, C.; Cavalera, S.; Giovannoli, C.; Spano, G.; Anfossi, L., Colour-encoded lateral flow immunoassay for the simultaneous detection of aflatoxin B1 and type-B fumonisins in a single Test line. *Talanta* **2019,** *192*, 288-294.
31. Cedillo-Alcantar, D. F.; Han, Y. D.; Choi, J.; Garcia-Cordero, J. L.; Revzin, A., Automated droplet-based microfluidic platform for multiplexed analysis of biochemical markers in small volumes. *Analytical chemistry* **2019,** *91* (8), 5133-5141.
32. Zhao, J.; You, Z., Spark-generated microbubble cell sorter for microfluidic flow cytometry. *Cytometry Part A* **2018,** *93* (2), 222-231.
33. Simonnet, C.; Groisman, A., High-throughput and high-resolution flow cytometry in molded microfluidic devices. *Analytical chemistry* **2006,** *78* (16), 5653-5663.
34. Kennedy, M. J.; Stelick, S. J.; Sayam, L. G.; Yen, A.; Erickson, D.; Batt, C. A., Hydrodynamic optical alignment for microflow cytometry. *Lab on a Chip* **2011,** *11* (6), 1138-1143.
35. Haandbæk, N.; Bürgel, S. C.; Heer, F.; Hierlemann, A., Characterization of subcellular morphology of single yeast cells using high frequency microfluidic impedance cytometer. *Lab on a Chip* **2014,** *14* (2), 369-377.
36. Yoo, H.-B.; Lee, C.; Hong, K. S.; Park, S.-R.; Yang, I., Quantification of single-strand DNA by sequence-specific counting in capillary flow cytometry. *Metrologia* **2020**.
37. Xuan, X.; Zhu, J.; Church, C., Particle focusing in microfluidic devices. *Microfluidics and nanofluidics* **2010,** *9* (1), 1-16.
38. Di Carlo, D., Inertial microfluidics. *Lab on a Chip* **2009,** *9* (21), 3038-3046.
39. Goda, K.; Ayazi, A.; Gossett, D. R.; Sadasivam, J.; Lonappan, C. K.; Sollier, E.; Fard, A. M.; Hur, S. C.; Adam, J.; Murray, C., High-throughput single-microparticle imaging flow analyzer. *Proceedings of the National Academy of Sciences* **2012,** *109* (29), 11630-11635.
40. Rane, A. S.; Rutkauskaite, J.; deMello, A.; Stavrakis, S., High-throughput multi-parametric imaging flow cytometry. *Chem* **2017,** *3* (4), 588-602.

41. Zhao, Q.; Zhang, J.; Yan, S.; Yuan, D.; Du, H.; Alici, G.; Li, W., High-throughput sheathless and three-dimensional microparticle focusing using a microchannel with arc-shaped groove arrays. *Scientific reports* **2017,** *7*, 41153.
42. Godin, J.; Lo, Y.-H., Two-parameter angular light scatter collection for microfluidic flow cytometry by unique waveguide structures. *Biomedical optics express* **2010,** *1* (5), 1472-1479.
43. Lim, E. J.; Ober, T. J.; Edd, J. F.; Desai, S. P.; Neal, D.; Bong, K. W.; Doyle, P. S.; McKinley, G. H.; Toner, M., Inertio-elastic focusing of bioparticles in microchannels at high throughput. *Nature communications* **2014,** *5* (1), 1-9.
44. Holzner, G.; Stavrakis, S.; DeMello, A., Elasto-inertial focusing of mammalian cells and bacteria using low molecular, low viscosity PEO solutions. *Analytical chemistry* **2017,** *89* (21), 11653-11663.
45. Destgeer, G.; Sung, H. J., Recent advances in microfluidic actuation and micro-object manipulation via surface acoustic waves. *Lab on a Chip* **2015,** *15* (13), 2722-2738.
46. Shi, J.; Yazdi, S.; Lin, S.-C. S.; Ding, X.; Chiang, I.-K.; Sharp, K.; Huang, T. J., Three-dimensional continuous particle focusing in a microfluidic channel via standing surface acoustic waves (SSAW). *Lab on a Chip* **2011,** *11* (14), 2319-2324.
47. Wang, L.; Flanagan, L. A.; Jeon, N. L.; Monuki, E.; Lee, A. P., Dielectrophoresis switching with vertical sidewall electrodes for microfluidic flow cytometry. *Lab on a Chip* **2007,** *7* (9), 1114-1120.
48. Labeed, F. H.; Coley, H. M.; Thomas, H.; Hughes, M. P., Assessment of multidrug resistance reversal using dielectrophoresis and flow cytometry. *Biophysical journal* **2003,** *85* (3), 2028-2034.
49. Kung, Y.-C.; Niazi, K. R.; Chiou, P.-Y., Tunnel dielectrophoresis for ultra-high precision size-based cell separation. *Lab on a Chip* **2021**.
50. Asghari, M.; Cao, X.; Mateescu, B.; Van Leeuwen, D.; Aslan, M. K.; Stavrakis, S.; deMello, A. J., Oscillatory Viscoelastic Microfluidics for Efficient Focusing and Separation of Nanoscale Species. *ACS nano* **2019,** *14* (1), 422-433.
51. Nebe-von-Caron, G.; Stephens, P.; Hewitt, C.; Powell, J.; Badley, R., Analysis of bacterial function by multi-colour fluorescence flow cytometry and single cell sorting. *Journal of microbiological methods* **2000,** *42* (1), 97-114.
52. Choi, H.; Jeon, C. S.; Hwang, I.; Ko, J.; Lee, S.; Choo, J.; Boo, J.-H.; Kim, H. C.; Chung, T. D., A flow cytometry-based submicron-sized bacterial detection system using a movable virtual wall. *Lab on a Chip* **2014,** *14* (13), 2327-2333.
53. Koydemir, H. C.; Gorocs, Z.; McLeod, E.; Tseng, D.; Ozcan, A. In *Field portable mobile phone based fluorescence microscopy for detection of Giardia lamblia cysts in water samples*, Optics and Biophotonics in Low-Resource Settings, International Society for Optics and Photonics: 2015; p 93140S.
54. Golden, J.; Verbarg, J.; Howell Jr, P.; Shriver-Lake, L.; Ligler, F., Automated processing integrated with a microflow cytometer for pathogen detection in clinical matrices. *Biosensors and Bioelectronics* **2013,** *40* (1), 10-16.
55. Yamaguchi, N.; Torii, M.; Uebayashi, Y.; Nasu, M., Rapid, semiautomated quantification of bacterial cells in freshwater by using a microfluidic device for on-chip staining and counting. *Applied and environmental microbiology* **2011,** *77* (4), 1536-1539.
56. Zordan, M. D.; Grafton, M. M.; Acharya, G.; Reece, L. M.; Cooper, C. L.; Aronson, A. I.; Park, K.; Leary, J. F., Detection of pathogenic E. coli O157: H7 by a hybrid microfluidic SPR and molecular imaging cytometry device. *Cytometry Part A: The Journal of the International Society for Analytical Cytology* **2009,** *75* (2), 155-162.
57. Mu, C.; Zhang, F.; Zhang, Z.; Lin, M.; Cao, X., Highly efficient dual-channel cytometric-detection of micron-sized particles in microfluidic device. *Sensors and Actuators B: Chemical* **2011,** *151* (2), 402-409.
58. Sakamoto, C.; Yamaguchi, N.; Nasu, M., Rapid and simple quantification of bacterial cells by using a microfluidic device. *Applied and environmental microbiology* **2005,** *71* (2), 1117-1121.

59. Gerdts, G.; Luedke, G., FISH and chips: Marine bacterial communities analyzed by flow cytometry based on microfluidics. *Journal of microbiological methods* **2006,** *64* (2), 232-240.
60. Mao, C.; Xue, C.; Wang, X.; He, S.; Wu, L.; Yan, X., Rapid quantification of pathogenic Salmonella Typhimurium and total bacteria in eggs by nano-flow cytometry. *Talanta* **2020**, 121020.
61. Yang, L.; Zhou, Y.; Zhu, S.; Huang, T.; Wu, L.; Yan, X., Detection and quantification of bacterial autofluorescence at the single-cell level by a laboratory-built high-sensitivity flow cytometer. *Analytical chemistry* **2012,** *84* (3), 1526-1532.
62. He, S.; Hong, X.; Zhang, M.; Wu, L.; Yan, X., Label-Free Detection of Bacteria in Fruit Juice by Nano-Flow Cytometry. *Analytical Chemistry* **2019,** *92* (3), 2393-2400.
63. Shriver-Lake, L. C.; Golden, J.; Bracaglia, L.; Ligler, F. S., Simultaneous assay for ten bacteria and toxins in spiked clinical samples using a microflow cytometer. *Analytical and bioanalytical chemistry* **2013,** *405* (16), 5611-5614.
64. Lee, G.-B.; Lin, C.-H.; Chang, G.-L., Micro flow cytometers with buried SU-8/SOG optical waveguides. *Sensors and Actuators A: Physical* **2003,** *103* (1-2), 165-170.
65. Suea-Ngam, A.; Howes, P. D.; Srisa-Art, M.; DeMello, A. J., Droplet microfluidics: from proof-of-concept to real-world utility? *Chemical Communications* **2019,** *55* (67), 9895-9903.
66. Boyd-Moss, M.; Baratchi, S.; Di Venere, M.; Khoshmanesh, K., Self-contained microfluidic systems: a review. *Lab on a Chip* **2016,** *16* (17), 3177-3192.
67. Zhang, Y.; Ozdemir, P., Microfluidic DNA amplification—A review. *Analytica chimica acta* **2009,** *638* (2), 115-125.
68. Boedicker, J. Q.; Li, L.; Kline, T. R.; Ismagilov, R. F., Detecting bacteria and determining their susceptibility to antibiotics by stochastic confinement in nanoliter droplets using plug-based microfluidics. *Lab on a Chip* **2008,** *8* (8), 1265-1272.
69. Huebner, A.; Srisa-Art, M.; Holt, D.; Abell, C.; Hollfelder, F.; Demello, A.; Edel, J., Quantitative detection of protein expression in single cells using droplet microfluidics. *Chemical communications* **2007,** (12), 1218-1220.
70. Köster, S.; Angile, F. E.; Duan, H.; Agresti, J. J.; Wintner, A.; Schmitz, C.; Rowat, A. C.; Merten, C. A.; Pisignano, D.; Griffiths, A. D., Drop-based microfluidic devices for encapsulation of single cells. *Lab on a Chip* **2008,** *8* (7), 1110-1115.
71. An, X.; Zuo, P.; Ye, B.-C., A single cell droplet microfluidic system for quantitative determination of food-borne pathogens. *Talanta* **2020,** *209*, 120571.
72. Khater, A.; Abdelrehim, O.; Mohammadi, M.; Azarmanesh, M.; Janmaleki, M.; Salahandish, R.; Mohamad, A.; Sanati-Nezhad, A., Picoliter agar droplet breakup in microfluidics meets microbiology application: numerical and experimental approaches. *Lab on a Chip* **2020**.
73. Duarte, J. M.; Barbier, I. v.; Schaerli, Y., Bacterial microcolonies in gel beads for high-throughput screening of libraries in synthetic biology. *ACS synthetic biology* **2017,** *6* (11), 1988-1995.
74. Guzman, L.-M.; Belin, D.; Carson, M. J.; Beckwith, J., Tight regulation, modulation, and high-level expression by vectors containing the arabinose PBAD promoter. *Journal of bacteriology* **1995,** *177* (14), 4121-4130.
75. Hondroulis, E.; Movila, A.; Sabhachandani, P.; Sarkar, S.; Cohen, N.; Kawai, T.; Konry, T., A droplet-merging platform for comparative functional analysis of m1 and m2 macrophages in response to e. coli-induced stimuli. *Biotechnology and Bioengineering* **2017,** *114* (3), 705-709.
76. Taylor, S. C.; Laperriere, G.; Germain, H., Droplet Digital PCR versus qPCR for gene expression analysis with low abundant targets: from variable nonsense to publication quality data. *Scientific reports* **2017,** *7* (1), 1-8.
77. Pabinger, S.; Rödiger, S.; Kriegner, A.; Vierlinger, K.; Weinhäusel, A., A survey of tools for the analysis of quantitative PCR (qPCR) data. *Biomolecular Detection and Quantification* **2014,** *1* (1), 23-33.

78. Selvaraj, V.; Maheshwari, Y.; Hajeri, S.; Yokomi, R., Droplet Digital PCR for Absolute Quantification of Plant Pathogens. In *Plant Biotechnology: Progress in Genomic Era*, Springer: 2019; pp 583-595.
79. Heyries, K. A.; Tropini, C.; VanInsberghe, M.; Doolin, C.; Petriv, I.; Singhal, A.; Leung, K.; Hughesman, C. B.; Hansen, C. L., Megapixel digital PCR. *Nature methods* **2011,** *8* (8), 649-651.
80. Kawakatsu, T.; Kikuchi, Y.; Nakajima, M., Regular-sized cell creation in microchannel emulsification by visual microprocessing method. *Journal of the American Oil Chemists' Society* **1997,** *74* (3), 317-321.
81. Vladisavljević, G. T.; Kobayashi, I.; Nakajima, M., Generation of highly uniform droplets using asymmetric microchannels fabricated on a single crystal silicon plate: effect of emulsifier and oil types. *Powder Technology* **2008,** *183* (1), 37-45.
82. Martin, A.; Storto, A.; Andre, B.; Mallory, A.; Dangla, R.; Visseaux, B.; Gossner, O., High-sensitivity COVID-19 group testing by digital PCR. *arXiv preprint arXiv:2006.02908* **2020**.
83. Veyer, D.; Kernéis, S.; Poulet, G.; Wack, M.; Robillard, N.; Taly, V.; L'Honneur, A.-S.; Rozenberg, F.; Laurent-Puig, P.; Bélec, L., Highly sensitive quantification of plasma SARS-CoV-2 RNA shelds light on its potential clinical value. *Clinical Infectious Diseases* **2020**.
84. Men, Y.; Li, J.; Ao, T.; Li, Z.; Wu, B.; Li, W.; Ding, Y.; Tseng, K.-H.; Tan, W.; Pan, T., Digital polymerase chain reaction in an array of microfluidic printed droplets. *bioRxiv* **2019**, 860411.
85. Sun, Y.; Zhou, X.; Yu, Y., A novel picoliter droplet array for parallel real-time polymerase chain reaction based on double-inkjet printing. *Lab on a Chip* **2014,** *14* (18), 3603-3610.
86. Tasrip, N.; Khairil Mokhtar, N.; Hanapi, U.; Abdul Manaf, Y.; Ali, M.; Cheah, Y.; Mustafa, S.; Desa, M., Loop mediated isothermal amplification; a review on its application and strategy in animal species authentication of meat based food products. *International Food Research Journal* **2019,** *26* (1).
87. Li, J.; Macdonald, J.; von Stetten, F., a comprehensive summary of a decade development of the recombinase polymerase amplification. *Analyst* **2018,** *144* (1), 31-67.
88. Lobato, I. M.; O'Sullivan, C. K., Recombinase polymerase amplification: basics, applications and recent advances. *Trac Trends in analytical chemistry* **2018,** *98*, 19-35.
89. Becherer, L.; Borst, N.; Bakheit, M.; Frischmann, S.; Zengerle, R.; von Stetten, F., Loop-mediated isothermal amplification (LAMP)–review and classification of methods for sequence-specific detection. *Analytical Methods* **2020,** *12* (6), 717-746.
90. Zhao, Y.; Chen, F.; Li, Q.; Wang, L.; Fan, C., Isothermal amplification of nucleic acids. *Chemical reviews* **2015,** *115* (22), 12491-12545.
91. Karami, A.; Gill, P.; Motamedi, M. H. K.; Saghafinia, M., A review of the current isothermal amplification techniques: applications, advantages and disadvantages. *J Global Infect Dis* **2011,** *3* (3), 293-302.
92. Shang, Y.; Sun, J.; Ye, Y.; Zhang, J.; Zhang, Y.; Sun, X., Loop-mediated isothermal amplification-based microfluidic chip for pathogen detection. *Critical reviews in food science and nutrition* **2020,** *60* (2), 201-224.
93. Notomi, T.; Okayama, H.; Masubuchi, H.; Yonekawa, T.; Watanabe, K.; Amino, N.; Hase, T., Loop-mediated isothermal amplification of DNA. *Nucleic acids research* **2000,** *28* (12), e63-e63.
94. Nagamine, K.; Hase, T.; Notomi, T., Accelerated reaction by loop-mediated isothermal amplification using loop primers. *Molecular and cellular probes* **2002,** *16* (3), 223-229.
95. Li, Y.; Fan, P.; Zhou, S.; Zhang, L., Loop-mediated isothermal amplification (LAMP): a novel rapid detection platform for pathogens. *Microbial pathogenesis* **2017,** *107*, 54-61.
96. Parida, M.; Sannarangaiah, S.; Dash, P. K.; Rao, P.; Morita, K., Loop mediated isothermal amplification (LAMP): a new generation of innovative gene amplification technique; perspectives in clinical diagnosis of infectious diseases. *Reviews in medical virology* **2008,** *18* (6), 407-421.

97. Zhang, H.; Xu, Y.; Fohlerova, Z.; Chang, H.; Iliescu, C.; Neuzil, P., LAMP-on-a-chip: Revising microfluidic platforms for loop-mediated DNA amplification. *TrAC Trends in Analytical Chemistry* **2019,** *113*, 44-53.
98. Sun, B.; Rodriguez-Manzano, J.; Selck, D. A.; Khorosheva, E.; Karymov, M. A.; Ismagilov, R. F., Measuring Fate and Rate of Single-Molecule Competition of Amplification and Restriction Digestion, and Its Use for Rapid Genotyping Tested with Hepatitis C Viral RNA. *Angewandte Chemie International Edition* **2014,** *53* (31), 8088-8092.
99. Rane, T. D.; Chen, L.; Zec, H. C.; Wang, T.-H., Microfluidic continuous flow digital loop-mediated isothermal amplification (LAMP). *Lab on a Chip* **2015,** *15* (3), 776-782.
100. Ma, Y.-D.; Luo, K.; Chang, W.-H.; Lee, G.-B., A microfluidic chip capable of generating and trapping emulsion droplets for digital loop-mediated isothermal amplification analysis. *Lab on a Chip* **2018,** *18* (2), 296-303.
101. Sun, B.; Shen, F.; McCalla, S. E.; Kreutz, J. E.; Karymov, M. A.; Ismagilov, R. F., Mechanistic evaluation of the pros and cons of digital RT-LAMP for HIV-1 viral load quantification on a microfluidic device and improved efficiency via a two-step digital protocol. *Analytical chemistry* **2013,** *85* (3), 1540-1546.
102. Ma, Y.-D.; Chang, W.-H.; Luo, K.; Wang, C.-H.; Liu, S.-Y.; Yen, W.-H.; Lee, G.-B., Digital quantification of DNA via isothermal amplification on a self-driven microfluidic chip featuring hydrophilic film-coated polydimethylsiloxane. *Biosensors and Bioelectronics* **2018,** *99*, 547-554.
103. Song, J.; Mauk, M. G.; Hackett, B. A.; Cherry, S.; Bau, H. H.; Liu, C., Instrument-free point-of-care molecular detection of Zika virus. *Analytical chemistry* **2016,** *88* (14), 7289-7294.
104. Liu, C.; Geva, E.; Mauk, M.; Qiu, X.; Abrams, W. R.; Malamud, D.; Curtis, K.; Owen, S. M.; Bau, H. H., An isothermal amplification reactor with an integrated isolation membrane for point-of-care detection of infectious diseases. *Analyst* **2011,** *136* (10), 2069-2076.
105. Wang, C.-H.; Lien, K.-Y.; Wang, T.-Y.; Chen, T.-Y.; Lee, G.-B., An integrated microfluidic loop-mediated-isothermal-amplification system for rapid sample pre-treatment and detection of viruses. *Biosensors and Bioelectronics* **2011,** *26* (5), 2045-2052.
106. Trinh, T. N. D.; Lee, N. Y., A rapid and eco-friendly isothermal amplification microdevice for multiplex detection of foodborne pathogens. *Lab on a Chip* **2018,** *18* (16), 2369-2377.
107. Fang, X.; Liu, Y.; Kong, J.; Jiang, X., Loop-mediated isothermal amplification integrated on microfluidic chips for point-of-care quantitative detection of pathogens. *Analytical chemistry* **2010,** *82* (7), 3002-3006.
108. Chen, C.; Liu, P.; Zhao, X.; Du, W.; Feng, X.; Liu, B.-F., A self-contained microfluidic in-gel loop-mediated isothermal amplification for multiplexed pathogen detection. *Sensors and Actuators B: Chemical* **2017,** *239*, 1-8.
109. Sayad, A.; Ibrahim, F.; Uddin, S. M.; Cho, J.; Madou, M.; Thong, K. L., A microdevice for rapid, monoplex and colorimetric detection of foodborne pathogens using a centrifugal microfluidic platform. *Biosensors and Bioelectronics* **2018,** *100*, 96-104.
110. Pang, B.; Ding, X.; Wang, G.; Zhao, C.; Xu, Y.; Fu, K.; Sun, J.; Song, X.; Wu, W.; Liu, Y., Rapid and quantitative detection of Vibrio parahemolyticus by the mixed-dye-based loop-mediated isothermal amplification assay on a self-priming compartmentalization microfluidic chip. *Journal of agricultural and food chemistry* **2017,** *65* (51), 11312-11319.
111. Azizi, M.; Zaferani, M.; Cheong, S. H.; Abbaspourrad, A., Pathogenic bacteria detection using RNA-based loop-mediated isothermal-amplification-assisted nucleic acid amplification via droplet microfluidics. *ACS sensors* **2019,** *4* (4), 841-848.
112. Duarte, C.; Salm, E.; Dorvel, B.; Reddy, B.; Bashir, R., On-chip parallel detection of foodborne pathogens using loop-mediated isothermal amplification. *Biomedical microdevices* **2013,** *15* (5), 821-830.

113. Park, B. H.; Oh, S. J.; Jung, J. H.; Choi, G.; Seo, J. H.; Lee, E. Y.; Seo, T. S., An integrated rotary microfluidic system with DNA extraction, loop-mediated isothermal amplification, and lateral flow strip based detection for point-of-care pathogen diagnostics. *Biosensors and Bioelectronics* **2017,** *91*, 334-340.
114. Seo, J. H.; Park, B. H.; Oh, S. J.; Choi, G.; Lee, E. Y.; Seo, T. S., Development of a high-throughput centrifugal loop-mediated isothermal amplification microdevice for multiplex foodborne pathogenic bacteria detection. *Sensors and Actuators B: Chemical* **2017,** *246*, 146-153.
115. Oh, S. J.; Park, B. H.; Jung, J. H.; Choi, G.; Lee, D. C.; Seo, T. S., Centrifugal loop-mediated isothermal amplification microdevice for rapid, multiplex and colorimetric foodborne pathogen detection. *Biosensors and Bioelectronics* **2016,** *75*, 293-300.
116. Sayad, A. A.; Ibrahim, F.; Uddin, S. M.; Pei, K. X.; Mohktar, M. S.; Madou, M.; Thong, K. L., A microfluidic lab-on-a-disc integrated loop mediated isothermal amplification for foodborne pathogen detection. *Sensors and Actuators B: Chemical* **2016,** *227*, 600-609.
117. Xia, Y.; Liu, Z.; Yan, S.; Yin, F.; Feng, X.; Liu, B.-F., Identifying multiple bacterial pathogens by loop-mediated isothermal amplification on a rotate & react slipchip. *Sensors and Actuators B: Chemical* **2016,** *228*, 491-499.
118. Uddin, S. M.; Ibrahim, F.; Sayad, A. A.; Thiha, A.; Pei, K. X.; Mohktar, M. S.; Hashim, U.; Cho, J.; Thong, K. L., A portable automatic endpoint detection system for amplicons of loop mediated isothermal amplification on microfluidic compact disk platform. *Sensors* **2015,** *15* (3), 5376-5389.
119. Huang, G.; Huang, Q.; Xie, L.; Xiang, G.; Wang, L.; Xu, H.; Ma, L.; Luo, X.; Xin, J.; Zhou, X., A rapid, low-cost, and microfluidic chip-based system for parallel identification of multiple pathogens related to clinical pneumonia. *Scientific reports* **2017,** *7* (1), 1-10.
120. Kim, J. H.; Kang, M.; Park, E.; Chung, D. R.; Kim, J.; Hwang, E. S., A Simple and Multiplex Loop-Mediated Isothermal Amplification (LAMP) Assay for Rapid Detection of SARS-CoV. *Biochip journal* **2019,** *13* (4), 341-351.
121. Lin, X.; Huang, X.; Urmann, K.; Xie, X.; Hoffmann, M. R., Digital loop-mediated isothermal amplification on a commercial membrane. *ACS sensors* **2019,** *4* (1), 242-249.
122. Ganguli, A.; Ornob, A.; Yu, H.; Damhorst, G.; Chen, W.; Sun, F.; Bhuiya, A.; Cunningham, B.; Bashir, R., Hands-free smartphone-based diagnostics for simultaneous detection of Zika, Chikungunya, and Dengue at point-of-care. *Biomedical microdevices* **2017,** *19* (4), 73.
123. Safavieh, M.; Kaul, V.; Khetani, S.; Singh, A.; Dhingra, K.; Kanakasabapathy, M. K.; Draz, M. S.; Memic, A.; Kuritzkes, D. R.; Shafiee, H., Paper microchip with a graphene-modified silver nano-composite electrode for electrical sensing of microbial pathogens. *Nanoscale* **2017,** *9* (5), 1852-1861.
124. Kaarj, K.; Akarapipad, P.; Yoon, J.-Y., Simpler, faster, and sensitive Zika virus assay using smartphone detection of loop-mediated isothermal amplification on paper microfluidic chips. *Scientific reports* **2018,** *8* (1), 1-11.
125. Gensberger, E. T.; Gössl, E.-M.; Antonielli, L.; Sessitsch, A.; Kostić, T., Effect of different heterotrophic plate count methods on the estimation of the composition of the culturable microbial community. *PeerJ* **2015,** *3*, e862.
126. Bartram, J.; Cotruvo, J.; Exner, M.; Fricker, C.; Glasmacher, A., *Heterotrophic plate counts and drinking-water safety*. IWA publishing: 2003.
127. Bartram, J.; Cotruvo, J.; Exner, M.; Fricker, C.; Glasmacher, A., Heterotrophic plate count measurement in drinking water safety management: report of an Expert Meeting Geneva, 24–25 April 2002. *International journal of food microbiology* **2004,** *92* (3), 241-247.
128. EPA, E. P. A., National primary drinking water regulations: long term 1 enhanced surface water treatment rule. Final rule. *Federal register* **2002,** *67* (9), 1811-1844.
129. Water, S.; Organization, W. H., Guidelines for drinking-water quality [electronic resource]: incorporating first addendum. Vol. 1, Recommendations. **2006**.

130. McFeters, G. A., *Drinking water microbiology: progress and recent developments*. Springer Science & Business Media: 2013.
131. Gillespie, S.; Lipphaus, P.; Green, J.; Parsons, S.; Weir, P.; Juskowiak, K.; Jefferson, B.; Jarvis, P.; Nocker, A., Assessing microbiological water quality in drinking water distribution systems with disinfectant residual using flow cytometry. *Water research* **2014,** *65*, 224-234.
132. Allen, M. J.; Edberg, S. C.; Reasoner, D. J., Heterotrophic plate count bacteria—what is their significance in drinking water? *International journal of food microbiology* **2004,** *92* (3), 265-274.
133. Van Nevel, S.; Koetzsch, S.; Proctor, C. R.; Besmer, M. D.; Prest, E. I.; Vrouwenvelder, J. S.; Knezev, A.; Boon, N.; Hammes, F., Flow cytometric bacterial cell counts challenge conventional heterotrophic plate counts for routine microbiological drinking water monitoring. *Water Research* **2017,** *113*, 191-206.
134. Whitton, R.; Fane, S.; Jarvis, P.; Tupper, M.; Raffin, M.; Coulon, F.; Nocker, A., Flow cytometry-based evaluation of the bacterial removal efficiency of a blackwater reuse treatment plant and the microbiological changes in the associated non-potable distribution network. *Science of The Total Environment* **2018,** *645*, 1620-1629.
135. Sgier, L.; Merbt, S. N.; Tlili, A.; Kroll, A.; Zupanic, A., Characterization of aquatic biofilms with flow cytometry. *Journal of visualized experiments: JoVE* **2018,** (136).
136. Kang, R.; Park, B.; Eady, M.; Ouyang, Q.; Chen, K., Classification of foodborne bacteria using hyperspectral microscope imaging technology coupled with convolutional neural networks. *Applied microbiology and biotechnology* **2020,** *104* (7), 3157-3166.
137. Coggins, L. X.; Larma, I.; Hinchliffe, A.; Props, R.; Ghadouani, A., Flow cytometry for rapid characterisation of microbial community dynamics in waste stabilisation ponds. *Water research* **2020,** *169*, 115243.
138. Aw, T. G.; Rose, J. B., Detection of pathogens in water: from phylochips to qPCR to pyrosequencing. *Current opinion in biotechnology* **2012,** *23* (3), 422-430.
139. Xavier, B. B.; Mysara, M.; Bolzan, M.; Ribeiro-Gonçalves, B.; Alako, B. T.; Harrison, P.; Lammens, C.; Kumar-Singh, S.; Goossens, H.; Carriço, J. A., BacPipe: A Rapid, User-Friendly Whole-Genome Sequencing Pipeline for Clinical Diagnostic Bacteriology. *Iscience* **2020,** *23* (1), 100769.
140. Epstein, S., The phenomenon of microbial uncultivability. *Current opinion in microbiology* **2013,** *16* (5), 636-642.
141. Liu, G.; Ling, F.; Magic-Knezev, A.; Liu, W.; Verberk, J.; Van Dijk, J., Quantification and identification of particle-associated bacteria in unchlorinated drinking water from three treatment plants by cultivation-independent methods. *Water research* **2013,** *47* (10), 3523-3533.
142. Shaw, J. L.; Monis, P.; Fabris, R.; Ho, L.; Braun, K.; Drikas, M.; Cooper, A., Assessing the impact of water treatment on bacterial biofilms in drinking water distribution systems using high-throughput DNA sequencing. *Chemosphere* **2014,** *117*, 185-192.
143. Dąbrowiecki, Z.; Dąbrowiecka, M.; Olszański, R.; Siermontowski, P., Developing a Methodology for Testing and Preliminary Determination of the Presence of Legionella Spp. and Legionella Pneumophila in Environmental Water Samples by Immunomagnetic Separation Combined with Flow Cytometry. *Polish Hyperbaric Research* **2019,** *68* (3), 71-92.
144. Hammes, F.; Egli, T., Cytometric methods for measuring bacteria in water: advantages, pitfalls and applications. *Analytical and bioanalytical chemistry* **2010,** *397* (3), 1083-1095.
145. Props, R.; Schmidt, M. L.; Heyse, J.; Vanderploeg, H. A.; Boon, N.; Denef, V. J., Flow cytometric monitoring of bacterioplankton phenotypic diversity predicts high population-specific feeding rates by invasive dreissenid mussels. *Environmental microbiology* **2018,** *20* (2), 521-534.
146. Props, R.; Monsieurs, P.; Mysara, M.; Clement, L.; Boon, N., Measuring the biodiversity of microbial communities by flow cytometry. *Methods in Ecology and Evolution* **2016,** *7* (11), 1376-1385.

147. Rockey, N.; Bischel, H. N.; Kohn, T.; Pecson, B.; Wigginton, K. R., The utility of flow cytometry for potable reuse. *Current opinion in biotechnology* **2019,** *57*, 42-49.
148. Safford, H. R.; Bischel, H. N., Flow cytometry applications in water treatment, distribution, and reuse: A review. *Water research* **2019,** *151*, 110-133.
149. Helmi, K.; David, F.; Di Martino, P.; Jaffrezic, M.-P.; Ingrand, V., Assessment of flow cytometry for microbial water quality monitoring in cooling tower water and oxidizing biocide treatment efficiency. *Journal of microbiological methods* **2018,** *152*, 201-209.
150. Santos, M.; Oliveira, H.; Pereira, J. L.; Pereira, M. J.; Gonçalves, F. J.; Vidal, T., Flow cytometry analysis of low/high DNA content (LNA/HNA) bacteria as bioindicator of water quality evaluation. *Ecological Indicators* **2019,** *103*, 774-781.
151. Grégori, G.; Denis, M.; Sgorbati, S.; Citterio, S., Resolution of Viable and Membrane-Compromised Free Bacteria in Aquatic Environments by Flow Cytometry. *Current protocols in cytometry* **2018,** *85* (1), e42.
152. Mirza, I.; Bulgakova, N. M.; Tomáštík, J.; Michálek, V.; Haderka, O.; Fekete, L.; Mocek, T., Ultrashort pulse laser ablation of dielectrics: Thresholds, mechanisms, role of breakdown. *Scientific reports* **2016,** *6* (1), 1-11.
153. Wlodarczyk, K. L.; Carter, R. M.; Jahanbakhsh, A.; Lopes, A. A.; Mackenzie, M. D.; Maier, R. R.; Hand, D. P.; Maroto-Valer, M. M., Rapid laser manufacturing of microfluidic devices from glass substrates. *Micromachines* **2018,** *9* (8), 409.
154. Book, S. F., Method 333.1: Determining the Total Cell Count and Ratios of High and Low Nucleic Acid Content Cells in Freshwater Using Flow Cytometry. *Federal Office of Public Health, Bern, Switzerland* **2012**.
155. Nescerecka, A.; Hammes, F.; Juhna, T., A pipeline for developing and testing staining protocols for flow cytometry, demonstrated with SYBR Green I and propidium iodide viability staining. *Journal of microbiological methods* **2016,** *131*, 172-180.
156. Prest, E.; Hammes, F.; Kötzsch, S.; van Loosdrecht, M. C.; Vrouwenvelder, J. S., Monitoring microbiological changes in drinking water systems using a fast and reproducible flow cytometric method. *Water research* **2013,** *47* (19), 7131-7142.
157. Xu, L.; Zhang, C.; Xu, P.; Wang, X. C., Mechanisms of ultraviolet disinfection and chlorination of Escherichia coli: culturability, membrane permeability, metabolism, and genetic damage. *Journal of Environmental Sciences* **2018,** *65*, 356-366.
158. Park, J.; Kim, Y.; Kim, M.; Lee, W. H., A novel method for cell counting of Microcystis colonies in water resources using a digital imaging flow cytometer and microscope. *Environmental Engineering Research* **2019,** *24* (3), 397-403.
159. Buysschaert, B.; Kerckhof, F. M.; Vandamme, P.; De Baets, B.; Boon, N., Flow cytometric fingerprinting for microbial strain discrimination and physiological characterization. *Cytometry Part A* **2018,** *93* (2), 201-212.
160. Prest, E. I.; Hammes, F.; van Loosdrecht, M.; Vrouwenvelder, J. S., Biological stability of drinking water: controlling factors, methods, and challenges. *Frontiers in microbiology* **2016,** *7*, 45.
161. Cook, N.; D'Agostino, M.; Thompson, K. C., *Molecular Microbial Diagnostic Methods: Pathways to Implementation for the Food and Water Industries*. Academic Press: 2015.
162. Egli, T.; Zimmermann, S.; Schärer, P.; Senouillet, J.; Künzi, S.; Köster, O.; Helbing, J.; Montandon, P.; Marguet, J.; Khajehnouri, F., Automatische Online Überwachung–Bestimmung der Bakterienzahl im Roh-und Trinkwasser: Resultate aus der Praxis. *Aqua & Gas* **2017,** *10* (2017), 52-59.
163. Schmid, N.; Graf, S.; Halvorsen, Z. A., Fluid dosing system. Google Patents: 2020.
164. Zhu, P.; Wang, L., Passive and active droplet generation with microfluidics: a review. *Lab on a Chip* **2017,** *17* (1), 34-75.

165. Sánchez Barea, J.; Lee, J.; Kang, D.-K., Recent advances in droplet-based microfluidic technologies for biochemistry and molecular biology. *Micromachines* **2019,** *10* (6), 412.
166. Weibel, D. B.; Whitesides, G. M., Applications of microfluidics in chemical biology. *Current opinion in chemical biology* **2006,** *10* (6), 584-591.
167. Jammes, F. C.; Maerkl, S. J., How single-cell immunology is benefiting from microfluidic technologies. *Microsystems & Nanoengineering* **2020,** *6* (1), 1-14.
168. Leeuwenhoek, M.; Groenewoud, F.; van Oosten, K.; Benschop, T.; Allan, M. P.; Gröblacher, S., Fabrication of on-chip probes for double-tip scanning tunneling microscopy. *Microsystems & Nanoengineering* **2020,** *6* (1), 1-9.
169. Eduati, F.; Utharala, R.; Madhavan, D.; Neumann, U. P.; Longerich, T.; Cramer, T.; Saez-Rodriguez, J.; Merten, C. A., A microfluidics platform for combinatorial drug screening on cancer biopsies. *Nature communications* **2018,** *9* (1), 1-13.
170. Shembekar, N.; Chaipan, C.; Utharala, R.; Merten, C. A., Droplet-based microfluidics in drug discovery, transcriptomics and high-throughput molecular genetics. *Lab on a Chip* **2016,** *16* (8), 1314-1331.
171. Maeki, M., Microfluidics for pharmaceutical applications. In *Microfluidics for Pharmaceutical Applications*, Elsevier: 2019; pp 101-119.
172. Urban, K.; Wagner, G.; Schaffner, D.; Röglin, D.; Ulrich, J., Rotor-stator and disc systems for emulsification processes. *Chemical Engineering & Technology: Industrial Chemistry-Plant Equipment-Process Engineering-Biotechnology* **2006,** *29* (1), 24-31.
173. Maa, Y.-F.; Hsu, C. C., Performance of sonication and microfluidization for liquid–liquid emulsification. *Pharmaceutical development and technology* **1999,** *4* (2), 233-240.
174. Pavlyuchenko, V.; Ivanchev, S., Composite polymer hydrogels. *Polymer Science Series A* **2009,** *51* (7), 743-760.
175. Hayward, R. C.; Utada, A. S.; Dan, N.; Weitz, D. A., Dewetting instability during the formation of polymersomes from block-copolymer-stabilized double emulsions. *Langmuir* **2006,** *22* (10), 4457-4461.
176. Garstecki, P.; Fuerstman, M. J.; Stone, H. A.; Whitesides, G. M., Formation of droplets and bubbles in a microfluidic T-junction—scaling and mechanism of break-up. *Lab on a Chip* **2006,** *6* (3), 437-446.
177. Gañán-Calvo, A. M., Enhanced liquid atomization: From flow-focusing to flow-blurring. *Applied Physics Letters* **2005,** *86* (21), 214101.
178. Anna, S. L.; Bontoux, N.; Stone, H. A., Formation of dispersions using “flow focusing” in microchannels. *Applied physics letters* **2003,** *82* (3), 364-366.
179. Herranz-Blanco, B.; Ginestar, E.; Zhang, H.; Hirvonen, J.; Santos, H. A., Microfluidics platform for glass capillaries and its application in droplet and nanoparticle fabrication. *International journal of pharmaceutics* **2017,** *516* (1-2), 100-105.
180. Ding, H.; Gilani, M. N.; Spelt, P. D., Sliding, pinch-off and detachment of a droplet on a wall in shear flow. *Journal of fluid mechanics* **2010,** *644* (217), 56.
181. Cramer, C.; Fischer, P.; Windhab, E. J., Drop formation in a co-flowing ambient fluid. *Chemical Engineering Science* **2004,** *59* (15), 3045-3058.
182. Squires, T. M.; Quake, S. R., Microfluidics: Fluid physics at the nanoliter scale. *Reviews of modern physics* **2005,** *77* (3), 977.
183. Cabezas, M.; Rebollo-Muñoz, N.; Rubio, M.; Herrada, M.; Montanero, J., Global stability analysis of axisymmetric liquid–liquid flow focusing. *Journal of Fluid Mechanics* **2021,** *909*.
184. Crawford, D.; Smith, C.; Whyte, G., Image-based closed-loop feedback for highly mono-dispersed microdroplet production. *Scientific reports* **2017,** *7* (1), 1-9.
185. Robinson, T., Microfluidic handling and analysis of giant vesicles for use as artificial cells: a review. *Advanced Biosystems* **2019,** *3* (6), 1800318.

186. Sato, Y.; Takinoue, M., Creation of artificial cell-like structures promoted by microfluidics technologies. *Micromachines* **2019,** *10* (4), 216.
187. Jeong, H.-H.; Yelleswarapu, V. R.; Yadavali, S.; Issadore, D.; Lee, D., Kilo-scale droplet generation in three-dimensional monolithic elastomer device (3D MED). *Lab on a Chip* **2015,** *15* (23), 4387-4392.
188. Conchouso, D.; Castro, D.; Khan, S.; Foulds, I. G., Three-dimensional parallelization of microfluidic droplet generators for a litre per hour volume production of single emulsions. *Lab on a Chip* **2014,** *14* (16), 3011-3020.
189. Headen, D. M.; García, J. R.; García, A. J., Parallel droplet microfluidics for high throughput cell encapsulation and synthetic microgel generation. *Microsystems & Nanoengineering* **2018,** *4* (1), 1-9.
190. Kamperman, T.; Teixeira, L. M.; Salehi, S. S.; Kerckhofs, G.; Guyot, Y.; Geven, M.; Geris, L.; Grijpma, D.; Blanquer, S.; Leijten, J., Engineering 3D parallelized microfluidic droplet generators with equal flow profiles by computational fluid dynamics and stereolithographic printing. *Lab on a Chip* **2020,** *20* (3), 490-495.
191. Nisisako, T.; Torii, T., Microfluidic large-scale integration on a chip for mass production of monodisperse droplets and particles. *Lab on a Chip* **2008,** *8* (2), 287-293.
192. Barbier, V.; Willaime, H.; Tabeling, P.; Jousse, F., Producing droplets in parallel microfluidic systems. *Physical Review E* **2006,** *74* (4), 046306.
193. Stolovicki, E.; Ziblat, R.; Weitz, D. A., Throughput enhancement of parallel step emulsifier devices by shear-free and efficient nozzle clearance. *Lab on a Chip* **2018,** *18* (1), 132-138.
194. Montessori, A.; Lauricella, M.; Succi, S.; Stolovicki, E.; Weitz, D., Elucidating the mechanism of step emulsification. *Physical Review Fluids* **2018,** *3* (7), 072202.
195. Yin, L.-J.; Saito, M.; Kobayashi, I.; Nakajima, M., Preparation and characterization of protein-stabilized emulsions by microchannel emulsification. *International Journal of Nanoscience* **2006,** *5* (06), 959-966.
196. Kobayashi, I.; Mukataka, S.; Nakajima, M., Novel asymmetric through-hole array microfabricated on a silicon plate for formulating monodisperse emulsions. *Langmuir* **2005,** *21* (17), 7629-7632.
197. Liu, Z.; Duan, C.; Jiang, S.; Zhu, C.; Ma, Y.; Fu, T., Microfluidic step emulsification techniques based on spontaneous transformation mechanism: A review. *Journal of Industrial and Engineering Chemistry* **2020**.
198. Sugiura, S.; Oda, T.; Izumida, Y.; Aoyagi, Y.; Satake, M.; Ochiai, A.; Ohkohchi, N.; Nakajima, M., Size control of calcium alginate beads containing living cells using micro-nozzle array. *Biomaterials* **2005,** *26* (16), 3327-3331.
199. Kobayashi, I.; Mukataka, S.; Nakajima, M., Production of monodisperse oil-in-water emulsions using a large silicon straight-through microchannel plate. *Industrial & engineering chemistry research* **2005,** *44* (15), 5852-5856.
200. Kobayashi, I.; Wada, Y.; Uemura, K.; Nakajima, M., Microchannel emulsification for mass production of uniform fine droplets: integration of microchannel arrays on a chip. *Microfluidics and Nanofluidics* **2010,** *8* (2), 255-262.
201. van Dijke, K.; Veldhuis, G.; Schroën, K.; Boom, R., Parallelized edge-based droplet generation (EDGE) devices. *Lab on a Chip* **2009,** *9* (19), 2824-2830.
202. Amstad, E.; Chemama, M.; Eggersdorfer, M.; Arriaga, L. R.; Brenner, M. P.; Weitz, D. A., Robust scalable high throughput production of monodisperse drops. *Lab on a Chip* **2016,** *16* (21), 4163-4172.
203. Sahin, S.; Schroën, K., Partitioned EDGE devices for high throughput production of monodisperse emulsion droplets with two distinct sizes. *Lab on a Chip* **2015,** *15* (11), 2486-2495.
204. Buryk-Iggers, S.; Kieda, J.; Tsai, S. S., Diamagnetic droplet microfluidics applied to single-cell sorting. *AIP Advances* **2019,** *9* (7), 075106.

205. Hess, D.; Yang, T.; Stavrakis, S., Droplet-based optofluidic systems for measuring enzyme kinetics. *Analytical and bioanalytical chemistry* **2020,** *412* (14), 3265-3283.
206. Ferreira, J.; Castro, F.; Rocha, F.; Kuhn, S., Protein crystallization in a droplet-based microfluidic device: Hydrodynamic analysis and study of the phase behaviour. *Chemical Engineering Science* **2018,** *191*, 232-244.
207. Kahkeshani, S.; Di Carlo, D., Drop formation using ferrofluids driven magnetically in a step emulsification device. *Lab on a Chip* **2016,** *16* (13), 2474-2480.
208. Schuler, F.; Paust, N.; Zengerle, R.; Von Stetten, F., Centrifugal step emulsification can produce water in oil emulsions with extremely high internal volume fractions. *Micromachines* **2015,** *6* (8), 1180-1188.
209. Shin, D.-C.; Morimoto, Y.; Sawayama, J.; Miura, S.; Takeuchi, S., Centrifuge-based step emulsification device for simple and fast generation of monodisperse picoliter droplets. *Sensors and Actuators B: Chemical* **2019,** *301*, 127164.
210. Clime, L.; Malic, L.; Daoud, J.; Lukic, L.; Geissler, M.; Veres, T., Buoyancy-driven step emulsification on pneumatic centrifugal microfluidic platforms. *Lab on a Chip* **2020,** *20* (17), 3091-3095.
211. Wang, J.; Li, Y.; Wang, X.; Wang, J.; Tian, H.; Zhao, P.; Tian, Y.; Gu, Y.; Wang, L.; Wang, C., Droplet microfluidics for the production of microparticles and nanoparticles. *Micromachines* **2017,** *8* (1), 22.
212. Marimuthu, M.; Kim, S., for Tissue Engineering. *Nanobiomaterials: Development and Applications* **2013**, 341.
213. Rosca, I. D.; Watari, F.; Uo, M., Microparticle formation and its mechanism in single and double emulsion solvent evaporation. *Journal of controlled release* **2004,** *99* (2), 271-280.
214. Ramazani, F.; Chen, W.; van Nostrum, C. F.; Storm, G.; Kiessling, F.; Lammers, T.; Hennink, W. E.; Kok, R. J., Strategies for encapsulation of small hydrophilic and amphiphilic drugs in PLGA microspheres: state-of-the-art and challenges. *International journal of pharmaceutics* **2016,** *499* (1-2), 358-367.
215. Ravivarapu, H. B.; Burton, K.; DeLuca, P. P., Polymer and microsphere blending to alter the release of a peptide from PLGA microspheres. *European Journal of Pharmaceutics and Biopharmaceutics* **2000,** *50* (2), 263-270.
216. Hung, L.-H.; Teh, S.-Y.; Jester, J.; Lee, A. P., PLGA micro/nanosphere synthesis by droplet microfluidic solvent evaporation and extraction approaches. *Lab on a Chip* **2010,** *10* (14), 1820-1825.
217. Hu, Y.; Wang, Q.; Wang, J.; Zhu, J.; Wang, H.; Yang, Y., Shape controllable microgel particles prepared by microfluidic combining external ionic crosslinking. *Biomicrofluidics* **2012,** *6* (2), 026502.
218. Hatori, M. N.; Kim, S. C.; Abate, A. R., Particle-templated emulsification for microfluidics-free digital biology. *Analytical chemistry* **2018,** *90* (16), 9813-9820.
219. Nishizuka, S. S.; Yaegashi, M.; Sasaki, N.; Iwaya, T., Digital PCR probe library for TP53 mutations in early relapse prediction. AACR: 2019.
220. Hindson, B. J.; Ness, K. D.; Masquelier, D. A.; Belgrader, P.; Heredia, N. J.; Makarewicz, A. J.; Bright, I. J.; Lucero, M. Y.; Hiddessen, A. L.; Legler, T. C., High-throughput droplet digital PCR system for absolute quantitation of DNA copy number. *Analytical chemistry* **2011,** *83* (22), 8604-8610.
221. Campbell, J.; Zhang, M.; Hwang, T.; Bailey, S.; Wilson, D.; Jia, Y.; Huang, D., Detailed vascular anatomy of the human retina by projection-resolved optical coherence tomography angiography. *Scientific reports* **2017,** *7* (1), 1-11.
222. Zhang, Q.; Wang, T.; Zhou, Q.; Zhang, P.; Gong, Y.; Gou, H.; Xu, J.; Ma, B., Development of a facile droplet-based single-cell isolation platform for cultivation and genomic analysis in microorganisms. *Scientific reports* **2017,** *7* (1), 1-11.

223. Klein, A. M.; Mazutis, L.; Akartuna, I.; Tallapragada, N.; Veres, A.; Li, V.; Peshkin, L.; Weitz, D. A.; Kirschner, M. W., Droplet barcoding for single-cell transcriptomics applied to embryonic stem cells. *Cell* **2015,** *161* (5), 1187-1201.
224. Yang, L.; George, J.; Wang, J., Deep Profiling of Cellular Heterogeneity by Emerging Single-Cell Proteomic Technologies. *Proteomics* **2020,** *20* (13), 1900226.
225. Liu, Y.; Chen, X.; Zhang, Y.; Liu, J., Advancing single-cell proteomics and metabolomics with microfluidic technologies. *Analyst* **2019,** *144* (3), 846-858.
226. Matuła, K.; Rivello, F.; Huck, W. T., Single-cell analysis using droplet microfluidics. *Advanced biosystems* **2020,** *4* (1), 1900188.
227. Demaree, B.; Weisgerber, D.; Dolatmoradi, A.; Hatori, M.; Abate, A. R., Direct quantification of EGFR variant allele frequency in cell-free DNA using a microfluidic-free digital droplet PCR assay. *Methods in cell biology* **2018,** *148*, 119-131.
228. Wang, C.-T.; Chen, Y.-M.; Hong, P.-A.; Wang, Y.-T., Tesla valves in micromixers. *International Journal of Chemical Reactor Engineering* **2014,** *1* (open-issue).
229. Yang, A.-S.; Chuang, F.-C.; Su, C.-L.; Chen, C.-K.; Lee, M.-H. In *Development of a 3D-tesla micromixer for bio-applications*, 2013 IEEE International Conference on Mechatronics and Automation, IEEE: 2013; pp 152-157.
230. Kirby, G. T.; White, L. J.; Rahman, C. V.; Cox, H. C.; Qutachi, O.; Rose, F. R.; Hutmacher, D. W.; Shakesheff, K. M.; Woodruff, M. A., PLGA-based microparticles for the sustained release of BMP-2. *Polymers* **2011,** *3* (1), 571-586.
231. Keohane, K.; Brennan, D.; Galvin, P.; Griffin, B. T., Silicon microfluidic flow focusing devices for the production of size-controlled PLGA based drug loaded microparticles. *International journal of pharmaceutics* **2014,** *467* (1-2), 60-69.
232. Ding, Y.; Howes, P. D.; deMello, A. J., Recent advances in droplet microfluidics. *Analytical chemistry* **2019,** *92* (1), 132-149.
233. Suea-Ngam, A.; Bezinge, L.; Mateescu, B.; Howes, P. D.; deMello, A. J.; Richards, D. A., Enzyme-Assisted Nucleic Acid Detection for Infectious Disease Diagnostics: Moving toward the Point-of-Care. *ACS sensors* **2020,** *5* (9), 2701-2723.
234. Zhu, Q.; Qiu, L.; Yu, B.; Xu, Y.; Gao, Y.; Pan, T.; Tian, Q.; Song, Q.; Jin, W.; Jin, Q., Digital PCR on an integrated self-priming compartmentalization chip. *Lab on a Chip* **2014,** *14* (6), 1176-1185.
235. Ding, G.; Jin, Z.; Zhang, Y.; Han, Y.; Li, G.; Jing, Y.; Li, W., Detection of Genetically Modified Rice by Loop-Mediated Isothermal Amplification Assays on a Self-Priming Compartmentalization Chip. *FOOD ANALYTICAL METHODS* **2020**.
236. Basu, A. S., Digital assays part I: partitioning statistics and digital PCR. *SLAS TECHNOLOGY: Translating Life Sciences Innovation* **2017,** *22* (4), 369-386.
237. Tellinghuisen, J., dPCR vs. qPCR: The role of Poisson statistics at low concentrations. *Analytical Biochemistry* **2020,** *611*, 113946.
238. Gou, T.; Hu, J.; Wu, W.; Ding, X.; Zhou, S.; Fang, W.; Mu, Y., Smartphone-based mobile digital PCR device for DNA quantitative analysis with high accuracy. *Biosensors and Bioelectronics* **2018,** *120*, 144-152.
239. Hu, F.; Li, J.; Zhang, Z.; Li, M.; Zhao, S.; Li, Z.; Peng, N., Smartphone-based droplet digital LAMP device with rapid nucleic acid isolation for highly sensitive point-of-care detection. *Analytical Chemistry* **2019,** *92* (2), 2258-2265.
240. Salipante, S. J.; Jerome, K. R., Digital PCR—An emerging technology with broad applications in microbiology. *Clinical chemistry* **2020,** *66* (1), 117-123.
241. Srisa-Art, M.; DeMello, A. J.; Edel, J. B., High-throughput DNA droplet assays using picoliter reactor volumes. *Analytical chemistry* **2007,** *79* (17), 6682-6689.

242. Wang, Y.-N.; Fu, L.-M., Micropumps and biomedical applications–A review. *Microelectronic Engineering* **2018,** *195*, 121-138.
243. Bick, A.; Khor, J. W.; Gai, Y.; Tang, S. K., Strategic placement of an obstacle eliminates droplet break-up in the flow of a microfluidic concentrated emulsion. *APS* **2019**, NP05. 149.
244. Demaree, B.; Weisgerber, D.; Dolatmoradi, A.; Hatori, M.; Abate, A. R., Direct quantification of EGFR variant allele frequency in cell-free DNA using a microfluidic-free digital droplet PCR assay. In *Methods in cell biology*, Elsevier: 2018; Vol. 148, pp 119-131.
245. Ahmadi, S.; Rabiee, N.; Bagherzadeh, M.; Karimi, M., Microfluidic devices for pathogen detection. In *Biomedical Applications of Microfluidic Devices*, Elsevier: 2020; pp 117-151.
246. Wang, Q.; Shen, Y.; Yao, H.; Ho, T.-Y.; Cai, Y. In *Practical functional and washing droplet routing for cross-contamination avoidance in digital microfluidic biochips*, Proceedings of the 51st Annual Design Automation Conference, 2014; pp 1-6.
247. Vladisavljević, G. T.; Ekanem, E. E.; Zhang, Z.; Khalid, N.; Kobayashi, I.; Nakajima, M., Long-term stability of droplet production by microchannel (step) emulsification in microfluidic silicon chips with large number of terraced microchannels. *Chemical Engineering Journal* **2018,** *333*, 380-391.
248. Shi, Z.; Lai, X.; Sun, C.; Zhang, X.; Zhang, L.; Pu, Z.; Wang, R.; Yu, H.; Li, D., Step emulsification in microfluidic droplet generation: mechanisms and structures. *Chemical Communications* **2020,** *56* (64), 9056-9066.
249. Organization, W. H., Global action plan for the prevention and control of noncommunicable diseases 2013-2020. **2013**.
250. Danish Khan, I.; Mohan Gupta, R.; Sen, S.; Rajmohan, K.; Kumar Jindal, A.; Makkar, A.; Rahman Razi, F.; Banerjee, P.; Panda, P.; Lakshmi Nair, G., Emerging antimicrobial resistance and evolving healthcare: Dangerous crossroads for the community and the military. *Journal of Archives in Military Medicine* **2017,** (In Pre).
251. Organization, W. H. *Technical consultation on in vitro diagnostics for AMR, 27–28 March 2019, WHO Headquarters, Geneva: meeting report*; World Health Organization: 2019.
252. Adeiza, S. S.; Onaolapo, J. A.; Olayinka, B. O., Prevalence, risk-factors, and antimicrobial susceptibility profile of methicillin-resistant Staphylococcus aureus (MRSA) obtained from nares of patients and staff of Sokoto state-owned hospitals in Nigeria. *GMS Hygiene and Infection Control* **2020,** *15*.
253. Morgan, D. J.; Zhan, M.; Goto, M.; Franciscus, C.; Alexander, B.; Vaughan-Sarrazin, M.; Roghmann, M.-C.; Pineles, L., The effectiveness of contact precautions on methicillin-resistant Staphylococcus aureus in long-term care across the United States. *Clinical Infectious Diseases* **2020**.
254. Algammal, A. M.; Hetta, H. F.; Elkelish, A.; Alkhalifah, D. H. H.; Hozzein, W. N.; Batiha, G. E.-S.; El Nahhas, N.; Mabrok, M. A., Methicillin-Resistant Staphylococcus aureus (MRSA): one health perspective approach to the bacterium epidemiology, virulence factors, antibiotic-resistance, and zoonotic impact. *Infection and Drug Resistance* **2020,** *13*, 3255.
255. Lagier, J.-C.; Edouard, S.; Pagnier, I.; Mediannikov, O.; Drancourt, M.; Raoult, D., Current and past strategies for bacterial culture in clinical microbiology. *Clinical microbiology reviews* **2015,** *28* (1), 208-236.
256. Stevenson, B., Common bacterial culture techniques and media. *Current protocols in microbiology* **2006,** (1), A. 4A. 1-A. 4A. 8.
257. Baylis, S.; Wallace, P.; McCulloch, E.; Niesters, H.; Nübling, C., Standardization of nucleic acid tests: the approach of the World Health Organization. *Journal of clinical microbiology* **2019,** *57* (1).
258. Yuan, H.; Chao, Y.; Shum, H. C., Droplet and Microchamber-Based Digital Loop-Mediated Isothermal Amplification (dLAMP). *Small* **2020,** *16* (9), 1904469.

259. Vieira, G.; Leal, N.; Rodrigues, A.; Chaves, C.; Rodrigues, F.; Osório, N., MRSA/MSSA causing infections: prevalence of mecA gene. *European Journal of Public Health* **2020,** *30* (Supplement_2), ckaa040. 052.
260. Suea-Ngam, A.; Choopara, I.; Li, S.; Schmelcher, M.; Somboonna, N.; Howes, P. D.; deMello, A. J., In Situ Nucleic Acid Amplification and Ultrasensitive Colorimetric Readout in a Paper-Based Analytical Device Using Silver Nanoplates. *Advanced Healthcare Materials* **2020**, 2001755.
261. Zhu, Y.; Li, J.; Lin, X.; Huang, X.; Hoffmann, M. R., A hydrogel beads based platform for single-cell phenotypic analysis and digital molecular detection. *bioRxiv* **2019**, 848168.
262. Raza, W.; Hossain, S.; Kim, K.-Y., A Review of Passive Micromixers with a Comparative Analysis. *Micromachines* **2020,** *11* (5), 455.
263. Fan, J.; Li, S.; Wu, Z.; Chen, Z., Diffusion and mixing in microfluidic devices. In *Microfluidics for Pharmaceutical Applications*, Elsevier: 2019; pp 79-100.

264. Bartkova, S.; Vendelin, M.; Sanka, I.; Pata, P.; Scheler, O., Droplet image analysis with user-friendly freeware CellProfiler. Analytical Methods 2020, 12 (17), 2287-2294.